ABSTRACT

| | |
|---|---|
| Title of Document: | A STUDY OF THE SULFUR ISOTOPIC COMPOSITION OF MARTIAN METEORITES |
| | Heather B. Franz, Ph.D., 2012 |
| Directed By: | Professor James Farquhar, Department of Geology and ESSIC |

Sulfur is an important tracer for geochemical processes because it possesses four stable isotopes and forms natural compounds in a range of oxidation states. This element has been shown to undergo mass-independent isotopic fractionation (S-MIF) during laboratory photochemical experiments, which may provide clues to processes that have occurred both in the solar nebula and in planetary atmospheres. The surface of Mars has been found to contain ubiquitous sulfate minerals, marking this planet as an ideal candidate for sulfur isotope study.

The shergottites comprise the youngest group of martian meteorites and the most representative of mantle-derived igneous rocks. Extraction and isotopic measurement of sulfur from 30 shergottites yield the first estimate of the juvenile martian sulfur composition, which matches within uncertainties that of Cañon Diablo Troilite. Analysis of martian meteorites spanning a range of ages from the shergottites, as young as ~150 Ma, to the nakhlites, ~1.3 Ga, reveals the presence of sulfur characterized by S-MIF compositions. These findings are interpreted as evidence for

cycling of sulfur between an atmospheric reservoir where photochemical processing of sulfur-bearing gases occurred and a surface reservoir in which photochemical products were ultimately deposited. Anomalous sulfur has been detected in both sulfate and sulfide minerals, implying assimilation of sulfur from the martian surface into magmas. Differences in the S-MIF compositions of the nakhlites and shergottites may preserve a record of complementary sulfur formed by a single process or may indicate the operation of multiple photochemical processes at different times or geographical locations.

Identification of the photochemical mechanism responsible for producing the anomalous sulfur observed in martian meteorites is important for constraining the atmospheric composition at the time the S-MIF signals were generated. Results of laboratory experiments with pure $SO_2$ gas suggest that self-shielding is insufficient to explain the anomalous sulfur isotopic composition. This implies that an optically thick $SO_2$ column in the martian atmosphere may not have been required for production of the observed signals.

A STUDY OF THE SULFUR ISOTOPIC COMPOSITION OF MARTIAN
METEORITES


By


Heather B. Franz


Dissertation submitted to the Faculty of the Graduate School of the
University of Maryland, College Park, in partial fulfillment
of the requirements for the degree of
Doctor of Philosophy
2012


Advisory Committee:
Professor James Farquhar, Chair
Professor Philip A. Candela
Assistant Professor Sarah Penniston-Dorland
Professor Richard J. Walker
Dean's Representative Professor Matthew C. Hansen

# Preface

This document contains original material that has not been published elsewhere except selected data presented in the following abstracts:

Franz, H. B., Farquhar, J., and Kim, S.-T. (2008) Sulfur isotopic composition of multiple mineral phases in shergottites. Lunar and Planetary Institute, #2433.

Franz, H. B., Farquhar, J., and Irving, A. J. (2010) Acid-volatile sulfur isotopic composition of seven shergottites from northwest Africa. Lunar and Planetary Institute, #2341.

Franz, H. B., Farquhar, J., and Irving, A. J. (2011) Acid-volatile sulfur isotopic composition of six shergottites. Lunar and Planetary Institute, #2338.

# Dedication

This work is dedicated to Phoebe, my only light through the darkest days.

I love you for all time, angel.

I miss you.

*"All the darkness in the world cannot extinguish the light of a single candle."*

*- Saint Francis of Assisi*

# Acknowledgements

I have so many people to acknowledge that I fear I will inadvertently miss someone. I must first thank my advisor, James Farquhar, for having the fortitude to travel this long and arduous path with me. I am grateful to many people at UM: Thanks to Rich Walker and Mike Brown for giving me the chance to pursue this crazy idea of becoming a geochemist (although Rich, you should have tried harder to talk me out of it); to my other committee members, Rich Walker, Phil Candela, Sarah Penniston-Dorland, and Matt Hansen, for their support; to Andy Campbell, who served on my proposal committee; to the many folks of the Farquhar group, past and present, who have provided lab assistance, especially Dave Johnston, Andy Masterson, Boz Wing, Sang-Tae Kim, Alexey Kamyshny, Harry Oduro, Nanping Wu, and Jon Banker; to Phil Piccoli for crucial and timely assistance with EPMA analyses; and to others in the Geology department who have been so helpful over the years – Sandy Romeo, Dorothy Brown, Todd Karwoski, Suzanne Martin, and Michelle Montero. I am also grateful to Mark Lewis, formerly of the Aerospace Engineering department, for being my stalwart supporter and friend.

From NASA Goddard Space Flight Center, I would like to thank Pan Conrad, Stephanie Getty, Jim Golder, Amy McAdam, Ed Patrick (now at SwRI), Craig Roberts, Jen Stern, and Inge ten Kate (now at University of Utrecht) for moral support; Inge also for translating ancient sulfur-related papers from their original German ☺; Alex Pavlov, Melissa Trainer, and Reggie Hudson for discussions about photochemistry; Manuel Quijada and Tim Madison for measuring the $D_2$ lamp spectrum; Mollie Powell for assistance with polishing the Y000593 meteorite section;

Last but certainly not least, I must thank my wonderful family, who have always been there for me – my parents, who raised me with an appreciation for education and the wonders of both art and science, and taught me that I could be whatever I wanted to be; my late grandparents on both sides, who provided unconditional love; my sisters, who have supported me throughout the journey with sympathetic ears; my furry four-legged kids, who remind me daily of what's truly important; and my husband Bryan, who is still my best friend after all these years.

# Table of Contents

# List of Tables

# List of Figures

# Chapter 1: Introduction[1]

[1] The text, tables, and figures in this chapter were written/created by H. B. Franz.

## 1.1 Introduction to Mars

### 1.1.1 A Brief History of Our Neighboring Planet

Humankind has long been fascinated with Mars, since even before it was known that Mars is the most Earth-like planet in our solar system. Beginning in the $17^{th}$ century, telescopic observations allowed new scientific discoveries, such as the first views of the Syrtis Major region by Huygens in 1659, which led to the first estimate of Mars' rotational period (Hartmann, 2003). Advancements in telescope technology brought Mars into increasingly better focus over time, but not quite well enough to discern the true nature of the features on its scarred surface. It was not until the advent of space missions in the 1960s that inhabitants of Earth were able to appreciate the spectacular landscapes on Mars, which include Olympus Mons, the highest volcano in the solar system, and Valles Marineris, the longest valley (Hartmann, 2003). Spacecraft currently in orbit about Mars are providing details of the planet's surface at incredibly high-resolution and spectroscopic perspectives that show patterns of mineralogical distributions on a global scale (e.g., Bibring et al., 2005; Murchie et al., 2009; Ehlmann et al., 2011).

Table 1-1 gives some basic statistics for Mars, which is about half the size of Earth but has approximately the same land area (Hartmann, 2003). The formation and differentiation of Mars into core, mantle, and crust occurred within a few tens of

millions of years after formation of the solar system (Lee and Halliday, 1997; Brandon et al., 2000). Due to its size and placement within the solar system, Mars holds a unique record of its past history throughout all stages of planetary evolution, preserved within its diverse surface features (Bibring and Erard, 2001). Extensive mapping of the surface by orbiting spacecraft in recent years has revealed a predominance of primary silicate minerals with basaltic to andesitic composition, including olivine, pyroxene, and plagioclase (Hamilton et al., 2003; Bandfield et al., 2004; Bibring et al., 2005). Widespread occurrences of secondary minerals including phyllosilicates and sulfates have also been detected (e.g., Bibring et al., 2005, 2006; Ehlmann et al., 2011).

**Table 1-1. Some Basic Data for Mars**

(Sources: Kallenbach et al., 2001; Taylor, 2011)

| Parameter | Value |
|---|---|
| Diameter | 6794 km |
| Mass | $6.42 \times 10^{23}$ kg |
| Gravitational acceleration | $3.73$ m/s$^2$ |
| Mean distance from the Sun | 1.524 AU |
| Orbital eccentricity | 0.093 |
| Obliquity | 23.98° |
| Rotational period | 24 h 39 m 35 s = 1 sol |
| Length of martian year | 1.88 Earth years = 669 sols |
| Surface temperature range | 140 – 295 K |
| Mean surface pressure | ~6.5 mbar |
|  |  |
| Main atmospheric constituents: | Mixing ratio: |
| $CO_2$ | 0.95 |
| $N_2$ | 0.027 |
| Ar | 0.016 |
| $H_2O$ | ~0.0003 |
| $O_2$ | 0.0013 |
| CO | 700 ppm |
| Ne | 2.5 ppm |

The martian surface has been dated through analysis of impact crater counts, which are calibrated for absolute ages based on extrapolation of the impact flux curve for the Moon and radiometric dating of lunar samples (Stöffler and Ryder, 2001). The cratering densities and superposition relationships for various surface regions have been used to define three major age periods: Noachian, Hesperian, and Amazonian (Scott and Carr, 1978; Tanaka, 1986). The earliest period of Mars' history is referred to as the pre-Noachian, which began at planetary formation and witnessed numerous large impacts. Some researchers believe that one or more large impacts may be responsible for the well-known Mars crustal dichotomy, characterized by differences in elevations, crustal thickness, and crater densities between northern and southern hemispheres (e.g., Wilhelms and Squyres, 1984; McGill and Squyres, 1991; Nimmo et al., 2008). Such large impacts would have released water and other volatiles, as well as vaporized rocks, into the atmosphere, potentially resulting in periods of time sufficiently warm for liquid water to exist on the surface (Segura et al., 2002). However, the characteristics of the atmosphere and surface conditions during this time are uncertain.

The marker for the end of the pre-Noachian and start of the Noachian period is taken as the formation of the Hellas Basin, dated from 4.1 to 3.8 Ga (Frey, 2008; Fassett and Head, 2011). The Noachian was characterized by high rates of impact cratering, erosion, and valley formation (Carr and Head, 2010). Volcanism during this period was probably dominated by buildup of the Tharsis province, which may have reached proportions of 5,000 km across and 9 km high by the end of the Noachian

(Phillips et al., 2001). Noachian terrains are much more eroded than younger terrains, suggesting that high erosion rates existed throughout the Noachian and then steeply declined (Craddock and Howard, 2002). Phyllosilicates have recently been discovered to be widespread in Noachian terrain (e.g., Bibring, 2005, 2006; Le Deit et al., 2012). It has been suggested that these minerals were formed primarily by hydrothermal groundwater circulation rather than weathering at the surface, where liquid water may have been present only during relatively brief transient episodes (Squyres and Kasting, 1994; Behlmann et al., 2011). During these episodes, an extensive network of valleys formed, most of which drained into local topographical lows (Carr and Head, 2010). Some of the water may have remained at the surface long enough to form temporary lakes that deposited evaporitic sulfate minerals (Grotzinger et al., 2005). The existence and duration of warm, wet periods on early Mars is a topic of debate, due to difficulties reconciling the need for a thick $CO_2$ atmosphere to allow stability of water at the surface with the lack of evidence for a sink or loss mechanism for the $CO_2$ in more recent epochs (Carr and Head, 2010). Most hypotheses proposed to counter this problem have invoked the presence of trace greenhouse gases, including $SO_2$, $H_2S$, and OCS, to raise the surface temperature above freezing (e.g., Kasting et al., 1989; Squyres and Kasting, 1994; Halevy et al., 2007; Johnson, 2008, 2009). It is likely that the buildup of the Tharsis province was accompanied by release of sulfur-bearing gases into the atmosphere. This topic will be revisited later.

Surface features formed during the Hesperian period, which followed the Noachian, are distinguished from those of the older Noachian surfaces based on the

number of impact craters (Scott and Carr, 1978; Scott and Tanaka, 1986). Crater densities suggest that this period extended from ~3.7 to 3 Ga (Hartmann and Neukum, 2001). Volcanism continued in the Hesperian, but was probably more episodic in nature than during earlier times (Carr and Head, 2010). The rate of valley formation declined, but large canyons and outflow channels including the Valles Marineris were formed, most likely by rapid release of large volumes of subsurface water under pressure (Carr, 1978; Ghatan et al., 2005; Russell and Head, 2007). The Hesperian was also characterized by very low rates of erosion, a steep decline in the rate of phyllosilicate formation, and an increase in formation of locally extensive sulfate deposits, particularly in the western hemisphere (e.g., Bibring et al., 2005, 2006; Carr and Head, 2010). Bibring et al. (2005) suggested that this observation indicates a transition from neutral to acidic pH conditions at the surface. The widespread detection of olivine on post-Noachian surfaces has been interpreted as evidence for low weathering rates during the past ~3.7 Ga of Mars' history (Bandfield et al. 2000).

The Amazonian period began ~3 Ga ago and continues to the present (Scott and Carr, 1978; Hartmann and Neukum, 2001). During this period, martian geological activity slowed further, with the average rate of volcanism decreasing by an order of magnitude, compared to that of the Hesperian, and volcanism was confined primarily to the regions of Tharsis and Elysium (Carr and Head, 2010). The Amazonian has also witnessed a low rate of resurfacing due to impact cratering, erosion, and weathering (Golombek et al., 2006). However, the effects of ice and wind are more evident in the Amazonian than in earlier periods, as are signs of obliquity-driven

processes, such as formation of polar layered deposits (Jakosky and Carr, 1985; Laskar et al., 2004). Ice is presently unstable at the surface except near the poles (Forget et al., 2006). However, modeling suggests that water ice may be stable at many locations within a few centimeters of the surface, as confirmed by the Phoenix lander (Mellon and Jakosky, 1995; Cull et al., 2010). In addition, neutron and gamma-ray spectrometers on orbiting spacecraft have detected ice at depths of tens of centimeters (Boynton et al., 2002; Feldman et al., 2004). While direct evidence of ice has not been detected from orbit at latitudes below 60º,  patterned ground occurs as low as 30º latitude (Levy et al., 2009). A few outflow channels in the Tharsis region have crater ages from 2 to 140 Ma (Berman and Hartmann, 2002), implying that liquid water may exist at depth and that it could be brought to the surface by tectonic or volcanic activity, even today.

### 1.1.2   *Sulfur on Mars*

Estimates of the bulk sulfur content of the Earth have been made based on the sulfur concentrations in chondritic meteorites and volatility trends of sulfur and other elements (Dreibus and Palme, 1996). For Earth, recent estimates have yielded 0.56% (Dreibus and Palme, 1996) and 0.46% (Allègre et al., 2001) bulk sulfur. Lodders and Fegley (1997) derived a bulk composition for Mars constrained by oxygen isotopes measured in martian meteorites and chondrites. They calculated that Mars comprises ~80% silicates, with a mantle FeO content of 17.2%. The remaining 20% of the planet consists of a metal-sulfide core containing ~10.6% sulfur, yielding a bulk sulfur abundance of 22,000 ppm (Lodders and Fegley, 1997).  The sulfur content of the silicate portion of the planets is based on analyses of mantle-derived samples. In

the Earth's case, McDonough and Sun (1995) estimated $250 \pm 50$ ppm sulfur in the upper mantle from mid-ocean ridge basalts and massif peridotites. Estimates for Mars have been based on analysis of martian meteorites, particularly the shergottites, which represent our youngest examples of material believed to derive from martian magmatic activity (e.g., McSween, 1994). Lodders and Fegley (1997) estimated 900 ppm sulfur in the martian mantle.

The amount of sulfur released into the atmosphere due to magmatic degassing is a function primarily of the oxygen fugacity, sulfur fugacity, FeO and $H_2O$ content of the melt, pressure, and temperature (Righter et al., 2009; Gaillard and Scaillet, 2009). It is uncertain whether the shergottite magmas were sulfide saturated upon melting and how much sulfur was lost through degassing during ascent. Righter et al. (2009) performed experiments with silicate melts at a range of compositions typical of shergottites and determined that the sulfur concentration for a sulfide-saturated magma from the martian mantle would be 3000 to 4000 ppm. In comparison, extraction of primary monosulfide minerals from shergottites analyzed for this study through acid-based distillation produced between 0 and 2363 ppm sulfur (Chapter 2). Righter et al. (2009) computed the quantity of sulfur that could have been injected into the atmosphere based on their calculated maximum mantle sulfur abundance of 4000 ppm, an assumed shergottite average sulfide content of 1600 ppm, and estimates of the eruptive mass on the martian surface. The total sulfur degassed on Mars during the past 4 Ga using their model amounts to $4.5 \times 10^{16}$ kg, equivalent to $1.1 \times 10^{17}$ kg of $SO_3$ (Righter et al., 2009). This is comparable to the value estimated for a similar degassing efficiency by Gaillard and Scaillet (2009), who concluded that this much

sulfur released by martian volcanic activity and later deposited on the surface could have produced a global layer of sulfate minerals 25 m thick. In comparison, the total volcanic sulfur flux on Earth is estimated as $9 - 46$ Tg per year (Oppenheimer et al., 2011).

In fact, planetary exploration missions have revealed that sulfur is present at significant abundance over most of the surface of Mars. The Viking landers detected sulfur concentrations of up to 10 wt% $SO_3$ (Baird et al., 1976; Clark et al., 1976), while Pathfinder found up to 8 wt% concentrations of $SO_3$ (Bell III et al., 2000, Rieder et al., 1997). Magnesium sulfates have been identified most abundantly (Banin et al., 1997). However, several hydrous iron sulfates present possible matches to absorption bands seen in mini-TES (Thermal Emission Spectrometer) and Pancam spectra acquired by the Mars Exploration Rover (MER) Spirit (Lane et al., 2004; Johnson et al., 2007). In addition to the sulfur present in the soil, the Mössbauer spectrometer on the MER rover Opportunity has detected concentrations of up to 25 wt% $SO_3$ in iron-rich sedimentary outcrops at Meridiani Planum (Klingelhöfer et al., 2004; Rieder et al., 2004; Squyres et al., 2004), part of a unit ~600 km across and several hundred meters thick that overlies typical Noachian cratered terrain (Arvidson et al., 2006). Recently the Observatoire pour la Minéralogie, l'Eau, les Glaces et l'Activité (OMEGA) instrument on the Mars Express orbiter and the Compact Reconnaissance Imaging Spectrometer for Mars (CRISM) instrument on the Mars Reconnaissance Orbiter have located several extensive sulfate mineral deposits in the martian surface, identified as gypsum ($CaSO_4 \cdot 2H_2O$), kieserite ($MgSO_4 \cdot H_2O$), and

polyhydrated sulfates (Langevin et al., 2005; Gendrin et al., 2005; Murchie et al., 2009; Lichtenberg et al., 2010).

Various formation mechanisms have been proposed for the martian sulfates. The sulfate-bearing layered terrains detected by OMEGA are tens of kilometers wide and a few kilometers thick (Bibring et al., 2005). While the formation of sulfate beds by evaporitic processes would require the presence of water, evaporation from standing bodies of water would impose strict constraints on atmospheric conditions (Gendrin et al., 2005). There are other processes that may explain the observed martian sulfates without the requirement for long-lived water reservoirs at the surface. For example, salts could precipitate from supersaturated water seeping out of ice deposits, followed by evaporation or sublimation of the water (Bibring et al., 2005). Other workers have suggested that large-scale deposits of hydrated minerals such as those at Meridiani Planum were created through a hydrological cycle of precipitation coupled with groundwater evaporation, producing alteration of regional topography that caused lateral spread of upwelling groundwater (Andrews-Hanna et al., 2010).

Other proposed formation mechanisms for martian sulfates involve the weathering of sulfide deposits, volcanic ash, or basaltic rock (Bibring et al., 2005; Burns, 1993). In situ oxidation of exposed iron (II) sulfide to sulfate should occur spontaneously by gas-solid reaction on both Earth and Mars (Gooding, 1978). On Mars, this process should produce $FeSO_4$ and possibly elemental sulfur in drier regions and $FeSO_4 \cdot H_2O$ in regions with abundant water vapor. If liquid water later interacted with these minerals, the dissolution of sulfate would allow oxidation of the $Fe^{2+}$ to $Fe^{3+}$ and precipitation of $FeO(OH)$ or $Fe_2O_3$ (Gooding, 1978). In addition to

the process just described, aqueous alteration of sulfides produces sulfuric acid-enriched water, which may dissolve surrounding silicate minerals and release other cations besides iron that could then precipitate as sulfate minerals (Gooding, 1978).

The $SO_2$ gas generated by martian volcanoes may also be oxidized to $H_2SO_4$ in the presence of water, forming an acid fog that can readily alter volcanic ash deposits or basaltic rocks to allow the crystallization of sulfates (Banin et al., 1997; Hurowitz et al., 2006). Since evidence suggests that Mars' volcanoes have been active until at least the past 100 million years, such a basalt alteration mechanism may have operated periodically over a long timescale (Hartmann et al., 1999). If so, there may be layers of ancient regolith hidden beneath that currently exposed at the surface. It has also been suggested that the predominant formation mechanism for sulfate minerals may have changed over time, with earlier processes inducing the precipitation of insoluble sulfates such as jarosite ($KFe^{3+}_3(OH)_6(SO_4)_2$), and later anhydrous weathering processes resulting in more soluble sulfates, including kieserite (Banin et al., 1997). Sulfates also represent a possible subsurface reservoir for martian water. Variations in atmospheric water vapor content could cause changes in the hydration phase of sulfate minerals and thus variations in the sulfate minerals identified by exploratory missions over time (Vaniman et al., 2004).

The Mars Science Laboratory (MSL) rover is scheduled to arrive at Mars' Gale Crater in August 2012. Gale crater is a Noachian-age crater ~155 km in diameter, located at the topographic boundary separating the ancient southern highlands and the younger terrain in the northern hemisphere (Milliken et al., 2010). The crater contains a central mound consisting of a 5-km thick stratigraphic sequence, interpreted to be

sedimentary in origin (Malin and Edgett, 2000). The crater has been partially excavated by subsequent erosion to reveal two sedimentary formations: a Lower formation that shows a net transition from clay/sulfate to sulfate/oxide mineralogy, and an Upper formation consisting of younger minerals with no evidence of clays or sulfates. While it is uncertain whether the clay and sulfate minerals in the mound are detrital or authigenic, it has been suggested that the mound was likely deposited by aeolian processes throughout Mars' history and lithified in place (Carr and Head, 2010; Milliken et al., 2010). In either case, the secular change in mineralogy upward through the sequence presumably records a transition in climate or sediment source on at least a regional scale (Milliken et al., 2010). The differences observed in the Lower and Upper formations are consistent with the hypothesis of Bibring et al. (2006) that a global transition occurred at ~3.8 to 3.6 Ga from a wetter climate conducive to clay mineral formation to a water-limited climate characterized by precipitation of sulfates and other salts. CRISM spectra suggest the presence of both mono- and polyhydrated Mg-sulfates in the Lower formation, but no Fe- or Al-sulfates indicative of highly acidic conditions have been detected yet from orbit (Milliken et al., 2010). Alternatively, the mound may record a period of intense volcanic activity, in which substantial quantities of sulfur-bearing gases were released into the atmosphere and subsequently deposited at the surface. Detailed study of the Gale Crater mound is expected to provide vital clues to past shifts in the martian climatic environment and volcanic history.

*1.1.3  Martian Meteorites*

To date, 65 unpaired meteorites have been identified as having originated on Mars (Irving, 2012a). They have historically been known as the "SNC meteorites" or simply "SNCs," based on the initials of the locations where the first three were recovered: Shergotty, India in 1865, Chassigny, France in 1815, and Nakhla, Egypt in 1911. The meteorites are classified as martian based primarily on analysis of atmospheric gases trapped in glass inclusions that match the composition of Mars' atmosphere as determined by the Viking mission (Bogard and Johnson, 1983). However, there are additional clues suggesting an unusual origin for these rocks. Most meteorites are pieces of asteroids, which crystallized at the dawn of the solar system around 4.5 Ga. In contrast, all but one of the SNCs were formed by igneous activity on a parent body less than 1.3 billion years ago, with Mars as the most likely candidate (Ashwal et al., 1982; Meyer, 2006).[1] Clayton and Mayeda (1983) also showed that the SNCs have a distinct oxygen isotopic composition compared to the Earth or other meteorite parent bodies, forming their own subgroup on an oxygen 3-isotope plot. Franchi et al. (1999) further showed that the oxygen isotopic composition of the SNCs is quite homogeneous, and that any oxygen heterogeneity inherited from the nebula was homogenized early in Mars' history.

The martian meteorites have traditionally been categorized as nakhlites, basaltic shergottites, lherzolitic shergottites, olivine-phyric and olivine-orthopyroxene-phyric

---

[1] The most ancient martian meteorite, ALH 84001, has an inferred crystallization age of ~4.1 Ga (Lapen et al., 2010). All other known martian meteorites have crystallization ages of 1.3 Ga or younger (Nyquist, 1995).

shergottites, chassignites, and orthopyroxenites (Meyer, 2006). The nakhlites are fine-grained clinopyroxenites comprised primarily of green cumulate augite crystals, minor olivine, and mesostasis containing fine-grained maskelynite, oxides, sulfides, and phosphate (Bunch and Reid, 1975; Berkley et al., 1980; Imae and Ikeda, 2005). They show indications of pre-terrestrial weathering in the form of salts and other alteration products (Dreibus et al., 2006). Basaltic shergottites are basaltic rocks with comparable amounts of pyroxene and plagioclase (Harvey et al., 1996; Barrat et al., 2002a). Lherzolitic shergottites contain large orthopyroxene crystals enclosing olivine and chromite phenocrysts, as well as accessory maskelynite, oxides, sulfides, and phosphates (Delaney, 1992; Ikeda, 1997). Olivine-phyric shergottites consist of olivine phenocrysts in a basaltic matrix (Goodrich et al., 2003; Greshake et al., 2004) and may contain minor amounts of orthopyroxene (Irving et al., 2002). The chassignites are cumulates consisting primarily of olivine with minor pyroxene, plagioclase, chromite, and phosphate (Prinz et al., 1974; Beck et al., 2005). The single orthopyroxenite (ALH 84001) is also a cumulate composed predominantly of orthopyroxene with minor maskelynite, augite, apatite, and chromite (Berkley, 1987; Boctor et al., 1998; Brearley, 2000). ALH 84001 also contains some carbonate-bearing assemblages believed to represent pre-terrestrial alteration (Treiman, 1995; Romanek et al., 1994).

A list of currently known martian meteorites is summarized in Table 1-2. The naming convention is typically based on the location where each meteorite was recovered. Specific abbreviations that appear in the table are NWA for Northwest Africa; Y for Yamato Mountain, Antarctica; MIL for the Miller Range, Antarctica;

EET for the Elephant Moraine at Victoria Land, Antarctica; QUE for Queen Alexandra Range, Antarctica; LEW for Lewis Cliffs, Antarctica; GRV for Grove Mountains, Antarctica; DaG for Dar al Gani, Sahara Desert, Africa; SaU for Sayh al Uhaymir, Oman, Asia; and ALH for Allan Hills, Antarctica.

## Table 1-2. List of Current Martian Meteorites

(Sources: Irving, 2012a; Classen, 2012)

| Meteorite | Mass (g) | Location where found | Year found |
|---|---|---|---|
| **Shergottites** | | | |
| *Mafic Shergottites* | | | |
| Shergotty | ~5,000 | Shergotty, India (August 25) | 1865 |
| Los Angeles 001 | 452.6 | | |
| Los Angeles 002 | 245.4 | California, USA | 1999 |
| Zagami | ~ 18,100 | Zagami, Nigeria (October 3) | 1962 |
| NWA 480 | 28.0 | | 2000 |
| NWA 1460 | 70.2 | Morocco | 2002 |
| NWA 856 | 320.0 | Morocco | 2001 |
| NWA 1669 | 35.9 | Morocco | 2001 |
| NWA 2800 | 686.0 | Algeria or Morocco | 2007 |
| NWA 2975 | 70.1 | | 2005 |
| NWA 2986 | 170.0 | | 2006 |
| NWA 2987 | 82.0 | | 2007 |
| NWA 4766 | 225.0 | | 2006 |
| NWA 4783 | 120.0 | | 2007 |
| NWA 4857 | 24.0 | | 2007 |
| NWA 4864 | 94.0 | | 2007 |
| NWA 4878 | 130.0 | Algeria | 2007 |
| NWA 4880 | 81.6 | | 2007 |
| NWA 4930 | 117.5 | | 2007 |
| NWA 5140 | 7.45 | | 2007 |
| NWA 5214 | 50.7 | | 2007 |
| NWA 5219 | 60.0 | | 2007 |
| NWA 5313 | 5.30 | | 2008 |
| NWA 5366 | 39.6 | | 2007 |
| NWA 3171 | 506.0 | Algeria | 2004 |
| NWA 4480 | 13.0 | Algeria or Morocco | 2006 |
| NWA 5029 | 14.7 | Morocco | 2003 |
| NWA 5298 | 445.0 | Bir Gandouz, Morocco | 2008 |
| NWA 5718 | 90.5 | Algeria or Morocco | 2006 |
| NWA 6963 | 83.3 | Morocco | 2011 |
| Dhofar 378 | 15.0 | | 2000 |
| Dhofar xxx "M12" | 209.0 | Oman | 2001 |
| Dhofar, unnamed | 209.1 | Oman | 2006 |
| Jiddat al Harasis 479 | 553.0 | Oman | 2008 |
| Ksar Ghilane 002 | 538.0 | Quibili, Tunisia | 2010 |
| EET 79001 (Lithology B) | 7,942.0 | Elephant Moraine, Antarctica | 1980 |
| QUE 94201 | 12.0 | Queen Alexandra Range, Antarctica | 1994 |
| *Permafic/Olivine-phyric or olivine-orthopyroxene-phyric Shergottites* | | | |
| DaG 476 | 2,015.0 | | 1998 |
| DaG 489 | 2,146.0 | | 1997 |
| DaG 670 | 1,619.0 | | 1999 |

| | | | |
|---|---|---|---|
| DaG 735 | 588.0 | | 1997 |
| DaG 876 | 6.22 | | 1998 |
| DaG 975 | 27.5 | Dar al Gani, Libya | 1999 |
| DaG 1037 | 4,012.4 | | 1999 |
| DaG xxx1 | 349.5 | | 1999 |
| DaG xxx2 "HH" | 19.0 | | 1999 |
| DaG xxx3 "NC2" | 1.7 | | 1999 |
| DaG xxx4 "AHA" | 40.1 | | 2000 |
| EET 79001 (Lithology A) | 7942.0 | Elephant Moraine, Antarctica | 1980 |
| NWA 1068 | 576.8 | | 2001 |
| NWA 1110 | 118.0 | | 2001 |
| NWA 1183 | 140.0 | | 2002 |
| NWA 1775 | 25.0 | Maarir, Morocco | 2002 |
| NWA 2373 | 18.1 | | 2004 |
| NWA 2969 | 11.7 | | 2005 |
| NWA xxxx | 15.0 | | 2005 |
| NWA 1195 | 315.0 | Safsaf, Morocco or Algeria | 2002 |
| NWA 1950 | 797.0 | Atlas Mountains, Morocco | 2001 |
| NWA 2046 | 63.0 | Lakhbi, Algeria | 2003 |
| NWA 2626 | 31.1 | Algeria | 2004 |
| NWA 2646 | 30.7 | Algeria or Morocco | 2004 |
| NWA 2990 | 363.0 | | 2007 |
| NWA 5960 | 147.0 | | 2009 |
| NWA 6234 | 55.7 | Mauritania | 2010 |
| NWA 6710 | 74.4 | | 2011 |
| NWA 4222 | 16.5 | Algeria or Morocco | 2006 |
| NWA 4468 | 675.0 | Southern Morocco | 2006 |
| NWA 4527 | 10.1 | | 2006 |
| NWA 4925 | 282.3 | Algeria | 2007 |
| NWA 5789 | 49.0 | Morocco | 2009 |
| NWA 5990 | 59.0 | Hamada du Drâa, Morocco | 2009 |
| NWA 6162 | 89.0 | Lbirat, Morocco | 2010 |
| NWA 7032 | 85.0 | Morocco | 2011 |
| NWA 7042 | 3,033.0 | Morocco | 2011 |
| Dhofar 019 | 1,056.0 | Dhofar, Oman | 2000 |
| SaU 005 | 1,344.0 | | 1999 |
| SaU 008 | 8,579.0 | | 1999 |
| SaU 051 | 436.0 | | 2000 |
| SaU 060 | 42.3 | | 2001 |
| SaU 090 | 94.8 | | 2002 |
| SaU 094 | 223.3 | Sayh al Uhaymir, Oman | 2001 |
| SaU 120 | 75.0 | | 2002 |
| SaU 125 | 31.7 | | 2003 |
| SaU 130 | 278.5 | | 2004 |
| SaU 150 | 107.7 | | 2002 |
| SaU xxx | 22.7 | | 2003 |
| LAR 06319 | 78.6 | Larkman Nunatak, Antarctica | 2006 |
| RBT 04261 | 78.8 | | |
| RBT 04262 | 204.6 | Roberts Massif, Antarctica | 2004 |

| | | | |
|---|---|---|---|
| Y 980459 | 82.5 | | 1998 |
| Y 980497 | 8.7 | Yamato Mountains, Antarctica | 1998 |
| Tissint | > 12,000 | Tanzou, Morocco | July 18, 2011 |
| *Ultramafic Shergottites* | | | |
| ALH 77005 | 482.5 | Allan Hills, Antarctica | 1977 |
| NWA 1950 | 797.0 | Morocco | 2001 |
| NWA 2646 | 9.3 | Algeria or Morocco | 2004 |
| NWA 4797 | 15.0 | Missour, Morocco | 2001 |
| NWA 6342 | 72.2 | Algeria | 2010 |
| GRV 99027 | 10.0 | Grove Mountains, Antarctica | 2000 |
| GRV 020090 | 7.5 | Grove Mountains, Antarctica | 2002 |
| LEW 88516 | 13.2 | Lewis Cliff, Antarctica | 1988 |
| Y 793605 | 16.0 | Yamato Mountains, Antarctica | 1979 |
| Y 984028 | 12.3 | | 1998 |
| Y 000027 | 9.68 | Yamato Mountains, Antarctica | 2000 |
| Y 000047 | 5.34 | | 2000 |
| Y 000097 | 24.5 | | 2000 |
| "YA1075" (Yanai) | 55.0 | Yamato Mountains, Antarctica | <1999 |
| **Nakhlites** | | | |
| Nakhla | ~ 10,000 | Nakhla, Egypt | 1911 |
| Lafayette | 800.0 | Indiana, USA | 2001 |
| Gov. Valadares | 158.0 | Governador Valadares, Brazil | 1958 |
| NWA 817 | 104.0 | Morocco | 2000 |
| NWA 998 | 456.0 | Algeria | 2001 |
| MIL 03346 | 715.2 | | 2003 |
| MIL 090030 | 452.6 | Miller Range, Antarctica | 2009 |
| MIL 090032 | 532.2 | | 2009 |
| MIL 090136 | 171.0 | | 2009 |
| Y 000593 | 13,713.0 | | 2000 |
| Y 000749 | 1,283.0 | Yamato Mountains, Antarctica | 2000 |
| Y 000802 | 22.0 | | 2000 |
| NWA 5790 | 145.0 | | 2008 |
| NWA 6148 | 280.0 | Mauritania | 2009 |
| **Chassignites** | | | |
| Chassigny | ~ 4,000 | Chassigny, France | 1815 |
| NWA 2737 | 611.0 | Morocco or Algeria | 2000 |
| **Orthopyroxenite** | | | |
| ALH 84001 | 1,930.9 | Allan Hills, Antarctica | 1984 |

## 1.2    Sulfur Isotopes

### 1.2.1    Sulfur Isotope Systematics

The four stable isotopes of sulfur, $^{32}$S, $^{33}$S, $^{34}$S, and $^{36}$S, have fractional abundances of approximately 95.04%, 0.75%, 4.20%, and 0.015%, respectively (Ding et al., 2001). On Earth, variations in the isotope ratios $^{33}$S/$^{32}$S, $^{34}$S/$^{32}$S, and $^{36}$S/$^{32}$S occur as a result of kinetic, thermodynamic, and biological processes that fractionate sulfur species in proportion to their relative mass differences (Thode et al., 1961; Ohmoto and Goldhaber, 1997). This effect is termed mass-dependent fractionation, and products tend to form highly correlated arrays of nearly constant $\Delta^{33}$S on plots of $\delta^{33}$S versus $\delta^{34}$S (Hulston and Thode, 1965; Thiemens, 1999; Farquhar and Wing, 2003).[2] This occurs because the mass difference between $^{33}$S and $^{32}$S is approximately half of that between $^{34}$S and $^{32}$S, and any mass-dependent fractionation effects in $\delta^{33}$S reflect this by being approximately half as large as those observed for $\delta^{34}$S. Analogous relationships may be described for the relative mass-dependent effects of $^{36}$S and the other stable isotopes. Measurements of $\delta^{36}$S and $\Delta^{36}$S are reported less frequently in the literature because the low natural abundance of $^{36}$S and the presence

---

[2] Sulfur isotopic compositions are usually reported in conventional delta notation with respect to a well-characterized reference:

$$\delta^{34}S = 1000[(^{34}S/^{32}S)_{sample}/(^{34}S/^{32}S)_{ref} - 1] \tag{1}$$
$$\delta^{33}S = 1000[(^{33}S/^{32}S)_{sample}/(^{33}S/^{32}S)_{ref} - 1] \tag{2}$$
$$\delta^{36}S = 1000[(^{36}S/^{32}S)_{sample}/(^{36}S/^{32}S)_{ref} - 1] \tag{3}$$
$$\Delta^{33}S = \delta^{33}S - 1000[(1 + \delta^{34}S/1000)^{0.515} - 1] \tag{4}$$
$$\Delta^{36}S = \delta^{36}S - 1000[(1 + \delta^{34}S/1000)^{1.90} - 1]. \tag{5}$$

of mass-interfering contaminants make this isotope very difficult to measure precisely (Hulston and Thode, 1965; Rumble and Hoering, 1994).

In addition to the mass-dependent fractionation described above, some processes fractionate sulfur isotopes in a manner that is not proportional to their mass differences (Thiemens, 1999). This was first documented in a robust way for oxygen isotopes during the formation of ozone from molecular oxygen by spark discharge (Thiemens and Heidenreich, 1983). It has since been documented for a number of reactions involving sulfur isotopes (Coleman et al., 1996; Farquhar et al., 2000, 2001). This effect is often referred to as sulfur mass-independent fractionation (S-MIF), although the terms non-mass-dependent fractionation and anomalous fractionation are also used. The most significant source of S-MIF is thought to be gas-phase photochemistry driven by ultraviolet (UV) radiation (Cooper et al., 1997; Farquhar et al., 2001; Rai et al., 2005). The resulting sulfur species carrying anomalous isotopic composition may subsequently transfer this signal to solid phases, which on Earth preserve this record in sedimentary deposits as $\Delta^{33}S$ and $\Delta^{36}S$ values that do not lie on predicted mass-dependent fractionation arrays. A similar effect is seen in some meteorites, which may contain sulfur-bearing phases with $\Delta^{33}S$ and $\Delta^{36}S$ values that do not lie on a predicted mass-dependent array. Mass-independent sulfur has been measured in many types of samples, including Archean terrestrial sediments (Farquhar et al., 2000c, 2007a; Farquhar and Wing, 2003; Ono et al., 2003, 2006a; Mojzsis et al., 2003; Cates and Mojzsis, 2006; Kaufman et al., 2007; Philippot et al., 2007), atmospheric sulfate aerosols (Romero and Thiemens, 2003), inclusions in kimberlite diamonds (Farquhar et al., 2002), mafic and ultramafic igneous rocks

(Penniston-Dorland et al., 2008), martian meteorites (Farquhar et al., 2000c; 2007a), other achondritic meteorites (Farquhar et al., 2000b; Rai et al., 2005), and chondritic meteorites (Cooper et al., 1997; Rai and Thiemens, 2007). Despite the presence of mass-independently fractionated sulfur phases in some meteorites, the majority of meteoritic sulfur shows mass-dependent isotopic composition (Hulston and Thode, 1965; Kaplan and Hulston, 1965; Gao and Thiemens, 1987; Gao and Thiemens, 1993).
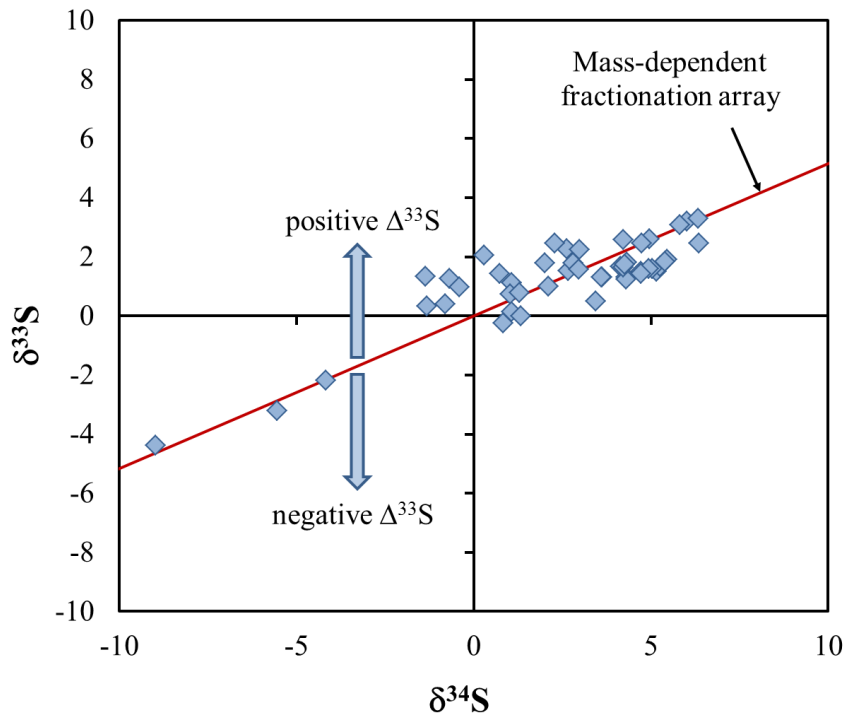


**Figure 1-1. Illustration of mass-independent sulfur fractionation.**

**Points on the red line display mass-dependent fractionation, while points above or below the red line (i.e., possessing non-zero values of $\Delta^{33}S$) display mass-independent fractionation. Data shown are for terrestrial Archean samples, reported by Farquhar et al. (2000a).**

Both mass-dependent and mass-independent isotope effects are measured and generally reported relative to an isotopic reference frame. For sulfur, the isotopic reference standard has evolved over time, from terrestrial to extraterrestrial materials. Early research into sulfur isotope systematics revealed that $\delta^{34}S$ for terrestrial samples exhibits a large range of values, on the order of 150‰, while similar measurements of meteorites showed remarkably constant $^{34}S/^{32}S$ (Thode et al., 1961; Greenwood et al., 2000b). In addition, the constant value of this ratio agrees closely with the median ratio for terrestrial sulfur and falls within the range of ratios for sulfur minerals believed to be of juvenile igneous origin (Thode et al., 1961). Macnamara and Thode (1950) suggested that the sulfur isotope ratio found in meteorites represents the primordial solar system value and that fractionation due to processes occurring within Earth's crust has created notable distribution above and below this primordial or base level. Although pyrite from Park City, Utah served as the reference material for the earliest studies of natural sulfur isotope abundances (Thode et al., 1949), it was soon replaced by meteoritic sulfur (Thode et al., 1961). Troilite (FeS) from the iron meteorite Cañon Diablo (denoted as CDT) was adopted as the isotopic reference standard for sulfur in 1962. However, workers discovered that the sulfur isotopic composition of CDT is slightly heterogeneous (Jensen, 1962; Beaudoin et al., 1994), and the supply of CDT began to diminish after a few decades of use.

For the reasons cited above, at a meeting held in Vienna in 1993, the IAEA advisory group on reference materials for stable isotope measurements proposed a new reference standard for sulfur, based on a set of synthetic $Ag_2S$ materials enriched in $^{32}S$, $^{33}S$, and $^{34}S$. This new scale, denoted as V-CDT, has been the recommended

reference for sulfur isotope analyses since 1995. It is defined by the IAEA-S-1 reference material, which has $\delta^{34}S_{\text{V-CDT}}$ = -0.3‰ relative to CDT (Robinson, 1993). The values of $\Delta^{33}S$ and $\Delta^{36}S$ of V-CDT were not defined, but it is assumed that they should also match the mean value of CDT. The calibration of IAEA-S-1 relative to V-CDT for $\Delta^{33}S$ and $\Delta^{36}S$ has been reported by three laboratories (the University of California at San Diego, the Geophysical Laboratory at the Carnegie Institute of Washington, and the University of Maryland) and a weighted average of these three determinations yields a value that is used as the assumed value for IAEA-S-1 on the V-CDT scale, $\Delta^{33}S$ = 0.094 ± 0.01‰ and $\Delta^{36}S$ = 0.69 ± 0.2‰ (Ono et al., 2006c).

While the synthetic $Ag_2S$ materials of V-CDT are used as the standards for modern sample analyses, measured sulfur isotope data in this work were normalized to measurements of CDT, to allow direct comparison with previously published results.

### 1.2.2   Applications of Sulfur Isotope Ratios

Sulfur-bearing minerals on Mars should preserve a record of sulfur isotopic fractionation processes that have occurred throughout the planet's history. The Earth's rock record may be viewed as an analog to that of Mars in this context, providing examples of the types of information that may be gathered from analysis of martian samples.

For instance, one important type of sulfur isotopic signature that has been detected in both terrestrial and martian samples involves mass-independent fractionation. Farquhar et al. (2000a) discovered a pattern of anomalous sulfur isotope

ratios in ancient terrestrial rocks and argued that it could be used to trace the rise in atmospheric oxygen levels. Samples older than 2450 Ma were found to have a wide range in $\Delta^{33}S$ values, while samples younger than 2090 Ma displayed $\Delta^{33}S$ values near zero, consistent with mass-dependent fractionation effects (Farquhar et al., 2000a). These data indicate that a significant change occurred in the sulfur cycle between 2450 and 2090 Ma. Farquhar et al. (2000a) hypothesized that the change in sulfur isotope compositions seen in the rock record may be attributed to an increase in oxygen level of the atmosphere. Gas-phase laboratory experiments have shown that several sulfur-bearing atmospheric species, including $H_2S$, $CS_2$, and $SO_2$, may incur MIF due to UV radiation (Farquhar et al., 2001; Zmolek et al., 1999). Farquhar et al. (2001) further found that $SO_2$ photochemistry can produce sulfur isotopic compositions similar to those observed in the ancient terrestrial rock record. However, ozone absorbs UV radiation at the wavelengths responsible for anomalous sulfur isotope fractionation. According to Farquhar et al. (2000a), generation of Earth's ozone layer apparently halted the photochemical reaction system involving sulfur, thus preventing formation and deposition of anomalous sulfur in terrestrial sediments for the past two billion years. Pavlov and Kasting (2002) determined that on the Archean Earth, S-MIF could only be preserved in sulfate aerosols if the $O_2$ concentration of the atmosphere was $< 10^{-5}$ times the present atmospheric oxygen level. They argued that in a highly oxygenated atmosphere, all products of atmospheric sulfur photochemistry would exit the atmosphere in an oxidized form, as $SO_2$ or $H_2SO_4$, where it would be homogenized in the oceanic reservoir and any S-MIF signal would be lost. At lower oxygen levels, however, sulfur would have been

removed from the atmosphere in a variety of oxidation states, each of which could have followed its own chemical pathway after deposition (Pavlov and Kasting, 2002).

Farquhar et al. (2000c) also reported mass-independent sulfur in some martian meteorites and extended the concept of atmospheric reactions in an optically thin atmosphere as a possible explanation. According to this hypothesis, volcanic $H_2S$ and $SO_2$ could have been photochemically processed in the martian atmosphere, producing sulfate with anomalous isotopic composition that subsequently was deposited on the planet's surface. If these sediments were then incorporated into rising magma during later volcanic episodes, the mass-independent signature could have been transferred to other sulfur mineral phases, as well (e.g., Jones, 1989; Herd et al., 2002; Rumble and Irving, 2009). This topic will be revisited in later chapters of this work.

Another major source of sulfur isotopic fractionation on Earth involves biological processing. Significant fractionation of sulfur isotopes occurs during the bacterial reduction of sulfate in shallow sediments on the terrestrial sea floor. This process is reflected in the isotopic composition of sea floor deposits, which generally contain sulfides highly depleted and sulfates highly enriched in the heavy isotopes of sulfur (Thode et al., 1949, 1961). The wide range of $\delta^{34}S$ measured in sedimentary rocks is primarily attributed to biological processes such as this, while geological processes tend to produce much smaller variations in $\delta^{34}S$ (Thode et al. 1953; Mojzsis et al., 2003). For this reason, natural samples on Earth that are highly depleted in heavy sulfur isotopes, relative either to CDT or to other associated sulfur minerals, are most often interpreted to have been influenced by biology.

In addition to sulfate reduction, other sulfur-metabolizing pathways are used by different types of Bacteria and Archaea on Earth. Comparative sequence analyses of genomes based on rRNA indicate that the reduction of elemental sulfur to $H_2S$, which is performed by many hyperthermophilic organisms near the root of the phylogenetic tree, may be a trait inherited from the last common ancestor of all terrestrial life (Canfield and Raiswell, 1999). The primitive nature of sulfur metabolism on Earth has led some researchers to suggest that sulfur-based life could have arisen on other planets, including Mars (Horneck, 2000). The tantalizing possibility that sulfur isotope ratios in martian meteorites could serve as biomarkers for extant or extinct microbial life provides an important motivation for their study. If a large sulfur isotopic fractionation were discovered between associated martian sulfate and sulfide minerals, then the possibility that this indicated a biological process would warrant further investigation. However, since large sulfur fractionation can also be produced by photochemical reactions in the atmosphere, the presence of isotopically light sulfur minerals on Mars is not sufficient to indicate life (Farquhar et al., 2000c). Additional evidence would be required to determine whether the sulfur signal could have been produced biologically.

### 1.3.3   Previous Studies of Sulfur in Martian Meteorites

Prior to this study, sulfur isotope data had only been published for a dozen martian meteorites, and data for multiple sulfur isotopes, required for the determination of mass-independent composition, had only been reported for five of them. This study was undertaken to exploit the opportunity afforded by the new

abundance of martian meteorites recovered from hot desert regions to enhance the understanding of Mars' sulfur composition and what it might reveal about the history of the red planet.

Burgess et al. (1989) used stepped combustion in pure oxygen to generate $SO_2$ from sulfur minerals in Shergotty, ALH 77005, Nakhla, and Chassigny. Based on comparison with data from pure mineral combustion, they concluded that all four meteorites contain troilite and gypsum and that the ratio of oxidized to reduced sulfur in these meteorites increases in the order Shergotty (0.1) < ALH 77005 (0.3) < Chassigny (1.5) < Nakhla (1.7). Combined with the same ratio determined for EET 79001 lithology A (0.2) and lithology C (0.5) in Gooding and Muenow (1986), these results indicate that the shergottites have a lower net sulfur oxidation state than the nakhlites or Chassigny. Because of the small sample masses analyzed, Burgess et al. (1989) were only able to obtain a sulfur isotope ratio from Shergotty, which gave $\delta^{34}S$ of -0.5 ± 1.5‰ for an unidentified sulfide mineral. Note that while the analytical method of Burgess et al. differed from typical techniques currently used for sulfur isotopic measurements, the $\delta^{34}S$ they report for Shergotty sulfide is consistent with a later result obtained by Greenwood et al. (1997b) via ion microprobe.

Gao and Thiemens (1990) measured the bulk sulfur isotopic composition in ALH 77005 via chemical extraction and fluorination. They found $\delta^{33}S = -0.07‰$, $\delta^{34}S = -0.17‰$, and $\delta^{36}S = -0.3‰$ in the acid soluble phase (presumed to be troilite), and $\delta^{33}S = 1.65‰$, $\delta^{34}S = 3.30‰$, and $\delta^{36}S = 6.2‰$ in the acid residue phase. Although not reported in the paper, these delta values yield $\Delta^{33}S = 0.018‰$ and $\Delta^{36}S = 0.025‰$ for the acid soluble phase and $\Delta^{33}S = -0.048‰$ and $\Delta^{36}S = -0.112‰$ for the acid

residue phase. For the acid soluble phase, Gao and Thiemens reported precision (1σ) of ± 0.03‰ for $\delta^{33}S$ and $\delta^{34}S$ and ± 0.2‰ for $\delta^{36}S$. Due to the small sample size for the acid residue phase, the cited precision (1σ) was ± 0.2‰ for $\delta^{33}S$ and $\delta^{34}S$ and ± 0.8‰ for $\delta^{36}S$. Gao and Thiemens attributed the acid residue signature to the gypsum reported for ALH 77005 in Burgess et al. (1989). Based on the assertion in Sakai (1957) that sulfide weathering favors the incorporation of lighter sulfur isotopes in the product sulfate, Gao and Thiemens concluded that the gypsum in ALH 77005 was not formed by sulfide weathering. However, they also acknowledged that the acid residue phase in their study had not been conclusively identified as gypsum and might actually represent a non-sulfate mineral phase.

Greenwood et al. (1997b) studied several shergottites using ion microprobe techniques. Their sulfur isotope results and average 1σ errors were reported as follows: Shergotty pyrrhotite, $\delta^{34}S$ = -0.5 to 0.2‰ (± 0.7‰); Zagami pyrrhotite, $\delta^{34}S$ = 1.4 to 3.1‰ (± 0.7‰); EET 79001 lithology A pyrrhotite, $\delta^{34}S$ = -2.6 to 0.2‰ (± 0.4‰); QUE 94201 pyrrhotite, $\delta^{34}S$ = 0.1 to 1.5‰ (± 0.6‰); LEW 88516 pyrrhotite, $\delta^{34}S$ = -2.9 to -0.9‰ (± 0.6‰); and EET 79001 lithology B pyrrhotite, $\delta^{34}S$ = -2.6 to -1.5‰ (± 0.4‰). Greenwood et al. (1997b) found that shergottite sulfur isotope ratios are similar to terrestrial ocean floor basalts, suggesting that the mantles of Earth and Mars have similar sulfur isotopic compositions.

Farquhar et al. (2000c) examined the sulfur isotopic composition of EET 79001A by trapping the $H_2S$ generated as a byproduct of carbonate acidification procedures for oxygen isotope study. They reported $\delta^{33}S$ = -0.07 to -0.43‰, $\delta^{34}S$ = -0.11 to

-0.92‰, and $\Delta^{33}S$ = -0.01 to 0.049‰, with cited   uncertainty on $\Delta^{33}S$ of $\pm$ 0.02‰ (1$\sigma$).

Farquhar et al. (1998) measured the oxygen isotopic composition of silicates and carbonates in ALH 84001 and found differences suggesting the existence of two separate oxygen isotopic reservoirs on Mars. They argued that the oxygen isotopes of the carbonates reflected the effects of atmospheric photochemistry. A recent study by Rumble and Irving (2009) revealed heterogeneity in the oxygen isotopic composition of silicate minerals in forty-two martian meteorites. They hypothesized that this could indicate assimilation of crustal minerals such as carbonates containing oxygen that had been photochemically processed in the atmosphere (Farquhar et al., 1998) into ascending magmas, producing localized heterogeneities in the oxygen isotopic composition of crystallizing silicates (Rumble and Irving, 2009). The authors suggest that the observed variation in oxygen isotopes could result either from mantle heterogeneities preserved since primary accretion or from incorporation of older, altered crustal material into the younger shergottite magma as it ascended.

If the variations in oxygen isotopes in martian meteorite silicates are the result of assimilation of crustal material as suggested by Rumble and Irving (2009), then the assimilation process would likely have introduced sulfur-bearing minerals or brines from the crust into ascending magmas, as well. If these surface deposits included sulfur that had experienced photochemical processing in the martian atmosphere, as suggested by  Farquhar et al. (2000c), then it could have transferred a record of that processing into igneous sulfide minerals that show S-MIF composition.

## 1.3 Research Goals

This section briefly defines the major goals of this research. Each topic is covered in more detail in subsequent chapters. Analytical techniques are described briefly in individual chapters, with more complete discussion in Appendix A and Appendix B.

### 1.3.1   Juvenile Martian Sulfur Isotopic Composition

The work described here significantly expands the database of sulfur isotopic composition in martian meteorites by examining numerous meteorites that have not previously been studied. Thirty shergottites were analyzed, representing a broad cross-section of the mineralogical categories. Since the shergottites are believed to derive from the martian mantle, measuring the sulfur isotopic composition for numerous samples allowed me to make the first estimate of the composition of martian mantle sulfur. This topic is covered in Chapter 2.

### 1.3.2   Evidence for Transfer of Sulfur from the Atmosphere to the Subsurface

Previous studies have found mass-independent sulfur in martian meteorites, suggesting incorporation of atmospherically-processed material into the subsurface (Farquhar et al., 2000c. 2007a; Kim and Farquhar, 2008). Three additional nakhlites were analyzed for this study to evaluate the extent of this process throughout the nakhlite cumulate pile. The presence of mass-independent sulfur was also evaluated for the shergottites and Chassigny. For each category of meteorite, the presence or absence of a S-MIF signal in sulfide and/or sulfate minerals was used to evaluate

hypotheses concerning assimilation of surface sediments into igneous rocks, either through recycling of crustal material or influx of sulfate. This topic is covered in Chapters 2 through 4.

### 1.3.3   *Evidence for Magmatic Reduction of Surface Sulfur*

While previous studies had reported significantly anomalous sulfur isotopic composition in Nakhla sulfate, comparatively small deviations from mass-dependent behavior were found in Nakhla sulfides through chemical extraction of both monosulfide and disulfide fractions (Farquhar et al., 2000c, 2007a). In contrast, more substantial S-MIF was found in the disulfide fraction of MIL 03346, but that meteorite produced negligible yield of monosulfide minerals upon chemical extraction (Kim and Farquhar, 2008). To test the hypothesis that igneous sulfide minerals in the martian meteorites could record evidence for assimilation of crustal material during magmatic processes, I turned to the ion microprobe technique. The Cameca IMS 1270 ion microprobe at UCLA was used to measure $\delta^{33}S$, $\delta^{34}S$, and $\Delta^{33}S$ of Nakhla, MIL 03346, and ALH 84001 to search for evidence of reduction-oxidation reactions in the melt that may have transformed atmospherically-derived sulfate or elemental sulfur assimilated by the melt into igneous sulfide minerals. This topic is covered in Chapter 4.

### 1.3.4 *SO$_2$ Photolysis Mechanisms*

Previous laboratory experiments with SO$_2$ and H$_2$S gas have indicated that UV photochemistry (Farquhar et al., 2000c, 2001) poses a viable process for generating S-MIF signatures analogous to those seen in ancient terrestrial sediments (Farquhar et al., 2000a), martian meteorites (Farquhar et al., 2000c, 2007a), and other types of achondritic and chondritic meteorites (Farquhar et al., 2000b; Rai et al., 2005, 2007). While the earlier studies provided valuable insight into the feasibility of a photochemical source for the observed S-MIF, however, they also prompted new questions concerning the precise wavelength(s) and photolytic mechanism(s) responsible for the signals. The current study included new broadband UV photochemical experiments with gas-phase SO$_2$ designed to probe more deeply into this issue and potentially illuminate the question from a new angle. These experiments investigated the effects on the S-MIF signal of intramolecular isotopic substitution of $^{18}$O for $^{16}$O in the SO$_2$. This topic is covered in Chapter 5.

### 1.3.5 *Summary*

This dissertation focuses on characterizing the sulfur isotopic composition of multiple sulfur-bearing phases in martian meteorites, with the intent of establishing the baseline sulfur isotopic composition of the martian mantle and evaluating the extent of evidence for cycling of sulfur through the atmosphere and back to the solid planet. To facilitate these goals, sulfur was extracted from sulfide and sulfate minerals of 34 martian meteorites for high-precision isotope ratio mass spectrometry

measurements. In addition, sulfide grains in three meteorites were examined via ion microprobe to search for S-MIF signatures that could be the fingerprints of reduction-oxidation processes involving atmospherically-processed sulfur that was assimilated into igneous melts. Photochemical experiments were performed to shed new light on the precise mechanism(s) responsible for producing mass-independent sulfur on Mars. The conclusions of this study, including potential avenues for follow-on work, are found in Chapter 6.

# Chapter 2: Shergottites Yield an Estimate of the Juvenile Martian Sulfur Composition and Reveal the Effects of Sulfur Mass-independent Fractionation[1,2]

[1] The text, tables, and figures in this chapter were written/created by H. B. Franz.

[2] All analyses presented in this chapter were performed by H. B. Franz.

## 2.1    Introduction

Sulfur has been a focus of geochemical study because it possesses four stable isotopes and occurs in several oxidation states from -2 to +6. It has been used to trace a variety of processes that occur in solid phase, liquid phase, and gas phase planetary environments. Like oxygen, sulfur has been shown to undergo mass-independent isotopic fractionation during laboratory photochemical experiments. The observation of mass-independent signatures in terrestrial samples and meteorites have been taken to provide clues to processes that have occurred both in the solar nebula and in planetary atmospheres (e.g., Thiemens and Heidenreich, 1983; Thiemens, 1999; Farquhar et al., 2000a, 2000b, 2000c, 2001).

Analyses of martian meteorites have shown that Mars possesses an oxygen isotopic composition characterized by a mass-independent enrichment in $^{17}O$ compared to the Earth and Moon, and displaying a distinctive signature for the martian hydrosphere compared to the bulk silicate planet (e.g., Clayton and Mayeda, 1983; Karlsson et al., 1992; Farquhar et al., 1998; Farquhar and Thiemens, 2000).

33

Studies of sulfur isotopes in the martian meteorite Nakhla have revealed sulfate and sulfide with a significantly anomalous sulfur isotopic composition (Farquhar et al., 2000c, 2007a), which is interpreted to indicate incorporation of atmospheric sulfur into the martian subsurface. Implicit in this interpretation is the inference that the juvenile sulfur isotopic reservoir of Mars is well-mixed in the martian mantle, and represented by a composition similar to that of troilite from Cañon Diablo.

The shergottites are the largest group of martian meteorites, numbering 54 of the 65 meteorites currently believed to come from Mars. They have mafic to ultramafic mineralogical compositions and are thought to represent melts derived from the martian mantle, displaying varying degrees of magmatic evolution but little evidence for aqueous alteration (e.g., Mikouchi et al., 2004; Irving et al., 2010; Rapp et al., 2012). The shergottites are classified into three subgroups which are defined on the basis of their chondrite-normalized light rare earth element (LREE) patterns as "enriched," "intermediate," or "depleted" (e.g., Longhi, 1991; McSween, 1994). The source of this variation is an active area of debate, and models are generally divided between those that favor a depleted martian mantle that acquires enrichment in trace elements through assimilation of crustal material into rising magmas (e.g., Jones, 1989; Herd et al., 2002; Rumble and Irving, 2009) and those that invoke a heterogeneous martian mantle with magmatic trace element content controlled by variable mixing between enriched and depleted mantle reservoirs (e.g., Borg et al., 1997; Brandon et al., 2000; Borg and Draper, 2003; Debaille et al., 2008).

For this study, the sulfur isotopic compositions of both sulfide and sulfate phases from 30 shergottites were measured. This suite provides representative sampling of

each mineralogical and trace element category of the shergottites. Analyses of these two sulfur-bearing phases allowed estimation of the juvenile martian sulfur composition from igneous sulfides and evaluation of potential contributions of photochemically-processed sulfur into the shergottites. The results indicate that the sulfur isotopic composition is within analytical uncertainty of that of Cañon Diablo Troilite. In addition, clearly-resolved mass-independent sulfur in both monosulfide and sulfate phases is observed in some shergottites, which likely indicates cycling between the martian atmosphere and subsurface.

## 2.2    Methods

Sequential chemical extraction procedures were applied for powdered whole rock samples to extract sulfur for measurement of sulfur isotope ratios from different mineral phases. Some meteorites were obtained as whole rock fragments and some had already been powdered.

Whole-rock samples were disaggregated in a steel mortar and then ground more finely with an agate mortar and pestle. The powder was transferred to a 15 mL centrifuge tube along with 10 mL of Milli-Q water. The tube was sonicated for 20 minutes to promote the dissolution of water-soluble sulfate from the sample. The tube was then centrifuged to allow separation of the solution from the solid sample by pipette. This process was repeated a second time to yield a total of 20 mL of solution containing water-soluble sulfate, which were transferred to a boiling flask. A few drops of 5 N HCl and several drops of 1 M $BaCl_2$ solution were added to the flask to precipitate $BaSO_4$. The solution in the flask was then evaporated to dryness at ~80 ℃

before the sulfate was reduced by a procedure similar to that described below for acid-soluble sulfate.

The powdered sample was transferred from the centrifuge tube to a double-necked boiling flask with silicone septum. The flask was assembled with a water-cooled condenser, a bubbler filled with Milli-Q water, and a sulfide trap into a distillation apparatus similar to that described by Forrest and Newman (1977). All ground glass joints were sealed with PTFE sleeves. The apparatus was assembled, checked for leaks, and then purged with nitrogen for 10 minutes. For the first extraction step, 25 mL of 5 N HCl were injected into the boiling flask through the septum with a syringe. The solution was then heated to ~60 °C. Acid-volatile sulfur (AVS) in the sample, presumed to consist primarily of monosulfides, reacted with the HCl to evolve $H_2S$ gas, which was captured in an acidic $AgNO_3$ solution. After completion of the AVS reduction reaction (approximately 3 hours), the sulfide trap with capture solution was replaced, and 25 mL of a reduction solution containing HI, $H_3PO_2$, and 12 N HCl were added to the boiling flask (Thode et al., 1961; Mayer and Krouse, 2004). The solution was heated to ~85 ºC. During the next four hours, acid-soluble sulfate in the sample reacted to form $H_2S$, which was captured in the manner described above. Upon completion of this reaction, 15 mL of an acidic chromium(II) solution were injected into the boiling flask, the sulfide trap was replaced again, and the solution was heated at 85 ºC for 3 more hours. During this final reduction step, chromium-reducible sulfur (CRS) minerals, presumed to be disulfides and elemental sulfur, were converted to $H_2S$ and captured in the $AgNO_3$ solution.

36

Most of the shergottites in this study were reduced using the method described above. The procedure followed for Tissint, NWA 7032, NWA 7042, and Chassigny differed from the above description in one detail. Upon completion of the acid-soluble sulfate step, the boiling flask was cooled and its contents were transferred to 30 mL centrifuge tubes. After separation of the acid solution from the solid sample powder, the sample was rinsed with Milli-Q water several times to clean it before being transferred back to the double-necked boiling flask. The following day, the distillation apparatus was reassembled, checked for leaks, and again purged with nitrogen for 10 minutes. A fresh sulfide trap with $AgNO_3$ capture solution was installed, and 15 mL each of the acidic chromium(II) solution and 5 N HCl were injected into the boiling flask, which was then heated at ~85 ºC for 3 hours.

The $H_2S$ evolved in each step of the extraction process reacted with the $AgNO_3$ in the capture solution to form $Ag_2S$, which was cleaned with Milli-Q water and 1 M $NH_4OH$ solution, then dried. The $Ag_2S$ was converted to $SF_6$ by reaction with 250 μmoles of fluorine gas in a nickel reaction vessel at 250° C for 8 hours. The $SF_6$ was subsequently condensed from the residual $F_2$ into a trap cooled with liquid nitrogen. Excess $F_2$ was passivated by reaction with KBr salt. Replacement of the liquid nitrogen coolant on the trap with ethanol slush at -115 °C allowed distillation of the $SF_6$ from the trap into the liquid-nitrogen-cooled injection loop of a gas chromatograph (GC). The $SF_6$ was purified by a 1/8-inch diameter, 6-foot long Molecular Sieve 5A GC column, followed by a 1/8-inch diameter, 12-foot long Haysep-Q™ GC column, with helium carrier gas flow rate of 20 mL/min. After its elution from the GC, the $SF_6$ was captured in spiral glass traps cooled with liquid

nitrogen, then transferred to the bellows of a Thermofinnigan MAT 253 dual-inlet gas source mass spectrometer. The sulfur isotopic composition of the $SF_6$ was measured by monitoring $SF_5^+$ ion beams at *m/z* of 127, 128, 129, and 131 Da.

## 2.3    Results

### 2.3.1    Sulfur Abundances

Sulfur abundances are estimated through gravimetric analysis of recovered $Ag_2S$ and are presented for the various sulfur-bearing phases in the shergottites and Chassigny in Table 2-1. Samples from which water-soluble sulfate was extracted first are shown with separate water-soluble and acid-soluble sulfate concentrations. Otherwise, only the total sulfate concentration is given. Figure 2-1 illustrates the sulfur concentrations in column-graph format to enable ready comparisons among the meteorites. Uncertainties in abundances are estimated as ± 2% of the values reported and are due primarily to uncertainties in the acid distillation process. Note that the inherent uncertainties due to sample heterogeneity are much larger than this and are not included in the estimate of analytical uncertainty reported here.

The average total sulfur concentration for all shergottites analyzed is 1031 ± 21 ppm (1σ), with a range from < 200 ppm to > 2400 ppm. The average contribution from AVS (monosulfide minerals) is 647 ± 13 ppm, with an average of 401 ± 8 ppm from total sulfate. The CRS fraction of shergottites (disulfide minerals and elemental sulfur) measures on average only 5 ppm and is generally too small for accurate isotope ratio measurements. Chassigny gave zero yield of AVS, 42 ± 1 ppm of acid-

soluble sulfate, 22 ± 1 ppm of water-soluble sulfate, and ~2 ± 1 ppm of CRS. However, the larger sample mass for Chassigny (~2 g) allowed determination of isotope ratios for both sulfate and CRS fractions.

Results for AVS and sulfate isotope ratios, including duplicate analyses of sulfate for some meteorites, are presented in Table 2-2. The table also includes isotope ratios for the CRS fraction from Chassigny. Shergottite samples generally produced too little CRS for accurate measurement of isotope ratios. Values for $\delta^{34}S$, $\Delta^{33}S$, and $\Delta^{36}S$ were normalized to measurements of Cañon Diablo Troilite (CDT) to facilitate comparison with results from previous studies. Uncertainties are estimated from repeated analyses of the sulfur isotopic ratios of IAEA reference materials and are generally better than 0.15‰, 0.008‰, and 0.15‰ (1σ) for $\delta^{34}S$, $\Delta^{33}S$, and $\Delta^{36}S$, respectively. Uncertainties for individual samples may be higher than these values, as shown in the table.

**Table 2-1. Sulfur concentrations for shergottites and Chassigny**

**Uncertainties are ± 2% of each measurement**.

| Meteorite | AVS (ppm) | Acid-soluble sulfate (ppm) | Water-soluble sulfate (ppm) | Total sulfate (ppm) | CRS (ppm) | Total sulfur (ppm) |
|---|---|---|---|---|---|---|
| EET 79001A | 1066 | -- | -- | 0 | 5 | 1071 |
| EET 79001B | 467 | -- | -- | 109 | 0 | 576 |
| NWA 2800 | 605 | 302 | 0 | -- | 10 | 917 |
| NWA 5718 | 302 | 143 | 0 | -- | 0 | 445 |
| NWA 2975 | 120 | 44 | 0 | -- | 12 | 176 |
| NWA 2986 | 287 | -- | -- | 72 | ** | 359 |
| NWA 3171 | 0 | 920 | 485 | -- | 8 | 1413 |
| NWA 5298 | 5 | 445 | 11 | -- | 4 | 465 |
| QUE 94201 | 511 | 0 | 295 | -- | ** | 806 |
| Shergotty | 1126 | 114 | 0 | -- | 2 | 1243 |
| Los Angeles | 1217 | 272 | 0 | -- | 21 | 1510 |
| Zagami | 918 | 33 | 0 | -- | 8 | 960 |
| RBT 04261 | 766 | -- | -- | 272 | 10 | 1048 |
| LAR 06319 | 725 | -- | -- | 572 | 0 | 1297 |
| Dhofar 019 | 770 | 841 | 15 | -- | 4 | 1630 |
| NWA 5960 | 479 | -- | -- | 428 | ** | 907 |
| NWA 2990 | 188 | 462 | 11 | -- | 8 | 669 |
| NWA 5990 | 2363 | 70 | 0 | -- | ** | 2433 |
| NWA 2046 | 731 | 104 | 12 | -- | 11 | 858 |
| NWA 4925 | 257 | 847 | 5 | -- | 10 | 1118 |
| NWA 5789 | 64 | 303 | 12 | -- | 0 | 379 |
| NWA 4468 | 395 | 169 | 17 | -- | 11 | 592 |
| NWA 6162 | 689 | -- | -- | 385 | ** | 1074 |
| SaU 005 | 601 | 901 | 8 | -- | 12 | 1522 |
| DaG 476 | 300 | 532 | 80 | -- | 4 | 916 |
| Y980459 | 388 | 172 | 0 | -- | 0 | 560 |
| ALH 77005 | 447 | -- | -- | 277 | 1 | 726 |
| NWA 6342 | 442 | -- | -- | 52 | ** | 494 |
| Chassigny | 0 | 42 | 22 | -- | <1 | 65 |

-- Sulfate is presented either as separate water- and acid-soluble phases or as total sulfate.
** Not recovered.
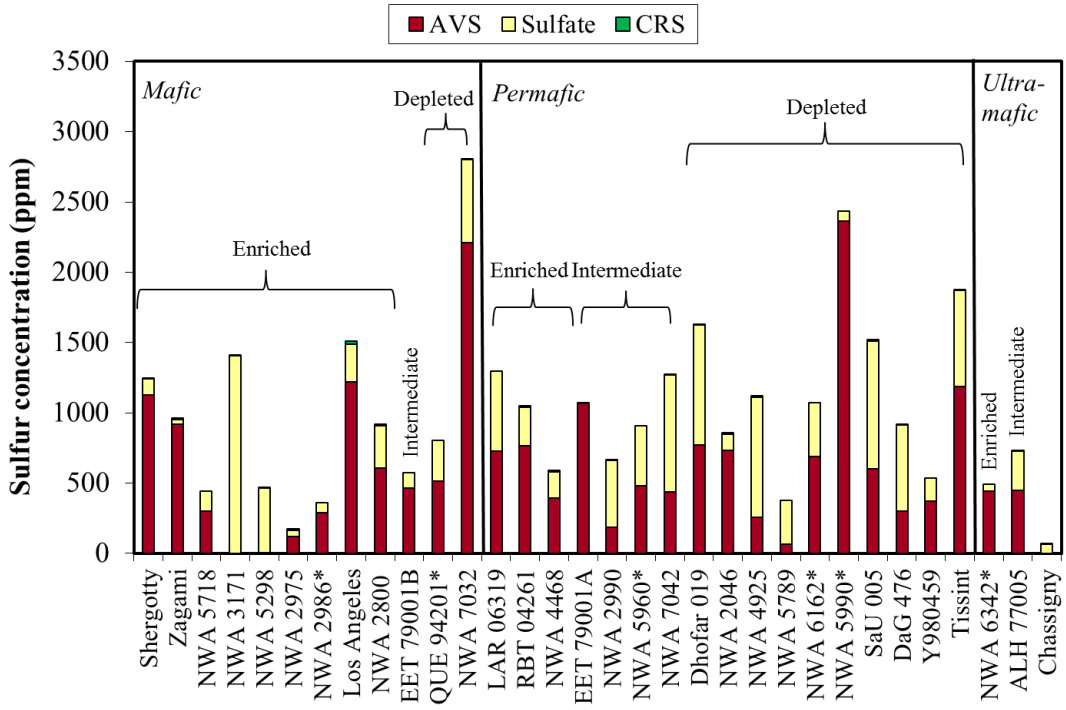
**Figure 2-1. Sulfur concentrations for the shergottites and Chassigny.**

**Asterisks indicate samples for which not all fractions were recovered.**

**(See Table 2-1.)**

**Table 2-2. Sulfur isotopic composition for shergottites and Chassigny.**

**Data are normalized to measurements of CDT. 1σ uncertainties are given in parentheses.**

| Meteorite | $\delta^{34}S$ | $\Delta^{33}S$ | $\Delta^{36}S$ |
|---|---|---|---|
| EET 79001A | | | |
| AVS | -0.13 (0.15) | 0.010 (0.008) | 0.10 (0.2) |
| EET 79001B | | | |
| AVS | -0.06 (0.15) | 0.013 (0.008) | 0.10 (0.2) |
| Total sulfate | 0.43 (0.15) | -0.008 (0.008) | 0.06 (0.2) |
| NWA 2800 | | | |
| AVS | 0.17 (0.15) | 0.009 (0.008) | -0.04 (0.2) |
| Acid-soluble sulfate | -0.50 (0.15) | 0.025 (0.008) | 0.14 (0.2) |
| NWA 5718 | | | |
| AVS | -0.15 (0.15) | -0.004 (0.008) | 0.23 (0.2) |
| Acid-soluble sulfate | 0.55 (0.15) | 0.260 (0.008) | 0.11 (0.2) |
| NWA 2975 | | | |
| AVS | -0.53 (0.15) | 0.014 (0.008) | 0.02 (0.2) |
| Acid-soluble sulfate | 0.40 (0.15) | 0.015 (0.026) | 0.78 (0.3) |
| NWA 2986 | | | |
| AVS | -0.22 (0.15) | 0.029 (0.008) | 0.10 (0.2) |
| Acid-soluble sulfate | -0.09 (0.15) | 0.021 (0.008) | 0.74 (0.3) |
| NWA 3171-1 | | | |
| Water-soluble sulfate | 6.39 (0.15) | 0.027 (0.008) | 0.32 (0.2) |
| Acid-soluble sulfate | 5.42 (0.15) | 0.025 (0.008) | 0.03 (0.2) |
| NWA 3171-2 | | | |
| Total sulfate | 6.14 (0.15) | 0.020 (0.008) | 0.16 (0.2) |
| NWA 5298-1 | | | |
| Acid-soluble sulfate | -0.25 (0.15) | 0.156 (0.009) | 0.28 (0.2) |
| NWA 5298-2 | | | |
| Total sulfate | 0.32 (0.15) | 0.169 (0.008) | -0.12 (0.2) |
| QUE 94201 | | | |
| AVS | 0.08 (0.15) | -0.007 (0.008) | 0.06 (0.22) |
| Water-soluble sulfate | 8.94 (0.15) | 0.014 (0.008) | 0.12 (0.2) |
| Shergotty | | | |
| AVS | -0.47 (0.15) | -0.003 (0.008) | 0.00 (0.2) |
| Acid-soluble sulfate | 0.36 (0.15) | -0.003 (0.008) | 0.39 (0.23) |
| Los Angeles | | | |
| AVS | 0.02 (0.15) | 0.054 (0.008) | 0.06 (0.2) |
| Acid-soluble sulfate | -0.39 (0.15) | 0.056 (0.008) | 0.15 (0.4) |

**Table 2-2, continued**

| Meteorite | $\delta^{34}S$ | $\Delta^{33}S$ | $\Delta^{36}S$ |
|---|---|---|---|
| Zagami | | | |
| AVS | -0.43 (0.15) | -0.018 (0.008) | 0.07 (0.15) |
| Acid-soluble sulfate | 0.22 (0.15) | 0.024 (0.019) | -0.11 (0.15) |
| NWA 7032 | | | |
| AVS | -0.17 (0.15) | 0.019 (0.008) | -0.13 (0.15) |
| Water-soluble sulfate | -0.11 (0.15) | 0.017 (0.008) | 0.57 (0.20) |
| Acid-soluble sulfate | 0.18 (0.15) | 0.012 (0.008) | -0.04 (0.15) |
| RBT 04261 | | | |
| AVS | -0.01 (0.15) | -0.007 (0.008) | 0.02 (0.15) |
| Total sulfate | 3.65 (0.15) | 0.011 (0.008) | 0.13 (0.15) |
| LAR 06319 | | | |
| AVS | 0.35 (0.15) | -0.002 (0.008) | 0.14 (0.15) |
| Total sulfate | 6.71 (0.15) | 0.057 (0.008) | 0.10 (0.15) |
| Dhofar 019 | | | |
| AVS | -0.33 (0.15) | 0.014 (0.008) | -0.04 (0.15) |
| Water-soluble sulfate | 7.63 (0.15) | 0.004 (0.028) | -- |
| Acid-soluble sulfate | 5.22 (0.15) | 0.019 (0.008) | -0.06 (0.15) |
| NWA 5960 | | | |
| AVS | -0.08 (0.15) | 0.093 (0.008) | -0.06 (0.15) |
| Total sulfate | 0.33 (0.15) | 0.086 (0.008) | 0.07 (0.15) |
| NWA 2990 | | | |
| AVS | 0.74 (0.15) | 0.063 (0.014) | 0.39 (0.15) |
| Acid-soluble sulfate | -0.56 (0.15) | 0.081 (0.008) | 0.24 (0.15) |
| NWA 5990 | | | |
| AVS | -0.15 (0.15) | 0.018 (0.008) | -0.18 (0.15) |
| Acid-soluble sulfate | 0.15 (0.15) | 0.012 (0.008) | 0.66 (0.15) |
| NWA 2046 | | | |
| AVS | -0.30 (0.15) | 0.007 (0.008) | -0.19 (0.15) |
| Acid-soluble sulfate | 1.27 (0.15) | 0.024 (0.008) | 0.14 (0.15) |
| NWA 4925 | | | |
| AVS | -0.25 (0.15) | 0.013 (0.008) | 0.05 (0.20) |
| Water-soluble sulfate | 1.63 (0.15) | -0.012 (0.020) | 0.66 (0.30) |
| Acid-soluble sulfate | 1.31 (0.15) | 0.020 (0.008) | 0.23 (0.15) |
| NWA 5789 | | | |
| AVS | 0.00 (0.15) | -0.013 (0.008) | 0.34 (0.15) |
| Acid-soluble sulfate | 0.43 (0.15) | 0.010 (0.008) | 0.07 (0.15) |
| NWA 4468 | | | |
| AVS | -0.38 (0.15) | 0.002 (0.008) | -0.01 (0.15) |
| NWA 4468-1 | | | |
| Water-soluble sulfate | 1.70 (0.15) | 0.117 (0.066) | 1.16 (0.44) |
| Acid-soluble sulfate | -4.61 (0.15) | 0.009 (0.008) | 0.99 (0.20) |
| NWA 4468-2 | | | |
| Total sulfate | 0.21 (0.15) | 0.000 (0.008) | 0.21 (0.15) |
| NWA 6162 | | | |
| AVS | -0.29 (0.15) | 0.027 (0.008) | 0.14 (0.15) |
| Total sulfate | 0.06 (0.15) | 0.023 (0.008) | 0.12 (0.15) |

**Table 2-2, continued**

| Meteorite | $\delta^{34}S$ | $\Delta^{33}S$ | $\Delta^{36}S$ |
|---|---|---|---|
| SaU 005 | | | |
| AVS | 0.03 (0.15) | 0.001 (0.009) | 0.11 (0.15) |
| Water-soluble sulfate | 9.39 (0.15) | 0.133 (0.126) | -0.19 (2.00) |
| Acid-soluble sulfate | 3.54 (0.15) | 0.021 (0.008) | -0.02 (0.15) |
| DaG 476 | | | |
| AVS | 0.08 (0.15) | 0.017 (0.008) | 0.02 (0.15) |
| Water-soluble sulfate | 11.78 (0.15) | 0.002 (0.034) | 1.04 (0.34) |
| Acid-soluble sulfate | 2.45 (0.15) | 0.056 (0.015) | 1.14 (0.55) |
| Y980459 | | | |
| AVS | -0.15 (0.15) | 0.006 (0.008) | 0.10 (0.15) |
| Acid-soluble sulfate | 1.92 (0.15) | -0.009 (0.008) | -0.03 (0.15) |
| NWA 7042 | | | |
| Water-soluble sulfate | 14.6 (0.15) | 0.032 (0.008) | -0.18 (0.20) |
| Acid-soluble sulfate | 3.26 (0.15) | 0.029 (0.008) | 0.02 (0.15) |
| Tissint | | | |
| AVS | -0.79 (0.15) | 0.024 (0.008) | -0.07 (0.15) |
| Acid-soluble sulfate | -0.07 (0.15) | 0.001 (0.008) | 0.13 (0.15) |
| ALH 77005 | | | |
| AVS | 0.45 (0.15) | -0.002 (0.008) | 0.02 (0.15) |
| Total sulfate | 0.99 (0.15) | 0.005 (0.008) | -0.04 (0.15) |
| NWA 6342 | | | |
| AVS | -0.24 (0.15) | 0.022 (0.008) | -0.02 (0.15) |
| Total sulfate | 1.68 (0.15) | -0.016 (0.019) | 1.02 (0.15) |
| Chassigny | | | |
| Water-soluble sulfate | 0.60 (0.15) | 0.033 (0.008) | 0.55 (0.20) |
| Acid-soluble sulfate | 0.54 (0.15) | 0.008 (0.008) | 0.34 (0.15) |
| CRS | -0.59 (0.15) | 0.004 (0.008) | 0.42 (0.15) |

*2.3.2   AVS Isotopic Compositions*

The sulfur isotope ratios for shergottite AVS were found to be uniform among the samples analyzed for this study, as seen in plots of $\Delta^{33}S$ vs. $\delta^{34}S$ and $\Delta^{36}S$ vs. $\delta^{34}S$ in Figure 2-2 (a) and (b). As the figure shows, the majority of shergottites form clusters close to the origins of these plots. Values of $\delta^{34}S$ in the main clusters range from -0.79 ± 0.15‰ to 0.45 ± 0.15‰, $\Delta^{33}S$ from -0.018 ±0.008‰ to 0.029 ± 0.008‰, and $\Delta^{36}S$ from -0.19 ± 0.15‰ to 0.35 ± 0.15‰. Weighted mean values for the main clusters – $\delta^{34}S$ (-0.11 ± 0.15‰), $\Delta^{33}S$ (0.007 ± 0.008‰), and $\Delta^{36}S$ (0.05 ± 0.15‰) –

are all identical within error to CDT. The symbols in Figure 2-2 are encoded with information pertaining to sample characteristics, as follows: triangles, circles, or diamonds indicate meteorites with mafic, permafic, or ultramafic composition, respectively. In addition, solid-filled, unfilled, or pattern-filled symbols indicate samples from an "enriched," "intermediate," or "depleted" shergottite mantle source. The data reveal no correlation between the AVS isotopic composition and either mineralogical or trace element characteristics.

There are four meteorites in Figure 2-2(a) that display clearly resolvable mass-independent $\Delta^{33}S$ compositions: NWA 2990, NWA 5960 (paired with the former), Los Angeles, and Tissint, with $\Delta^{33}S$ of 0.063 ± 0.014‰, 0.093 ± 0.008‰, 0.054 ± 0.008‰, and 0.024 ± 0.008‰, respectively. These values were not factored into the weighted mean reported above, since these meteorites appear to carry an anomalous sulfur-bearing component distinct from the primary shergottite signature, as seen in the relatively tight cluster of points formed by the remaining shergottites. In contrast, all values of $\Delta^{36}S$ are within error of zero. The potential implications of these findings are discussed in Section 2.4 below.

*2.3.3   Sulfate Isotopic Compositions*

The sulfur isotope ratios for the shergottite sulfate fractions display a wider range of values than the AVS fractions. This is attributed to variable contributions from martian and/or terrestrial weathering and possibly from exogenous sulfate that was assimilated by the melts from which the shergottite parents crystallized. Plots of sulfate $\Delta^{33}S$ vs. $\delta^{34}S$ and $\Delta^{36}S$ vs. $\delta^{34}S$ are shown in Figures 2-3 and 2-4, with

45

**Figure 2-2(a). AVS of shergottites: $\Delta^{33}S$ vs. $\delta^{34}S$.**

**Triangles = mafic; Circles = permafic; Diamonds = ultramafic. Solid-filled symbols = enriched source; Pattern-filled symbols = depleted source; Unfilled symbols = intermediate source. Weighted mean does not include NWA 2990, NWA 5960, Los Angeles, or Tissint. Error bars are 2σ.**

**Figure 2-2(b). AVS of shergottites: $\Delta^{36}$S. vs. $\delta^{34}$S.**

**Triangles = mafic; Circles = permafic; Diamonds = ultramafic. Solid-filled symbols = enriched source; Pattern-filled symbols = depleted source; Unfilled symbols = intermediate source. Weighted mean does not include NWA 2990, NWA 5960, Los Angeles, or Tissint. Error bars are 2σ.**

symbols in Figure 2-4 displaying sample characteristics as described for Figure 2-2. In general, the acid-soluble fractions have $\delta^{34}$S from -4.6 ± 0.15‰ to 6.7 ±0.15‰, $\Delta^{33}$S from -0.016 ± 0.019‰ to 0.260 ± 0.008‰, and $\Delta^{36}$S from -0.14 ±0.15‰ to 1.0‰. Values for the water-soluble sulfate fractions range from -0.25 ± 0.15‰ to 11.8 ±0.15‰ for $\delta^{34}$S, -0.012 ±0.020‰ to 0.133 ±0.126‰ for $\Delta^{33}$S, and -0.19 ± 2.00‰ to 0.66 ± 0.30‰ for $\Delta^{36}$S. Note that for all of these samples, the highest values of $\Delta^{36}$S typically carry higher uncertainties because of their small sizes, which makes them more susceptible to contamination that can lead to mass spectrometric interferences.

The $^{34}$S enrichments of shergottite sulfate fractions, ranging as high as 14.6 ± 0.15‰ for NWA 7042 water-soluble sulfate, are interpreted to represent addition of terrestrial sulfate during weathering on Earth. While a martian photochemical origin is not ruled out, it is considered unlikely because of the absence of significant nonzero $\Delta^{33}$S. Other sulfate fractions in martian meteorites possess significant $^{33}$S anomalies without as enriched $^{34}$S. The effects of terrestrial sulfate on martian S-MIF will be addressed for specific meteorites in Section 2.4.

Chassigny has acid-soluble sulfate with $\delta^{34}$S of 0.54 ± 0.15‰, $\Delta^{33}$S of 0.008 ± 0.008‰, and $\Delta^{36}$S of 0.34 ± 0.15‰ and water-soluble sulfate with $\delta^{34}$S of 0.60 ± 0.15‰, $\Delta^{33}$S of 0.033 ± 0.008‰, and $\Delta^{36}$S of 0.55 ± 0.20‰. The small positive $\Delta^{33}$S of Chassigny water-soluble sulfate is consistent with positive $\Delta^{33}$S values observed in several shergottites and may reflect addition of a small quantity of atmospherically-processed sulfate to Chassigny through aqueous alteration.
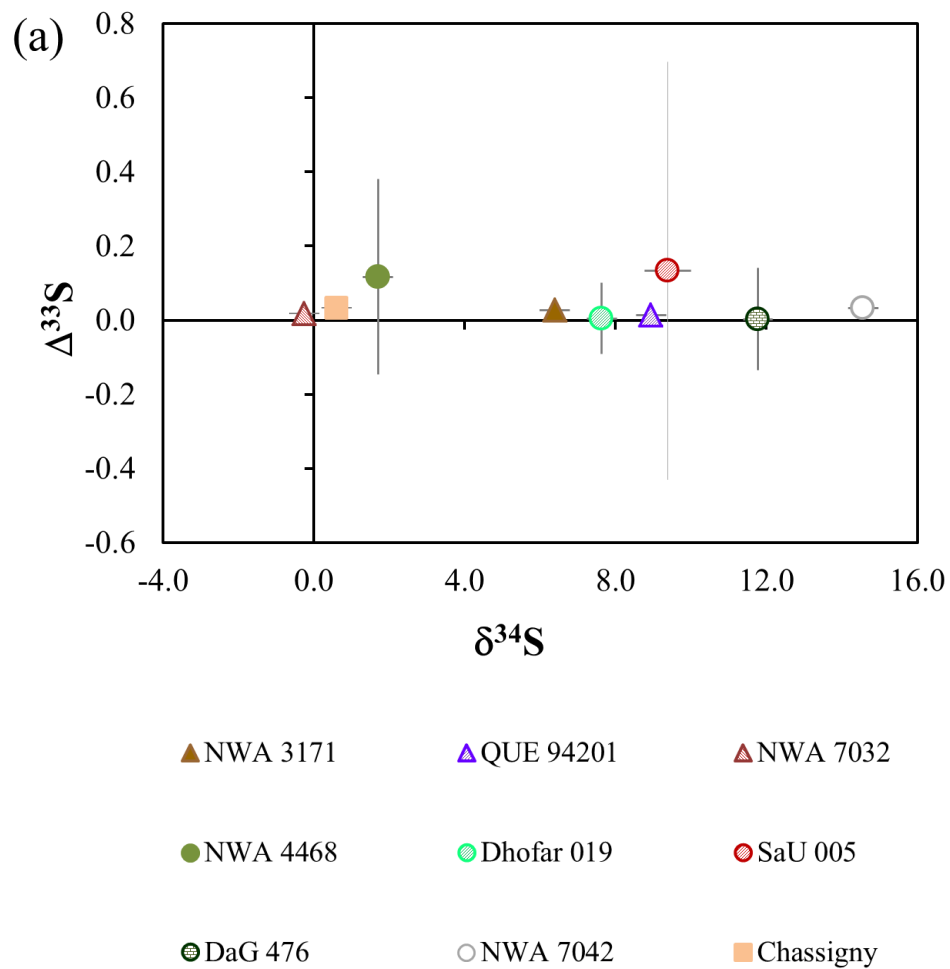
**Figure 2-3(a). Water-soluble sulfate of shergottites and Chassigny: $\Delta^{33}S$ vs. $\delta^{34}S$. Triangles = mafic; Circles = permafic; Diamonds = ultramafic. Solid-filled symbols = enriched source; Pattern-filled symbols = depleted source; Unfilled symbols = intermediate source. Error bars are 2$\sigma$.**
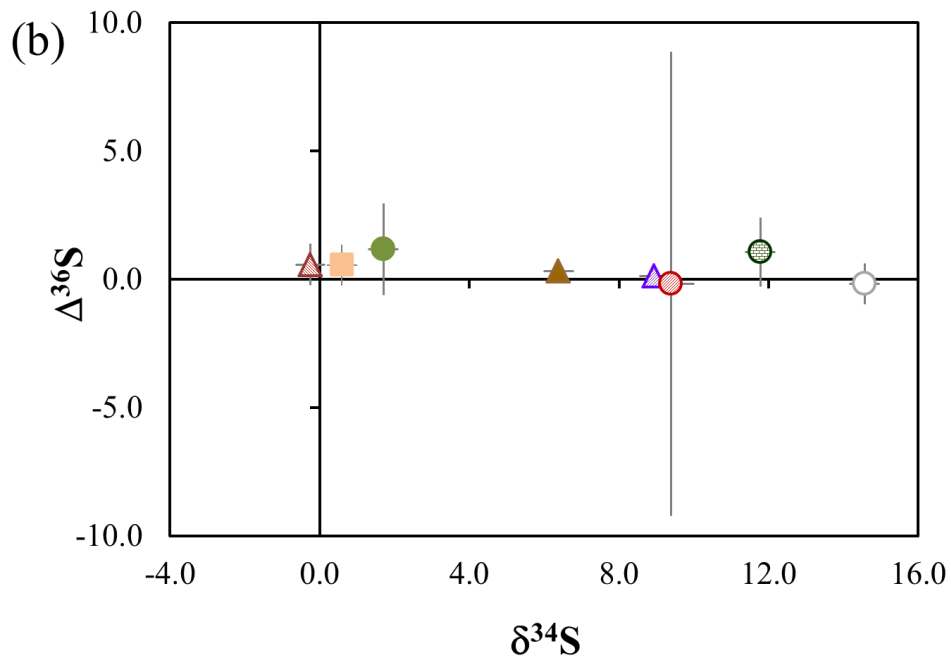
**Figure 2-3(b). Water-soluble sulfate of shergottites and Chassigny: $\Delta^{36}S$ vs. $\delta^{34}S$. Triangles = mafic; Circles = permafic; Diamonds = ultramafic. Solid-filled symbols = enriched source; Pattern-filled symbols = depleted source; Unfilled symbols = intermediate source. Error bars are 2σ.**

**Figure 2-4(a). Acid-soluble and total sulfate for shergottites and Chassigny: $\Delta^{33}$S vs. $\delta^{34}$S.**

**Triangles = mafic; Circles = permafic; Diamonds = ultramafic. Solid-filled symbols = enriched source; Pattern-filled symbols = depleted source; Unfilled symbols = intermediate source. Error bars are 2$\sigma$.**

**Figure 2-4(b). Acid-soluble and total sulfate for shergottites and Chassigny: $\Delta^{36}S$ vs. $\delta^{34}S$.**

**Triangles = mafic; Circles = permafic; Diamonds = ultramafic. Solid-filled symbols = enriched source; Pattern-filled symbols = depleted source; Unfilled symbols = intermediate source. Error bars are 2$\sigma$.**

## 2.4 Discussion

### 2.4.1 Sulfur Abundances

As seen in Figure 2-1, there is no correlation between total sulfur abundance and either mineralogical classification or trace element enrichment characteristics. There is also no correlation between the relative abundances of sulfide and sulfate phases and these classifying parameters. Shergottite magmas primarily experienced reducing conditions, with initial oxygen fugacity ($fO_2$) from ~1 to 3 log units below the QFM buffer (e.g., McSween et al., 1996; Wadhwa et al., 2001; Herd et al., 2004). Magmatic sulfur at this range of $fO_2$ should have existed predominantly in the $S^{2-}$ valence state (Wallace and Carmichael, 1992; Jugo et al., 2005). Jugo et al. (2005) reported that the sulfur speciation in a basaltic melt switches from sulfide dominance to sulfate dominance between approximately QFM and QFM + 2. Some of the shergottites show evidence for evolution of their magmatic $fO_2$ to higher values as crystallization proceeded, with late-stage $fO_2$ as high as QFM + 0.3 (Herd, 2003; Gross et al., 2012). According to the model of Jugo et al. (2005), the proportion of sulfur present as sulfate should increase from a few percent of the total sulfur at QFM to approximately 10% at QFM + 0.3.

The sulfate yields from the chemical extraction of shergottites ranged from no sulfate for EET 79001A to > 99% of sulfur as sulfate for NWA 3171. It is clear from the above discussion that most of the shergottites were found to contain more sulfate than could have been produced by closed-system igneous crystallization. This implies either that the meteorites experienced extensive weathering that oxidized much of

their primary sulfides to sulfate or that exogenous sulfate was introduced at some time after crystallization.

Exogenous sulfate could have been introduced either on Mars or on Earth. Assimilation of crustal material into shergottite magmas has been invoked as a possible explanation for the elevated $f$O$_2$ observed in some martian meteorites as well as enrichments in incompatible trace elements (e.g., Jones, 1989; Herd et al., 2002; Rumble and Irving, 2009). This process also could have introduced sulfate from the martian crust into magmas. Several shergottites revealed S-MIF compositions in their sulfate fractions, interpreted as evidence for assimilation of surface-derived sulfur. In these cases, the sulfate is thought to be of martian origin due to the S-MIF signal, which could not have been introduced during weathering on Earth. One of these meteorites was NWA 5298, which produced too little AVS for isotopic analysis (5 ± 1 ppm), but substantial sulfate (456 ± 9 ppm). The shergottites with anomalous sulfate isotopic compositions are discussed further in Section 2.4.3.

Another shergottite that produced particularly low AVS yield was NWA 3171. While petrographic examination indicated the presence of pyrrhotite in NWA 3171 (Irving et al., 2004), sulfur extraction of two separate splits of this meteorite, with sample masses of 275 mg and 644 mg respectively, produced no AVS. This suggests either that the sulfides are heterogeneously distributed and these splits contained little to no pyrrhotite, or that the original pyrrhotite was oxidized to sulfate prior to analysis. It is possible that this reflects weathering that occurred both on Mars and on Earth. Thin fractures containing rust-colored alteration material have been reported in NWA 3171 (Irving et al., 2004; Russell et al., 2005). Electron microprobe analysis

revealed that hydrous mineral assemblages in this alteration material, dominated by an iron hydroxide mineral similar to goethite, is not typical of terrestrial hot weathering environments, but may indicate hydrothermal alteration or weathering processes on Mars (Irving et al., 2004; Russell et al., 2005). Such processes could have caused oxidation of primary igneous pyrrhotite to sulfate. Rare barite and calcite have also been reported in NWA 3171, assumed to have precipitated from groundwater in the terrestrial desert (Irving et al., 2004). It is likely that desert weathering on Earth resulted in further oxidation of pyrrhotite, as evidenced by the recovery of all sulfur in NWA 3171 as sulfate in this study.

Although Chassigny was a meteorite fall and not a find, implying that it should have experienced less severe terrestrial weathering than most martian meteorites, it still may have experienced oxidizing conditions during its almost 200 years in curation. As with NWA 3171, over 99% of the sulfur recovered from Chassigny was in the form of sulfate, although the total sulfate yield was only $65 \pm 1$ ppm, with < 1 ppm of CRS. Previous studies have generally agreed upon a low abundance of sulfur in Chassigny, as expected for a dunite. Dyakonova and Kharitonova (1960) detected no sulfides. Floran et al. (1978) reported troilite, marcasite, and pentlandite among the accessory minerals in Chassigny, but indicated that the marcasite may be a terrestrial alteration product of primary troilite. By oxidation of powdered samples in oxygen at 1600 °C, Gibson and Moore (1983) measured Chassigny's total sulfur abundance as $360 \pm 50$ ppm. Burgess et al. (1989) used stepped combustion to estimate the contents of multiple sulfur-bearing phases, detecting sulfur abundances of 85 ppm from sulfides, 80 ppm from sulfates, and at least 50 ppm from elemental sulfur. Burgess et

al. (1989) concluded that Chassigny contained a lower abundance of sulfate sulfur than the shergottites, but a higher ratio of oxidized/reduced sulfur phases, indicating a higher net oxidation state. The implication of the current results compared to previous reports is that the sulfur content in Chassigny is heterogeneously distributed.

Wentworth and Gooding (1994) examined interior chips of Chassigny via scanning electron microscopy and energy-dispersive X-ray spectrometry and reported discontinuous veins of Ca-sulfate, Ca-carbonate, and Mg-carbonate along fractures in primary igneous minerals. Based on grain morphologies, the authors suggested that the sulfate salts were probably gypsum ($CaSO_4 \cdot 2H_2O$) or bassanite ($CaSO_4 \cdot \frac{1}{2}H_2O$). The sulfates commonly occurred in close proximity to carbonates, in some places displaying fine-scale intergrowths. The salts were also found to contain traces of Cl and P, consistent with precipitation from short-lived, cold, saline, aqueous solutions that postdated igneous crystallization. Unlike similar minerals in the nakhlites, Wentworth and Gooding (1994) found that the Chassigny salts occur as isolated deposits, without associated ferric oxides or aluminosilicate clay minerals, complicating the interpretation of the sulfate source.

Wentworth and Gooding (1994) reported that some vugs in Chassigny's fusion crust contain traces of massive, fine-grained Ca-sulfate, which could be interpreted as evidence for either terrestrial contamination or postfall leaching of hygroscopic, pre-terrestrial salts from the interior. Ion probe analyses of Chassigny amphiboles by Watson et al. (1994) indicated D/H ratios that were higher than expected for magmatic water, prompting the suggestion that amphibole structural water had experienced isotopic exchange with deuteric or meteoric water on Mars. Wentworth

and Gooding (1994) concluded that given this additional evidence for aqueous martian fluids in Chassigny, a pre-terrestrial origin of the Chassigny sulfates is most probable.

The question of martian versus terrestrial weathering is especially interesting for the Tissint meteorite, which was witnessed to fall in a remote, rocky region of Morocco on July 18, 2011 (Irving et al., 2012b). While the first fragments of the meteorite were not recovered until about 4 months later, Irving et al. (2012b) reported that even pieces with broken fusion crust, presumably reflecting impact at the Earth's surface, showed no signs of terrestrial weathering. The sulfate extracted from Tissint comprised ~37% of the total sulfur yield. Given the lack of evidence for terrestrial weathering upon petrographic analysis (Irving et al., 2012b), the sulfate extracted from Tissint most likely formed on Mars. As a depleted, permafic shergottite (Irving et al., 2012b), the trace element abundances of Tissint do not provide evidence for assimilation of enriched crustal material into the magma. This suggests that if sulfate from the martian surface was added to the melt, it must have occurred without simultaneous incompatible element enrichment. The AVS fraction of Tissint displayed a positive $\Delta^{33}$S anomaly of 0.024 ± 0.008%, suggesting assimilation of sulfur that had been cycled through the atmosphere into the Tissint magma, followed by reduction of sulfate to sulfide. However, the sulfate extracted from this meteorite, with $\Delta^{33}$S of 0.001 ± 0.008‰, showed no evidence for anomalous sulfur. The sulfate could have derived from multiple sources, including oxidative weathering of primary sulfide minerals and further addition of martian sulfate bearing no S-MIF signal during post-crystallization alteration on Mars. The isotopic composition and degree of

57

homogeneity of crustal sulfur deposits on Mars are not known, but the variations in $\Delta^{33}S$ observed in Tissint AVS and sulfate fractions may indicate heterogeneities in the isotopic composition of surface sulfur.

### 2.4.2    *Juvenile Martian Sulfur Isotopic Composition*

The weighted mean for the shergottite AVS fractions without $\Delta^{33}S$ anomalies yields the first estimate of the juvenile martian sulfur isotopic composition: $\delta^{34}S = -0.14 \pm 0.15‰$, $\Delta^{33}S = 0.008 \pm 0.008‰$, and $\Delta^{36}S = 0.04 \pm 0.19‰$.[3] As seen in Figure 2-2, there is no correlation between degree of trace element enrichment or mineralogical classification and AVS sulfur composition. Data for meteorites of enriched versus depleted and mafic versus ultramafic groups are distributed about the mean. It is notable that the sulfur isotopic composition of Y980459, which is generally regarded as the most primitive shergottite and thus most characteristic of the martian mantle composition (Mikouchi et al., 2004), lies closest to the mean of all the shergottites.

The unexpectedly high concentrations of sulfate recovered from most shergottites in this study raises questions about the source of the sulfate and potential effects on

---

[3] The calculated $1\sigma$ uncertainty on the weighted mean is $\delta^{34}S \pm 0.12‰$, $\Delta^{33}S \pm 0.001‰$, and $\Delta^{36}S \pm 0.19‰$. The larger uncertainties given in the text for $\delta^{34}S$ and $\Delta^{33}S$ represent the standard error of repeated measurements of reference standards, which encompasses sources of error in the fluorination and cleaning procedure as well as in the mass spectrometric measurements.

AVS composition. The observed sulfate could have been incorporated into the magmas by assimilation of crustal material or it could have resulted from weathering processes on Mars or Earth. The former mechanism is invoked to explain the S-MIF composition observed in selected shergottites, as discussed in the next section. Three meteorites, NWA 2990/5960 and Los Angeles, possessed AVS with S-MIF composition, and thus their AVS data were not factored into the weighted mean. It was assumed that the AVS fractions of the remaining shergottites reflect their mantle-derived sulfide compositions and that the sulfate extracted from them was most likely produced by weathering processes that did not affect the AVS.

Figure 2-5 illustrates the shergottite sulfur isotopic composition, as well as data for other types of meteorites for comparison. The figure includes data for chondrites, various types of achondrites (acapulcoites-lodranites, aubrites, and ureilites), and iron meteorites. Chondrites are the most primitive group of meteorites, with chemical compositions similar to that of a volatile-free Sun (Hutchison, 2004). They contain abundant chondrules, some of the earliest-formed solids in the solar system (Grossman, 1988). Chondrules are mm-sized, rounded objects composed primarily of Fe-Mg silicates with Fe-Ni metal and minor sulfides (Hutchison, 2004). Acapulcoites and lodranites form a coherent group representing perhaps the best examples of primitive achondrites. They have textures typical of achondrites but chondritic compositions, with oxygen isotopic compositions depleted in [17]O compared to the terrestrial fractionation line (McSween, 1999). The aubrites comprise a small group of achondrites poor in iron, producing unusual translucent, cream-colored fusion crusts that contrast with the dark crusts formed on most stony meteorites (Hutchison,

59

2004). Aubrites are the most sulfur-rich group of achondrites, with average sulfur abundance of approximately 0.5 wt% (Gibson and Moore, 1983). Their sulfide mineral complement includes oldhamite (CaS), indicating formation under highly reducing conditions (Hutchison, 2004). Oxygen isotopes of the aubrites plot along the terrestrial mass fractionation line (McSween, 1999). The ureilites are an unusual group of achondrites displaying an odd mix of characteristics, some of which suggest they are highly fractionated igneous rocks and others that indicate primitive origins. Their oxygen isotopic compositions lie along a mixing line defined by refractory inclusions in carbonaceous chondrites, characteristic of unprocessed nebular material (McSween, 1999). Several sulfide phases have been identified in the ureilites, including troilite (FeS), oldhamite, daubreelite ($Cr_2FeS_4$), and niningerite (MgS) or alabandite (MnS) (Berkley et al., 1976; Ramdohr, 1972). Farquhar et al. (2000b) reported an average $\Delta^{33}S$ in the ureilites of 0.042 ± 0.007‰.

Iron meteorites, or "irons," are broadly classified into twelve groups according to their chemical compositions. These groups may also be classified as magmatic (Groups IC, IIAB, IIC, IID, IIF, IIIAB, IIIE, IIIF, IVA, and IVB) and non-magmatic (Groups IAB/IIICD and IIE) types (Hutchison, 2004). The Cañon Diablo meteorite, from which the sulfide reference standard CDT is obtained, is a member of non-magmatic Group IAB. Recent analysis of troilite nodules from several iron meteorites revealed a small enrichment in $^{33}S$ in magmatic irons compared to non-magmatic irons (Antonelli et al., 2012). This finding was interpreted as evidence for heterogeneities in the materials that accreted to form the meteorite parent bodies,

possibly reflecting photochemical processes in the solar nebula (Antonelli et al., 2012).

The mean value for shergottite AVS isotopic composition is within $1\sigma$ error of CDT, suggesting a similarity between sulfur in the martian mantle and that of Group IAB iron meteorites. This average composition is not [33]S-enriched as seen in some achondrite groups (acpulcoite-lodranites, aubrites, and ureilites), components of chondrites, and IIIAB and IVA iron meteorites (Farquhar et al., 2000b; Rai et al., 2005; Rai and Thiemens, 2007).It can be seen in Figure 2-5(a) that the main cluster formed by shergottite AVS values in $\Delta^{33}S$-$\delta^{34}S$ space displays less variation than that in the FeS phases of iron meteorites measured by Gao and Thiemens (1991). Antonelli et al. (2012) reported a smaller range for Group IAB, IIIAB, and IVA iron meteorites that is similar in range to the shergottite data. This suggests efficient mixing of sulfur within the martian mantle.

Figure 2-5(a) also displays data for sulfur isotopic compositions of chondritic and achondritic meteorites, indicating the existence of S-MIF signatures in planetary precursor materials (Farquhar et al., 2000b; Rai et al., 2005; Rai and Thiemens, 2007). The three leading candidate processes for producing the S-MIF observed in the meteorites are cosmic ray spallation, nucleosynthetic effects, and gas-phase photochemistry (Farquhar et al., 2000c, 2007a; Rai et al., 2005; Rai and Thiemens, 2007). Cosmic ray spallation has been discounted because the measured $\Delta^{36}S/\Delta^{33}S$, cosmic ray exposure ages, and abundances of target elements for spallation do not match observations for these meteorites (Farquhar et al., 2000c, 2007a; Rai et al., 2005; Rai and Thiemens, 2007). Previous workers have argued against stellar

nucleosynthesis as the source of S-MIF based on the uniformity in $^{36}S/^{32}S$ ratios. It was assumed that given the low relative abundance of $^{36}S$ compared to other sulfur isotopes, the addition of even small quantities of nucleosynthetic $^{36}S$ would be readily apparent as variable $^{36}S/^{32}S$ ratios. The absence of such variations has been interpreted as evidence for efficient mixing in the solar nebula (Farquhar et al., 2000c; Rai et al., 2005). New questions appear to have been raised by a recent report of anomalies in $^{33}S$ and $^{34}S$ abundances in SiC grains extracted from the Murchison meteorite, which the authors attributed to molecular chemistry in supernova ejecta that resulted in preferential uptake of sulfur from the innermost supernova zones by the SiC grains (Hoppe et al., 2012). Evidence for photochemical effects in sulfonic acid extracts of the Murchison chondritic meteorite was presented by Cooper et al. (1997), and nebular photochemistry remains a leading hypothesis for the source of the S-MIF signal in the chondrites and achondrites.

It is believed that the solar nebula was a `reducing environment, with $H_2S$ as the dominant sulfur-bearing species (Pasek et al., 2005). To explain the observation of S-MIF in several major groups of meteorites that formed in distinct regions of the nebula, Rai et al. (2005) proposed that photochemical reactions occurred near the protosun, producing sulfur with anomalous isotopic composition that was incorporated into fluffy grains (i.e., with high surface area to volume ratio) (Fegley, 2000). Later, these grains were redistributed to various regions in the nebula by an x-wind, formed through interaction of accreting mass from the nebular disk with the magnetosphere of the protostar (Shu et al., 1996, 1997). The redistributed grains then accreted to form the various meteorite parent bodies (Rai et al., 2005).

Because sulfur in the martian mantle should have been well-mixed during the putative magma ocean stage (e.g., Elkins-Tanton et al., 2005), the variation in $\Delta^{33}S$ in the shergottites is interpreted to reflect processes that occurred on Mars and not a primordial signal. As seen in Figure 2-5(b), the S-MIF signal of shergottite sulfates and some sulfides is greater than that observed in chondritic or achondritic meteorites and is interpreted to reflect photochemical processing in the martian atmosphere, as discussed in the next section.
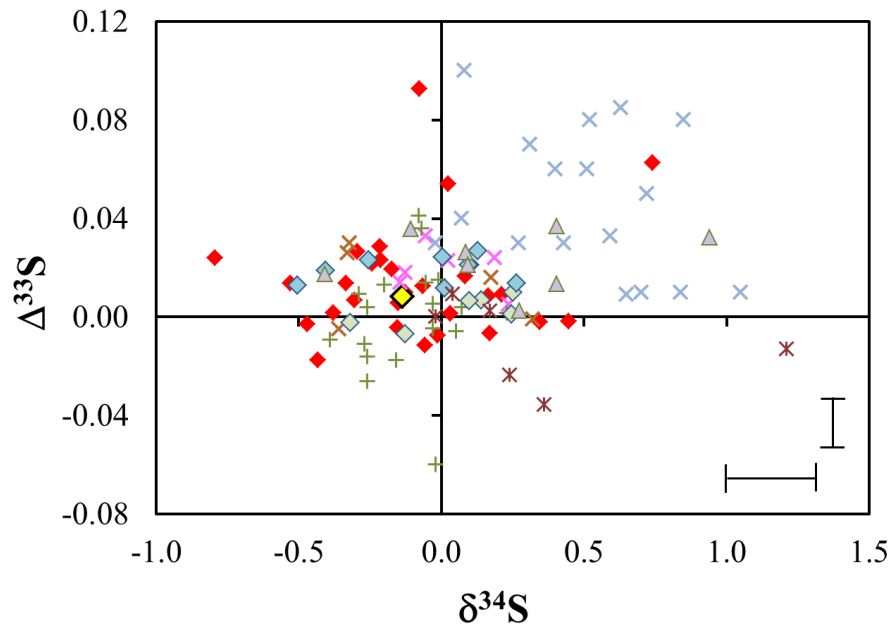
**Figure 2-5(a). Shergottite AVS composition with other meteorites.**

**Representative 2σ error bars at lower right corner. [1] Farquhar et al., 2000b;**

**[2] Rai et al., 2005; [3] Gao and Thiemens, 1993; [4] Rai and Thiemens, 2007; [5]**

**Antonelli et al., 2012; [6] Gao and Thiemens, 1991; [7] Peters et al., 2010.**
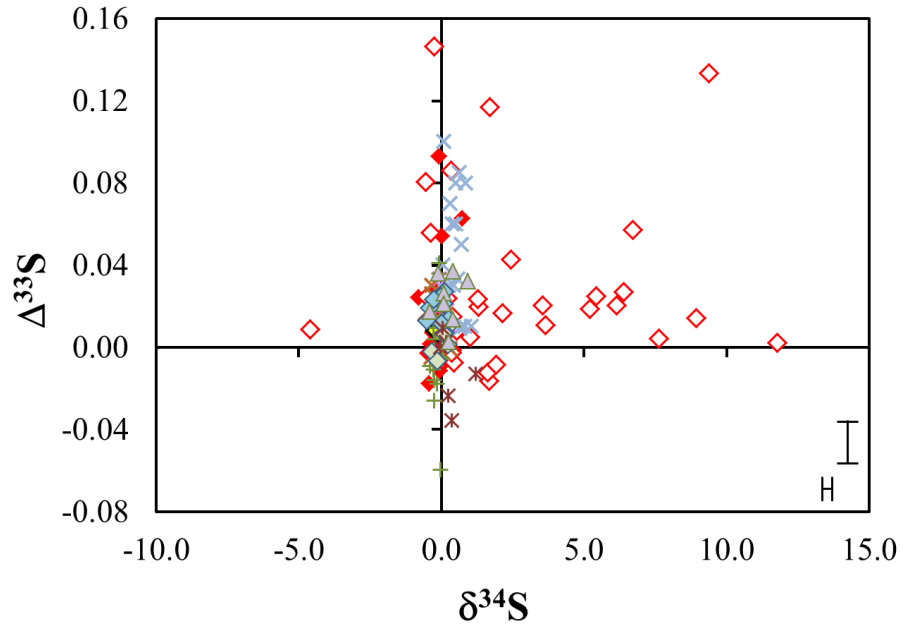
**Figure 2-5(b). Shergottite AVS and sulfate composition with other meteorites. Representative 2σ error bars at lower right. [1] Farquhar et al., 2000b; [2] Rai et al., 2005; [3] Gao and Thiemens, 1993; [4] Rai and Thiemens, 2007; [5] Antonelli et al., 2012; [6] Gao and Thiemens, 1991; [7] Peters et al., 2010.**

*2.4.3   Sulfur Isotopic Anomalies in the Shergottites*

Very few known processes are capable of fractionating sulfur in a mass-independent manner. The most likely candidate for producing the anomalous sulfur signatures observed in ancient terrestrial sediments (Farquhar et al., 2000), modern-day sulfate aerosols (Romero and Thiemens, 2003), and sulfur inclusions in kimberlitic diamonds (Farquhar et al., 2002) is ultraviolet (UV) photochemistry. UV photochemistry may also contribute to isotopic variations in different groups of meteorites, as discussed in the preceding section (Cooper et al., 1997; Farquhar et al., 2000c, 2007a; Rai et al., 2005; Rai and Thiemens, 2007).

Previous studies of martian meteorites have revealed sulfur with significant mass-independent isotopic composition, with Nakhla sulfate possessing the most extreme $\Delta^{33}$S of -1.25 ± 0.01‰ (Farquhar et al., 2007a). In contrast, the $\Delta^{36}$S of Nakhla sulfate was -0.16 ± 0.2‰, indicating no clearly resolved S-MIF (Farquhar et al., 2007a). Based on comparison with results of laboratory gas-phase photochemical experiments using $SO_2$ and $H_2S$, Farquhar et al. (2000c) suggested that the anomalous sulfur isotopic composition observed in Nakhla was generated by UV photochemistry of volcanic gases in the martian atmosphere, followed by incorporation of photochemical products into surface sediments. The covariation between $\Delta^{33}$S and $\Delta^{36}$S in Nakhla (Farquhar et al., 2007a) appears to be different than that observed for terrestrial and other types of meteorite samples (Farquhar et al., 2000a, 2000b, 2000c). This relationship may be similar to that observed for elemental sulfur

products of $SO_2$ photochemistry experiments with a Hg lamp source (Farquhar et al., 2001).

All of the shergottites with mass-independent $\Delta^{33}S$ AVS compositions also show similar positive values of $\Delta^{33}S$ in their respective sulfate fractions. In addition to these four samples, positive $\Delta^{33}S$ sulfate anomalies are seen in three other meteorites: two separate splits of NWA 5298 were analyzed, yielding $\Delta^{33}S$ of $0.146 \pm 0.009$‰ for acid-soluble sulfate and $0.169 \pm 0.008$‰ for total sulfate, although its AVS yield was insufficient for accurate isotope ratio measurements. NWA 5718 shows the highest $\Delta^{33}S$ of any martian meteorite analyzed to date, with acid-soluble sulfate of $0.244 \pm 0.008$‰. LAR 06319 total sulfate has $\Delta^{33}S$ of $0.057 \pm 0.008$‰, similar to sulfate of Los Angeles. However, both NWA 5718 and LAR 06319 have AVS with mass-dependent composition, yielding $\Delta^{33}S$ of $-0.004 \pm 0.008$‰ and $-0.002 \pm 0.008$‰, respectively. The water-soluble sulfate fractions of NWA 5298 and NWA 5718 were too small for isotope ratio measurements.

Results for $\Delta^{36}S$ versus $\Delta^{33}S$ of shergottite AVS and sulfate phases are shown in Figure 2-6. The main cluster of AVS data in Figure 2-6(a) forms an array with negative slope on this diagram. The meteorites that possess S-MIF form a secondary array parallel to the main cluster but offset due to their positive $\Delta^{33}S$. As seen most clearly in Figure 2-6(b), the sulfate fractions from shergottites with S-MIF compositions form an array roughly perpendicular to that formed by the AVS fractions. This S-MIF sulfate array resembles the sulfate array formed by the nakhlites (Farquhar et al., 2007a; Chapter 3 of this work), and consequently that of the Hg-lamp $SO_2$ photolysis products described above. However, given the

**(a)**

Δ³⁶S (y-axis)

Δ³³S (x-axis)
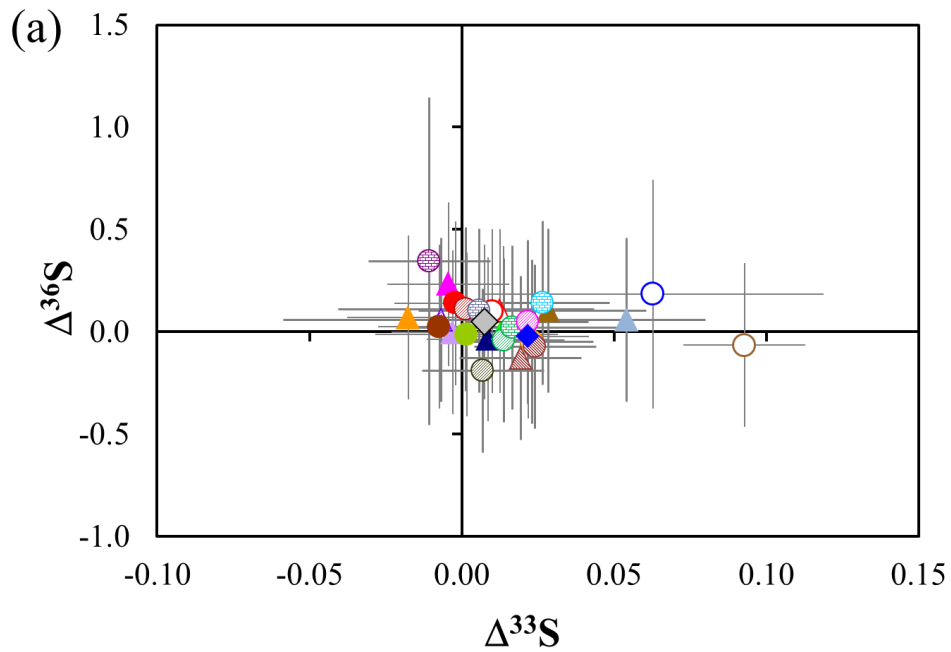
Legend:
- ▲ NWA 2800
- ▲ Los Angeles
- ▲ NWA 5718
- ▲ NWA 2975
- ▲ NWA 2986
- ▲ Shergotty
- ▲ Zagami
- △ EET 79001B
- △ QUE 94201
- ▲ NWA 7032
- ● RBT 04261
- ● LAR 06319
- ● NWA 4468
- ○ EET 79001A
- ○ NWA 5960
- ○ NWA 2990
- ◉ Dhofar 019
- ◉ NWA 5990
- ◉ NWA 2046
- ◉ NWA 6162
- ◉ SaU 005
- ◉ DaG 476
- ◉ NWA 4925
- ◉ NWA 5789
- ◉ Y980459
- ◉ Tissint
- ◆ NWA 6342
- ◇ ALH 77005
- ◇ Weighted mean

**Figure 2-6(a). AVS of shergottites: Δ³⁶S vs. Δ³³S.**

**Triangles = mafic; Circles = permafic; Diamonds = ultramafic. Solid-filled symbols = enriched source; Pattern-filled symbols = depleted source; Unfilled symbols = intermediate source. Weighted mean does not include NWA 2990, NWA 5960, Los Angeles, or Tissint. Error bars are 2σ.**

**Figure 2-6(b). Acid-soluble and total sulfate of shergottites and Chassigny: $\Delta^{36}S$ vs. $\Delta^{33}S$.**

**Triangles = mafic; Circles = permafic; Diamonds = ultramafic. Solid-filled symbols = enriched source; Pattern-filled symbols = depleted source; Unfilled symbols = intermediate source. Weighted mean does not include NWA 2990, NWA 5960, Los Angeles, or Tissint. Error bars are 2σ. Dashed lines indicate slopes formed by products of laboratory photochemistry experiments (Farquhar et al., 2000c, 2001).**

uncertainties in the data, the shergottite sulfates may also fit the array formed by products of $H_2S$ photochemistry experiments (Farquhar et al., 2000c). These two experiments show different relationships but the data do not allow this to be resolved.

The anomalous sulfur observed in the shergottites all carries a positive $\Delta^{33}S$, and may be the complement of anomalous sulfur in the nakhlites, which is characterized by negative $\Delta^{33}S$. The similar covariation between $\Delta^{36}S$ and $\Delta^{33}S$ in the nakhlites and shergottites could indicate the fingerprint of a single photochemical process. If this is true, then the opposite signs of nakhlite and shergottite $\Delta^{33}S$ may represent either a temporal change in transfer mechanism between atmospheric and surface reservoirs from the time of nakhlite alteration to the time of shergottite alteration, or a geographic difference in the deposition of sulfur with anomalous $\Delta^{33}S$. Some regions may have been characterized by [33]S enrichments while others were characterized by [33]S depletions. Alternatively, the differences in $\Delta^{33}S$ and the $\Delta^{36}S$-$\Delta^{33}S$ relationships could reflect distinct photochemical processes that are recorded in the nakhlites versus the shergottites.

There are two general pathways through which anomalous sulfur could have entered the shergottite parent rocks. The observation of S-MIF in the AVS fraction of NWA 2990/5960, Los Angeles, and Tissint implies its incorporation into igneous minerals through assimilation of surface materials bearing atmospherically-processed sulfur into ascending magmas. Similar arguments have been advanced to account for variations in mineralogy, trace element abundances, and oxygen isotopic compositions among the shergottites (e.g., Jones, 1989; Herd et al., 2002; Rumble and Irving, 2009). Jones (1989) proposed that the shergottite bulk compositions may be

70

approximated by mixing among three components: (1) a depleted mantle source similar to that which produced Chassigny and the nakhlites; (2) a source, possibly in the crust, enriched in light rare earth elements (LREE), with high Rb/Sr and (U, Th)/Pb ratios; and (3) a second crustal source depleted in LREE or in REE overall, but with highly enriched (U, Th)/Pb ratio. Herd et al. (2002) noted a correlation in the oxygen fugacity ($f$O$_2$) of basaltic shergottites and their $^{87}$Sr/$^{86}$Sr, $^{143}$Nd/$^{144}$Nd, and La/Yb ratios and suggested that the shergottite mantle source is reduced, with $f$O$_2$ controlled by assimilation of crustal material. Rumble and Irving (2009) reported variations in silicate oxygen isotopic compositions in the shergottites. They hypothesized that this could indicate assimilation of crustal minerals such as carbonates containing oxygen that had been photochemically processed in the atmosphere (Farquhar et al., 1998) into ascending magmas, producing localized heterogeneities in the oxygen isotopic composition of crystallizing silicates (Rumble and Irving, 2009). Applied to the sulfur data, this argument suggests that the S-MIF of NWA 2990/5960, Los Angeles, and Tissint was acquired by assimilation of crustal sulfur, presumably derived from elemental sulfur or sulfate aerosols that had been deposited on the martian surface after UV photochemical processing in the atmosphere. Upon incorporation into ascending magmas, the sulfur would have been reduced in the melt to form igneous sulfide minerals bearing the S-MIF signal. Note that the sulfur isotope ratios only provide direct evidence for incorporation of sulfur-bearing materials from the surface and cannot identify other lithologies that may have been assimilated contemporaneously. It is likely, however, that the assimilative events suggested by the anomalous AVS isotopic signatures also involved addition of

71

other minerals, evidence of which may be recorded in trace element abundances and other isotope systems.

Arguments for crustal assimilation models have been based in part on the correlation between the degree of incompatible element enrichment and the $fO_2$ of the enriched shergottite magmas, assuming that addition of surface materials with higher oxidation state would raise the late-stage $fO_2$ of the magma. Assimilation of sulfate to produce sulfide would raise the $fO_2$ of the magma, depending on the iron content of the magma and the quantity of sulfate added. A simplistic model of the reduction of assimilated Mg-sulfate by ferrous iron would be represented by the following reaction:

$$SiO_2(l) + MgSO_4(s) + 9FeO(l) \rightarrow 4Fe_2O_3(l) + FeS(po) + MgSiO_3(pyx) \qquad (1)$$
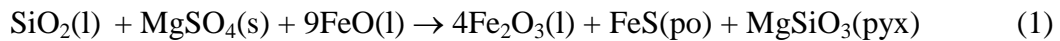
where $MgSO_4(s)$ indicates an unspecified solid sulfate phase. This reaction suggests that nine moles of reduced iron would be required to complete the reduction of one mole of sulfate to sulfide, producing one mole of FeS and four moles of $Fe_2O_3$. If the $Fe_2O_3$ on the right-hand side were replaced with $Fe_3O_4$, the reaction would be more representative of the mineralogy observed in martian meteorites:

$$SiO_2(l) + MgSO_4(s) + 13FeO(l) \rightarrow 4Fe_3O_4(s) + FeS(po) + MgSiO_3(pyx) \qquad (2)$$
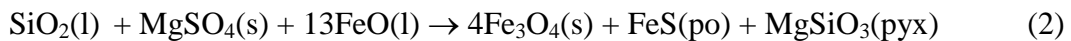
where $Fe_3O_4(s)$ indicates spinel solid solution. This reaction suggests that assimilation of $MgSO_4$ by a melt with high abundance of reduced iron would favor production of magnetite over hematite.

Preliminary studies of $fO_2$ from Fe-Ti oxide pairs in olivine-phyric shergottite NWA 6234 indicate that late-stage oxides in this meteorite and its pairs, including NWA 2990 and NWA 5960, formed at very oxidizing conditions of QFM + 0.3

72

(Gross et al., 2012). Taking NWA 2990 as an example, $188 \pm 4$ ppm sulfur was recovered from the AVS extraction step, or ~1.6 µmol/g. According to equation (2) above, assuming that all of the AVS fraction of NWA 2990 was derived from assimilation of surface sulfate in the form of $MgSO_4$, ~20.8 µmol/g of FeO would have been required to reduce this much sulfate, producing ~6.4 µmol/g of magnetite, as well.

Rubin et al. (2000) reported that the Los Angeles magma experienced late-stage $fO_2$ approximately at QFM. A similar estimate of 1 to 2 units below QFM was given by Xirouchakis et al. (2002). Warren et al. (2004) concluded that Los Angeles is the most "crustal" shergottite, based on its enrichment in incompatible elements (Rubin et al., 2000) and initial $^{143}Nd/^{144}Nd$ and $^{87}Sr/^{86}Sr$ ratios, which support a high degree of assimilation (Nyquist et al., 2001). However, Warren et al. (2004) also note that these trace element characteristics are similar to those of other enriched shergottites such as Shergotty and Zagami and that the $fO_2$ could have been controlled by differences in water content alone.

The observation of significant non-zero $\Delta^{33}S$ in the sulfate fractions of NWA 5718 and LAR 06319 but not in their AVS fractions indicates that these meteorites experienced different magmatic conditions than NWA 2990/5960, Los Angeles, and Tissint. While it appears that the magmas that produced the latter four meteorites reduced a portion of the sulfur acquired through assimilation of surface material to the $S^{2-}$ state, resulting in its incorporation into sulfide minerals, either this process did not occur in the magmas that produced NWA 5718 and LAR 06319 or it occurred to such a minor extent that their measured AVS compositions are dominated by the

original mantle-derived sulfur. This implies that the magmas that produced NWA 5718 and LAR 06319 were less reducing than those that produced NWA 2990/5960, Los Angeles, and Tissint, that their magmas cooled too quickly to allow for extensive reduction of assimilated sulfate to occur, or that the S-MIF observed in the sulfate fraction represents surface sulfate that was added to the parent rocks through post-crystallization alteration processes.

Alteration on Mars by low- or high-temperature S-MIF-bearing fluids after crystallization of monosulfide minerals was completed represents a second pathway for incorporating anomalous sulfur into the shergottites. This mechanism could have introduced S-MIF into sulfate phases without affecting the AVS composition. The presence of S-MIF in NWA 5718 and LAR 06319 sulfate but not AVS is consistent with this pathway. The lack of AVS data for NWA 5298, which also shows anomalous sulfate composition, does not allow discrimination between these two scenarios. The sulfur abundance of NWA 5298 was among the lower part of the range for shergottites, with $465 \pm 9$ ppm total sulfur, over 96% of which was recovered as sulfate. Hui et al. (2011) reported that REE patterns in NWA 5298 bulk rock, clinopyroxene, plagioclase, and phosphate indicate closed-system chemical behavior with no evidence for crustal contamination or post-crystallization disturbance of REE contents in those minerals. This suggests that this meteorite did not obtain its anomalous sulfate by assimilation of surface sediments, since that would likely have altered the REE patterns. Likewise, alteration by late-stage influx of sulfur-bearing fluid would be feasible only with assertion of severe constraints on the fluid composition, such that REE patterns were not affected.

74

Microscopic barite crystals, which have been interpreted as terrestrial alteration products, have been observed in NWA 5298 petrographic analyses, both as secondary crack-fill and as grains within clinopyroxene (Crozaz et al., 2003). This is not the source of the observed S-MIF, however. Incorporation of terrestrial sulfate from the Moroccan desert would instead dilute the S-MIF signal, and would reduce any pre-existing (martian) $\Delta^{33}$S anomaly.

Oxygen fugacity estimates for LAR 06319 indicate formation at $f$O$_2$ approximately QFM − 1.7, more reducing than NWA 2990/5960 and NWA 5298, but more oxidizing than depleted shergottites (Sarbadhikari et al., 2009). Like NWA 5718, LAR 06319 has AVS with mass-dependent isotopic composition, but in contrast to that meteorite, LAR 06319 sulfate shows $\delta^{34}$S of 6.71 ± 0.15‰, substantially more positive than typical for martian sulfate. It is possible that this indicates dilution of a martian S-MIF signal by terrestrial sulfate, thus reducing the $\Delta^{33}$S from an initially more positive value to the 0.057 ± 0.008‰ that we observe.

Sarbadhikari et al. (2009) reported that while LAR 06319 has a similar quantity of mafic minerals as olivine-phyric shergottites Y980459 and Dhofar 019, its rare earth element pattern is more consistent with those of LREE-enriched basaltic shergottites such as Shergotty and Los Angeles. Because the composition of early-trapped melt inclusions is similar to that of LAR 06319 whole rock, those authors concluded that for crustal assimilation to explain the enriched character of this meteorite, it would have had to occur prior to crystallization of the olivine megacrysts. For this reason, Sarbadhikari et al. (2009)  determined that LAR 06319 more likely derived from partial melting of an enriched and oxidized mantle reservoir, which did not involve

assimilation of crustal material. These arguments, combined with the presence of a S-MIF signal in the sulfate but not AVS, suggest that the S-MIF signal in LAR 06319 indicates alteration on Mars by a fluid containing anomalous sulfur.

The shergottite with the largest S-MIF signal, NWA 5718, has not been studied extensively to date by other workers. Wittke et al. (2010) reported that NWA 5718 is an enriched mafic shergottite, with higher REE abundance than petrologically similar meteorites NWA 2975/2986. NWA 5718 was among those shergottites with lower abundances of sulfur, yielding only $445 \pm 9$ ppm total sulfur, ~32% of which was sulfate. Its sulfate $\delta^{34}S$ of $0.55 \pm 0.15$‰ does not provide strong evidence for addition of terrestrial sulfate. The $\Delta^{33}S$ of $0.260 \pm 0.008$‰ in its sulfate but $-0.004 \pm 0.008$‰ in its AVS fraction implies that the anomalous sulfate could have been introduced as a weathering product, similar to LAR 06319. The lack of any sulfur anomaly in the AVS fraction also argues against substantial reduction of assimilated sulfur within the melt. As more information about this meteorite comes to light through analyses of other elements, the mechanism of S-MIF introduction may become more clear.

In summary, the above discussion suggests that the S-MIF signal observed in shergottite sulfate could have been derived either by assimilation of solid crustal material by the magma or by post-crystallization alteration of the meteorite parent rocks by fluids containing anomalous sulfur. In the former case, the solid material could have been assimilated as elemental sulfur or sulfate minerals followed by reduction in the melt to form sulfides, as observed in NWA 2990/5960, Los Angeles, and Tissint. If the late-stage $fO_2$ allowed for minimal reduction, the AVS isotopic composition could be dominated by an original mass-dependent mantle-derived

signature that masks evidence for assimilation into monosulfide minerals while maintaining S-MIF composition in sulfate. This could explain the observation of anomalous sulfate but mass-dependent AVS in NWA 5718 and LAR 06319. Alternatively, the latter two meteorites could preserve evidence for post-crystallization addition of anomalous sulfate through aqueous alteration processes. This alteration would have had to occur on Mars rather than on Earth to introduce the S-MIF signal. Additional weathering in the terrestrial environment may have contributed to their total sulfate contents and diluted the anomalous martian $\Delta^{33}$S.

## 2.5    Conclusions

Analysis of AVS fractions, representing igneous monosulfide minerals, from 30 shergottites has yielded the first estimate of the juvenile martian sulfur isotopic composition, which is identical within measurement errors to CDT. However, four of these meteorites (NWA 2990/5960, Los Angeles, and Tissint) revealed mass-independent sulfur characterized by $\Delta^{33}$S of 0.024 ± 0.008‰ to 0.093 ± 0.008‰ in their AVS fractions. Mass-independently fractionated sulfate was found in three of these meteorites, as well as in three additional shergottites (NWA 5298, NWA 5718, and LAR 06319), with $\Delta^{33}$S as high as 0.260 ± 0.008‰. The anomalous sulfur was most likely generated through UV photochemical processing of volcanic sulfur-bearing gases in the martian atmosphere, followed by deposition of products carrying S-MIF onto the planet's surface and later introduction into shergottite parent rocks. In the case of NWA 2990/5960, Los Angeles, and Tissint, anomalous sulfur was likely introduced into their magmas, followed by partial reduction of the assimilated sulfur

within the melt to form igneous sulfide minerals, producing the S-MIF signal observed in AVS fractions. Aqueous alteration by fluids bearing photochemically processed sulfur after crystallization of the meteorite parent rocks could have introduced S-MIF into sulfate phases of NWA 5718 and LAR 06319 without affecting the AVS compositions. These processes would have had to occur on Mars to introduce the anomalous sulfur that is observed, since influx of modern terrestrial sulfate would not introduce S-MIF. In addition, weathering of igneous sulfides characterized by mass-dependent sulfur composition, either on Mars on Earth, would not produce a S-MIF signal.

# Chapter 3: Sulfur Isotopes in the Nakhlites Suggest Assimilation of Surficial Deposits and a Multi-stage Alteration History[1,2]

[1] The text, tables, and figures in this chapter were written/created by H. B. Franz.

[2] All analyses presented in this chapter were performed by H. B. Franz.

## 3.1    Introduction

Mars exploration missions have revealed the presence of sulfate minerals at significant abundance over most of the planet's surface (e.g., Baird et al., 1976; Clark et al., 1976; Bell et al., 2000, Rieder et al., 1997; Lane et al., 2004; Johnson et al., 2007; Klingelhöfer et al., 2004; Rieder et al., 2004; Squyres et al., 2004; Langevin et al., 2005; Gendrin et al., 2005; Wiseman et al., 2008; Murchie et al., 2009; Lichtenberg et al., 2010). The formation of the oxoanion, sulfate, has been attributed to a variety of mechanisms, including oxidation of sulfides in volcanic ash and basaltic rocks through interaction with groundwater or hydrothermal solutions, impact-related oxidation of sulfides, and photochemical oxidation of sulfur-bearing gases introduced into the martian atmosphere by volcanic and hydrothermal activity (e.g., Burns, 1993; Banin et al., 1997; Bibring et al., 2005; Gendrin et al., 2005; Grotzinger et al., 2005; Knauth et al., 2005; Zolotov and Shock, 2005; Arvidson et al., 2006; Andrews-Hanna et al., 2010).   The deposition and concentration of the sulfate oxoanion in minerals have been attributed to further chemical and physical processing involving dissolution of sulfate in water, followed by precipitation of various sulfate minerals.   The martian inventory of sulfate minerals also includes

evidence that some were formed in high-temperature environments associated with the transport, emplacement, and subsequent cooling of lava flows. Studies of martian meteorites have provided significant information about sulfide and sulfate minerals that formed on Mars, including clues to the origin and processing of sulfur that occurred prior to the meteorites' ejection from the planet (e.g., Bunch and Reid, 1975; Clark and Baird, 1976; Gibson and Moore, 1983; Burgess et al., 1989; Gooding and Muenow, 1986; McSween et al., 1996; Bridges and Grady, 2000; Lorand et al., 2005; Chevrier et al., 2011). In some cases, alteration minerals formed on Earth during the terrestrial residence of certain meteorites still retain geochemical signatures of martian chemistry inherited from the precursor sulfur-bearing minerals that formed on Mars (e.g, Farquhar et al., 2000c, 2007).

The focus of this chapter is the nakhlites, a group comprised of eight distinct martian meteorites (accounting for pairs) sharing similar clinopyroxene-dominated mineralogy, crystallization ages of ~1.3 Ga, and cosmic ray exposure ages of 10-12 Ma. These shared characteristics have been interpreted as evidence that the nakhlites derive from the same igneous complex on Mars and were excavated from Mars' surface and ejected into Earth-crossing orbits by an impact that occurred within the past 20 million years (e.g., Stauffer, 1962; Papanastassiou and Wasserburg, 1974; Nakamura et al., 1982; Harvey and McSween, 1992a, 1992b; Wadhwa and Crozaz, 1995; Eugster et al., 2002; Shih et al., 2002; Garrison et al., 2005).

The nakhlites preserve multiple lines of evidence for interaction with liquid water at some time during their history on Mars, including association of sulfate minerals with "iddingsite" alteration material and isotopic compositions that imply formation

by martian surface processes (e.g., Bunch and Reid, 1975; Gooding et al., 1991; Treiman et al., 1993; Bridges and Grady, 2000; Treiman and Goodrich, 2002; Changela and Bridges, 2010, Farquhar and Thiemens, 2000; Farquhar et al., 2000c; 2007). Previous studies of the sulfur isotopic composition of nakhlites have documented mass-independent (S-MIF) signatures, ascribed to photochemical reactions and oxidation of volcanic gases in the martian atmosphere (Farquhar et al., 2000c; Farquhar et al., 2007a; Kim and Farquhar, 2008). Sulfate from Nakhla has also been shown to carry a mass-independent oxygen isotopic signal distinct from those of carbonates and hydrous minerals, implying different pathways for the oxidants involved in their formation (Karlsson et al., 1992; Romanek et al., 1998; Farquhar and Thiemens, 2000).

Numerous questions have been raised by these studies concerning the relationships between martian sulfide and sulfate minerals, the pathways leading to formation of sulfate, and the possibility of assimilation and incorporation of sulfosalts into magmas in the subsurface and at the surface of Mars. Adding to the intrigue is the recent observation that the S-MIF signature observed in nakhlites differs from mass-independent signals found in terrestrial analogs, including present-day sulfate aerosols, sulfate from the ice core record, and sulfate and sulfide from the ancient Earth (older than ~2.4 Ga) (Farquhar et al., 2000a; Lee et al., 2001; Romero et al., 2003; Baroni et al., 2007). Here I report new measurements of $\delta^{34}S$, $\Delta^{33}S$, and $\Delta^{36}S$ from Y000593, NWA 6148, and NWA 998 obtained by sequential chemical processing of whole-rock material, designed to extract sulfur from multiple mineral phases. Sulfate fractions of all three meteorites reveal mass-independent sulfur

isotopic composition, with negative values of $\Delta^{33}$S bracketed by those previously determined for sulfate in Nakhla (Farquhar et al., 2000c, 2007a). Results provide evidence for spatially and/or temporally localized assimilation of atmospherically processed sulfur into magmas in the nakhlite igneous complex and suggest that the aqueous alteration of these meteorites occurred during multiple events.

## 3.2 Methods

A sequential chemical extraction procedure was performed on powdered whole rock that allowed the measurement of sulfur isotope ratios for different mineral phases. For each meteorite, rock fragments with total mass of 1.5 to 2 grams were disaggregated in a steel mortar and then ground more finely with an agate mortar and pestle. The powder was transferred to a 15 mL centrifuge tube along with 10 mL of Milli-Q water. The tube was sonicated for 20 minutes to promote the dissolution of water-soluble sulfate from the sample. The tube was then centrifuged to allow separation of the solution from the solid sample by pipette. This process was repeated a second time to yield a total of 20 mL of solution containing water-soluble sulfate, which were transferred to a boiling flask. A few drops of 0.5 N HCl were added to the flask to reduce the pH to ~3, followed by several drops of 1 M $BaCl_2$ solution to precipitate any dissolved sulfate as $BaSO_4$. The flask was then allowed to evaporate to dryness before the sulfate was reduced by a procedure similar to that described below for acid-soluble sulfate.

The powdered sample was transferred from the centrifuge tube to a double-necked boiling flask with silicone septum. The flask was assembled with a water-

cooled condenser, a bubbler filled with Milli-Q water, and a sulfide trap into a distillation apparatus similar to that described by Forrest and Newman (1977). All ground glass joints were sealed with PTFE sleeves. The apparatus was assembled, checked for leaks, and then purged with nitrogen for at least 10 minutes. For the first extraction step, 25 mL of 5 N HCl were injected into the boiling flask through the septum with a syringe. The solution was then heated to ~60 °C. Acid-volatile sulfur (AVS) in the sample, presumed to consist primarily of monosulfides, reacted with the HCl to evolve $H_2S$ gas, which was captured in an acidic $AgNO_3$ solution.

After the AVS extraction step, the sulfide trap with capture solution was replaced, and 25 mL of a solution containing HI, $H_3PO_2$, and 12 N HCl ("Thode solution"; Thode et al., 1961; Mayer and Krouse, 2004) were added to the boiling flask, which was then heated to ~85 ℃ to extract acid-soluble sulfur from the sample. Upon completion of this reaction, the flask was cooled and its contents were transferred to 30 mL centrifuge tubes. After separation of the acid solution from the solid sample powder, the sample was rinsed with Milli-Q water several times to clean it before being transferred back to the double-necked boiling flask.

The following day, the distillation apparatus was reassembled, checked for leaks, and again purged with nitrogen for at least 10 minutes. A fresh sulfide trap with $AgNO_3$ capture solution was installed. For the final reduction step, 15 mL each of acidic chromium(II) solution and 5 N HCl were injected into the boiling flask, which was then heated to ~60 ℃ for extraction of disulfides and elemental sulfur.

The $H_2S$ evolved in each step of the extraction process reacted with the $AgNO_3$ in the capture solution to form $Ag_2S$, which was cleaned with Milli-Q water and 1 M

NH$_4$OH solution, then dried. The Ag$_2$S was converted to SF$_6$ by reaction with 250 µmol of fluorine gas in a nickel reaction vessel at 250° C for 8 hours. The SF$_6$ was subsequently condensed from the residual F$_2$ into a trap cooled with liquid nitrogen. Excess F$_2$ was passivated by reaction with KBr salt. Replacement of the liquid nitrogen coolant on the trap with ethanol slush at -115 °C allowed distillation of the SF$_6$ from the trap into the liquid-nitrogen-cooled injection loop of a gas chromatograph (GC). The SF$_6$ was purified by a 1/8-inch diameter, 6-foot long Molecular Sieve 5A GC column, followed by a 1/8-inch diameter, 12-foot long Haysep-Q™ GC column, with helium carrier gas flow rate of 20 mL/min. After its elution from the GC, the SF$_6$ was captured in spiral glass traps cooled with liquid nitrogen, then transferred to the bellows of a Thermofinnigan MAT 253 dual-inlet gas source mass spectrometer. The sulfur isotopic composition of the SF$_6$ was measured by monitoring SF$_5^+$ ion beams at *m/z* of 127, 128, 129, and 131 Da. Uncertainties, estimated from repeated analyses of the sulfur isotopic ratios of IAEA reference materials, are generally better than 0.15‰, 0.008‰, and 0.15‰ (1σ) for δ$^{34}$S, Δ$^{33}$S, and Δ$^{36}$S, respectively.

## 3.3 Results

Values for δ$^{34}$S, Δ$^{33}$S, and Δ$^{36}$S were normalized to measurements of Cañon Diablo Troilite (CDT) to facilitate comparison with results from previous studies. The results for sulfur isotopic compositions and concentrations obtained via chemical extraction are presented in Table 3-1 and are briefly summarized as follows. The AVS extraction step of all three meteorites produced negligible yields, as did the CRS

extraction of Y000593 and NWA 998 and the water-soluble sulfate extraction of NWA 998.

**Table 3-1. Sulfur isotopic compositions and sulfur concentrations of nakhlites.**

**Data are normalized to measurements of CDT. 1σ uncertainties in parentheses.**

| Sample | Sulfur concentration (± 2% of value) | $\delta^{34}S$ | $\Delta^{33}S$ | $\Delta^{36}S$ |
|---|---|---|---|---|
| Y000593 | | | | |
| Water-soluble sulfate | 11 ppm | 10.03 (0.15) | -0.576 (0.008) | 0.18 (0.15) |
| Acid-soluble sulfate | 23 ppm | 2.93 (0.15) | -0.224 (0.008) | 0.25 (0.15) |
| | | | | |
| NWA 6148 | | | | |
| Water-soluble sulfate | 1 ppm | 4.38 (0.15) | -0.038 (0.030) | * |
| Acid-soluble sulfate | 79 ppm | 2.26 (0.15) | -0.070 (0.008) | 0.18 (0.15) |
| | | | | |
| NWA 998 | | | | |
| Acid-soluble sulfate | 63 ppm | 1.86 (0.15) | -0.084 (0.008) | -0.02 (0.15) |

*Sample was too small for accurate measurement of this quantity.

Of these nakhlites, Y000593 proved particularly low in sulfur, showing water-soluble sulfate and acid-soluble sulfate concentrations of 11 ± 1 ppm and 23 ± 1 ppm, respectively. The $\delta^{34}S$ of water-soluble sulfate (10.03 ± 0.15‰) was considerably more positive than that of acid-soluble sulfate (2.93 ± 0.15‰). The water-soluble sulfate also showed a larger $^{33}S$ anomaly, with $\Delta^{33}S$ of -0.576 ± 0.008‰, compared to $\Delta^{33}S$ of -0.224 ± 0.008‰ for the acid-soluble sulfate. The $\Delta^{36}S$ of these two fractions was identical within measurement precision, giving 0.18 ± 0.15‰ for the water-soluble sulfate and 0.25 ± 0.015‰ for the acid-soluble sulfate.

NWA 6148 was found to have a very small water-soluble sulfate fraction with ~1 ppm concentration and acid-soluble sulfate of 79 ± 2 ppm. Like Y000593, NWA

6148 revealed water-soluble sulfate enriched in $^{34}$S, with $\delta^{34}$S of 4.38 ± 0.15‰. The $\delta^{34}$S of 2.26 ± 0.15‰ for acid-soluble sulfate was similar to that of Y000593. Both sulfate fractions showed small negative $^{33}$S anomalies, with $\Delta^{33}$S of -0.038 ± 0.030‰ for water-soluble sulfate and -0.070 ± 0.008‰ for acid-soluble sulfate. The $\Delta^{36}$S of acid-soluble sulfate was 0.18 ± 0.15‰, while the water-soluble sulfate fraction was too small for accurate determination of $\Delta^{36}$S.

The only sulfur fraction of NWA 998 large enough for isotopic analysis was the acid-soluble sulfate, with concentration of 63 ± 2 ppm. Its isotopic composition was almost identical to that of NWA 6148, with $\delta^{34}$S of 1.86 ± 0.15‰, $\Delta^{33}$S of -0.084 ± 0.008‰, and $\Delta^{36}$S of -0.02 ± 0.15‰.

Data for Y000593, NWA 6148, and NWA 998 sulfate isotopic compositions are shown in Figures 3-1 and 3-2, along with previously reported data for other nakhlites.
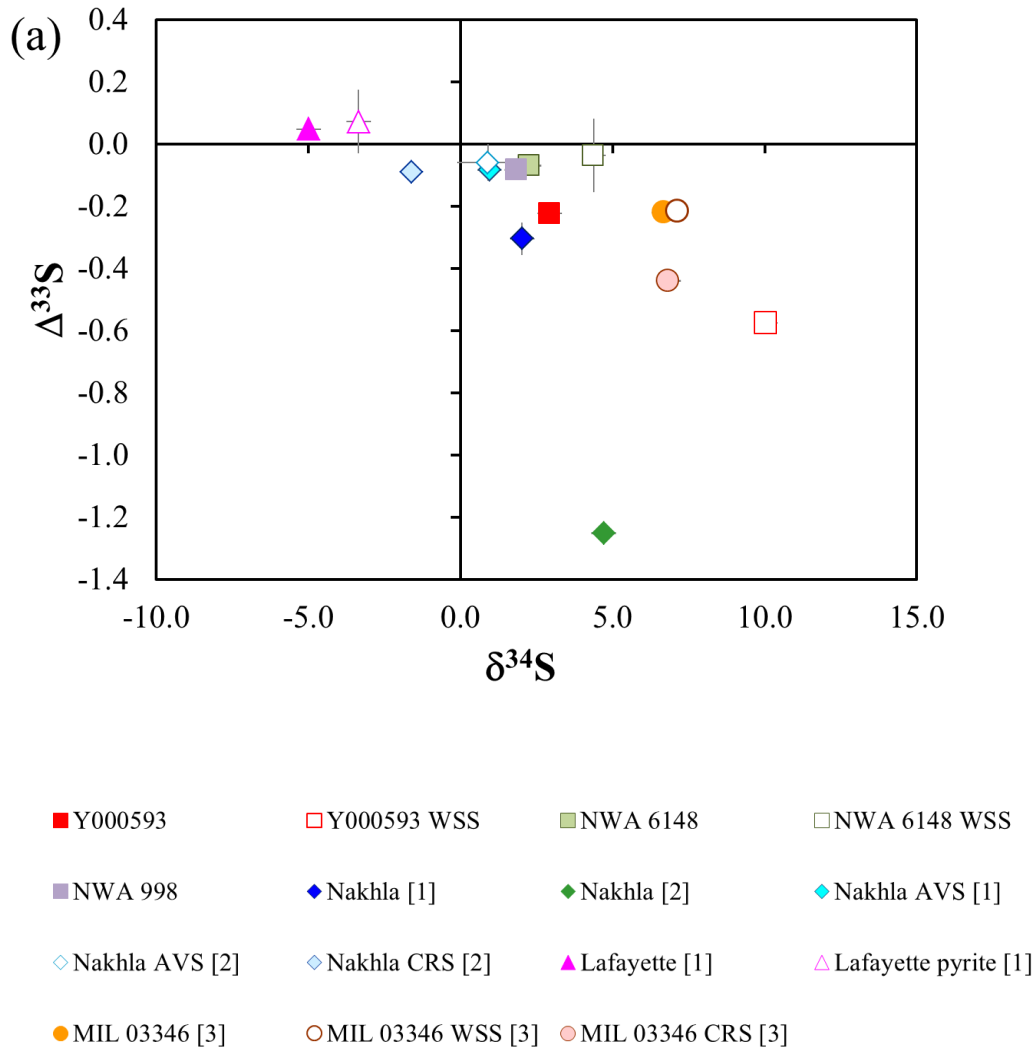
**Figure 3-1(a). $\Delta^{33}S$ vs. $\delta^{34}S$ for nakhlites.**

**Acid-soluble sulfate (no parentheses), water-soluble sulfate (WSS), acid-volatile sulfur (AVS), and pyrite or chromium-reducible sulfur (CRS). Y000593, NWA 6148, and NWA 998, this study; other nakhlites from previous studies. Error bars represent $2\sigma$ deviations; if error bars are not visible, they are smaller than the symbol. [1] Farquhar et al., 2000c; [2] Farquhar et al., 2007a; [3] Kim and Farquhar, 2008.**
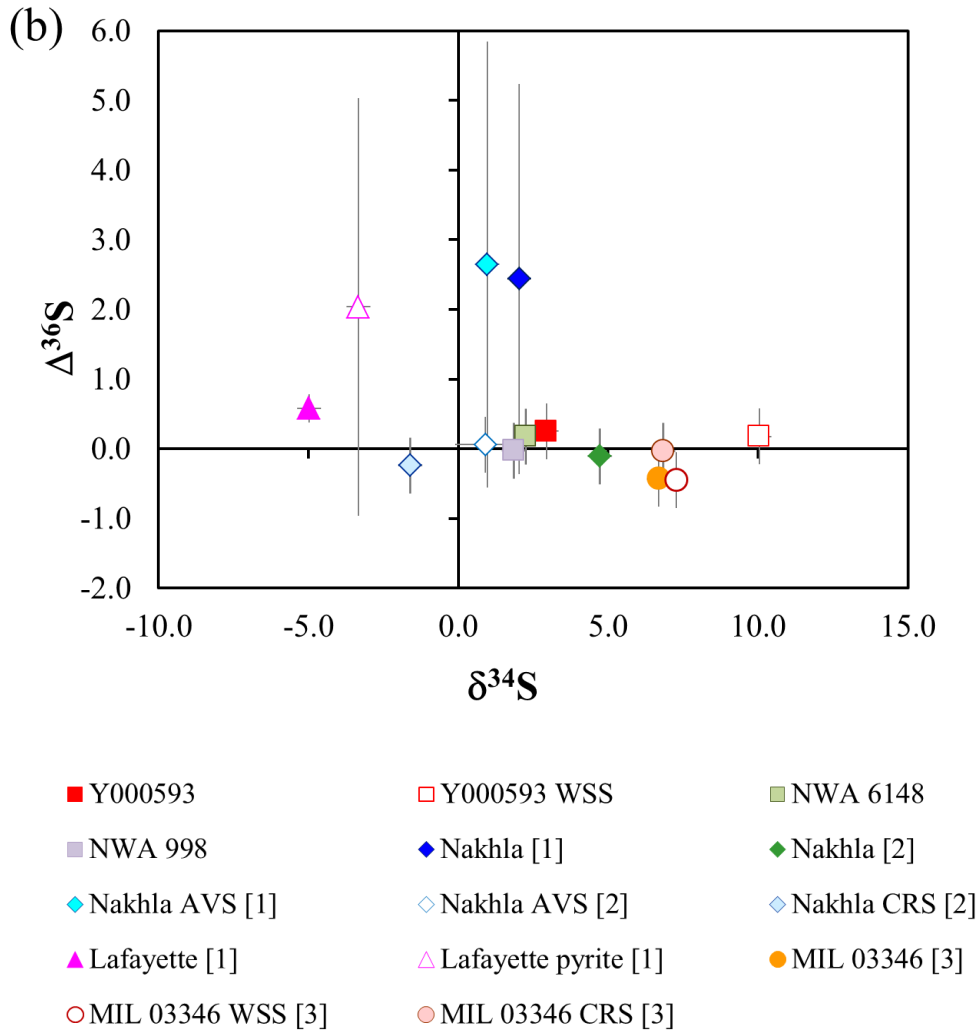
**Figure 3-1(b). $\Delta^{36}$S vs. $\delta^{34}$S for nakhlites.**

**Acid-soluble sulfate (no parentheses), water-soluble sulfate (WSS), acid-volatile sulfur (AVS), and pyrite or chromium-reducible sulfur (CRS). Y000593, NWA 6148, and NWA 998, this study; other nakhlites from previous studies. Error bars represent 2σ deviations. [1] Farquhar et al., 2000c; [2] Farquhar et al., 2007a; [3] Kim and Farquhar, 2008.**

## 3.4    Discussion

### 3.4.1    Sulfur Concentrations

Chevrier et al. (2011) found magmatic sulfides in the nakhlites NWA 817, NWA 998, Nakhla, and Governador Valadares to be only ~20% as high in abundance as is typical of shergottites. The current study observed even lower nakhlite sulfur concentrations. The sample of Y000593 analyzed in this study showed unexpectedly low abundance of sulfur, with zero yields for both AVS and CRS and low concentrations of both water-soluble and acid-soluble sulfate phases. It is unclear why this was observed. Iron sulfide, tentatively identified as either pyrrhotite or pyrite, has been detected in Y000593 mesostasis (Mikouchi et al., 2003; Imae et al., 2005). Rochette et al. (2005) reported that while pyrrhotite is very rare in nakhlites, Y000593 is believed to contain a significant quantity of pyrrhotite, based on magnetic properties. The abundance of mesostasis, where sulfides in martian meteorites are typically concentrated, is ~10 vol% in Y000593, intermediate to the abundances in Nakhla and Lafayette (7-8%) and NWA 817 and MIL 03346 (20-24%) (Mikouchi et al., 2003, 2006; Imae and Ikeda, 2007). In the sequential extraction procedure, pyrrhotite should be reduced during the AVS step and pyrite during the CRS step. Farquhar et al. (2007a) obtained Nakhla sulfur concentrations of 12 ppm AVS and 94 ppm CRS by a similar sequential extraction procedure, indicating the presence of sulfide minerals, albeit at low abundance. Burgess et al. (1989) reported 75 ppm of reduced sulfur in Nakhla. However, MIL 03346, with a larger quantity of mesostasis,

like Y000593 produced negligible AVS yield (Kim and Farquhar, 2008), although pyrrhotite grains were observed in petrographic analysis (Chapter 4 of this work).

The abundance of sulfate in Nakhla was measured as 170 ppm (Farquhar et al., 2007a), but Y000593 yielded a total sulfate of only 34 ppm. It did, however, show significant, clearly-resolved S-MIF signals in its sulfate fractions, with water-soluble sulfate $\Delta^{33}$S anomaly second in magnitude only to sulfate of Nakhla (Farquhar et al., 2007a). The implications of the S-MIF signature are further discussed in the next section.

Like Y000593 and MIL 03346, NWA 6148 and NWA 998 produced negligible AVS. NWA 6148 did contain a small amount of CRS, but NWA 998 produced none. Treiman and Irving (2008) detected pyrrhotite and chalcopyrite in the mesostasis of one NWA 998 petrographic section, but the grains were commonly altered on their edges to hematite. They found another section to contain almost no sulfide but more hematite, suggesting that the original sulfides had been completely oxidized. Chevrier et al. (2011) similarly observed that sulfides in NWA 998 were 50% altered, with iron hydroxides and oxyhydroxides occurring either at grain boundaries or as pseudomorphs. They saw no pyrite, consistent with the lack of yield from the CRS chemical extraction step. Treiman and Irving (2008) observed structured distribution of apatite in NWA 998, such that apatite is concentrated in planar zones separating apatite-free regions. They interpreted this finding, in conjunction with the low abundance of mesostasis in this meteorite, to indicate that late magma was expelled from large portions of the cumulate, possibly along fractures and channels.

Detailed petrography of NWA 6148 has not yet been reported. Jambon et al. (2010) estimated that NWA 5790, believed to be paired with NWA 6148, contains ~40 vol% glassy mesostasis, the highest of any nakhlite, but did not mention the presence of sulfides.

Collectively, these results suggest that these meteorites carry sulfur in heterogeneously-distributed minor mineral phases. Further implications of these observations are discussed below.

### 3.4.2   Implications for the Origin of Sulfate in the Nakhlites

Like other nakhlites, Y000593 and NWA 998 contain "iddingsite," a reddish-brown alteration product characterized by Fe-rich smectites and oxyhydroxides, carbonates, and sulfates that occurs along olivine fractures (e.g., Bunch and Reid, 1975; Gooding et al., 1991; Harvey and McSween, 1992a; Treiman et al., 1993; Bridges and Grady, 2000; Treiman and Goodrich, 2002; Treiman and Irving, 2008; Noguchi et al., 2009; Changela and Bridges, 2010). These veins appear to be pre-terrestrial based on cross-cutting relationships with cracks and fusion crust (e.g., Gooding et al., 1991; Treiman et al., 1993; Bridges and Grady, 2000). Misawa et al. (2003) reported that Rb-Sr dating of olivine separates from Y000593 suggests that an aqueous alteration event occurred at approximately $614 \pm 29$ to $650 \pm 80$ Ma. These findings coincide with results from K-Ar dating of Lafayette, which indicated an iddingsite formation age of $670 \pm 91$ Ma (Swindle et al., 2000).

In addition to iddingsite, Y000593 contains pre-terrestrial laihunite, formed by fluid-assisted high-temperature oxidation of olivine, and jarosite of less certain origin that is associated with iddingsite veins (Noguchi et al., 2009). Based on textural

91

relationships and thermal stabilities, Noguchi et al. (2009) determined that the laihunite formed prior to the iddingsite. The fact that laihunite also forms under alkaline rather than acidic conditions asserts an additional constraint on the formation history of these phases (Iishi et al., 1997; Noguchi et al., 2009). Noguchi et al. (2009) argued that the presence of jarosite in both Y000593 and MIL 03346 suggests that the near-surface nakhlites may have experienced a late-stage acidic oxidation event. This is consistent with the hypothesis of a global acidic aqueous reservoir posed by Greenwood and Blake (2006), based on positive correlations between sulfur, chlorine, and phosphorus at both Mars Exploration Rover landing sites. Vicenzi et al. (2007b) reported significant deuterium enrichment in jarosite veins of MIL 03346, indicating a martian origin, and noted that a number of the veins were truncated by fusion crust. Vicenzi et al. (2007a) reported that the jarosite veins in MIL 03346 cross-cut phyllosilicate-bearing veins, suggesting that the sulfate formed during the last stages of alteration, characterized by a shift from neutral pH to acidic fluids. McCubbin et al. (2009) determined that at least some of the jarosite in MIL 03346 formed from magmatic fluid within acidic microenvironments in melt inclusions, isolated from external input. However, Hallis and Taylor (2011) noted that the cleavage structure of the host augite examined by McCubbin et al. (2009) could have allowed breaches to occur, and thus the jarosite could have been acquired through an exogenous, perhaps even terrestrial, source. Thus the martian origin of jarosite in the nakhlites continues to be debated.

The $\delta^{34}S$ of acid-soluble sulfate in Y000593 was 2.93 ± 0.15‰, similar to the value reported for Nakhla total sulfate by Farquhar et al. (2000c). The $\delta^{34}S$ of water-

soluble sulfate was substantially more positive at $10.03 \pm 0.15$‰. This is among the most positive values of $\delta^{34}S$ reported for martian meteorites to date, possibly reflecting sulfate formed on Mars, sulfate formed on Earth, or a combination of these. However, the significantly negative $\Delta^{33}S$ values of sulfate minerals measured in Y000593 indicate that like other nakhlites, this meteorite carries sulfur that has experienced isotopic fractionation by a process that does not obey mass-dependent rules. According to arguments of Farquhar et al. (2000c), the most likely candidate is photochemical processing of sulfur-bearing gases in the martian atmosphere. The source of these gases could be volcanic activity, release of sulfur from the regolith during contact heating of rocks, or photochemical decomposition of sulfate in surface minerals or dust (Muhkin et al., 1996; Farquhar et al., 2000; Navrotsky et al., 2005). The photochemically altered sulfur could have undergone gas-phase oxidation in the atmosphere to form sulfate aerosols that were later deposited on the planet's surface or exchanged isotopically with surface minerals (Settle, 1979; Farquhar et al., 2000). Anomalous sulfur could have been subsequently incorporated into the nakhlite unit either by aqueous alteration event(s) or through assimilation of surface sulfate into ascending magma (Jones, 1989; Herd et al., 2002; Rumble and Irving, 2009).

In addition, since $SO_2$ photochemistry generates products enriched in $^{34}S$, incorporation of photochemically processed sulfur into surface rocks also represents a potential mechanism for introducing variable $\delta^{34}S$ as observed in the nakhlites and ALH 84001 (Farquhar et al., 2000c, 2001). Isotopically heavy pyrite grains, with $\delta^{34}S$ as high as $7.8 \pm 0.65$‰, have previously been reported for ALH 84001 by Shearer et al. (1996) and Greenwood et al. (1997). Values of $\delta^{34}S$ reported for Lafayette lie at

the opposite end of the range, representing the lightest sulfur measured in martian meteorites. Farquhar et al. (2000c) reported $\delta^{34}S$ of -4.98 ± 0.2‰ for sulfate and -3.34 ± 0.2‰ for pyrite in Lafayette, while Greenwood et al. (2000) measured $\delta^{34}S$ as light as -6.4 ± 2.1‰ for Lafayette pyrrhotite. Collectively, these observations suggest that the current sulfur isotopic compositions of the nakhlites and ALH 84001 reflect a complex multi-stage history potentially involving aqueous alteration, isotopic exchange, oxidation and reduction reactions, and both high and low temperature processes.

It is possible that terrestrial sulfate was introduced to the nakhlites during their residence on Earth before collection. Wadhwa et al. (2004) found evidence from trace element patterns that Y000593 experienced severe weathering in the Antarctic environment, including the addition of LREE. They noted, however, that Ce anomalies observed in augite grains did not apply to whole rock analyses, suggesting that the LREE enrichment occurred in microenvironments at length scales of hundreds of micrometers or less. Seawater sulfate carries an average $\delta^{34}S$ of ~21‰ (Paytan et al., 1998). A small amount of terrestrial sulfate with this composition mixed with martian sulfate could raise the $\delta^{34}S$ while retaining an anomalous $\Delta^{33}S$ signal. However, the low concentrations of sulfate and the significant $\Delta^{33}S$ anomaly allow for only very limited quantities of terrestrial input, analogous to the findings of Wadhwa et al. (2004) for trace elements. The majority of the sulfate in Y000593 must be pre-terrestrial, since modern terrestrial sulfate does not possess the negative $\Delta^{33}S$ observed in Y000593.

Hallis and Taylor (2011) also report evidence for extensive Antarctic weathering of MIL 03346 and its pairs. Those authors noted a gradient in abundance and mineralogical composition of sulfates with distance from the exterior surface, including a decrease in gypsum occurrences and an absence of jarosite toward the interior of the meteorite. Like Y000593, MIL 03346 showed elevated values of $\delta^{34}$S compared to Nakhla, with 7.1 ± 0.2‰ for water-soluble sulfate and 6.7 ± 0.2‰ for average acid-soluble sulfate (Kim and Farquhar, 2008). In contrast, Nakhla total sulfate showed $\delta^{34}$S of 2.03 ± 0.2‰ (Farquhar et al., 2000c) and 4.7 ± 0.2‰ (Farquhar et al., 2007a). Since Nakhla was a meteorite fall and thus collected immediately after arrival on Earth, it should show minimal effects from terrestrial contamination. As with Y000593, the enriched signature of MIL 03346 water-soluble sulfate may reflect input of terrestrial sulfate, which would imply dilution of the intrinsic martian sulfur and decrease of the true $\Delta^{33}$S magnitude. The agreement between values for the water-soluble and acid-soluble sulfate fractions of MIL 03346, which both showed $\Delta^{33}$S of -0.22 ± 0.01‰ (Kim and Farquhar, 2008), differs from Y000593, in which the water-soluble sulfate fraction actually showed significantly more negative $\Delta^{33}$S than the acid-soluble fraction. Since it is possible that the enrichments in $\delta^{34}$S observed in these meteorites reflect photochemical processes on Mars, the contribution of terrestrial sulfate to the samples analyzed remains uncertain.

As a hot-desert find, NWA 998 shows more evidence for terrestrial alteration than the Antarctic nakhlites, including disturbance of Sm-Nd and Pb-Pb systems (Carlson and Irving, 2004) and addition of LREE (Wadhwa et al., 2004). Bridges and Hicks (2011) also reported jarosite in NWA 5790 (paired with NWA 6148) believed to

95

represent a terrestrial weathering product. Contrary to Y000593, both NWA 998 and NWA 6148 display comparatively minor sulfur isotope anomalies. The $\Delta^{33}S$ of -0.070 $\pm$ 0.008‰ for acid-soluble sulfate and -0.038 $\pm$ 0.030‰ for water-soluble sulfate of NWA 6148 and -0.084 $\pm$ 0.008‰ for acid-soluble sulfate of NWA 998 match within error the $\Delta^{33}S$ of Nakhla AVS (Farquhar et al., 2000c, 2007a). Values of $\delta^{34}S$ range from 1.86 $\pm$ 0.15‰ to 4.38 $\pm$ 0.15‰, the latter representing the water-soluble sulfate fraction of NWA 6148 and matching within error the $\delta^{34}S$ of 4.7 $\pm$ 0.2‰ measured for Nakhla sulfate by Farquhar et al. (2007a). These values of $\delta^{34}S$ are not consistent with significant terrestrial sulfate input, especially given that Nakhla is a fall and was not subjected to extensive terrestrial weathering.

*3.4.3    Assessment of Sulfur Results in Terms of Models for Nakhlite Relative Burial Depths*

The relative abundance of mesostasis in the nakhlites, in conjunction with other systematic differences related primarily to cooling rate, has been interpreted as an indicator of their varying burial depths (Mikouchi et al., 2006; Day et al., 2006; Chevrier et al., 2011). Mikouchi and Miyamoto (2002) estimated nakhlite cooling rates based on analysis of Fe-Mg and Ca zoning profiles in olivines. They assumed that the initial core compositions of nakhlite olivines were uniform and that the observed differences in zoning profiles were produced by varying degrees of subsolidus atomic diffusion related to temperature. Mikouchi and Miyamoto (2002) took the core composition of NWA 817 olivine as representative of the initial composition for all nakhlites, since the olivine and augite cores from that meteorite

appear to be nearly in Fe-Mg equilibrium (Mikouchi and Miyamoto, 2001). They modeled Fe-Mg diffusion based on diffusion rates of Misener (1974), modified for an oxygen fugacity at the QFM buffer, as estimated for the nakhlites (Reid and Bunch, 1975). The recent discovery of the NWA 5790 nakhlite prompted a revision of their assumptions, since this meteorite displays olivine cores significantly more Fe-rich than those of the other nakhlites, suggesting that its olivines may have crystallized from evolving intercumulus melt (Mikouchi et al., 2012). Their revised calculations incorporated variable initial olivine core compositions based on the abundance of mesostasis. Analyses by multiple workers places NWA 5790 at the top of the pile (Jambon et al., 2010; Mikouchi et al., 2012). Mikouchi et al. (2012) estimate the following burial depths for the other nakhlites: NWA 817 ~1-2 m, MIL 03346 ~4 m, Y000593 ~7 m, Nakhla and Governador Valadares ~10 m, and Lafayette and NWA 998 > 30 m.

It is of interest to evaluate the relative sulfur isotopic compositions of the nakhlites in light of this hypothesis. Greenwood et al. (2000) argued that the sequence of decreasing $\delta^{34}S$ for sulfides of Nakhla, Governador Valadares, and Lafayette may reflect increasing degrees of subsolidus re-equilibration during late-stage nakhlite magmatism, prior to a later low-temperature alteration event that resulted in iddingsite formation. This later event was addressed by Bridges and Grady (2000), who developed a model for formation of the alteration assemblages in these meteorites through progressive evaporation of a low-temperature acidic brine. In this model, the assemblage in Lafayette formed with >25% of the water remaining and that in Nakhla with <10% of the water remaining. Bridges et al. (2004) reported that

the range of siderite compositions in Y000593 is consistent with the brine evaporation model of Bridges and Grady (2000).

The new $\delta^{34}S$ values for sulfates of Y000593, NWA 998, and NWA 6148 lie within the range established for Nakhla and MIL 03346 sulfate in previous studies (Farquhar et al., 2000c, 2007a; Kim and Farquhar, 2008). The $\Delta^{33}S$ of Y000593 water-soluble sulfate (-0.576 ± 0.008‰) lies approximately one-third of the way between the mean value for MIL 03346 sulfates (-0.22 ± 0.01‰) of Kim and Farquhar (2008) and that of Nakhla sulfate (-1.25 ± 0.01‰) reported by Farquhar et al. (2007a), consistent with the purported location of Y000593 between MIL 03346 and Nakhla in the nakhlite cumulate pile (Mikouchi et al., 2006; Day et al., 2006). However, $\Delta^{33}S$ of Y000593 acid-soluble sulfate (-0.224 ± 0.008‰) is very similar to both sulfate fractions of MIL 03346 and the earlier value determined for Nakhla total sulfate (-0.302 ± 0.026‰) (Farquhar et al., 2000c; Kim and Farquhar, 2008). As mentioned above, sulfate from both NWA 998 and NWA 6148, believed to derive from the bottom and top of the nakhlite pile, respectively, carries only a small negative $\Delta^{33}S$.

The range of $\Delta^{33}S$ among these meteorites suggests highly variable degrees of input from a sulfur pool distinct from the primary mantle signature, which displays the fingerprint of atmospheric processing in the form of significantly negative $\Delta^{33}S$. Assuming that Nakhla, Y000593, and MIL 03346 were altered by the same event, it is conceivable that the infiltration of a surface brine carrying anomalous sulfate varied with depth, such that Nakhla received more of this component than the shallower Y000593 and MIL 03346, contributing to its higher concentration of sulfate and more

negative $\Delta^{33}S$. However, the fact that the two available measurements of Nakhla sulfate span this same range of $\Delta^{33}S$ values suggests that the distribution of the anomalous sulfur may have been heterogeneous and not systematically related to burial depth. The paucity of data, including only single samples of Y000593 and MIL 03346, precludes a definitive answer to this question. It is also possible that the anomalous sulfur that infiltrated the nakhlite unit was heterogeneous and characterized by a range of $\Delta^{33}S$.

If it is assumed that the entire nakhlite unit was emplaced prior to a single alteration event that produced all of the negative $\Delta^{33}S$ values, then the lack of significant sulfur anomalies in NWA 998 and NWA 6148 seen in this study and in Lafayette (Farquhar et al., 2000c) carries potential implications for the pathway through which the alteration fluid entered the nakhlites. If the uppermost and lowermost portions of the cumulate pile were relatively unaffected by the anomalous sulfur, this would suggest lateral migration of fluid into middle portions of the pile, rather than simple top-down or bottom-up migration as has been proposed by Bridges and Hicks (2011).

There are indications, however, that the nakhlites may have formed during multiple magmatic events, rather than representing a single lava flow. Shirai and Ebihara (2008) reported that variable Zr/Hf ratios in the nakhlites cast doubt on their origins within a single cumulate pile. They suggested that Nakhla and Y000593 derived from one magma source, while MIL 03346 derived from another. Shih et al. (2010) compared Sm-Nd isotope systematics of seven nakhlites (all except NWA 998) and concluded that based on calculated ages and $\varepsilon_{Nd}$ values, the nakhlite parent

magmas represent at least three different flows that occurred over 20 Ma or more, assuming derivation from the same mantle source: Nakhla + Governador Valadares ± Lafayette, Y000593, and MIL 03346 + NWA 5790. However, uncertainties in the data allow the possibility that NWA 5790 was produced later than MIL 03346. Jambon et al. (2010) reported that NWA 5790 augite phenocrysts preserve complex primary zoning unique among the nakhlites. In addition, preliminary analyses by Mikouchi et al. (2012) revealed that augite and olivine core compositions in NWA 5790 are more Fe-rich than those of other nakhlites. It has also been reported that augite cores in NWA 5790 have higher REE abundances than those of other nakhlites (Jambon et al., 2010; Sanborn et al., 2011), which together with the Fe-rich composition suggests possible derivation from a more evolved parent melt (Mikouchi et al., 2012). For a top-down migration of fluid to introduce anomalous surface-derived sulfur into MIL 03346, Y000593, and Nakhla, it would have had to be injected between eruption of magmas that produced MIL 03346 and NWA 5790/6148.

The absence of monosulfide minerals detected in AVS extraction of Y000593, NWA 998, and NWA 6148, as well as MIL 03346 (Kim and Farquhar, 2008), suggests that these meteorites may have experienced a high degree of oxidation, which resulted in extensive conversion of primary pyrrhotite to sulfate. The late-stage oxidation event for near-surface nakhlites proposed by Noguchi et al. (2009) based on the presence of jarosite in Y000593 and MIL 03346 is consistent with this idea. In addition, Day et al. (2006) reported that MIL 03346 groundmass crystallized at a higher oxygen fugacity than other nakhlites. The values of $\Delta^{33}S$ determined for

separate analyses of Nakhla AVS were -0.08 ± 0.01% and -0.06 ± 0.03‰ (Farquhar et al., 2000c, 2007a). Homogeneity of sulfur within a common nakhlite mantle source would imply that mantle-derived igneous pyrrhotite of the other nakhlites had isotopic compositions similar to this. If so, they would retain the same $\Delta^{33}S$ upon oxidation to sulfate, which is a mass-dependent process. This is consistent with values of $\Delta^{33}S$ (-0.038 ± 0.008‰ to -0.084 ± 0.008‰) measured for NWA 998 and NWA 6148 sulfates. The presence of a greater percentage of sulfate with this smaller-magnitude $\Delta^{33}S$ would dilute the signal of any anomalous sulfur from a surficial source and could also contribute to the variation in $\Delta^{33}S$ measured for Nakhla, MIL 03346, and Y000593.

Recent ion microprobe analysis of pyrrhotite grains in MIL 03346 showed clear evidence for S-MIF in primary igneous sulfides (Chapter 4 of this work). It is thought that sulfate with negative $\Delta^{33}S$ was generated through photochemical reactions in the martian atmosphere and deposited on the surface, as described above. It was then assimilated into the nakhlite magma. The exogenous sulfur was at least partially reduced to the $S^{2-}$ state within the magma and incorporated into primary igneous pyrrhotite grains. This idea is explored more fully in Chapter 4.

Following emplacement into surface or shallow crustal depth, the nakhlite unit experienced episodes of aqueous alteration, during which oxidation of igneous sulfides containing anomalous sulfur, produced as described above, would have contributed to production of sulfate with negative $\Delta^{33}S$. These alteration episodes could have also provided additional influx of isotopically anomalous sulfate into the nakhlite unit. It is likely that this occurred during multiple events, at different periods

during the nakhlite post-crystallization history. There is some evidence for alteration during late magmatic stages. As mentioned in the previous section, Greenwood et al. (2000a) reported increasingly negative $\delta^{34}$S in sulfides of Nakhla, Governador Valadares, and Lafayette and noted that this correlates with the relative degrees of subsolidus equilibration in these meteorites reported by Harvey and McSween (1992a). Greenwood et al. (2000a) suggested that influx of sulfur-bearing fluids into the nakhlite unit as the magma cooled may have driven the pyrrhotites in Nakhla and Governador Valadares to more sulfur-rich compositions and resulted in partial replacement of pyrrhotite in Lafayette by pyrite, as they observed.

Day et al. (2006) reported pervasive alteration in MIL 03346, including incipient alteration around pyrrhotite grains. Those authors noted that portions of MIL 03346 pyrrhotite grains armored by Fe-rich pyroxene do not show evidence for alteration, but that unarmored portions in contact with intercumulus material have been altered to hematite. They suggested that this may indicate localized alteration events that occurred upon introduction of aqueous fluids to the cooling lava.

Most researchers favor a low-temperature origin for the bulk of secondary alteration minerals in the nakhlites. In particular, a low-temperature origin for some of the sulfates is bolstered by cross-cutting relationships of sulfate and phyllosilicate veins, indicating that the sulfates formed later (Vicenzi et al., 2007a). As mentioned in the previous section, isotopic dating of olivine separates and alteration products in Y000593 and Lafayette indicate that an alteration event occurred ~650 Ma (Swindle et al., 2000; Misawa et al., 2003), well after formation of the igneous unit. If these dates are accurate, then this implies that water must have been present in the vicinity

of the nakhlites at a time well after cessation of the nakhlite magmatic activity. The shergottite formation ages provide substantial evidence for the occurrence of high-temperature geological processes on Mars after formation of the nakhlites. While the relative geography between regions that produced the shergottites and nakhlites is unknown, the presence of volcanic activity on Mars within the past few hundred million years indicates a potential source of heat for melting ice and forming alteration brines.

Another possible source of liquid water is impact-related hydrothermal activity. Recent work by Changela and Bridges (2011) has revealed additional evidence that variations in alteration assemblages among the nakhlites are correlated with their depth in the vertical sequence. They reported that fracture-filled veins in Lafayette, believed to derive from the lowermost depths of the nakhlite unit, contain a hydrated gel consisting of siderite, phyllosilicates, and an iron oxide phase, but did not report any sulfates in Lafayette. Changela and Bridges (2011) found many veins with crystalline siderite along their margins and silicate gel in the center, but no phyllosilicates. They also observed zones of gypsum in Nakhla. Y000593 was found to contain traces of sulfur concentrated along the edges of silicate gel veins, along with an olivine alteration product identified as laihunite (Noguchi et al., 2009), but no carbonates. Due to the non-crystalline nature of the gel, Changela and Bridges (2011) concluded that it formed during rapid cooling in the latter stages of a hydrothermal event. They proposed that the fluid responsible for the alteration derived from melting of ice from a subsurface reservoir such as permafrost, followed by migration upward through the nakhlites.

The scenario proposed by Changela and Bridges (2011), origin of an alteration brine in the subsurface and subsequent migration upward through the nakhlites, would be consistent with some of the observed variations in sulfur isotopic compositions among these meteorites. The sulfur isotopic composition of Lafayette is distinct from those of other nakhlites, displaying a uniquely positive $\Delta^{33}$S signature (Farquhar et al., 2000c). This suggests that Lafayette, located approximately three times as deep as Nakhla and Governador Valadares in the nakhlite sequence (Mikouchi et al., 2006), experienced a different alteration history. Karlsson et al. (1992) found that Lafayette contained the highest abundance of extraterrestrial water of any martian meteorite. Treiman et al. (1993) reported that Lafayette also shows the greatest content of pre-terrestrial alteration material among the nakhlites, but that the distribution of these products suggests episodic influx of fluid at low water-to-rock ratio rather than long-term exposure to aqueous fluids or flooding by a large volume of water. Based on estimates of the pH of the fluid that altered Lafayette and the assumption that the evaporation sequence model for nakhlite alteration assemblages is correct, it has been suggested that the fluid could not have contained substantial $SO_3$ prior to its migration through the nakhlites (Changela and Bridges, 2011; Hallis and Taylor, 2011). However, if Lafayette was altered by multiple pulses of fluid input as suggested by Treiman et al. (1993) rather than a single event, then perhaps the evaporation sequence model explains one chapter of the nakhlite alteration history but not the entire story. Nakhla, Y000593, and MIL 03346 may have experienced a separate event – or multiple events – involving fluid containing photochemically processed sulfur that may not have penetrated to the Lafayette burial depth. This is

consistent with the suggestion by Hallis and Taylor (2011) that the differences in mineralogical structure and composition of olivine alteration veins in Lafayette and the Miller Range nakhlites indicate chemical differences in the fluids that affected them. The positive $\Delta^{33}$S determined for Lafayette sulfate and pyrite by Farquhar et al. (2000c) could reflect incorporation of anomalous sulfur from a different part of the crust that was generated independently from that detected in the shallower nakhlites.

Hallis and Taylor (2011) argued that the relative lack of halite and siderite in alteration assemblages of MIL 03346 and Y000593 indicates that they were altered by a slightly different fluid than that which altered Nakhla. This raises the possibility that these meteorites were altered in a separate event by a fluid containing a different proportion of anomalous sulfur, and suggests that the nakhlites that do not display large $\Delta^{33}$S anomalies, including NWA 6148 and NWA 998, were also altered separately.

### 3.4.4    $\Delta^{36}$S and the Nature of the Covariation of $\Delta^{33}$S and $\Delta^{36}$S in the Nakhlites

Due to the very low abundance of $^{36}$S, measurements of $\Delta^{36}$S are more difficult and subject to greater uncertainties than those of $\Delta^{33}$S. As seen in Figure 3-1(b), values of $\Delta^{36}$S determined for sulfur-bearing phases in the nakhlites are all near zero, and error bars for all measurements except Lafayette sulfate and the acid-soluble sulfate from MIL 03346 cross the X-axis. Although the expected ratio of $\Delta^{36}$S/$\Delta^{33}$S varies depending on the mechanism that produced the S-MIF, the presence of significant non-zero $\Delta^{33}$S with no clearly resolvable $\Delta^{36}$S led Farquhar et al. (2007a)

to explore whether the mechanism that produced the mass-independent sulfur fractionation could involve hyperfine coupling, which affects only odd-mass isotopologues (Buchachenko, 2001). The new measurements of Y000593, NWA 6148, and NWA 998 all showed $\Delta^{36}S$ within $2\sigma$ error of zero. Viewed within the context of the nakhlite group, these data appear consistent with scatter about the X-axis and offer no resolution to the issue of hyperfine coupling versus other photochemical mechanisms.

Farquhar et al. (2007a) noted a covariation in $\Delta^{33}S$ and $\Delta^{36}S$ of Nakhla that appeared to deviate from that seen in ancient terrestrial samples, other meteorites, and products of photochemical experiments (Farquhar et al., 2000a, 2001). Figure 3-2 shows the relationship between $\Delta^{33}S$ and $\Delta^{36}S$ measured for the nakhlites, including the range of AVS and sulfate data from shergottites for comparison (Chapter 2 of this work). As seen in the figure, $\Delta^{36}S$ values given by Farquhar et al. (2000c) for Nakhla AVS and sulfate and for Lafayette pyrite were associated with large uncertainties. If the true values of these quantities were close to those of other measurements of nakhlites, as allowed by their uncertainties, then they could be consistent with a trend defined by Nakhla sulfate from Farquhar et al. (2007a), Y000593 sulfates, MIL 03346 CRS, and Lafayette sulfate, which is approximately perpendicular to the array formed by AVS data from other meteorites. The bidirectional nature of these arrays suggests that they may preserve the signatures of separate and distinct sulfur processing.

Figure 3-2 shows that the nakhlites display a similar covariation between $\Delta^{33}S$ and $\Delta^{36}S$ as seen in selected shergottites that display anomalous sulfur characterized by

positive rather than negative values of $\Delta^{33}S$. This array is also roughly parallel to that formed by elemental sulfur products of $SO_2$ photochemistry experiments with a Hg lamp source (Farquhar et al., 2000c). These results may indicate that the anomalous sulfur seen in the nakhlites, which show negative $\Delta^{33}S$, and in the shergottites and Lafayette, with positive $\Delta^{33}S$, reflects complementary sulfur pools formed by a single photochemical process in the martian atmosphere. The observation that Lafayette sulfate composition lies along the array formed by Nakhla and Y000593 sulfate in $\Delta^{36}S$ vs. $\Delta^{33}S$ space is consistent with this possibility. Alternatively, it may indicate input of sulfur from different surface reservoirs, bearing the signature of distinct photochemical processes.
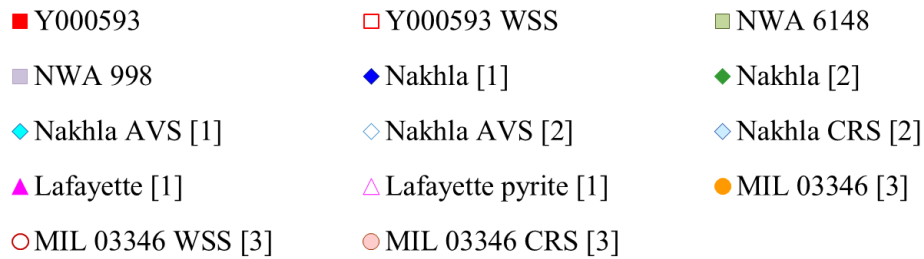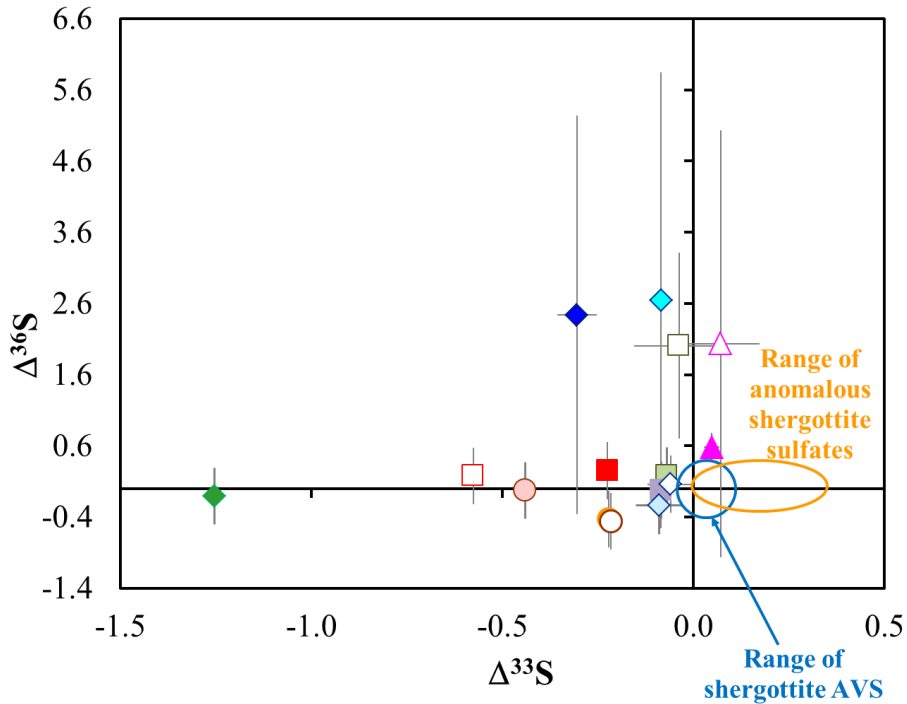
**Figure 3-2.** $\Delta^{36}S$ vs. $\Delta^{33}S$ for nakhlites.

**Acid-soluble sulfate (no parentheses), water-soluble sulfate (WSS), acid-volatile sulfur (AVS), and pyrite or chromium-reducible sulfur (CRS). Y000593, NWA 6148, and NWA 998, this study; other nakhlites from previous studies. Error bars represent 2σ deviations. Ranges of shergottite data from Chapter 2 are shown for comparison. [1] Farquhar et al., 2000c; [2] Farquhar et al., 2007a; [3] Kim and Farquhar, 2008.**

## 3.5    Conclusions

The new measurements of the sulfur isotopic compositions of Y000593, NWA 6148, and NWA 998 presented here confirm previous reports that nakhlite sulfate phases display evidence of mass-independent fractionation. These findings suggest that sulfur has been exchanged between the martian surface and another reservoir, potentially the atmosphere, where photochemical processing of sulfur-bearing gases occurred. The identity of the exact mechanism that produced the anomalous sulfur remains unresolved but this is currently an active area of research. Comparison of data for nakhlites believed to have formed at different depths below the martian surface reveals distinct differences in their sulfur isotopic compositions as well as mineralogical and textural properties, suggesting that aqueous alteration of these meteorites on Mars occurred during multiple, separate events, rather than a single event. The data suggest that fluids containing anomalous sulfur from a surface reservoir in communication with the atmosphere was introduced to the nakhlites at multiple times during their history, during the magmatic stage as well as during a later alteration event or series of events precipitated by transient availability of liquid water. This process affected the sulfur isotope systematics of nakhlite sulfides as well as sulfates, producing variable non-zero values of $\Delta^{33}$S in igneous pyrrhotites, pyrite, and sulfate minerals. The variability in nakhlite sulfur isotope ratios suggests that individual events occurred over limited spatial extents within the nakhlite unit. While it likely that the later alteration event ~650 Ma introduced additional anomalous sulfur to the nakhlites, the variations in sulfate $\Delta^{33}$S as well as the compositions of other secondary minerals believed to have formed at that time indicate localized S-

MIF effects. It is likely that the post-crystallization alteration of the nakhlites also involved mass-dependent processes that oxidized primary igneous sulfides to sulfate.

# Chapter 4: Ion Microprobe Analysis of Individual Sulfide Grains in Martian Meteorites Reveals Evidence for Assimilation of Martian Surface Materials[1,2,3,4]

[1] The text, tables, and figures in this chapter were written/created by H. B. Franz.

[2] Ion microprobe analyses described in this chapter were performed by K. McKeegan, R, Economos, and A. Schmitt with assistance from H. B. Franz.

[3] Electron microprobe analyses of Nakhla and ALH 84001 presented in this chapter were performed by H. B. Franz with assistance from P. Piccoli.

[4] Electron microprobe analyses of MIL 03346 presented in this chapter were performed by S. T. Kim and J. M. D. Day.

## 4.1    Introduction

The source of variations observed in incompatible trace element abundances among martian meteorites is the subject of a long-standing and lively debate. Incompatible elements typically have high charge or large size and preferentially partition into the liquid fraction during partial melting and crystallization processes (Walther, 2005). The shergottites, which crystallized between ~150 and 575 Ma, display a wide range of trace element and isotopic compositions, indicating derivation from multiple sources (McSween, 1994). The "depleted" shergottites are characterized by rare earth element (REE) patterns that are depleted in light REE

compared to chondrites and have radiogenic isotopic compositions (e.g., Sm-Nd, Rb-Sr, Lu-Hf isotope systems) consistent with origin from source regions with long-term depletions in incompatible elements. In contrast, the "enriched" shergottites have flat chondrite-normalized REE patterns and radiogenic isotopic compositions that indicate derivation from source regions with long-term enrichment in incompatible elements (Borg and Draper, 2003). The nakhlites crystallized ~1.3 Ga and display trace element characteristics that differ from those of the shergottites. The nakhlites are highly enriched in incompatible elements, but their radiogenic isotopic compositions indicate derivation from a strongly depleted source (Treiman, 2005).

There are two general models that seek to explain these observations, both of which invoke mixing between reservoirs either depleted or enriched in trace elements, although the reservoirs in the two models were formed by different means. In the first model, the two reservoirs are assumed to be the mantle, which is reduced and depleted in trace elements, and the martian crust, which is oxidized and enriched in trace elements (e.g., Jones, 1989; Herd et al., 2002; Rumble and Irving, 2009). This model assumes that the meteorite compositions were produced by assimilation of crustal material into magmas. The second model assumes that the two reservoirs comprise distinct depleted and enriched source areas within the mantle that were established during a global magma ocean stage (e.g., Borg et al., 1997; Brandon et al., 2000; Borg and Draper, 2003; Debaille et al., 2008). The depleted reservoir in this scenario consists of cumulate crystals formed from a martian magma ocean and the enriched reservoir represents late-stage intercumulus melt containing higher

abundances of incompatible trace elements (e.g., Borg et al., 1997; Brandon et al., 2000; Borg and Draper, 2003; Debaille et al., 2008).

Sulfur isotope systematics have the potential to provide an additional tracer for assimilation of surface deposits into igneous rocks. Like oxygen, sulfur has multiple stable isotopes that are susceptible to fractionations that deviate from those predicted solely on the basis of isotopic mass differences (e.g., Thiemens and Heidenreich, 1983; Thiemens et al., 1999). The foremost cause of such sulfur mass-independent fraction (S-MIF) in planetary atmospheres and the solar nebula is believed to be ultraviolet photochemistry (Thiemens et al., 1999; Farquhar et al., 2000a, 2000c, 2001; Thiemens, 2006). The discovery by Farquhar et al. (2000a, 2000c) that ancient terrestrial sediments and selected martian meteorites possess S-MIF signatures similar to products of laboratory photochemical experiments with sulfur-bearing gases opened a new avenue of investigation into possible interactions between atmospheric and surface reservoirs on both planets.

The largest S-MIF signals measured by Farquhar et al. (2000c, 2007a) were found in the sulfate fraction of the Nakhla meteorite, although the AVS fraction of Nakhla was also shown by those studies to possess a small negative $\Delta^{33}S$ anomaly. Farquhar et al. (2000c, 2007) suggested that this could indicate incorporation of surface sulfur into igneous sulfide minerals. The subsequent observation by Kim and Farquhar (2008) of significant S-MIF in a sulfide fraction of the MIL 03346 nakhlite confirmed the suggestion of high-temperature sulfur assimilation processes, likely including chemical reduction. The study described in this chapter was undertaken to

investigate this question further by examining the sulfur isotopic composition of individual sulfide grains in three martian meteorites via ion microprobe.

## 4.2 Methods

### 4.2.1 Ion Microprobe

The secondary ion mass spectrometry (SIMS) technique, also known as the ion microprobe, offers the best spatial resolution for *in situ* analysis of individual mineral grains for measurements of $\delta^{33}S$, $\delta^{34}S$, and $\Delta^{33}S$. This method was used to examine sulfides in two nakhlites (Nakhla and MIL 03346) as well as ALH 84001, with the goal of determining whether the anomalous sulfur isotopic composition obtained via chemical extraction of bulk rock material was also evident in individual grains. The SIMS analyses were performed at the University of California at Los Angeles (UCLA), using a Cameca IMS 1270 high-resolution ion microprobe in multicollector mode. Polished meteorite samples first were mapped with reflected-light optical microscopy to locate sulfide grains large enough (i.e., > ~20 μm diameter) for SIMS analysis. Prior to loading in the ion microprobe sample chamber, the sections were cleaned by sonication in Milli-Q water and methanol, then coated with a ~100 Å layer of carbon to ensure conductivity across the sample surface. Ion microprobe analyses in January 2012 utilized a 5 nA $Cs^+$ primary ion beam at 20 keV impact energy with 100 μm Kohler illumination, focused to a 25-30 μm spot. A mass resolving power of ~4000 and energy filtering were used to minimize the contributions from the $^{32}SH^-$ ion to the $^{33}S^-$ peak. Positive charge buildup on the sample was prevented by applying an electron flood gun normal to the primary beam. Prior to each analysis, the

surface was pre-sputtered for up to 150 seconds, followed by 30 cycles (60 cycles in some cases) of 10-second integrations. The resulting secondary ions of $^{32}S^-$, $^{33}S^-$, and $^{34}S^-$ were simultaneously collected by multiple Faraday cups, located in a temperature-controlled vacuum chamber (Mojzsis et al., 2003). Measurements of Nakhla in January 2008 employed similar operating conditions to those described above, but with mass resolution of ~6000.

The precision achieved during SIMS analysis is highly dependent on mineral grain and primary beam characteristics, which affect the number of sulfur ions produced. Isotope ratios determined by SIMS also exhibit a mass-dependent fractionation resulting from the measurement process, causing deviations from the true isotope ratios that can be predicted and corrected in a systematic manner. The fractionation may be due to the ionization process of sputtering, the transport of secondary ions to the detector, and mass-dependent detector response (Mojszis et al., 2003). These errors are corrected by calibration with matrix-matched standards under the same instrumental conditions. Note that fractionation due to matrix effects are solely mass-dependent and do not affect $\Delta^{33}S$ measurements.

Results for analyses of reference standards during these sessions are presented in Tables A-1 and A-2 of the appendix. Note that the 1σ errors listed in the tables represent only "internal" errors, or the standard error measured in an individual spot over the number of integration cycles. The true uncertainty in measurements of sulfide grains in the meteorite sections was taken as the greatest of the internal error, the standard error of repeated analyses of mineral standards (i.e., "external reproducibility"), or the standard error of multiple analyses of a given grain.

Measurements of MIL 03346 in January 2012 achieved average $1\sigma$ precision of $\pm$ 0.07‰ for $\Delta^{33}S$ and $\pm$ 0.07‰ for $\delta^{34}S$, based on repeatability of reference standards. The uncertainty on $\Delta^{33}S$ measurements of ALH 84001 was a little higher, $\pm$ 0.25‰, due to smaller grain sizes. Average $1\sigma$ precision for Nakhla analyses in January 2008 was $\pm$ 0.21‰ for $\Delta^{33}S$ and $\pm$ 0.71‰ for $\delta^{34}S$, based on repeatability of the CDT standard. Note that only data for ion probe spots yielding $\geq 2.2 \times 10^{8}$ counts/s on $^{32}S^{-}$ were included in the results.

### 4.2.2 *Electron Microprobe*

The composition of sulfide grains analyzed via SIMS was verified using the JEOL JXA-8900 SuperProbe (EPMA) with a ZAF correction at the University of Maryland. Wavelength dispersive spectrometry (WDS) scans were performed with an accelerating potential of 15 kV, beam current of 10 nA, spot size of 1 μm, and dwell times of 20 s for iron and sulfur and 30 s for the remaining elements. Precision of sulfur and iron measurements based on repeated analyses of a pyrrhotite standard was approximately 0.2 wt% ($1\sigma$). Uncertainties on other elements were approximately 3 wt% for Ni, 5 wt% for Cr, 7 wt% for Co, and 2 – 5 wt% for Cu, varying on concentration. Note that EPMA analyses of MIL 03346 were performed by J. M. D. Day and S-T. Kim using similar instrument settings.

## 4.3  Results

The sulfur isotopic compositions determined for sulfide grains in Nakhla, MIL 03346, and ALH 84001 are presented in Table 4-1. The table includes weighted means for repeated measurements of individual grains, as well as the weighted mean for each meteorite. The data are depicted graphically in Figures 4-1 through 4-3, which show $\Delta^{33}$S vs. $\delta^{34}$S for each meteorite. Figure 4-4 compares $\Delta^{33}$S vs. $\delta^{34}$S of nakhlites measured via SIMS with data obtained by chemical extraction. Table 4-2 gives composition data for each grain, determined by electron microprobe. Images of the sulfide grains may be found in Appendix B.

Nakhla pyrrhotite grains had average metal/sulfur (M/S) ratio of 0.94. The weighted mean sulfur isotopic composition of all grains showed $\delta^{34}$S of -0.51 ± 0.70‰ and $\Delta^{33}$S of 0.06 ± 0.20‰.

MIL 03346 pyrrhotite showed average M/S ratio of 0.90. A few grains showed marked elevation in Cu concentration, as high as 14.0 ± 2.0% for grain 104 (6). That particular grain had the highest value of $\delta^{34}$S, at 4.96 ± 0.23‰, but its $\Delta^{33}$S was -0.71 ± 0.13‰, the same as the weighted mean for all grains of this meteorite. The $\delta^{34}$S of the weighted mean for all grains was 3.02 ± 0.23‰.

The sulfide grains in ALH 84001 were sulfur-rich compared to the other meteorites, with average M/S ratio of 0.57. Although this does not represent stoichiometric pyrite, the IMF for ALH 84001 was based on a pyrite standard rather than pyrrhotite, since pyrite provided a closer match to its composition. The $\delta^{34}$S values obtained with IMF based on the pyrite standard are approximately 0.23‰ lower than the $\delta^{34}$S values obtained with IMF based on the pyrrhotite standard. Only

two grains in ALH 84001 produced sufficient count rates, with weighted mean sulfur isotopic composition of 2.48 ± 0.07‰ for $\delta^{34}S$ and 0.02 ± 0.25‰ for $\Delta^{33}S$.

**Table 4-1. Sulfur isotopic compositions determined by ion microprobe analysis (1σ uncertainties of individual measurements are given in parentheses; uncertainties for weighted means are acquired from repeated analyses of mineral standards)**

| Grain – spot[*] | $\delta^{34}S$ | $\Delta^{33}S$ |
|---|---|---|
| *Nakhla* | | |
| 9 (1) - 1 | -0.47 (0.02) | 0.33 (0.14) |
| 9 (1) - 2 | -3.16 (0.02) | -0.11 (0.15) |
| 9 (1) - 3 | -0.64 (0.02) | 0.24 (0.15) |
| 9 (1) - 4 | -3.35 (0.02) | 0.02 (0.16) |
| 9 (1) - 5 | -5.72 (0.02) | -0.12 (0.16) |
| | | |
| *Weighted mean for grain 9 (1)* | *-2.57 ± 0.97* | *0.08 ± 0.16* |
| | | |
| 9 (4) - 1 | 0.96 (0.02) | 0.58 (0.18) |
| 9 (4) - 2 | 0.87 (0.03) | -0.04 (0.24) |
| 9 (4) - 3 | 1.65 (0.02) | 0.12 (0.16) |
| 9 (4) - 4 | -0.11 (0.02) | -0.15 (0.14) |
| 9 (4) - 5 | -1.13 (0.02) | -0.04 (0.15) |
| | | |
| *Weighted mean for grain 9 (4)* | *0.33 ± 0.48* | *0.07 ± 0.16* |
| | | |
| 9 (11) | 1.69 (0.03) | 0.12 (0.22) |
| 9 (16) | 1.12 (0.03) | -0.33 (0.22) |
| 17 (6) | -0.40 (0.03) | -0.07 (0.22) |
| 17 (14) | 2.11 (0.03) | -0.11 (0.23) |
| | | |
| 17 (19) - 1 | 2.16 (0.03) | 0.15 (0.22) |
| 17 (19) – 2 | 1.94 (0.03) | 0.10 (0.23) |
| | | |
| *Weighted mean for grain 17 (19)* | *2.05 ± 0.11* | *0.13 ± 0.22* |
| | | |
| **Weighted mean for Nakhla** | **-0.51 ± 0.72** | **0.06 ± 0.21** |

[*]Section (grain) – spot. Nakhla sections: USNM-9, USNM-17, and USNM-18.

**Table 4-1, continued**

| | | |
|---|---|---|
| *MIL 03346* | | |
| 6 (1) – 1 | 2.04 (0.23) | -0.94 (0.16) |
| 6 (1) – 2 | 2.42 (0.23) | -0.80 (0.16) |
| 6 (1) – 3 | 3.51 (0.23) | -0.68 (0.16) |
| *Weighted mean for grain 6 (1)* | *3.02 ± 0.23* | *-0.75 ± 0.16* |
| 6 (17) | 4.35 (0.23) | -1.02 (0.16) |
| 93 (2) – 1 | 2.45 (0.23) | -1.23 (0.13) |
| 93 (2) – 2 | 4.27 (0.23) | -0.97 (0.13) |
| *Weighted mean for grain 93 (2)* | *3.31 ± 0.23* | *-1.11 ± 0.13* |
| 93 (5) | 3.75 (0.23) | -0.55 (0.13) |
| 93 (7) – 1 | 2.89 (0.23) | -0.44 (0.13) |
| 93 (7) – 2 | 3.00 (0.23) | -0.68 (0.13) |
| *Weighted mean for grain 93 (7)* | *2.96 ± 0.23* | *-0.60 ± 0.13* |
| 104 (2) | 2.46 (0.23) | -0.78 (0.13) |
| 104 (6) – 1 | 5.95 (0.23) | -1.06 (0.13) |
| 104 (6) – 2 | 3.81 (0.23) | -0.30 (0.13) |
| *Weighted mean for grain 104 (6)* | *4.96 ± 0.23* | *-0.71 ± 0.13* |
| 104 (8) | 1.62 (0.23) | -0.71 (0.13) |
| 132 (1) | 1.31 (0.23) | -0.46 (0.13) |
| 132 (2) | 0.89 (0.23) | -0.40 (0.23) |
| 132 (3) | 2.56 (0.23) | -0.73 (0.13) |
| ***Weighted mean for MIL 03346*** | ***3.02 ± 0.23*** | ***-0.72 ± 0.13*** |
| *ALH 84001* | | |
| 352 (G6) | *2.59 (0.05)* | 0.11 (0.28) |
| 352 (G9) | *2.45 (0.03)* | 0.00 (0.15) |
| ***Weighted mean for ALH 84001*** | ***2.48 ± 0.07*** | ***0.02 ± 0.25*** |

**Table 4-2. Electron microprobe analyses of sulfide grains**

**included in ion microprobe study**

| Grain – spot[*] | Fe | Cu | Ni | Co | Cr | S | Total |
|---|---|---|---|---|---|---|---|
| *Nakhla* | | | | | | | |
| 9 (1) – 1 | 60.58 | 0.02 | 0.53 | 0.17 | 0.08 | 37.40 | 98.78 |
| 9 (1) – 2 | 60.43 | 0.01 | 0.46 | 0.18 | 0.06 | 37.47 | 98.61 |
| 9 (4) – 1 | 61.56 | 0.05 | 0.35 | 0.19 | 0.13 | 38.59 | 100.87 |
| 9 (4) – 2 | 59.64 | b.d. | 0.36 | 0.19 | 0.12 | 38.61 | 98.93 |
| 9 (11) – 1 | 61.36 | 0.01 | 0.25 | 0.21 | 0.07 | 37.52 | 99.41 |
| 9 (11) – 2 | 61.04 | 0.06 | 0.27 | 0.16 | 0.09 | 37.72 | 99.34 |
| 9 (16) – 1 | 60.41 | b.d. | 0.37 | 0.15 | 0.08 | 37.61 | 98.63 |
| 9 (16) - 2 | 61.86 | b.d. | 0.36 | 0.19 | 0.04 | 37.34 | 99.80 |
| 17 (6) – 1 | 61.50 | 0.31 | 0.35 | 0.24 | 0.07 | 37.45 | 99.92 |
| 17 (6) – 2 | 60.60 | 1.14 | 0.31 | 0.22 | 0.05 | 38.46 | 100.84 |
| 17 (14) – 1 | 61.26 | 0.32 | 0.27 | 0.19 | 0.11 | 37.44 | 99.58 |
| 17 (19) – 1 | 62.90 | b.d. | 0.33 | 0.19 | 0.09 | 38.38 | 101.89 |
| 17 (19) – 2 | 62.92 | 0.01 | 0.33 | 0.17 | 0.06 | 37.75 | 101.23 |
| 17 (19) – 3 | 62.27 | b.d. | 0.30 | 0.16 | 0.06 | 36.84 | 99.63 |
| *MIL 03346* | | | | | | | |
| 6 (1) – 1 | 61.33 | b.d. | 0.05 | 0.15 | - | 38.99 | 100.52 |
| 6 (1) – 2 | 61.42 | 0.02 | 0.03 | 0.16 | - | 38.91 | 100.54 |
| 6 (1) – 3 | 59.67 | b.d. | b.d. | 0.16 | - | 39.39 | 99.25 |
| 6 (17) – 1 | 61.21 | b.d. | b.d. | 0.14 | - | 39.14 | 100.49 |
| 93 (2) - 1 | 60.99 | 0.01 | b.d. | 0.14 | - | 38.93 | 100.07 |
| 93 (5) - 1 | 60.75 | b.d. | 0.03 | 0.15 | - | 39.23 | 100.15 |
| 93 (7) – 1 | 61.37 | 0.04 | b.d. | 0.14 | - | 38.88 | 100.42 |
| 104 (2) – 1 | 61.20 | 0.08 | b.d. | 0.14 | - | 38.94 | 100.56 |
| 104 (6) – 1 | 61.06 | b.d. | 0.03 | 0.13 | - | 38.87 | 100.09 |
| 104 (6) – 2 | 61.03 | 0.02 | b.d. | 0.16 | - | 39.18 | 100.39 |
| 104 (8) – 1 | 61.42 | b.d. | b.d. | 0.15 | - | 39.23 | 100.80 |
| 132 (1) - 1 | 61.19 | 0.01 | 0.04 | 0.14 | - | 39.29 | 100.67 |
| 132 (2) – 1 | 59.43 | 1.39 | 0.01 | 0.14 | - | 39.52 | 100.49 |
| 132 (2) – 2 | 61.26 | 0.06 | b.d. | 0.17 | - | 39.12 | 100.61 |
| 132 (3) - 1 | 61.11 | 0.03 | 0.02 | 0.12 | - | 39.08 | 100.36 |
| *ALH 84001* | | | | | | | |
| 352 (G6) – 1 | 48.82 | 0.01 | 0.01 | 0.07 | 0.06 | 51.14 | 100.11 |
| 352 (G9) – 1 | 49.66 | 0.01 | 0.01 | 0.07 | 0.10 | 48.64 | 98.49 |
| 352 (G9) - 2 | 48.65 | b.d. | b.d. | 0.09 | 0.07 | 51.57 | 100.38 |

[*]Nomenclature: Section (grain) – spot. Nakhla sections: USNM-9, USNM-17, and USNM-18.
"b.d." = below detection limit: Fe < 220 ppm; Cu > 23 ppm; Ni < 160 ppm; Co < 140 ppm; Cr < 150 ppm; S < 110 ppm.
"-" = not analyzed.
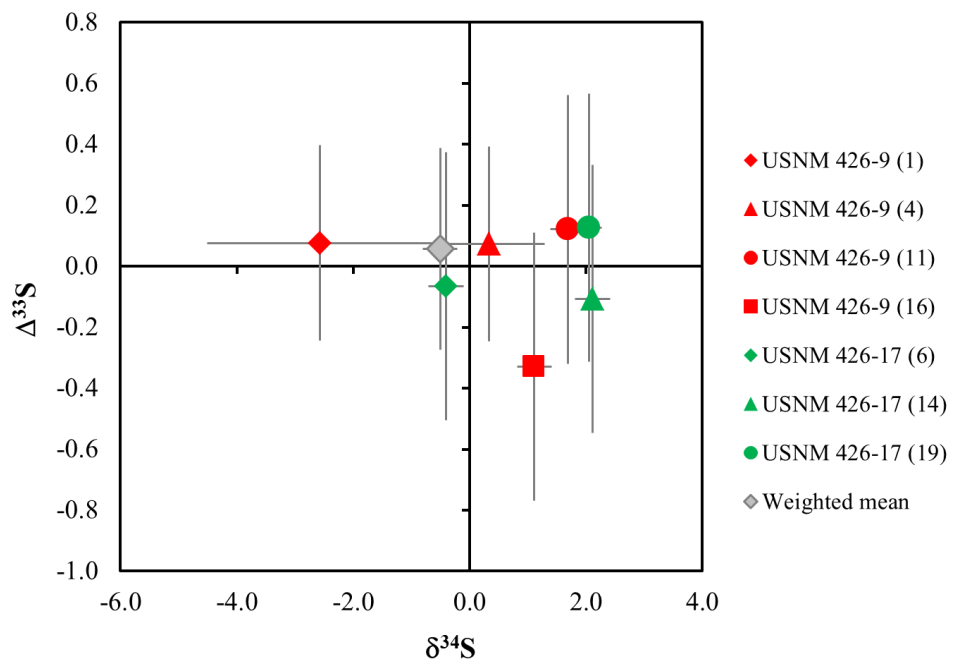
**Figure 4-1. Nakhla sulfur isotopic composition obtained via ion microprobe.**

**Weighted mean for each grain is shown. 2σ error bars.**
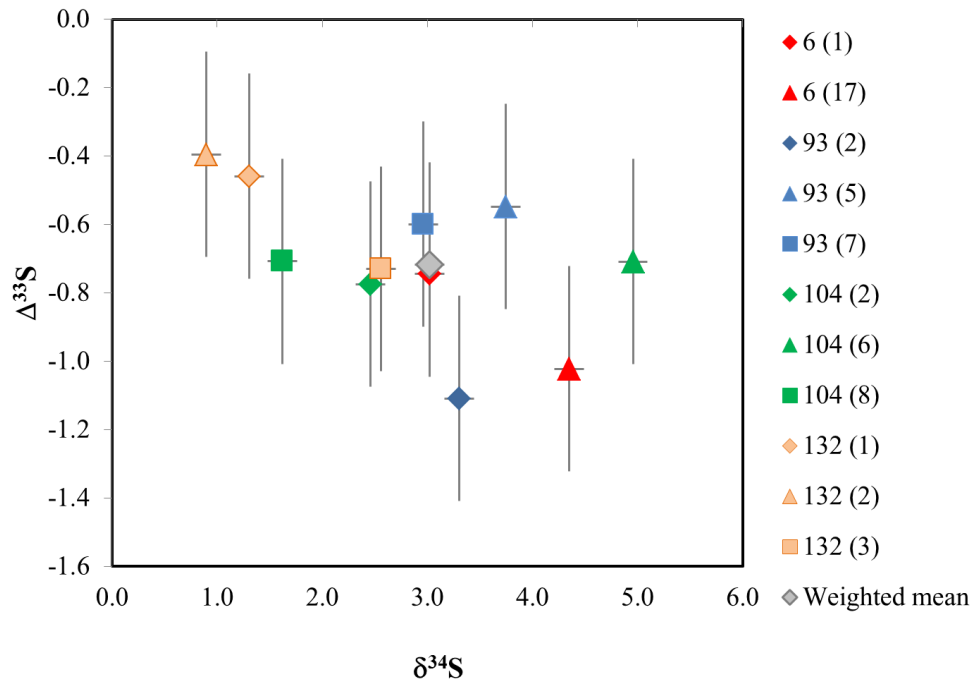
**Figure 4-2. MIL 03346 sulfur isotopic composition obtained via ion microprobe.**

**Weighted mean for each grain is shown. 2σ error bars.**
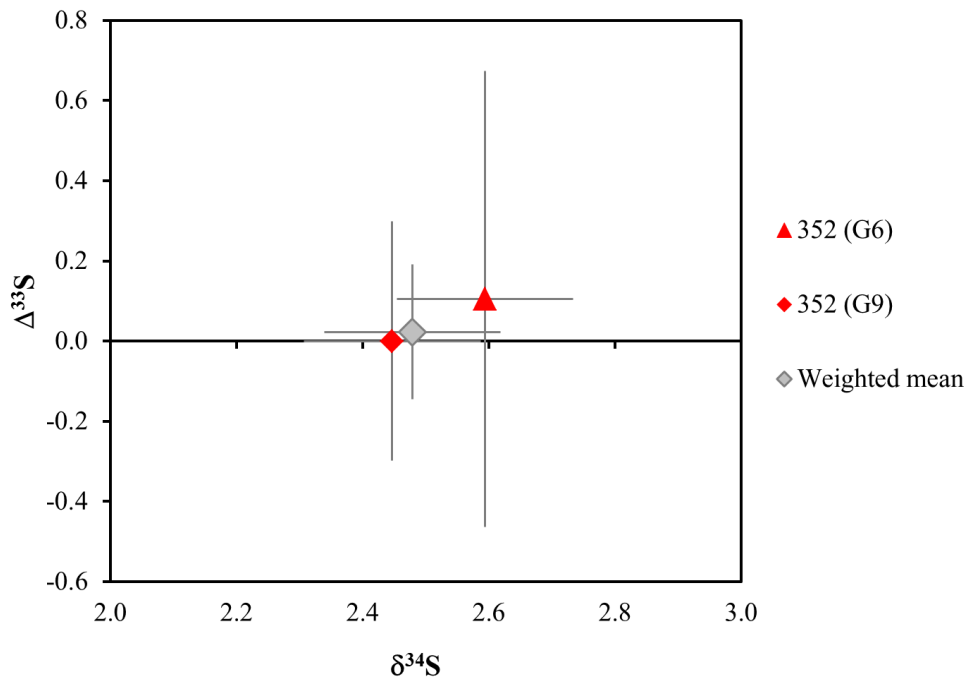
**Figure 4-3. ALH 84001 sulfur isotopic composition obtained via ion microprobe.**

**Weighted mean for each grain is shown. 2σ error bars.**
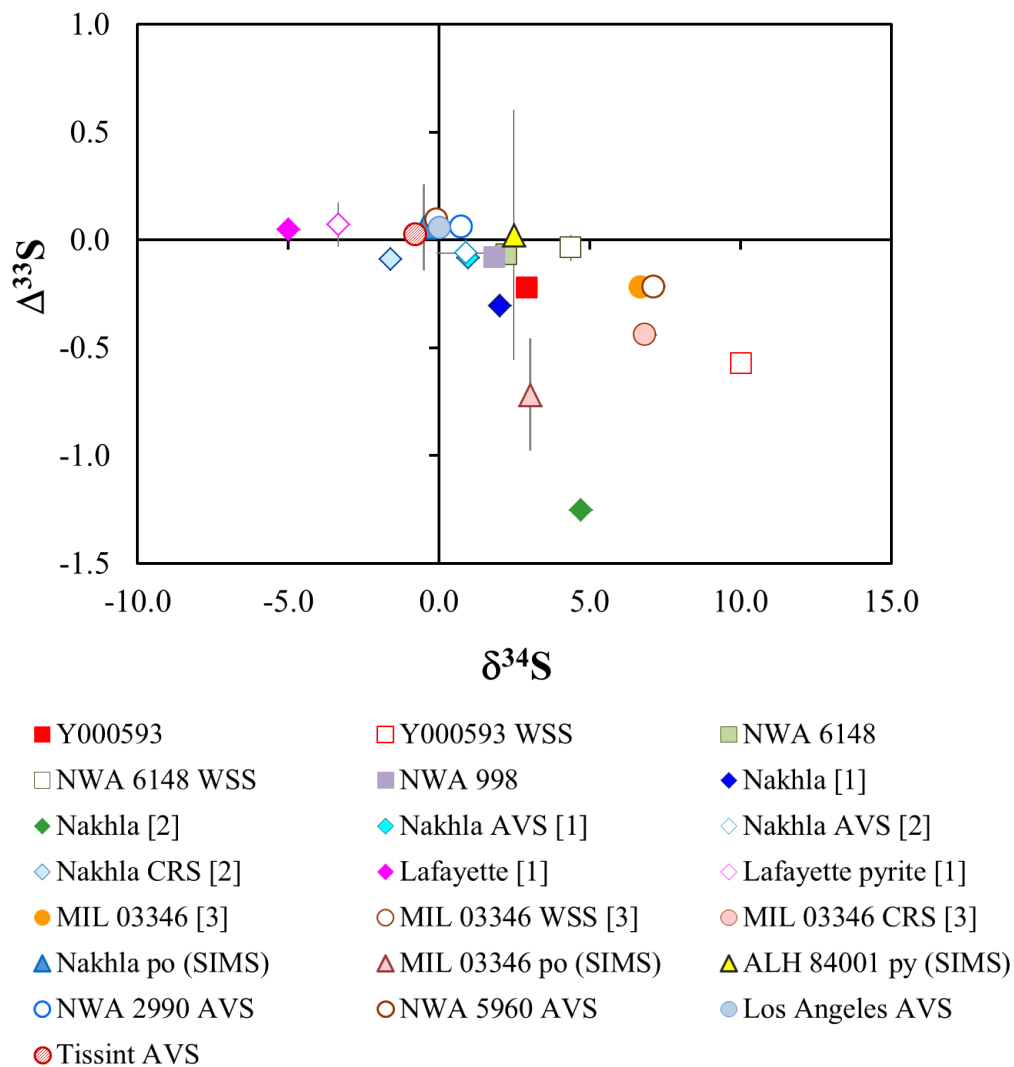
**Figure 4-4.** $\Delta^{33}$S vs. $\delta^{34}$S of nakhlites: SIMS and chemical extraction data. po = pyrrhotite; py = pyrite; [1] Farquhar et al., 2000c; [2] Farquhar et al., 2007a; [3] Kim and Farquhar, 2008. SIMS data are shown as the weighted mean for all grains of a given meteorite.

## 4.4    Discussion

### 4.4.1    Sulfide Mineralogy and Sulfur Isotopic Compositions

Two sulfide grains in ALH 84001 showed no evidence for S-MIF, with weighted mean $\Delta^{33}S$ of $0.02 \pm 0.25$‰ ($1\sigma$). Analyses of Nakhla pyrrhotite grains also did not show evidence for anomalous sulfur composition. The mean $\Delta^{33}S$ for Nakhla grains was $0.06 \pm 0.21$‰, compared to values of $-0.06 \pm 0.03$‰ and $-0.09 \pm 0.01$‰ for its acid-volatile sulfur (AVS, or monosulfides) and chromium-reducible sulfur (CRS, disulfides and elemental sulfur) phases reported by Farquhar et al. (2007a). The mean $\delta^{34}S$ determined by SIMS, $-0.51 \pm 0.72$‰, is bracketed by the AVS ($0.9 \pm 0.5$‰) and CRS ($-1.6 \pm 0.2$‰) compositions reported by Farquhar et al. (2007a).

Individual sulfide grains of MIL 03346 had mean $\Delta^{33}S$ of $-0.72 \pm 0.13$‰. This represents a clearly resolved S-MIF signal. In comparison, chemical extraction of MIL 03346 bulk rock yielded $\Delta^{33}S$ of $-0.22 \pm 0.01$‰ for both the water-soluble and acid-soluble sulfate fractions and $-0.44 \pm 0.01$‰ for the CRS fraction (Kim and Farquhar, 2008). Day et al. (2006) reported that although the olivine and augite compositions of MIL 03346 suggest that it derived from the same or a similar lava flow as the other nakhlites, it experienced less equilibration and faster cooling. As Day et al. (2006) explained, diffusive subsolidus re-equilibration between Mg-rich cores and Fe-rich rims is much faster for olivine for pyroxene (Harvey and McSween, 1992b). In MIL 03346 olivines, Fe-Mg diffusion occurred in a zone of only ~100 mm from the grain boundaries, indicating that MIL 03346 is the least equilibrated nakhlite (Day et al., 2006). As seen in figures B-4 through B-7 of the appendix, pyrrhotite

grains in MIL 03346 are intergrown with skeletal titanomagnetite in the intercumulus matrix, similar to features that commonly occur in quenched terrestrial basaltic flows (Haggerty, 1976) and another indicator of fast cooling of the parent magma.

It is possible that sulfate in alteration veins within pyrrhotite grains contributed to the signal measured during SIMS analysis. Sulfate in these veins could have been added via post-crystallization influx of fluids, or it could have been formed from alteration of the pyrrhotite itself. The latter is suggested by the observation of sulfate veins that appear to originate in MIL 03346 pyrrhotite grains (Day et al., 2006). Hallis and Taylor (2011) reported a gradient in sulfate abundance and composition in veins of the Miller Range nakhlites, concluding that the outermost portions of these meteorites contain substantial amounts of terrestrial sulfate acquired through Antarctic weathering. Since terrestrial sulfate would be expected to possess $\Delta^{33}$S of zero, addition of terrestrial sulfate would dilute any martian S-MIF signal and reduce the magnitude of the true $\Delta^{33}$S anomaly. Likewise, addition of martian sulfate characterized by $\Delta^{33}$S with greater magnitude than that of the pyrrhotite grains would tend to increase the magnitude of the $\Delta^{33}$S anomaly. Values for individual grains in MIL 03346 ranged from -0.30 ± 0.13‰ to -1.11 ± 0.13‰, indicating variation outside the range of analytical uncertainty. Either or both of the processes described above could have affected the MIL 03346 samples and contributed to the variability observed in $\Delta^{33}$S for individual SIMS measurements. However, the alteration veins are quite narrow, with widths < 5 μm as measured by Hallis and Taylor (2011). Thus the areal extent of the veins is very small compared to the microprobe spot, such that the measured signal is dominated by pyrrhotite. For the observed S-MIF to be derived

solely from sulfate in veins within the pyrrhotite, the anomalous $\Delta^{33}$S of the sulfate would have to carry an extremely large negative magnitude. For these reasons, the detected S-MIF is interpreted to reside in the pyrrhotite.

### 4.4.2   Implications for Nakhlite Magmatism and Atmosphere-surface Interactions

Farquhar et al. (2000c) reported the first detections of S-MIF in martian meteorites, including $\Delta^{33}$S in Nakhla sulfate of -0.302 ± 0.026‰ and a smaller $\Delta^{33}$S of -0.080 ± 0.012‰ in the AVS fraction. Later analyses expanded the range of variability, with Farquhar et al. (2007a) reporting $\Delta^{33}$S of -1.25 ± 0.01‰ for Nakhla sulfate and -0.06 ± 0.03‰ in its AVS. The observation by Kim and Farquhar (2008) of significantly negative $\Delta^{33}$S of -0.44 ± 0.01‰ in the CRS fraction of MIL 03346 highlighted the fact that some mechanism must have operated to generate S-MIF in reduced phases, not just in sulfate.

Analysis of AVS extracted from 27 shergottites implies that the sulfur isotopic composition of the martian mantle matches that of CDT (Chapter 2 of this work). The three shergottites that showed anomalous AVS compositions were all characterized by positive $\Delta^{33}$S, in contrast to the negative $\Delta^{33}$S seen in the nakhlites. This suggests that the anomalous sulfur detected in these nakhlites represents a distinct reservoir. It is not likely that this distinct sulfur reservoir is a primordial martian mantle signature, because sulfur in the mantle should have been homogenized during the putative magma ocean stage (e.g., Elkins-Tanton, 2005). It is also unlikely that the anomalous sulfur was acquired through late accretion of chondritic materials to the mantle after cessation of core formation, as suggested to explain abundances of highly siderophile

elements (HSE) in the shergottites (Walker, 2009). Walker (2009, 2012) concluded from mass balance computations that late-accreted material could have comprised 0.5 to 1 wt% of the shergottite mantle source. Applying 1 wt% as an upper limit to the contribution from late accretion, similar mass balance calculations indicate that for the S-MIF observed in martian meteorites to derive from this source, the S-MIF signature of the late-accreted material would have had to be many times greater than that observed in any chondritic or achondritic meteorites to date. This implies that the S-MIF observed in igneous sulfides must have been acquired through other means.

Farquhar et al (2000c, 2001) performed a suite of experiments examining the effects of UV radiation on sulfur isotopic fractionation of $SO_2$ and $H_2S$ gas and determined that UV photochemistry is capable of generating S-MIF signatures analogous to those observed in Nakhla sulfate (Farquhar et al., 2000c, 2007). Farquhar et al. (2000c, 2007) proposed that the observed signal provides evidence for deposition of atmospherically-processed sulfur onto the martian surface, where it was incorporated into the meteorite parent rocks. There are three general ways in which sulfide with anomalous sulfur could have been produced: by recycling of early martian crust bearing anomalous sulfur back into the mantle, by assimilation of crustal material containing anomalous sulfur into ascending magma, or by introduction of anomalous sulfur into the source region, magma, or lithologic unit dissolved or suspended in fluid. In any case, the atmospherically-processed sulfur would presumably reside in a more oxidized state, having been deposited as sulfate or elemental sulfur aerosols, and thus chemical reduction would be required to transform the sulfur into sulfide phases.

Assimilation of crustal material is consistent with the hypothesis of Jones (1989) for the shergottites, which proposed that the variations in shergottite REE patterns reflect late-stage assimilation of enriched crustal material into magma from a depleted mantle source. However, Jones (1989) concluded that the nakhlites in contrast show little evidence for interaction with the martian crust. Later studies have confirmed the apparent closed-system crystallization of nakhlites based on zoning patterns in cumulus minerals and the intercumulus matrix (e.g., Longhi, 1991; Harvey and McSween, 1992b; Wadhwa and Crozaz, 1995; Day et al., 2006). This implies that the assimilative mechanism that introduced anomalous sulfur into the nakhlite magmas may have allowed closed-system crystallization processes for silicates but open-system behavior for sulfur.

Sulfur that had been deposited on the martian surface following photochemical processing in the atmosphere could have been transported into the nakhlite parent unit by an alteration brine. This represents a mechanism for introducing the anomalous sulfur isotopic signature observed in Nakhla sulfate minerals without need for the involvement of high-temperature processes and may be responsible for at least a portion of the S-MIF signal observed in the nakhlites. Petrographic studies of nakhlites have revealed the presence of secondary minerals, including carbonates, sulfates, and phyllosilicates, believed to have formed by low-temperature alteration processes (e.g., Bunch and Reid, 1975; Gooding et al., 1991; Harvey and McSween, 1992a; Treiman et al., 1993; Bridges and Grady, 2000; Treiman and Goodrich, 2002; Treiman and Irving, 2008; Noguchi et al., 2009; Changela and Bridges, 2010). The nakhlites also show evidence for subsolidus alteration during the cooling phase.

Greenwood et al. (2000a) reported increasingly negative $\delta^{34}$S in sulfides of Nakhla, Governador Valadares, and Lafayette and noted that this correlates with the relative degrees of subsolidus equilibration in these meteorites reported by Harvey and McSween (1992). Greenwood et al. (2000a) suggested that influx of sulfur-bearing fluids into the nakhlite unit as the magma cooled may have driven the pyrrhotites in Nakhla and Governador Valadares to more sulfur-rich compositions and resulted in partial replacement of pyrrhotite in Lafayette by pyrite, as they observed.

Day et al. (2006) also reported evidence for circulation of fluids through MIL 03346, noting incipient alteration around pyrrhotite grains. Those authors observed that portions of MIL 03346 pyrrhotite grains armored by Fe-rich pyroxene do not show evidence for alteration, but that unarmored portions in contact with intercumulus material have been altered to hematite. They suggested that this may indicate localized alteration events that occurred upon introduction of aqueous fluids to the cooling magma.

To generate the S-MIF observed in igneous sulfides, assimilation of anomalous sulfur must have occurred during a high-temperature magmatic phase. This could have occurred at any time during magmatic activity, but models for the assimilative mechanism must consider the variations in $\Delta^{33}$S between sulfides in MIL 03346 and Nakhla. Models for the relative burial depths of the nakhlites place them in the vertical sequence of NWA 998 < Lafayette < Nakhla, Governador Valadares < Y000593 < MIL 03346 < NWA 5790/6148, NWA 817 (Mikouchi et al., 2006; Day et al., 2006; Jambon et al., 2010; Chevrier et al., 2011; Mikouchi et al., 2012). These models are based on similarities in mineralogical compositions but differences in

textures among the nakhlites, suggesting that they may be samples of a single cumulate pile with crystals loosely packed near the surface and more densely packed with increasing depth (Harvey and McSween, 1992a, 1992b; Mikouchi et al, 2012).

Assuming that the nakhlites represent samples from different depths in a single magmatic flow, as described above, the simplest mechanism for introducing variable S-MIF into the nakhlite sulfides would involve localized assimilation of sulfur from the crustal reservoir upon emplacement of the magma, due to variations in the sulfur concentration and/or isotopic composition with depth in the crust. The crustal sulfur could have been assimilated from a brine or as solid minerals. The assimilated sulfur was then reduced within the magma to form igneous sulfide minerals, imparting different isotopic signatures at different depths. This localized assimilation model suggests that the depth at which MIL 03346 crystallized was a particularly sulfur-rich zone, containing significantly negative $\Delta^{33}S$ that was incorporated into pyrrhotite grains. The smaller $\Delta^{33}S$ anomaly in Nakhla AVS (Farquhar et al., 2000c, 2007a) and the lack of clearly resolved S-MIF in Nakhla grains examined via SIMS suggests either that the local sulfur content of the crust at the Nakhla depth was characterized by a different isotopic composition than that in the region where MIL 03346 formed or that less exogenous sulfur was assimilated into the Nakhla magma. It is also possible that the differences in their sulfide compositions reflect a combination of these two effects. Furthermore, the variability in Nakhla sulfide compositions measured by chemical extraction and SIMS suggests that the assimilation-reduction may have occurred on a local scale.

While the magma was cooling, it was likely infiltrated by additional fluids that altered primary igneous minerals and deposited various salts. Some of these fluids could have introduced additional sulfate from the surface reservoir, with sulfur isotopic composition characterized by negative $\Delta^{33}S$. There is evidence that the different regions of the nakhlite unit were altered in separate events (see Chapter 3), which would be consistent with the observed variations in sulfate $\Delta^{33}S$ magnitudes.

Some researchers have suggested that rather than deriving from a single magma source, the nakhlites represent multiple flows from distinct sources, possibly within a complex igneous system (Lentz et al., 2005; Shirai and Ebihara, 2008). Shirai and Ebihara (2008) reported that variable Zr/Hf ratios in the nakhlites cast doubt on their origins within a single cumulate pile. They suggested that Nakhla and Y000593 derived from one magma source, while MIL 03346 derived from another. If the parent rocks of these meteorites were produced by multiple flows, then the differences in sulfide $\Delta^{33}S$ could still represent variations in sulfur that was assimilated upon emplacement, as described above. However, derivation from multiple magma sources would also allow the possibility that the variations in sulfur isotope ratios reflect differences in the parent magma compositions. Since the magma produced in the mantle would not carry an anomalous composition, the S-MIF would presumably have been introduced by assimilation of wall rock bearing anomalous sulfur during magmatic ascent. Different pathways through the crust would have allowed variations in the isotopic composition or quantity of sulfur assimilated by the magmas, producing variable $\Delta^{33}S$ between Nakhla and MIL 03346. The post-crystallization history could have proceeded as described above, through multiple

pulses of sulfate-bearing brines that deposited evaporites and generated secondary alteration minerals from primary phases.

## 4.5 Conclusions

Recent SIMS analysis of individual pyrrhotite grains in the MIL 03346 nakhlite revealed a clearly resolved S-MIF signal characterized by negative $\Delta^{33}S$. These data are consistent with results of high-precision sulfur isotope measurements obtained via chemical extraction of MIL 03346 (Kim and Farquhar, 2008). While chemical extraction of Nakhla monosulfide minerals also revealed the presence of S-MIF characterized by negative $\Delta^{33}S$ (Farquhar et al., 2000c, 2007), SIMS analysis of Nakhla pyrrhotite grains did not show evidence for anomalous sulfur. These results are believed to represent evidence for variable assimilation of sulfur from the martian surface during nakhlite magmatic processes. The assimilated sulfur was characterized by S-MIF composition generated through photochemical processing of sulfur-bearing gases in the martian atmosphere, followed by deposition onto the surface. This anomalous sulfur was subsequently incorporated into nakhlite magmas during their emplacement in the crust or through assimilation of altered wall rock during magmatic ascent. The sulfur was finally reduced to $S^{2-}$ within the melt to form pyrrhotite with S-MIF compositions. The differences in $\Delta^{33}S$ observed for MIL 03346 and Nakhla likely reflect differences in the quantity and/or isotopic composition of locally assimilated sulfur. Following crystallization, the nakhlite parent unit probably experienced alteration by fluids carrying atmospherically-processed sulfur, generating

variable negative $\Delta^{33}S$ observed in sulfate fractions of MIL 03346 and Nakhla as well as other nakhlites (Chapter 3). SIMS analysis of sulfide grains in ALH 84001 revealed no resolvable sulfur isotopic anomaly.

# Chapter 5: Mass-Independent Fractionation of Sulfur Isotopes during Broadband $SO_2$ Photochemistry: Comparative Systematics of $^{16}O$- and $^{18}O$-rich $SO_2$[1,2]

[1] The text, tables, and figures in this chapter were written/created by H. B. Franz.

[2] All analyses presented in this chapter were performed by H. B. Franz.

## 5.1 Introduction

Laboratory experiments have indicated that mass-independent isotopic fractionation (S-MIF) is produced in gas-phase ultraviolet (UV) photochemistry of sulfur-bearing molecules, including $SO_2$, $H_2S$, and $CS_2$ (Farquhar et al., 2000c, 2001; Zmolek et al., 1999), and many of the specific causes of this chemistry remain to be understood. Comparison of sulfur isotopic fractionation produced by laboratory photochemistry experiments and the S-MIF signals observed in the ancient terrestrial rock record and in martian meteorites provide compelling hints of a cause-and-effect relationship (e.g., Farquhar et al., 2000c, 2001, 2007a). If this relationship were fully characterized, it would imply constraints on the chemical and physical composition of the respective planetary atmospheres at the times the anomalous signals were generated. Such characterization requires determination of the mechanism responsible for producing the observed fractionation.

Possible mechanisms for generating the S-MIF signal include shielding effects within the gas and isotopologue-specific absorption or kinetics. The concept of self-

shielding has been invoked most frequently to explain mass-independent fractionations due to photochemical processes, as first proposed by Thiemens and Heidenreich (1983) for oxygen isotopic anomalies in ozone formation. Self-shielding generally refers to a phenomenon in which one isotopologue of a gaseous species interferes with absorption of radiation by another isotopologue of the same gas. One type of self-shielding may arise due to the column density of the absorbing species, resulting in saturation of absorption by the major isotope and enrichment of photochemical products in the minor isotopes. Another type of shielding effect may be produced by overlapping peaks in the absorption spectra for the isotopologues, such that absorption by the minor isotopes is inhibited (Bally and Langer, 1982). Lyons (2007) argued that self-shielding during $SO_2$ photolysis is theoretically predicted to generate S-MIF analogous to that observed in Archean samples (Farquhar et al., 2000a, 2007c).

Mass-independent fractionation may also result from variations in absorption cross-section that favor certain isotopes over others (Okabe, 1978). Danielache et al. (2008) reported spectroscopic measurements of the UV absorption spectrum of $SO_2$, noting rich vibrational structure and complex shifts in position, width, and height of peaks with isotopic substitution. In addition, isotopologue-dependent variations in lifetime of excited states produced upon photon absorption may produce mass-independent effects in the products of secondary reactions (Okabe, 1978).

The current database of sulfur isotopic compositions measured in martian meteorites (Farquhar et al., 2000c, 2007; Kim and Farquhar, 2008; Chapters 2 through 4 of this work) suggests that the martian atmosphere has hosted

photochemical processes of a nature distinct from those that dominated the Archean Earth, which were characterized by $\Delta^{36}S/\Delta^{33}S \approx$ -2 to -0.8 (Farquhar et al., 2000a, 2000c, 2001, 2007c). In contrast, the nakhlites and several shergottites possess S-MIF signatures characterized by significant variation in $\Delta^{33}S$ with little variation in $\Delta^{36}S$ and a small positive slope of 0.5 to 0.6 in $\Delta^{36}S$-$\Delta^{33}S$ space (Farquhar et al., 2000c, 2007a; Chapters 2 and 3). Recent analyses have shown that the sulfur isotopic record of early Earth includes time intervals with a similar pattern of substantial non-zero $\Delta^{33}S$ and zero $\Delta^{36}S$, interpreted to indicate atmospheric processes (Ono et al., 2006a; Farquhar et al., 2000b).

Previous laboratory experiments with $SO_2$ gas using a Hg lamp source generated elemental sulfur with composition forming an array characterized by $\Delta^{36}S/\Delta^{33}S \approx 0.6$ (Farquhar et al., 2001), similar to the relationship between $\Delta^{36}S$ and $\Delta^{33}S$ observed in martian meteorites (Farquhar et al., 2000c, 2007; Chapters 2 and 3). The Hg lamp produces two emission lines at 184.9 and 253.7 nm, which access regions of the $SO_2$ UV absorption spectrum dominated by different photochemical processes (Farquhar et al., 2001). The region below 219.2 nm is dominated by predissociation of $SO_2$, while the region from ~240 to 360 nm is dominated by photoexcitation (Okabe, 1978; Farquhar et al., 2001). Other experiments with alternative UV sources have yielded products characterized by different $\Delta^{36}S$-$\Delta^{33}S$ covariation. Experiments with an Ar laser at 193 nm produced $\Delta^{36}S/\Delta^{33}S \approx$ -1.1, while a KrF laser at 248 nm produced $\Delta^{36}S/\Delta^{33}S \approx$ -4.2 (Farquhar et al., 2001). Experiments with a Xe lamp, generating a continuum > 220 nm, produced $\Delta^{36}S/\Delta^{33}S \approx$ -1.2 (Farquhar et al., 2001). While experiments with these latter three sources yielded products with S-MIF

characteristics approaching those of most Archean samples, to date only the Hg lamp experiments have demonstrated a means to generate S-MIF from $SO_2$ photochemistry that is similar to the signature seen in martian meteorites (Farquhar et al., 2000a, 2000c, 2007a; Chapters 2 and 3).

Since the discrete lines of the Hg lamp and laser sources are not representative of solar radiation, it was desirable to perform additional experiments with a broadband source that would more closely model the natural environment experienced in the martian atmosphere than previous experiments. The study described here utilized a deuterium lamp source to examine the photochemical effects on pure $SO_2$ gas produced by broadband radiation from 180 to 360 nm. This range extends below the 220 nm lower limit of the Xe lamp utilized by Farquhar et al. (2001) to access the spectral region where $SO_2$ dissociation occurs. The experiments included a set using $^{16}O$-rich $SO_2$, characterized by natural abundance of oxygen isotopes, and a set using $^{18}O$-rich $SO_2$, fully-substituted by $^{18}O$. The experiments with $^{16}O$-rich $SO_2$ provided a baseline for comparison of photochemical effects of the broadband source with those of previous experiments using other types of UV sources. The experiments with $^{18}O$-rich $SO_2$ were designed to provide potential clues to the mechanism responsible for producing the S-MIF signal. Previous studies have shown that both primary and secondary photoprocesses are sensitive to intramolecular isotopic substitution (Bhattacharya et al., 2000; Zmolek et al., 1999). For example, S-MIF has been observed during photopolymerization of carbon disulfide; experiments using $^{13}CS_2$ as a reactant yield polymers with significantly larger fractionation than polymers resulting from irradiation of $^{12}CS_2$ (Zmolek et al., 1999). The presence or absence of

such effects upon intramolecular isotopic substitution of oxygen atoms during $SO_2$ photochemistry could help identify the mechanism responsible for the S-MIF generation.

Hereafter, the term "$SO_2$" is used to denote $SO_2$ with natural abundance of oxygen isotopes and "$S^{18}O_2$" to denote $^{18}O$-rich $SO_2$.

## 5.2    Methods

The experiments described here were performed with a 300-watt Oriel-66136 deuterium source operated at 2 A, generating broadband UV radiation from 180-360 nm. Each experiment was run with one of two glass reaction cells of 4-mm wall thickness: a cylindrical cell with inner diameter of 1.9 cm, length of 44 cm, and volume of 164.8 $cm^3$, and a spherical cell with diameter of 10.9 cm and volume of 536.1 $cm^3$. Each reaction cell was epoxy-sealed to a 4-mm fused silica window with diameter of 2.3 cm. The reaction cell was connected to a modular photolysis flow reactor assembly constructed from glass and flexible stainless steel tubing.

Prior to each experiment, the photolysis assembly was evacuated to a pressure below 15 mTorr. $SO_2$ gas was introduced into the evacuated manifold to achieve an experimental pressure of 10-20 Torr. The $SO_2$ was then cryogenically purified with liquid nitrogen. A small amount of non-reacted $SO_2$ was preserved at the beginning of each experiment for measurement of the initial sulfur isotopic composition. The remainder was isolated in the reaction cell, which was placed with its fused silica window adjacent to the deuterium lamp aperture. The entire reaction cell was

wrapped with aluminum foil to isolate the lighting conditions inside the cell from the ambient laboratory environment.

After the $SO_2$ in the reaction cell was irradiated for 2.5 to 4.5 hours, the products and residual $SO_2$ were extracted and processed using standard laboratory methods (Farquhar et al., 2001; Johnston et al., 2006). The preserved initial $SO_2$ and the residual $SO_2$ were converted to sulfate by reaction with 30% hydrogen peroxide solution at room temperature. The resulting sulfuric acid was extracted with Milli-Q water and then precipitated as barium sulfate by the addition of several drops of 10% barium chloride solution. The barium sulfate was rinsed with milliQ water and dried in a 90° C oven prior to reduction. The dried barium sulfate was reduced in a boiling flask with 25 mL of a solution prepared from 12 N hydrochloric, 48% hydroiodic, and 50% hypophosphorous acids (Thode et al., 1961). The boiling flask was connected to the lower adapter of a distillation apparatus that was actively purged with nitrogen gas. The solution was heated to ~85 ℃ for approximately 3 hours, reducing the barium sulfate to $H_2S$. After passing through a Milli-Q water trap, purified $H_2S$ was carried through a centrifuge tube containing 14 mL of 0.1 M zinc acetate solution, where it reacted to form zinc sulfide. Dropwise addition of 0.2 M silver nitrate solution after the distillation process converted the zinc sulfide to silver sulfide, $Ag_2S$. After allowing at least several hours for the exchange reaction to complete, the resulting precipitate was filtered on a 0.2 μm cellulose filter and rinsed with 150 mL of Milli-Q water, washed with 15 mL of 0.1 M ammonium hydroxide solution to remove excess silver ions, then rinsed with an additional 150 mL of Milli-Q water.

Ag$_2$S was transferred from the filter paper to aluminum foil packets that had been cleaned with ethanol and dried overnight in a 90° C oven.

A similar method was used for the reduction of product elemental sulfur, which was extracted from the reaction cell with carbon tetrachloride and evaporated to dryness in a double-necked boiling flask with septum seal. The flask was connected to the lower adapter of a distillation apparatus purged with nitrogen gas. Chromium (II) reduction solution (CRS) was prepared in a nitrogen atmosphere by overnight reaction of chromium (III) chloride in a solution of 0.5 N HCl and zinc metal. Fifteen mL of CRS and 15 mL of 5 N HCl were injected through the septum into the boiling flask containing the elemental sulfur sample, with nitrogen flowing through the distillation apparatus. Solutions were heated to ~60 ºC for approximately 3 hours, generating H$_2$S that was captured and converted to Ag$_2$S as described above, with one exception. In some experiments, particularly when the irradiation duration was relatively short, the product yield of elemental sulfur may have been too low for cellulose filtering of the Ag$_2$S. In these cases, the Ag$_2$S was instead purified by centrifugation and washing with Milli-Q water and ammonium hydroxide solution.

Ag$_2$S was converted to SF$_6$ by reaction with 250 µmol of fluorine gas in a nickel reaction vessel at 250° C for 8 hours. The SF$_6$ was subsequently condensed from the residual F$_2$ into a trap cooled with liquid nitrogen. Excess F$_2$ was passivated by reaction with KBr salt. Replacement of the liquid nitrogen coolant on the trap with ethanol slush at -115° C allowed distillation of the SF$_6$ from the trap into the liquid-nitrogen-cooled injection loop of a gas chromatograph (GC). The SF$_6$ was purified by a 1/8-inch diameter, 6-foot long Molecular Sieve 5A GC column, followed by a 1/8-

inch diameter, 12-foot long Haysep-Q™ GC column. Both columns were held at 50°C, with helium carrier gas flow rate of 20 mL/min. After its elution from the GC column, the $SF_6$ was captured in spiral glass traps cooled with liquid nitrogen, then transferred to the bellows of a Thermofinnigan MAT 253 dual-inlet gas source mass spectrometer. The sulfur isotopic composition of the $SF_6$ was measured by monitoring $SF_5^+$ ion beams at *m/z* of 127, 128, 129, and 131 Da. Results of the experiments were renormalized with respect to the initial $SO_2$ isotopic composition to facilitate understanding of the photochemical fractionation effects. Estimated $1\sigma$ uncertainties based on repeated measurements of IAEA reference materials in this laboratory are generally better than 0.15‰, 0.008‰, and 0.15‰ for $\delta^{34}S$, $\Delta^{33}S$, and $\Delta^{36}S$, respectively. However, the uncertainties in mass spectrometric measurements for specific values are reported when they exceed these values, to represent more accurately the larger uncertainties encountered in measuring isotope ratios of extremely small quantities of analyte.

## 5.3    Results

Table 5-1(a) presents the data collected from the $SO_2$ and $S^{18}O_2$ photolysis experiments, with uncertainties given in Table 5-1(b). The data as shown in Table 5-1(a) represent fractionation with respect to the sulfur isotopic composition of the initial gas. The corresponding uncertainties in Table 5-1(b) include error propagation from the renormalization of raw data with respect to the initial gas. The data indicate reduced magnitude of fractionation for the experiments with $^{18}O$-rich $SO_2$ as compared to $^{16}O$-rich $SO_2$. Products and residual gas from the $S^{18}O_2$ experiments

show both smaller delta values for each sulfur isotope and smaller deviations from mass-dependent behavior, quantified as $\Delta^{33}S$ and $\Delta^{36}S$.

The measured $\delta^{34}S$ of elemental sulfur from the $S^{18}O_2$ experiments ranges from $92.05 \pm 0.15‰$ to $114.89 \pm 0.15‰$ (average $104.38 \pm 0.15‰$). In comparison, the $SO_2$ experiments yield product elemental sulfur with $\delta^{34}S$ ranging from $167.81 \pm 0.15‰$ to $177.22 \pm 0.11‰$ (average $172.76 \pm 0.15‰$). On average, the difference in $\delta^{34}S$ for the $SO_2$ and $S^{18}O_2$ experiments ($SO_2$ - $S^{18}O_2$) is $68.38‰$. The residual sulfur dioxide gas displays less pronounced or consistent differences between $^{18}O$-rich $SO_2$ and $^{16}O$-rich $SO_2$, as there is some overlap between the data, but generally indicates a lower range of fractionation for the $S^{18}O_2$ experiments than for those performed with $^{16}O$-rich $SO_2$. The residual $S^{18}O_2$ shows $\delta^{34}S$ of $-1.25 \pm 0.15‰$ to $-2.48 \pm 0.15‰$ (average $-2.03 \pm 0.15‰$). For the $^{16}O$-rich $SO_2$ experiments, residual $SO_2$ shows $\delta^{34}S$ of $-1.37 \pm 0.15‰$ to $-5.56 \pm 0.15‰$ for (average $-3.04 \pm 0.15‰$). On average, the difference in $\delta^{34}S$ for the $SO_2$ and $S^{18}O_2$ experiments ($SO_2$ - $S^{18}O_2$) is $-1.01‰$.

Deviation from mass-dependent fractionation is illustrated on plots of $\Delta^{33}S$ versus $\delta^{34}S$ and $\Delta^{36}S$ versus $\delta^{34}S$ in Figure 5-1. Figure 5-1(a) shows $\Delta^{33}S$ versus $\delta^{34}S$ for both residual $SO_2$ and product elemental sulfur, while Figure 5-1(b) shows a detailed perspective of the residual gas data. Elemental sulfur has $\Delta^{33}S$ values of $8.33 \pm 0.05‰$ to $16.30 \pm 0.05‰$ (average $13.25 \pm 0.06‰$) for experiments with $S^{18}O_2$ and $16.56 \pm 0.05‰$ to $23.19 \pm 0.05‰$ (average $18.60 \pm 0.05‰$) for experiments with $SO_2$. Figure 5-1(b) shows $\Delta^{33}S$ for residual gas of $-0.02 \pm 0.05‰$ to $-0.25 \pm 0.05‰$ (average $-0.15 \pm 0.05‰$) for $S^{18}O_2$ and $-0.10 \pm 0.04‰$ to $-0.52 \pm 0.05‰$ (average $-0.27 \pm 0.05‰$) for $SO_2$ experiments. As expected from mass balance considerations,

Figure 1(a) shows that the $\Delta^{33}S$ for elemental sulfur lies above the baseline, which represents mass-dependent fractionation, while the residual gas data in Figure 5-1(b) lies below the baseline.

Similar data for $\Delta^{36}S$ are shown in Figures 5-1(c) and 5-1(d). Figure 5-1(c) displays $\Delta^{36}S$ versus $\delta^{34}S$ for both residual $SO_2$ and product elemental sulfur, while Figure 5-1(d) shows a detailed perspective of the residual gas data. The $\Delta^{36}S$ for elemental sulfur ranges from $-21.33 \pm 2.16‰$ to $-41.86 \pm 0.48‰$ (average $-33.59 \pm 1.03‰$) for experiments with $S^{18}O_2$ and $-41.09 \pm 0.38‰$ to $-48.63 \pm 0.43‰$ (average $-43.47 \pm 0.38‰$) for experiments with $SO_2$. As detailed in Figure 5-1(d), $\Delta^{36}S$ for residual gas ranges from $-0.20 \pm 0.22‰$ to $0.67 \pm 0.22‰$ (average $0.18 \pm 0.25‰$) for $S^{18}O_2$ and $0.06 \pm 0.23‰$ to $0.35 \pm 0.21‰$ (average $0.19 \pm 0.22‰$) for $SO_2$ experiments. Figure 5-1(c) shows that the $\Delta^{36}S$ for elemental sulfur lies below the mass-dependent fractionation baseline, while the residual gas data illustrated in Figure 5-1(d) lie primarily above the baseline.

It is immediately clear from Figures 5-1(a) through 5-1(d), which graphically display the differences in sulfur fractionation between the $S^{18}O_2$ and $SO_2$ experiments, that the elemental sulfur produced during photolysis of $S^{18}O_2$ is less fractionated with respect to the initial gas than that produced during experiments with $SO_2$. It is also evident from the figures that the experimental products do not exhibit mass-dependent isotopic composition. The $\Delta^{33}S$ and $\Delta^{36}S$ of the elemental sulfur products do not show strong correlation with $\delta^{34}S$, but are clustered within small ranges of $\delta^{34}S$ for the $^{18}O$-rich and $^{16}O$-rich $SO_2$ samples. The $\Delta^{33}S$ and $\Delta^{36}S$ of residual gas samples in Figures 5-1(b) and 5-1(d) show significantly less consistency

and order than those of the elemental sulfur samples, which may be due to reformation of $SO_2$ from fractionated photo-fragments during the experiments.

**Table 5-1(a). Sulfur isotopic data from photolysis experiments presented as per mil deviation from isotopic composition of initial gas**

| | Residual $SO_2$ | | | Product elemental sulfur | | |
|---|---|---|---|---|---|---|
| | $\delta^{34}S$ | $\Delta^{33}S$ | $\Delta^{36}S$ | $\delta^{34}S$ | $\Delta^{33}S$ | $\Delta^{36}S$ |
| $SO_2$ | -5.04 | -0.52 | 0.35 | 175.33 | 23.19 | -48.63 |
| | -1.37 | -0.10 | 0.10 | 177.22 | 17.40 | -43.74 |
| | -1.66 | -0.13 | 0.15 | 167.81 | 16.56 | -41.09 |
| | -1.57 | -0.18 | 0.06 | 170.41 | 17.92 | -41.37 |
| | -5.56 | -0.40 | 0.30 | 173.03 | 17.93 | -42.54 |
| $S^{18}O_2$ | -1.88 | -0.18 | 0.01 | 114.89 | 15.23 | -41.44 |
| | -2.38 | -0.25 | 0.67 | 113.05 | 16.30 | -41.86 |
| | -2.16 | -0.02 | -0.20 | 103.43 | 8.33 | -35.96 |
| | -1.25 | -0.12 | 0.24 | 92.05 | 12.56 | -21.33 |
| | -2.48 | -0.19 | 0.19 | 98.47 | 13.82 | -27.37 |
| | Averages | | | | | |
| | $\delta^{34}S$ | $\Delta^{33}S$ | $\Delta^{36}S$ | $\delta^{34}S$ | $\Delta^{33}S$ | $\Delta^{36}S$ |
| $SO_2$ | -3.04 | -0.27 | 0.19 | 172.76 | 18.60 | -43.47 |
| | ± 0.15 | ± 0.05 | ± 0.22 | ± 0.15 | ± 0.05 | ± 0.38 |
| $S^{18}O_2$ | -2.03 | -0.15 | 0.18 | 104.38 | 13.25 | -33.59 |
| | ± 0.15 | ± 0.05 | ± 0.25 | ± 0.15 | ± 0.06 | ± 1.03 |

**Table 5-1(b). Errors (1$\sigma$) in sulfur isotopic data from photolysis experiments**

| | Residual $SO_2$ | | | Product elemental sulfur | | |
|---|---|---|---|---|---|---|
| | $\delta^{34}S$ | $\Delta^{33}S$ | $\Delta^{36}S$ | $\delta^{34}S$ | $\Delta^{33}S$ | $\Delta^{36}S$ |
| $SO_2$ | ± 0.15 | ± 0.05 | ± 0.21 | ± 0.15 | ± 0.05 | ± 0.43 |
| | ± 0.15 | ± 0.04 | ± 0.22 | ± 0.15 | ± 0.05 | ± 0.36 |
| | ± 0.15 | ± 0.05 | ± 0.22 | ± 0.15 | ± 0.05 | ± 0.38 |
| | ± 0.15 | ± 0.05 | ± 0.23 | ± 0.15 | ± 0.05 | ± 0.35 |
| | ± 0.15 | ± 0.04 | ± 0.21 | ± 0.15 | ± 0.05 | ± 0.39 |
| $S^{18}O_2$ | ± 0.15 | ± 0.04 | ± 0.24 | ± 0.15 | ± 0.06 | ± 0.33 |
| | ± 0.15 | ± 0.05 | ± 0.22 | ± 0.15 | ± 0.05 | ± 0.48 |
| | ± 0.15 | ± 0.04 | ± 0.22 | ± 0.15 | ± 0.05 | ± 0.30 |
| | ± 0.15 | ± 0.05 | ± 0.37 | ± 0.15 | ± 0.08 | ± 2.16 |
| | ± 0.15 | ± 0.05 | ± 0.22 | ± 0.15 | ± 0.07 | ± 1.85 |
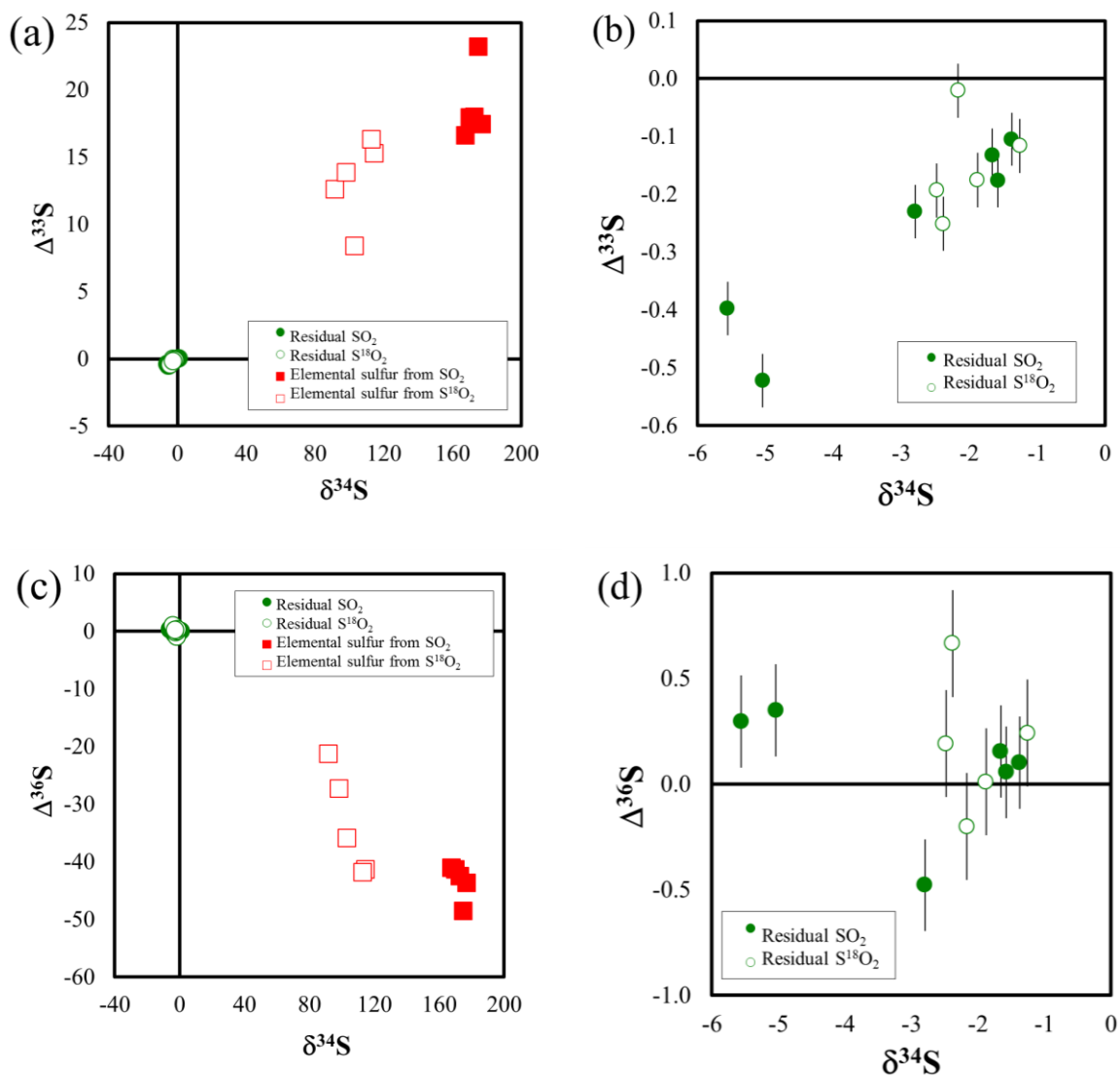
**Figure 5-1. Isotopic composition of products and residues of photolysis experiments.**

Results are reported with respect to initial gas composition. If 2σ error bars are not visible, they are smaller than the symbols. (a) $\Delta^{33}S$ vs. $\delta^{34}S$ for residual gas and elemental sulfur product. (b) $\Delta^{33}S$ vs. $\delta^{34}S$ for residual gas. (c) $\Delta^{36}S$ vs. $\delta^{34}S$ for residual gas and elemental sulfur product. (d) $\Delta^{36}S$ vs. $\Delta^{34}S$ for residual gas.

## 5.4    Discussion

### 5.4.1    SO₂ Absorption Spectrum

SO$_2$ exhibits a complex absorption spectrum in the near UV as well as vacuum UV regions. According to Okabe (1978), there are three main SO$_2$ absorption regions in the UV. A very weak absorption at 340-390 nm and a moderate absorption at 260-340 nm are characterized by photoexcitation resulting in fluorescence, phosphorescence, or self-quenching products of SO$_2$, SO and SO$_3$. Product SO$_3$ from this process can also hydrate to produce H$_2$SO$_4$. A strong absorption system at 180-235 nm produces a reaction network similar to that of the 260-340 nm region. Absorption at 180-235 nm is attributed to competition between fluorescence, which predominates above 219.2 nm, and predissociation leading to the production of SO, predominating below 219.2 nm. Photodissociation of sulfur monoxide to elemental sulfur is also attributed to predissociation near 200 nm (e.g., Speth et al., 1998; Archer et al., 2000).

Because of the characteristics of the deuterium lamp, these experiments principally probe the absorption system from 180-235 nm, with some longer wavelength contributions. Figure 5-2 displays the absorption spectrum of SO$_2$ as well as the normalized deuterium lamp spectrum as a function of wavelength. The lamp spectrum from 180-300 nm was measured at the NASA Goddard Space Flight Center with an Acton Research Corporation UV spectrometer, comprising a monochromator and reflectometer connected to a photomultiplier tube. To replicate the conditions of the photolysis experiments, the deuterium lamp was placed with its window in room

air, adjacent to the $MgF_2$ window of the spectrometer chamber. A fused silica filter in front of the detector mimicked the attenuation effects of the photocell window during the experiments. A second deuterium lamp spectrum, generated from a different source with its output inside the spectrometer vacuum chamber, is also shown in the figure for comparison. It is evident that absorption below ~190 nm by components of air prevents a portion of radiation at the shortest wavelengths from reaching the photocell. However, there is still substantial radiation available from 190-220 nm, the region dominated by photodissociation. The lamp spectrum from 300-390 nm was extrapolated based on data provided by Oriel.
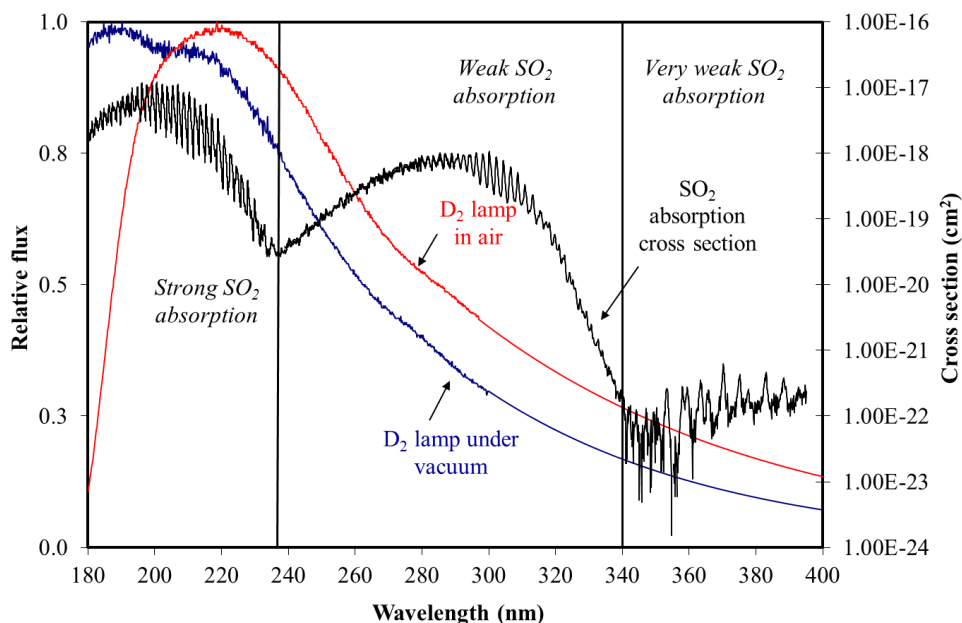
**Figure 5-2. Deuterium lamp spectrum and $SO_2$ absorption spectrum.**

**The lamp spectrum in air is representative of the conditions for the experiments described here. Another lamp spectrum under vacuum is included for comparision, showing the loss of intensity from absorption by air below ~190 nm. Lamp spectra are measured from 180-300 nm; spectra from 300-390 nm were obtained by extrapolation based on data provided by Oriel. The $SO_2$ absorption spectrum is from Wu et al. (2000) and Bogumil et al. (2003).**

150

Fully interpreting the S-MIF observed in the rock record involves pinpointing the specific process or processes and thus the spectral wavelengths responsible for generating the anomalous sulfur compositions. This in turn carries potential implications constraining the chemical makeup and optical depth of the atmosphere at the time the reactions occurred. The experiments described here were designed to reveal clues to the origin of the S-MIF effects given certain possibilities, such as self-shielding, isotopologue-dependent variations in absorption cross section, or spin-forbidden reactions that would favor $^{33}$S over other isotopes (Bhattacharya et al., 2000; Lyons, 2007, 2009; Danielache et al., 2008).

It is not possible in these broadband UV experiments to isolate definitively the specific wavelength responsible for the sulfur fractionation, although it is notable that the deuterium lamp source provides significantly less radiation in the region dominated by photoexcitation (260-340 nm) than in the region where predissociation occurs (< 235 nm). The fact that the large S-MIF of these experiments is seen in elemental sulfur products implicates dissociation of $SO_2$ as a critical step in its formation. There are multiple pathways through which this dissociation could occur. Kawasaki and Sato (1987) determined that the dissociation of $SO_2$ at 193 nm is due to predissociation because the angular distribution of fragments indicates a long dissociative lifetime and because intersystem crossing to a repulsive triplet state allows dissociation to take place. There are reports that direct dissociation to form S and $O_2$ can occur from single-photon absorption at shorter wavelengths that were not

accessed in the current experiments (e.g., Wisniewski and Castleman, 2002; Knappenberger and Castleman, 2004). However, several studies have shown that multi-photon absorption at longer wavelengths can also produce elemental sulfur. According to Effenhauser et al. (1990), absorption of two photons at 248 nm produces SO + O and S + $O_2$ as fragments. They also stated that absorption of two photons at 308 nm gives SO + O in various states, and S + $O_2$ as a minor pathway. Sato et al. (1992) reported sulfur fragments from two-photon absorption at 286-309 nm and determined that three-body dissociation at 308 nm would require the absorption of three photons. They directly observed only two-photon processes, which occur due to the long-lived $\tilde{B}$ state of $SO_2$, and suggested that perhaps two-photon dissociation occurs before a third photon can be absorbed in nanosecond excitation sources. Wisniewski and Castleman (2002) stated that the production of elemental sulfur at 312 nm appears to result from secondary fragmentation of SO, rather than three-photon absorption to yield S + O + O. They suggested that S forms from two-photon dissociation through the $\tilde{E}$ state.

Previous studies have attempted to ascribe the observed S-MIF from $SO_2$ photolysis to one or another of these pathways. Modeling of previous gas-phase $SO_2$ experiments at 200 nm was interpreted to indicate that photochemical self-shielding may have caused the sulfur isotopic fractionation (Lyons, 2007). Self-shielding can occur if the optical depth of the gas column causes saturation of the major isotope, resulting in disproportionately high absorption by minor isotopes and enrichment of them in photochemical products. Gas pressures of 10–30 Torr within the photocell during these experiments produced a $^{32}SO_2$ column density of approximately $2 \times 10^{18}$

cm$^{-2}$ and optical depth of about 20, which represent strongly self-shielding conditions for $^{32}SO_2$ (Lyons, 2007, 2009). However, elemental sulfur products in these experiments displayed depletion in $^{36}S$ compared to mass-dependent behavior and enrichment in $^{33}S$. A set of companion experiments performed in the same UM laboratory to examine the effects of pressure and third-body interactions on the sulfur isotopic fractionation during broadband $SO_2$ photolysis also suggested that self-shielding likely plays only a minor role in producing the observed mass-independent sulfur compositions (Masterson et al., 2011). Instead, those authors postulated a kinetic origin for the large fractionation observed, produced from predissociative excited state dynamics of $SO_2$.

Interpretation of $SO_2$ photolysis data in light of the current results must account for the new observation that substitution of $^{18}O$ for $^{16}O$ in the $SO_2$ significantly alters the magnitude of the S-MIF signal in elemental sulfur products. Another type of shielding mechanism that could potentially create S-MIF effects would occur in the presence of overlapping peaks in the $SO_2$ absorption spectrum. Specifically, if the $^{36}SO_2$ peak for a given quantum number in the bending mode progression were shifted sufficiently in wavelength that it coincided with the $^{32}SO_2$ peak of the next quantum number, the more-prevalent $^{32}SO_2$ could absorb most or all of the photons at that wavelength and thus deplete the products in $^{36}S$ (Lyons et al., 2009). Unlike simple self-shielding due solely to column density, this mechanism could produce enrichment in one minor isotopologue and depletion in another, as observed in the experiments. However, theoretical calculations of shifts in $SO_2$ absorption spectra

upon intramolecular isotopic substitution of sulfur and oxygen do not predict such overlap to occur in the region of interest (Danielache et al., 2008; Danielache, 2012).

Few previous studies have examined the effects of intramolecular isotopic substitution on $SO_2$ photochemistry. Knappenberger and Castleman (2004) saw an inverse kinetic isotope effect in excited state dynamics with substitution of $^{34}S$ for $^{32}S$ in gas-phase $SO_2$ experiments. They observed that excited states of $^{34}SO_2$ had slightly longer lifetimes than those of $^{32}SO_2$, implying greater probability of dissociation due to secondary processes for $^{34}SO_2$. Nelson and Borkman (1975) performed isotopic substitution experiments with solid-phase $SO_2$, finding that $S^{18}O_2$ displayed a longer phosphorescence lifetime for the $^3\tilde{B}_1$ state than $S^{16}O_2$. Both of these reports provide evidence that isotopic substitution within $SO_2$ molecules can alter the dynamics such that modified fractionation could manifest in photochemical products, and further suggest that the relative lifetimes of excited molecular states may play a key role in defining the fractionation effects for various isotopologues. The observation that elemental sulfur products have reduced magnitude of S-MIF in both $\Delta^{33}S$ and $\Delta^{36}S$ with $S^{18}O_2$ photolysis, but that the arrays formed by the products and residual $SO_2$ have slopes roughly identical to those seen in experiments with $^{16}O$-rich $SO_2$, supports this idea.

### 5.4.3   *Implications for the S-MIF in Martian Meteorites*

Despite concerted search efforts using ground-based spectroscopy, no $SO_2$ has been detected in the modern martian atmosphere (Krasnopolsky, 2005, 2012; Nakagawa et al., 2009). Recent observations have established a disk-averaged upper limit of 0.3 ppb (Encrenaz et al., 2011; Krasnopolsky, 2012). However, substantial

quantities of $SO_2$ may have been released into the atmosphere during past episodes of volcanic activity (e.g., Gaillard and Scaillet, 2009; Righter et al., 2009). Besides ultimately contributing to the inventory of sulfur at the surface of Mars, these volcanic pulses of $SO_2$ should have produced global climate effects (e.g., Settle, 1979; Postawko and Kuhn, 1986; Halevy et al., 2007; Johnson et al., 2008, 2009; Tian et al., 2010). The concentration of $SO_2$ in the atmosphere during these periods would have determined whether the net impact was that of warming due to greenhouse effects or cooling due to an increase in planetary albedo upon formation of sulfate aerosols (Tian et al., 2010).

If self-shielding were the dominant mechanism controlling production of S-MIF during $SO_2$ photochemistry, it would imply constraints on the column density of $SO_2$ in the atmosphere when the anomalous sulfur was generated. The results reported here suggest that self-shielding is insufficient to explain the S-MIF signatures observed in products of UV photochemistry with $^{16}O$- and $^{18}O$-rich $SO_2$, implying less-stringent constraints on optical depth. Isotopologue-dependent processes could have generated S-MIF in an atmosphere even with low levels of $SO_2$.

Another outstanding question regarding the source of S-MIF in natural samples involves the specific pathway responsible for producing the signals. Assuming that the S-MIF was generated from $SO_2$, there are two potential pathways for its formation, depending on absorption wavelength. As discussed in previous sections, the region from $180 - 235$ nm is characterized by a strong absorption that promotes predissociation of $SO_2$, while the region from $260 - 340$ nm sees moderate absorption leading to photoexcitation (Okabe, 1978). Previous experiments by Farquhar et al.

(2001) probed these two regions through the use of UV sources at different wavelengths. Specifically, these sources included an ArF laser at 193 nm; a KrF laser at 248 nm; a Hg lamp with two discrete lines at 184.7 and 253.7 nm; and a Xe lamp producing a continuum > 220 nm (Farquhar et al., 2001). Products of experiments with these various sources were shown to possess distinct relationships between $\Delta^{33}S$ and $\Delta^{36}S$.

Figure 5-3 shows this covariation for the results reported by Farquhar et al. (2001) as well as the products of the current experiments. The array formed by the residual $SO_2$ and product elemental sulfur of the new broadband experiments with the $D_2$ lamp has a slope of -2.4 on the plot of $\Delta^{36}S$ versus $\Delta^{33}S$. In comparison, the slopes reported for products of previous experiments ranged from -4.2 to 0.6, as noted on the figure. The array formed by the broadband experiments lies between those formed by experiments with the ArF laser (193 nm) and the KrF laser (248 nm), which accessed separate absorption regions. This implies that the results of the broadband experiments may reflect the combined effects of more than one photochemical process.

The Hg lamp products in Figure 5-3 stand apart from those of the other UV sources, having a uniquely positive slope in $\Delta^{36}S$-$\Delta^{33}S$ space that provides the closest analog to the S-MIF signal observed in martian meteorites of the $SO_2$ experiments performed to date. Since the 184.7 nm line of the Hg lamp accessed a region deeper in the UV than those of the other sources, this may indicate that a different mechanism operative in that region is responsible for the observed martian S-MIF.
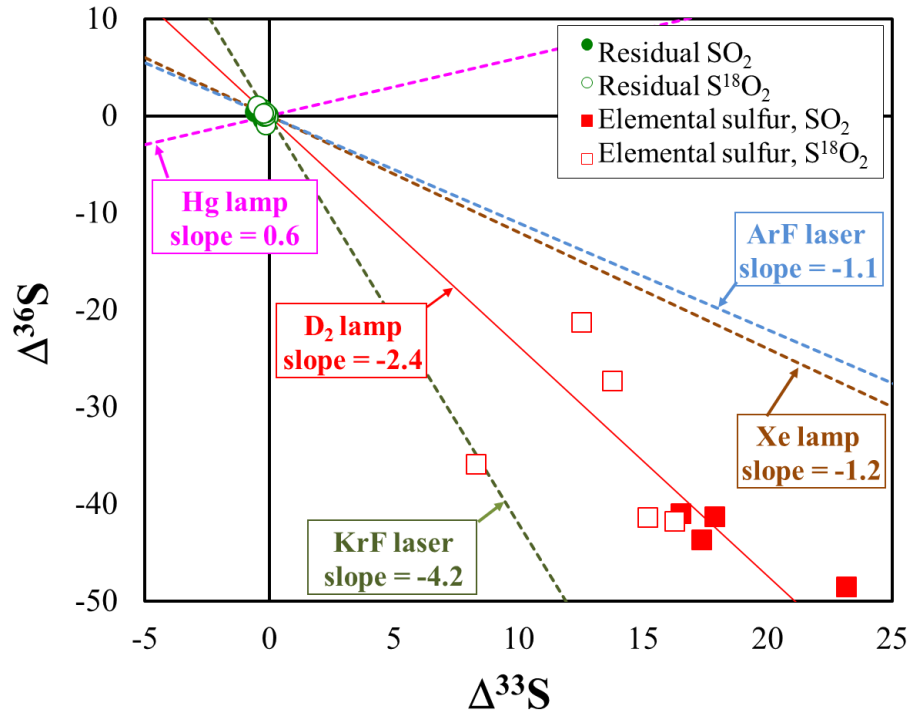
**Figure 5-3. $\Delta^{36}S$ versus $\Delta^{33}S$ for products and residues of photolysis experiments. Delta values are with respect to the initial gas composition. Line fit to products of current experiments with $D_2$ lamp has slope of -2.4. Slopes of data from previous $SO_2$ experiments with different UV sources are indicated with dotted lines: ArF laser, 193 nm; KrF laser, 248 nm; Hg lamp, 184.7 and 253.7 nm; Xe lamp, continuum > 220 nm (Farquhar et al., 2001). Martian meteorite data with S-MIF forms an array with small positive slope, most similar to that of the Hg-lamp experiments reported by Farquhar et al. (2001).**

## 5.5  Conclusions

Large mass-independent fractionation (S-MIF) of sulfur isotopes is produced in laboratory experiments of gas-phase photochemistry of $SO_2$ driven by UV radiation (Farquhar et al., 2001).  This report described results of a suite of experiments designed to investigate the mechanism responsible for the observed S-MIF by comparing sulfur isotopic fractionation produced during the UV photolysis of ^{16}O-rich and ^{18}O-rich $SO_2$. Results reveal generally reduced sulfur fractionation for ^{18}O-rich $SO_2$ as compared to ^{16}O-rich $SO_2$. Disproportionate absorption by minor isotopologues due to self-shielding does not satisfactorily explain these results. In addition, comparison of theoretical absorption spectra for the various $SO_2$ isotopologues does not implicate other types of shielding due to overlapping peaks in the spectra. These results suggest that the mechanism responsible for producing the S-MIF lies in isotopologue-specific absorption or excited-state dynamics of $SO_2$. This implies that S-MIF could have been produced in the martian atmosphere without imposing constraints on column density of $SO_2$.

# Chapter 6:  Summary and Future Directions[1]

[1] The text and figures in this chapter were written/created by H. B. Franz.

## 6.1    Summary of Study Components

As a heterovalent element with multiple stable isotopes, sulfur has become a valuable tracer for geochemical processes on Earth, with applications to a variety of areas from igneous to biological systems. Sulfur has also been found to be ubiquitous on the surface of Mars and is believed to occur at higher abundance in Mars than in Earth (e.g., Gibson et al., 1985; Dreibus and Palme, 1996; McDonough and Sun, 1995; Gaillard and Scaillet, 2009). Sulfur-bearing gases in the atmosphere even at low concentrations can produce global climatic effects (Settle, 1979; Halevy et al., 2007; Johnson et al., 2009), and high levels of sulfate can reduce the pH of fluids at the surface, resulting in enhanced weathering of silicate minerals and suppression of carbonate precipitation (Halevy et al., 2007). Preliminary studies of the sulfur isotopic composition of martian meteorites revealed evidence for cycling of sulfur between atmospheric and surficial reservoirs on Mars, carrying potential implications for martian magmatic processes and climate history (Farquhar et al., 2000c, 2007a).

This dissertation set out to delve more deeply into several areas of martian sulfur geochemistry, to provide contextual data and constraints on issues pertaining to igneous activity, aqueous alteration processes, and atmospheric composition. The main goals and findings in each of these areas are synthesized in this final chapter,

159

which concludes with an overall summary of the broad implications of this work and potential avenues for further study.

### 6.1.1 Juvenile Martian Sulfur Isotopic Composition

Sulfur is the only element besides oxygen that has been shown to undergo mass-independent isotopic fractionation during laboratory photochemical experiments, which may provide clues to processes that have occurred both in the solar nebula and in planetary atmospheres (e.g., Thiemens and Heidenreich, 1983; Thiemens, 1999; Farquhar et al., 2000a, 2000b, 2000c, 2001). Analyses of martian meteorites have shown that martian high-temperature silicates possess an oxygen isotopic composition characterized by relatively uniform mass-independent enrichment in $^{17}O$ compared to the Earth and Moon, but that low-temperature weathering products display a distinctive signature for the martian hydrosphere compared to the bulk silicate planet (e.g., Clayton and Mayeda, 1983; Karlsson et al., 1992; Farquhar et al., 1998). A recent study by Rumble and Irving (2009) revealed heterogeneity in the oxygen isotopic composition of forty-two martian meteorites, most of which were shergottites. Rumble and Irving (2009) suggested that the observed variation in oxygen isotopes could result either from mantle heterogeneities preserved since primary accretion or from incorporation of older, altered crustal material into the younger shergottite magma as it ascended. If the latter interpretation is correct, then a similar heterogeneity in sulfur isotopic composition, consistent with possible photochemical cycling of sulfur through the atmosphere (Farquhar, 2000c), could exist. Studies of sulfur isotopes in the martian meteorite Nakhla have revealed sulfate and possibly sulfide with significantly anomalous sulfur isotopic composition

(Farquhar et al., 2000c, 2007a), which is believed to indicate incorporation of atmospheric sulfur into the martian subsurface. However, full interpretation of the Nakhla sulfur signature hinges upon knowledge of the juvenile sulfur isotopic composition of Mars.

The shergottites are the largest group of martian meteorites, numbering 54 of the 65 meteorites currently believed to come from Mars. They have mafic to ultramafic mineralogical compositions and are thought to represent melts derived from the martian mantle, displaying varying degrees of magmatic evolution but little evidence for aqueous alteration (e.g., Mikouchi et al., 2004; Irving et al., 2010; Rapp et al., 2012). The shergottites also fall into three subgroups based on whether their chondrite-normalized light rare earth element (LREE) patterns are "enriched," "intermediate," or "depleted" (e.g., Longhi, 1991; McSween, 1994). The source of this variation is an active area of debate, with models generally divided between those that favor a depleted martian mantle that acquires enrichment in trace elements through assimilation of crustal material into rising magmas (e.g., Jones, 1989; Herd et al., 2002; Rumble and Irving, 2009) and those that invoke a heterogeneous martian mantle with magmatic trace element content controlled by variable mixing between enriched and depleted mantle reservoirs (e.g., e.g., Borg et al., 1997; Brandon et al., 2000; Borg and Draper, 2003; Debaille et al., 2008).

For this dissertation, the sulfur isotopic compositions of both sulfide and sulfate phases from 30 shergottites were analyzed, providing representative sampling of each mineralogical and trace element category. Separation of the various sulfur-bearing phases allows estimation of the juvenile martian sulfur composition from

igneous sulfides and evaluation of potential contributions of photochemically-processed sulfur into the shergottites. The work described here significantly expands the database of sulfur isotopic composition in martian meteorites by including a number of meteorites that have not previously been studied.

Analysis of the shergottite AVS fractions, representing igneous monosulfide minerals, for this dissertation yields the first estimate of the juvenile martian sulfur isotopic composition, which is identical within measurement errors to that of Cañon Diablo Troilite (CDT). However, four of these meteorites (NWA 2990/5960, Los Angeles, and Tissint) possess mass-independent sulfur (S-MIF) characterized by $\Delta^{33}$S of 0.054 ± 0.013‰ to 0.093 ± 0.008‰ in their AVS fractions. In addition, mass-independent sulfate was found in NWA 2990/5960 and Los Angeles, and also in three additional shergottites (NWA 5298, NWA 5718, and LAR 06319). The anomalous sulfur is interpreted to have been generated through UV photochemical processing of volcanic sulfur-bearing gases in the martian atmosphere, followed by deposition of products carrying S-MIF onto the planet's surface and later introduction into shergottite melts. Reduction and oxidation reactions within the melt then reduced a portion of this surface-derived sulfur to the $S^{2-}$ oxidation state, resulting in its incorporation into igneous pyrrhotite.

The discovery of clearly resolved S-MIF in several shergottites represents a significant contribution by this dissertation, especially given the magnitudes of the sulfate $\Delta^{33}$S anomaly, which are several times as large as those identified by Farquhar et al. (2000c). The direct evidence that this provides for assimilation of martian surface materials into shergottite magmas confirms previous hypotheses of crustal

assimilation based on trace elements (e.g., Jones, 1989; Herd et al., 2002; Rumble and Irving, 2009). Furthermore, comparison of the shergottite S-MIF signature with that of the nakhlites carries potential implications for the long-term evolution of the martian environment. This topic is discussed more fully in the following sections.

### 6.1.2 Evidence for Transfer of Sulfur from the Atmosphere to the Subsurface

Sulfate minerals are found at significant abundance over most of the planet's surface (e.g., Baird et al., 1976; Clark et al., 1976; Bell et al., 2000, Rieder et al., 1997; Lane et al., 2004; Johnson et al., 2007; Klingelhöfer et al., 2004; Rieder et al., 2004; Squyres et al., 2004; Langevin et al., 2005; Gendrin et al., 2005; Wiseman et al., 2008; Murchie et al., 2009; Lichtenberg et al., 2010). Their formation has been attributed to a variety of mechanisms, including oxidation of sulfides in volcanic ash and basaltic rocks through interaction with groundwater or hydrothermal solutions, impact-related oxidation of sulfides, and photochemical oxidation of sulfur-bearing gases introduced into the martian atmosphere by volcanic and hydrothermal activity (e.g., Burns, 1993; Banin et al., 1997; Bibring et al., 2005; Gendrin et al., 2005; Grotzinger et al., 2005; Knauth et al., 2005; Zolotov and Shock, 2005; Arvidson et al., 2006; Andrews-Hanna et al., 2010). The deposition and concentration of the sulfate ion in minerals have been attributed to further chemical and physical processing involving dissolution of sulfate in water, followed by precipitation of various sulfate minerals.

The nakhlites represent a group comprised of eight distinct martian meteorites believed to derive from the same igneous complex on Mars (e.g., Stauffer, 1962;

Papanastassiou and Wasserburg, 1974; Nakamura et al., 1982; Harvey and McSween, 1992a, 1992b; Wadhwa and Crozaz, 1995; Eugster et al., 2002; Shih et al., 2002; Garrison et al., 2005). They preserve multiple lines of evidence for interaction with liquid water at some time during their history on Mars, including associations of sulfate minerals with "iddingsite" alteration material and isotopic compositions that imply formation by martian surface processes (e.g., Bunch and Reid, 1975; Gooding et al., 1991; Treiman et al., 1993; Bridges and Grady, 2000; Treiman and Goodrich, 2002; Changela and Bridges, 2010, Farquhar and Thiemens, 2000; Farquhar et al., 2000; 2007a). Previous analyses of the sulfur isotopic composition of sulfide and sulfate phases in two of these meteorites, Nakhla and MIL 03346, detected S-MIF signatures, suggesting incorporation of atmospherically-processed material (Farquhar et al., 2000c. 2007a; Kim and Farquhar, 2008). The S-MIF isotopic signature observed in nakhlites differs from mass-independent signals found in terrestrial analogs, including present-day sulfate aerosols, sulfate from the ice core record, and sulfate and sulfide from the ancient Earth (older than ~2.4 Ga) (Farquhar et al., 2000a; Lee et al., 2001; Romero et al., 2003; Baroni et al., 2007). In addition, sulfate from Nakhla has been shown to carry a mass-independent oxygen isotopic signal distinct from those of carbonates and hydrous minerals, implying different pathways for the oxidants involved in their formation (Karlsson et al., 1992; Romanek et al., 1998; Farquhar et al., 1998; Farquhar and Thiemens, 2000).

Numerous questions have been raised by these studies concerning the relationships between martian sulfide and sulfate minerals, the pathways leading to formation of sulfate, and the possibility of assimilation and incorporation of sulfosalts

into magmas in the subsurface and at the surface of Mars. This dissertation presents new measurements of $\delta^{34}S$, $\Delta^{33}S$, and $\Delta^{36}S$ from the nakhlites Y000593, NWA 6148, and NWA 998 obtained by sequential chemical processing of whole-rock material, designed to extract sulfur from multiple mineral phases. Sulfate fractions of all three meteorites show S-MIF compositions, with negative values of $\Delta^{33}S$ bracketed by those previously determined for sulfate in Nakhla (Farquhar et al., 2000c, 2007a). Comparison of data for nakhlites believed to have formed at different depths below the martian surface reveals distinct differences in their sulfur isotopic compositions as well as mineralogical and textural properties. The results of this dissertation suggest that aqueous alteration of these meteorites on Mars occurred during multiple, separate events, rather than a single event.

### 6.1.3 *Evidence for Magmatic Reduction of Surface Sulfur*

Assimilation of crustal material into martian magmas is one of the leading candidates for the mechanism responsible for producing variations in trace element abundance among martian meteorites (e.g., Jones, 1989; Herd et al., 2002; Rumble and Irving, 2009). An alternative model assumes mixing between distinct depleted and enriched source reservoirs within the mantle that were established during a global magma ocean stage (e.g., Borg et al., 1997; Brandon et al., 2000; Borg and Draper, 2003; Debaille et al., 2008). Sulfur isotope systematics have the potential to shed light on this debate by providing an additional tracer for assimilation of surface deposits into igneous rocks. Like oxygen, sulfur has multiple stable isotopes that are susceptible to isotope effects that deviate from those predicted solely on the basis of isotopic mass differences (e.g., Thiemens and Heidenreich, 1983; Thiemens et al.,

1999). An important cause of such S-MIF in planetary atmospheres and the solar nebula is believed to be ultraviolet photochemistry (Thiemens et al., 1999; Farquhar et al., 2000a, 2000c, 2001). The effects of photochemistry include primary processes, which include the initial photon absorption and the immediately subsequent formation of an electronically excited state, and secondary processes, which include unimolecular processes such as fluorescence, phosphorescence, and dissociation as well as bimolecular reactions such as collisional deactivation or reactions of the excited state (Okabe, 1978).

The largest S-MIF signals measured by Farquhar et al. (2000c, 2007a) were found in the sulfate fraction of the Nakhla meteorite, although the AVS fraction of Nakhla was also shown by those studies to possess a small negative $\Delta^{33}$S anomaly. Farquhar et al. (2000c, 2007) suggested that this could indicate incorporation of surface sulfur into igneous sulfide minerals. The subsequent observation by Kim and Farquhar (2008) of significant S-MIF in a sulfide fraction of the MIL 03346 nakhlite confirmed the suggestion of high-temperature sulfur assimilation processes, likely including chemical reduction. This question was further investigated for this dissertation by determining the sulfur isotopic composition of individual sulfide grains in four martian meteorites via ion microprobe (SIMS).

Recent SIMS analysis of individual pyrrhotite grains in the Nakhla, MIL 03346, and NWA 6148 nakhlites reveal clearly resolved S-MIF characterized by negative $\Delta^{33}$S in MIL 03346, and small but not clearly resolved negative $\Delta^{33}$S anomalies in Nakhla and NWA 6148. These data are consistent with results of high-precision sulfur isotope measurements obtained via chemical extraction techniques for these

and other nakhlites (Chapter 3) and are interpreted as evidence for assimilation of sulfur from the martian surface during nakhlite magmatic processes. Results for sulfur isotopic compositions measured by both SIMS and chemical extraction techniques are shown in Figure 6-1.

The simplest explanation for the sulfide isotopic variations in the nakhlite sulfides would be variable assimilation of local sulfate deposits in sediments or salts during emplacement of magma at the surface or shallow subsurface. This explanation has the advantage of assimilating shallow crustal materials in place, without the need to invoke processes of sulfur transfer and distribution within the crust prior to nakhlite magmatism. A potential problem with this scenario is that the pyrrhotite grains, some of which are > 100 μm in size for MIL 03346, would have had to form rapidly as the magma cooled.

An alternative explanation for the variations in nakhlite sulfide isotopic compositions invokes penetration of a sulfate-bearing hydrothermal fluid into a deep region of the crust that hosted the nakhlite magma chamber. This anomalous sulfur could have been subsequently incorporated into nakhlite magmas through assimilation of altered wall rock, followed by reduction to $S^{2-}$ within the melt and formation of pyrrhotite with S-MIF compositions. In this scenario, explanations for the cause of variation in S-MIF magnitudes among the nakhlite sulfides depend on assumptions regarding single versus multiple mantle source regions. If all of the nakhlites derived from a single magma chamber, then variations in pyrrhotite isotopic compositions suggest either that physical segregation of magma occurred in the chamber to produce poorly mixed regions reflecting localized assimilation of wall

167

rock material or that temporal changes in assimilated contents are reflected in nakhlites produced by separate flows. If the nakhlites instead derived from multiple magma chambers, the isotopic variations may be explained more simply by separate assimilation processes that occurred in the different chambers.

Sulfides in several sections of the ALH 84001 meteorite were also analyzed by SIMS for this dissertation. The average isotopic composition of these grains has a negative value of $\Delta^{33}S$ similar to that measured in several nakhlite phases, but smaller than the S-MIF reported for two ALH 84001 pyrite grains by Greenwood et al. (2000b) of -0.74 ± 0.38‰ and -0.51 ± 0.38‰. A small negative $\Delta^{33}S$, comparable to that of Nakhla, was also found during chemical extraction of ALH 84001 whole rock material (Kim and Farquhar, unpublished data). If the S-MIF signal in ALH 84001 is real, it may indicate that the a similar assimilative process of photochemically-derived sulfur operated during time periods of ~4.1 Ga and 1.3 Ga. However, the ALH 84001 SIMS data carry large uncertainties due to small grain sizes, and they do not represent a clearly resolved S-MIF detection. The results of this dissertation combined with those of Kim and Farquhar and Greenwood et al. (2000b) suggest that further study of the ALH 84001 sulfur composition is warranted.
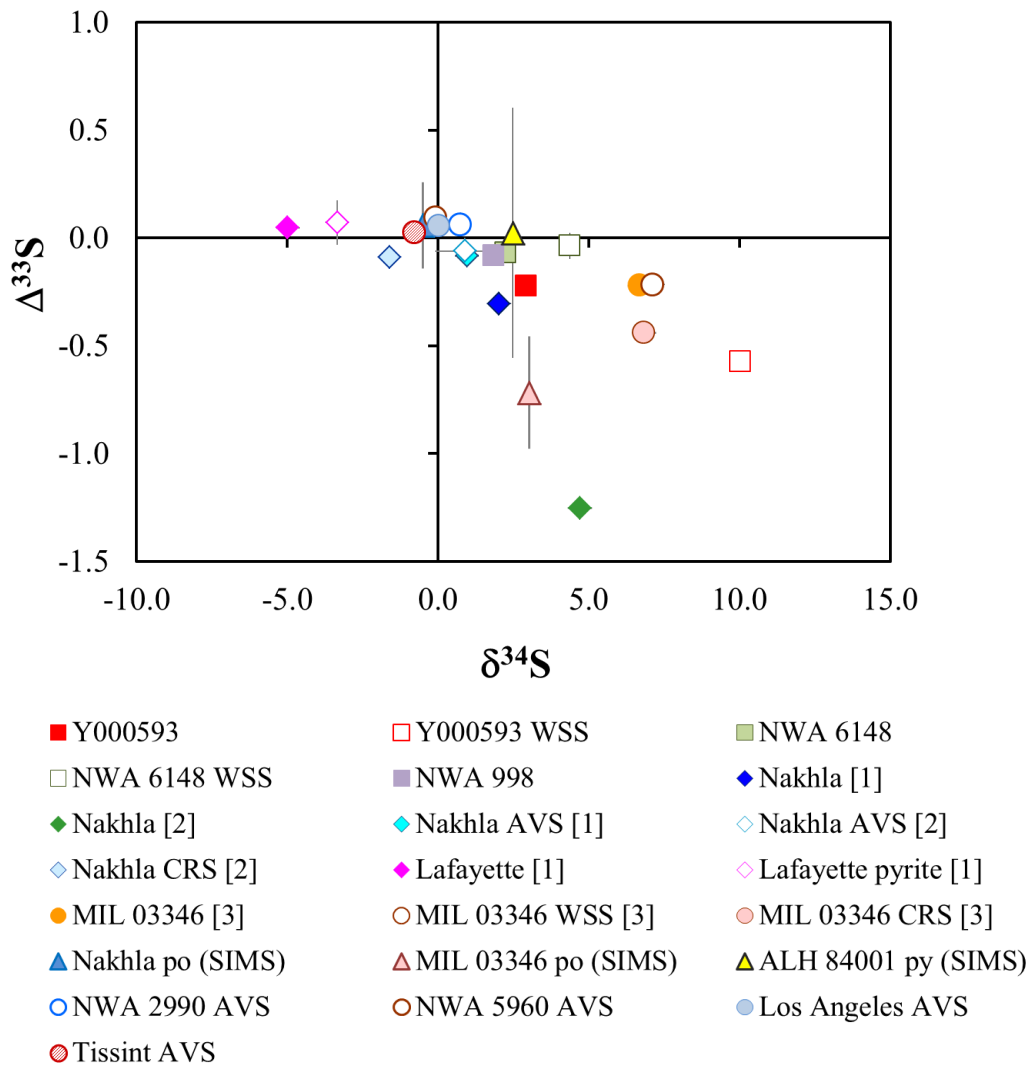
**Figure 6-1.** $\Delta^{33}S$ vs. $\delta^{34}S$ of nakhlites: SIMS and chemical extraction data.
po = pyrrhotite; py = pyrite; [1] Farquhar et al., 2000c; [2] Farquhar et al., 2007a; [3] Kim and Farquhar, 2008.

*6.1.4 SO₂ Photolysis Mechanisms*

Previous laboratory experiments have indicated that S-MIF is produced in gas-phase UV photochemistry of sulfur-bearing molecules, including $SO_2$, $H_2S$, and $CS_2$ (Farquhar et al., 2001; Zmolek et al., 1999), and many of the specific causes of this chemistry remain to be understood. Comparison of sulfur isotopic fractionation produced by laboratory photochemistry experiments and the S-MIF signals observed in the ancient terrestrial rock record and in martian meteorites provide compelling hints of a cause-and-effect relationship (e.g., Farquhar et al., 2000, 2001, 2007a). If this relationship were fully characterized, it would imply constraints on the chemical and physical composition of the respective planetary atmospheres at the times the anomalous signals were generated. Such characterization requires determination of the precise mechanism(s) responsible for producing the observed fractionation.

This study included a suite of experiments designed to investigate the mechanism(s) responsible for the observed S-MIF by comparing sulfur isotopic fractionation produced during the UV photolysis of $^{16}O$-rich and $^{18}O$-rich $SO_2$. Results reveal generally reduced sulfur fractionation for $^{18}O$-rich $SO_2$ as compared to $^{16}O$-rich $SO_2$. Disproportionate absorption by minor isotopologues due to self-shielding does not satisfactorily explain these results. In addition, comparison of theoretical absorption spectra for the various $SO_2$ isotopologues does not implicate other types of shielding due to overlapping peaks in the bending mode progression. These results suggest that the mechanism responsible for producing the S-MIF lies in isotopologue-specific absorption or excited-state dynamics of $SO_2$.

## 6.2    The Larger Picture

This study has shown compelling evidence for assimilation of surface-derived sulfur into martian magmas during formation of the nakhlite lithologic unit at ~1.3 Ga. From this it can logically be inferred that similar processes may have occurred throughout Mars' history. Other results of this study reveal a distinctly different S-MIF in the much younger shergottites, raising new questions based on this variation in sulfur isotopic composition. It cannot be determined whether the S-MIF signals carried by the nakhlites and shergottites were produced by atmospheric processes close in time to their respective volcanic events or whether they were generated during earlier periods and retained in surface reservoirs until assimilation by nakhlite or shergottite magmas. While models of crustal production show that there has been a steady decline in volcanic activity throughout Mars' history,  application of refined cratering age techniques to recent data from spacecraft orbiting Mars has revealed episodes of volcanic activity as recent as ~100 Ma (Hartmann et al., 1999; Neukum et al., 2010).  Furthermore, the analysis by Neukum et al. (2010) argued for pulses in intensity of both volcanic and fluvial or glacial processes on Mars at time periods corresponding to the formation ages of nakhlites and shergottites. Therefore it is reasonable to assume that photochemical S-MIF production could have occurred in the martian atmosphere during any or all of these episodes.

The quantity of sulfur that could have been released into Mars' atmosphere by volcanic activity is dependent on the amount of sulfur that could have been dissolved in martian silicate melts, which in turn depends on sulfur fugacity ($f\mathrm{S}_2$), oxygen

fugacity ($f$O$_2$), temperature, pressure, and melt composition (e.g., Haughton et al., 1974; Wallace and Carmichael, 1992). Sulfur may occur in multiple valence states in basaltic magmas, predominately sulfide (S$^{2-}$) and sulfate (S$^{6+}$) (Wallace and Carmichael, 1992). The speciation of sulfur in a melt significantly affects its solubility, with sulfate-dominated magmas able to dissolve more sulfur (Carroll and Rutherford, 1985; Jugo, 2009). Studies have shown that at magmatic temperatures, sulfur should occur as >80% sulfide at $f$O$_2$ below the quartz-fayalite-magnetite (QFM) buffer, characteristic of nearly all known martian magmas based on meteorite compositions (e.g., Wallace and Carmichael, 1985; Wadhwa, 2001; Herd et al., 2002; Chevrier et al., 2011).

While most studies of magmatic sulfur content have been based on terrestrial systems, recent work by Righter et al. (2009) provided experimental data for melts more characteristic of shergottites, which are FeO-rich and Al$_2$O$_3$-poor compared to basaltic melts on Earth. Righter et al. (2009) determined that primitive martian magmas would be capable of dissolving at most 4000 ppm of sulfur at sulfide saturation, representing a fundamental controlling variable in the quantity of sulfur degassed on Mars. Gaillard and Scaillet (2009) emphasized that in addition to magmatic $f$O$_2$ and atmospheric pressure during degassing, the species of sulfur-bearing gases released by martian volcanoes would depend strongly on H$_2$O content of the magmas, with H$_2$O-rich vapor increasing the efficiency of volcanic degassing. They estimated that volcanic gases emitted at later stages of martian evolution, such as during activity of the Tharsis province, should contain sulfur at abundances 10-100 times higher than that seen with basaltic volcanism on Earth. In addition, Gaillard and

Scaillet (2009) found that martian volcanic degassing into an atmosphere of less than 1 bar should have been dominated by $SO_2$ or $S_2$ rather than $H_2S$. The relative proportions of $SO_2$ and $S_2$ would be controlled by $fO_2$ and water content, with an increase in either quantity favoring sulfur release as $SO_2$ (Gaillard and Scaillet, 2009). Based on assumptions regarding these variables and the total volume of basalt produced, Gaillard and Scaillet (2009) estimated that the buildup of the Tharsis province could have released enough sulfur into the atmosphere to form a global layer of sulfate minerals up to 25 m deep.

Products of laboratory experiments with both $SO_2$ and $H_2S$ gas have been shown to carry S-MIF signatures, but most experimental studies have focused on $SO_2$ because the S-MIF effects are more pronounced and provide a better match to the Archean rock record (Farquhar et al., 2000c, 2001; Masterson et al., 2011; Chapter 5 of this work). The conclusion of Gaillard and Scaillet (2009) that martian basaltic magmas should have released substantial quantities of $SO_2$ into the atmosphere implies potentially direct relevance of the laboratory photochemical studies to the S-MIF observed in martian meteorites. There are several possible pathways through which $SO_2$ UV photochemistry may generate products that are ultimately incorporated into elemental sulfur or sulfate aerosols. Elemental sulfur may be formed by single- or multi-photon absorption, depending on wavelength (see Chapter 5), followed by self-reaction to form $S_8$ aerosols or re-oxidation to $SO_2$ (Kasting et al., 1989; Johnson et al., 2009). The model of Johnson et al. (2009) predicts that when photolysis is limited, formation of $S_8$ aerosols is inhibited. $SO_2$ can also undergo photoexcitation, followed by self-reaction that induces disproportionation to SO and

SO$_3$ (Lyons, 2009). Tian et al. (2010) estimated that based on the rate-limiting step

SO$_3$ + H$_2$O → H$_2$SO$_4$, the timescale for formation of sulfate aerosols from SO$_3$ in the early martian atmosphere was only a few months, with an e-folding time for reduction of SO$_2$ in the atmosphere of hundreds of years (Johnson et al., 2009; Tian et al., 2010). Once formed, submicron-sized aerosol particles would travel around Mars several dozen times, being dispersed around the globe at a wide range of equatorial and mid-latitudes before their ultimate removal from the atmosphere by gravitational settling (Settle, 1979). This is one way by which isotopically anomalous sulfur produced through atmospheric photochemical reactions could have been transferred to surface reservoirs.

Halevy et al. (2010) modeled the Archean sulfur cycle based on high-precision measurements of the UV absorption spectrum of SO$_2$ by Danielache et al. (2008). Their model predicted that both predissociation of SO$_2$ at 193 nm and photoexcitation at 248 nm could generate products carrying positive $\Delta^{33}$S, as observed in the shergottites. However, the magnitude and distribution of the predicted S-MIF signal among the various sulfur species were different at these two wavelengths. At 193 nm, Halevy et al. (2010) predicted formation of S$_8$ product with large positive $\Delta^{33}$S and both residual SO$_2$ and H$_2$SO$_4$ product with moderately negative $\Delta^{33}$S, similar to results from laboratory photochemical experiments (Farquhar et al., 200c, 2001; Masterson et al., 2011; Chapter 5). At 248 nm, their model predicted that both S$_8$ and H$_2$SO$_4$ products would carry small positive $\Delta^{33}$S, while residual SO$_2$ would still possess small negative $\Delta^{33}$S. This result implies

multiple pathways for formation of positive $\Delta^{33}S$, in products with different sulfur oxidation states, during $SO_2$ photochemical processing.

The preservation of the S-MIF signal would depend on the atmospheric composition, not only of sulfur-bearing gases, but of other species, as well. Pavlov and Kasting (2002) determined that on the Archean Earth, S-MIF could only be preserved in sulfate aerosols if the $O_2$ concentration of the atmosphere was $< 10^{-5}$ times the present atmospheric oxygen level. They argued that in a highly oxygenated atmosphere, all sulfur species would be oxidized to sulfate, and any S-MIF would be lost due to mixing. At lower oxygen levels, however, sulfur would have been removed from the atmosphere in a variety of oxidation states, each of which could have followed its own chemical pathway after deposition (Pavlov and Kasting, 2002).

Recent modeling of an ancient martian atmosphere assumed to contain 500 mbar of $CO_2$ showed that the predominant removal mechanism of $SO_2$ from the atmosphere would have been rainout, rather than aerosol formation (Johnson et al., 2009). For the conditions chosen for that model, $S_8$ aerosols would have accounted for less than 1% of atmospheric $SO_2$ loss, with ~10% removed through sulfate aerosols. The only other case addressed by Johnson et al. (2009) was present-day Mars, with $CO_2$ level set at 6 mbar but including no sulfur species. While there remains a great deal of uncertainty concerning the actual atmospheric pressure throughout Mars' history (e.g., Gillman et al., 2009, 2011), the results of Johnson et al. (2009) suggest that rainout of anomalous $SO_2$, followed by oxidation to sulfate within surface reservoirs, represents another potential mechanism for preservation of S-MIF.

Once deposited on the surface of Mars, the products of atmospheric sulfur processing would have experienced different environmental conditions than those prevalent on Earth. Mars' history has most likely been dominated by cold, arid conditions at the surface, with only transient episodes during which liquid water existed in localized areas (Squyres and Kasting, 1994; Ehlmann et al., 2011). As a result, weathering processes on Mars would be dominated by solid-vapor reactions or solid-liquid reactions at low water-to-rock ratios (Gooding, 1978; Ehlmann et al., 2011). Sulfate aerosols deposited at the surface would contain aqueous solutions of sulfuric acid, which would react with silicate minerals at the surface to initiate acidic weathering processes, releasing Fe, Ca, and Mg cations that would then be free to precipitate sulfate minerals (Gooding, 1978; Settle, 1979; Burns and Fisher, 1988, 1993; Hurowitz et al., 2006). During episodes when liquid water was present on the surface, fluvial systems could have served as a mechanism for transporting and concentrating surficial sulfur into closed basins, forming temporary lakes that deposited evaporitic sulfate minerals (Grotzinger et al., 2005). Aeolian activity also would have contributed to widespread redistribution of sulfur deposited at the surface (Greeley et al., 2001; Carr and Head, 2010; Hobbs et al., 2010; Tirsch et al., 2011).

Figure 6-2 shows a plot of $\Delta^{36}S$ vs. $\Delta^{33}S$ for nakhlites as well as the sulfate fractions of those shergottites that carry anomalous sulfur. S-MIF observed in both sulfide and sulfate phases in these shergottites is characterized by positive $\Delta^{33}S$, while the S-MIF in the nakhlites shows almost solely negative $\Delta^{33}S$. If we assume that the S-MIF in the shergottites reflects assimilation of photochemically-processed sulfur as
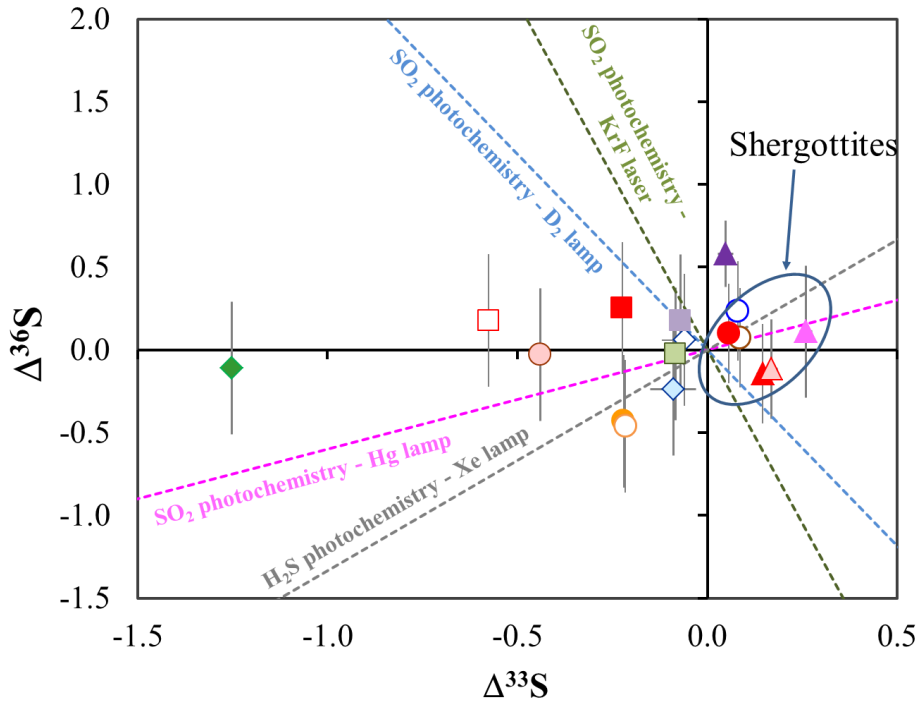
**Figure 6-2. $\Delta^{36}S$ vs. $\Delta^{33}S$ of nakhlites and shergottites possessing S-MIF.**
**[1] Farquhar et al., 2000c; [2] Farquhar et al., 2007a; [3] Kim and Farquhar,**
**2008.**

suggested for the nakhlites, then there are various possible explanations for this observation. The opposite $\Delta^{33}S$ signs may reflect complementary sulfur pools resulting from a single photochemical process, as suggested by the similar slope of nakhlite and shergottite compositions in $\Delta^{36}S$-$\Delta^{33}S$ space. For example, laboratory

experiments with $SO_2$ gas have shown that elemental sulfur produced during UV photochemistry is highly enriched in $^{33}S$, carrying significantly positive $\Delta^{33}S$ values, while the residual $SO_2$ gas from the experiments shows a small negative $\Delta^{33}S$ (Chapter 5 of this work). For this to explain the different $\Delta^{33}S$ signs in the meteorites, it could imply transfer of S-MIF from atmospheric or surface to subsurface reservoirs through different chemical species and oxidation states of sulfur during different periods of martian history. This in turn could indicate a fundamental change in the martian environment that affected S-MIF generation and/or preservation.

The source or sources of the S-MIF are not well understood, but some general principles may be observed. The generation of S-MIF could be affected by a change in sulfur species degassed from magmas, for example, or a change in atmospheric composition that altered the photochemical environment. Preservation of S-MIF could be affected by changes in atmospheric chemistry, also dependent on the photochemical environment, which modified available pathways for deposition of sulfur at the surface.

Environmental changes between the time of nakhlites and shergottites could have affected the pathways for generation and preservation of S-MIF in various ways. In the scenario described above, for example, a reduction in atmospheric water content could have reduced the efficiency of sulfate aerosol formation and caused a shift toward greater deposition of elemental sulfur at the surface. Changes in water abundance at the surface could have affected the quantity and species of sulfur transported into the subsurface.

Differences in the species of sulfur degassed from the parent magmas also could have altered the prevalent photochemical pathways for S-MIF generation, producing different isotopic signatures in the nakhlites and shergottites. As discussed above, the speciation of sulfur in a basaltic melt is dependent on the melt water content. Estimates of the water content of martian magmas through analysis of meteorites vary widely. Jones et al. (2012) calculated a parent melt water content for Y980459, believed to be the most primitive shergottite, of ~80 ppm, based on analysis of melt inclusions. This result contrasts those of 1.5 wt% water for the Nakhla melt (Harvey and McSween, 1992b) and ~1.8 wt% water for Shergotty (McSween et al., 2001). However, it has been suggested that the elevated $fO_2$ of enriched compared to depleted shergottites could have resulted from assimilation of crustal water into ascending magmas (e.g., Warren et al., 2004). Thus variations in magmatic composition and degree of crustal assimilation, as well as heterogeneities in water content of assimilated crust, could have resulted in varying proportions of $SO_2$ and $S_2$ degassed from magmas, affecting the subsequent photochemical production of S-MIF. No laboratory experiments have yet been performed to test for S-MIF during $S_2$ photolysis, but it does absorb UV radiation from 240 to 360 nm (Okabe, 1978) and should be investigated for possible contributions to S-MIF production from $S_2$ in addition to $SO_2$.

The difference in $\Delta^{33}S$ observed in the different groups of martian meteorites may reflect a broader change in environmental conditions. While Gaillard and Scaillet (2009) concluded that $H_2S$ would have comprised only a very small fraction of the sulfur degassed from martian volcanoes into an atmosphere of less than 1 bar, it

represents another potential source of S-MIF on Mars that cannot be entirely discounted. Products of laboratory photochemical experiments with $H_2S$ have also been shown to display S-MIF signatures (Farquhar et al., 2000c) with slope in $\Delta^{36}S$-$\Delta^{33}S$ space similar to that seen in the nakhlites and shergottites. Figure 6-2 includes dotted lines depicting the slopes of arrays formed by products of photochemical experiments with both $SO_2$ and $H_2S$. As seen in the figure, photochemical processing of either of these gases is capable of generating S-MIF with characteristics similar to those observed in nakhlites and shergottites in this study. If early martian history did include a period with a substantially thicker atmosphere that allowed for appreciable degassing of $H_2S$ (Gaillard and Scaillet, 2009), then this period may have been characterized by generation and preservation of S-MIF characterized by negative $\Delta^{33}S$. The S-MIF detected in the nakhlites may represent anomalous sulfur produced during ancient volcanic activity and preserved in a subsurface or near-surface reservoir until being later assimilated into the magma that produced the nakhlites, or it could derive from volcanic activity at the time of nakhlite magmatism. Later volcanic episodes degassing into a thinner atmosphere may have produced less $H_2S$ and more $SO_2$, resulting in generation and preservation of S-MIF with positive $\Delta^{33}S$ as observed in the shergottites.

Alternatively, the opposite signs of $\Delta^{33}S$ could indicate geographical differences in the characteristic sulfur isotopic signatures of the nakhlite and shergottite source areas. While aeolian processes would be expected to homogenize the surface fines on a wide geographic scale over time, topographic features could have facilitated sequestration of sulfur bearing isotopically distinct signatures due to fluvial or aeolian

180

transport. These distinct pools could have been tapped during later assimilative processes associated with magmatic activity, resulting in variations in the observed isotopic compositions of the meteorites.

Given the evidence presented by the nakhlites for assimilation of anomalous sulfur from the atmosphere and its reduction within the melt, the data presented in this dissertation are interpreted to indicate that a similar process occurred within selected shergottite melts as well, producing the S-MIF observed in their sulfate and AVS fractions. The major outstanding questions then concern the speciation of sulfur and photochemical pathways that generated the signals, as well as the broader implications the observations may carry concerning martian geological and climate history.

## 6.3    Future Directions

While this study has vastly expanded our knowledge of martian sulfur isotopic systematics, it has also provided a framework for deeper inquiry into the mechanisms that produced the observed S-MIF signatures. Some areas of interest for future research include the following:

- *Pathways for S-MIF production and preservation* – Preliminary experiments have indicated that gas-phase photochemistry of $SO_2$ and $H_2S$ can produce S-MIF compositions similar to those detected in the meteorites. However, much work remains to be done to determine the precise mechanisms that were likely at work in the martian atmosphere. Further experiments designed to isolate

181

specific regions of the $SO_2$ absorption spectrum would help untangle potential contributions of photodissociation (< 220 nm) and/or photoexcitation (260 – 340 nm) to the S-MIF signal. An understanding of the precise photochemical mechanism(s) responsible for producing the anomalous sulfur, such as distinguishing between self-shielding versus isotopologue-selective processes, is vital to identifying broader implications of the sulfur isotope data for martian atmospheric history. While work to date has focused on $SO_2$ and $H_2S$, other gases that may have existed in the past martian atmosphere and could have contributed to S-MIF production, such as $S_2$ and OCS, should also be considered. In addition, modeling of atmospheric chemistry that includes potential trace gases and also examines a targeted range of pressures suggested based on the latest volcanic degassing models would help inform models for assimilation of anomalous sulfur into the subsurface.

- *Other evidence for assimilation of surface materials in the shergottites* – The shergottites that showed the largest S-MIF signals in this study were discovered quite recently and have not been analyzed extensively by other research groups. For example, NWA 5718 yielded the greatest magnitude $\Delta^{33}S$ anomaly, but besides the initial petrographic analysis by Wittke et al. (2010), no other analysis of this meteorite has been reported. The results presented here suggest that NWA 5718 is a promising candidate for studies searching for other evidence of assimilative processes on Mars and particularly in the shergottites.

- *Re-examination of ALH 84001* – Future analysis of ALH 84001 should consider techniques more suited to small sulfide grain sizes to look for S-MIF signatures. Firm identification of such a signal and its relationship to those observed in the nakhlites and shergottites could carry implications for the history of the martian atmosphere.

Finally, the ultimate next step to advance our knowledge of the martian sulfur cycle would be analysis of samples returned from Mars, which could be placed in well-characterized geological context to provide the clearest interpretation of measured isotopic compositions. This would allow the highest-fidelity measurements of martian samples and, barring significant advancements in instrumentation for *in situ* planetary exploration, might represent the only means by which we could measure the sulfur isotopic composition of fine-grained regolith or sedimentary materials.

# Appendix A. Analytical Methods[1,2]

[1] All text and tables in this appendix were written/created by H. B. Franz.

[2] Ion microprobe standard analyses presented in this appendix were performed by K. McKeegan, R. Economos, and A. Schmitt.

[3] Electron microprobe standard analyses presented in this appendix were performed by P. Piccoli.

## A.1    Acid-based Chemical Extraction

### A.1.1    Sequential Extraction Procedure

The most precise laboratory technique for measuring sulfur isotope ratios involves the conversion of all sulfur-bearing phases to $SF_6$, which removes the potential for isobaric interference during mass spectrometric analysis (Hulston and Thode, 1965; Farquhar et al., 2001). This study was performed with a sequential chemical extraction procedure on powdered whole rock that allowed the measurement of sulfur isotope ratios for different mineral phases. Meteorite samples were received either as rock chips or already powdered. Samples received as rock chips were disaggregated in a steel mortar and then ground more finely with an agate mortar and pestle. Each powdered sample was transferred to a 15 mL centrifuge tube along with 10 mL of Milli-Q water. The tube was sonicated for 20 minutes to promote the dissolution of water-soluble sulfate from the sample. The tube was then centrifuged to allow separation of the solution from the solid sample by pipette. This process was repeated a second time to yield a total of 20 mL of solution containing water-soluble

sulfate, which were transferred to a boiling flask. A few drops of 0.5 N HCl were added to the flask to reduce the pH to ~3, followed by several drops of 1 M $BaCl_2$ solution to precipitate any sulfate in the solution as $BaSO_4$. The flask was then allowed to evaporate to dryness before the sulfate was reduced by a procedure similar to that described below for acid-soluble sulfate.

The powdered sample was transferred from the centrifuge tube to a double-necked boiling flask with silicone septum. The flask was assembled with a water-cooled condenser, a bubbler filled with Milli-Q water, and a sulfide trap into a distillation apparatus similar to that described by Forrest and Newman (1977). All ground glass joints were sealed with PTFE sleeves. The apparatus was assembled, checked for leaks, and then purged with nitrogen for at least 10 minutes. For the first extraction step, 25 mL of 5 N HCl were injected into the boiling flask through the septum with a syringe. The solution was then heated to ~60 °C. Acid-volatile sulfur (AVS) in the sample, presumed to consist primarily of monosulfides, reacted with the HCl to evolve $H_2S$ gas, which was captured in an acidic $AgNO_3$ solution. After completion of the AVS reduction reaction (approximately three hours), the sulfide trap with capture solution was replaced, and 25 mL of a reduction solution prepared from 12 N hydrochloric acid, 48% hydriodic acid, and 50% hypophosphorus acid were added to the boiling flask ("Thode solution" - Thode et al., 1961; Mayer and Krouse, 2004). The solution was heated to ~85 ºC. During the next 4.5 hours, acid-soluble sulfate in the sample reacted to form $H_2S$, which was captured in the manner described above.

At this point, two slightly different techniques were employed to extract the final sulfur-bearing fraction. For all but the last three shergottites analyzed, upon completion of the acid-soluble sulfur reduction, the sulfide trap was again replaced with fresh AgNO$_3$ solution. Fifteen mL of an acidic chromium(II) solution were injected into the boiling flask containing the AVS and Thode solution, already heated to ~85 ℃. During the next ~3 hours, chromium-reducible sulfur (CRS) minerals, presumed to be disulfides and elemental sulfur, were converted to H$_2$S and captured in the AgNO$_3$ solution.

The sulfur isotope ratios for the shergottite CRS fractions obtained with the above procedure showed an anomalous pattern of depletion in [34]S and enrichment in [33]S, prompting the concern that complex chemical reactions had occurred between the Thode and CRS solutions to produce isotopically biased CRS results. For this reason, the following modified procedure was used to extract the CRS fraction from Chassigny, Y000593, NWA 6148, NWA 998, NWA 7032, NWA 7042, and Tissint. Upon completion of the acid-soluble sulfate reduction, the boiling flask was cooled and its contents were transferred to 30 mL centrifuge tubes. After separation of the acid solution from the solid sample powder, the sample was rinsed with Milli-Q water several times to clean it before being transferred back to the double-necked boiling flask. The following day, the distillation apparatus was reassembled, checked for leaks, and again purged with nitrogen for 10 minutes. A fresh sulfide trap with AgNO$_3$ capture solution was installed. For the final reduction step, 15 mL of the CRS solution and 15 mL of 5 N HCl were injected into the boiling flask, which was then

heated to ~85 ºC. Disulfide minerals and elemental sulfur in these samples were thus converted to $H_2S$ and captured in the $AgNO_3$ solution, as previously described.

The $H_2S$ evolved in each step of the extraction process reacted with the $AgNO_3$ in the capture solution to form $Ag_2S$, which was cleaned with Milli-Q water and 1 M $NH_4OH$ solution, then dried. The $Ag_2S$ was converted to $SF_6$ by reaction with 250 μmoles of fluorine gas in a nickel reaction vessel at 250° C for 8 hours. The $SF_6$ was subsequently condensed from the residual $F_2$ into a trap cooled with liquid nitrogen. Excess $F_2$ was passivated by reaction with KBr salt. Replacement of the liquid nitrogen coolant on the trap with ethanol slush at -115 °C allowed distillation of the $SF_6$ from the trap into the liquid-nitrogen-cooled injection loop of a gas chromatograph (GC). The $SF_6$ was purified by a 1/8-inch diameter, 6-foot long Molecular Sieve 5A GC column, followed by a 1/8-inch diameter, 12-foot long Haysep-Q™ GC column. Both columns were held at 50 °C, with helium carrier gas flow rate of 20 mL/min.  After its elution from the GC, the $SF_6$ was captured in spiral glass traps cooled with liquid nitrogen, then transferred to the bellows of a Thermofinnigan MAT 253 dual-inlet gas source mass spectrometer. The sulfur isotopic composition of the $SF_6$ was measured by monitoring $SF_5^+$ ion beams at *m/e* of 127, 128, 129, and 131 Da. Uncertainties, estimated from repeated analyses of the sulfur isotopic ratios of IAEA reference materials, are generally better than ±0.4‰, ±0.02‰, and ±0.4‰ (2σ) for $\delta^{34}S$, $\Delta^{33}S$, and $\Delta^{36}S$, respectively (Farquhar et al., 2007a).

*A.1.2   Chromium-Reducible Sulfur Fractions*

Results for the chromium-reducible sulfur (CRS) fractions of the shergottites were not discussed in Chapter 2 due to observations of unexpected fractionation effects suspected to represent analytical artifacts. The sequential extraction procedure employed for this study was identical to that used by Farquhar et al. (2007a) to analyze the Nakhla meteorite.

Yields for the CRS fractions of shergottites were uniformly low, except for one extraction group that produced anomalously high abundances of $97 - 328$ ppm. These results were traced to sulfate-contaminated $CrCl_3$ reagent used in preparation of the CRS reduction solution, and the CRS fractions of those meteorites were discounted on that basis. The remaining shergottites yielded $0 - 21$ ppm of CRS. Since discovery of the contaminated reagent, $CrCl_3$ from a different manufacturer, which is not believed to contain similar sulfate impurities, has been used for all subsequent analyses. However, as a precaution, 1 M $BaCl_2$ solution was added to the CRS solution at 5 times stoichiometric excess to precipitate any sulfate contaminants as barium sulfate prior to use of the CRS solution for sequential extractions.

The CRS fractions were not expected to be large, given the pyrrhotite-dominated sulfide mineralogy of the shergottites, so the low abundances were not cause for suspicion about the procedure. However, the sulfur isotope ratios of the CRS fractions that were extracted through the "one-pot" method – i.e., injection of the CRS solution into the boiling flask already containing AVS and Thode solutions – were found to form an array on a plot of $\Delta^{33}S$ versus $\delta^{34}S$ suggesting mass-independent compositions. No such array was seen on the plot of $\Delta^{36}S$ versus $\delta^{34}S$, where the $\Delta^{36}S$

values were scattered above and below the x-axis. These results are tabulated in Table A-1 and depicted graphically in Figure A-1. Values for CRS $\delta^{34}S$ obtained with the one-pot extraction method ranged from $-17.78 \pm 0.15‰$ to $-4.36 \pm 0.15‰$, with $\Delta^{33}S$ from $0.048 \pm 0.013‰$ to $0.131 \pm 0.025‰$.

Since Chassigny was expected to contain more CRS than AVS, based on the report of Greenwood et al. (2000a), its CRS was extracted by a different method, as described in the previous section. Instead of introducing the CRS solution into the boiling flask containing the AVS and Thode solutions, the residue from AVS and Thode extractions was separated from the reduction solution and returned to the boiling flask. The distillation apparatus was then reassembled for the CRS extraction. It was noted that the sulfur isotope ratios obtained for Chassigny CRS did not lie along the mass-independent array formed by the shergottites previously analyzed, but instead were close to zero.

For the last two shergottites analyzed, Tissint and NWA 7032, the CRS extraction was performed in a separate step, as for Chassigny. As seen in Figure A-1(a), the isotope ratios of the Tissint and NWA 7032 CRS fractions were close to zero and did not lie along the $\Delta^{33}S$ versus $\delta^{34}S$ array formed by the other shergottites. The same was true for $\Delta^{36}S$ of Tissint. (The CRS fraction of NWA 7032 was too small for accurate determination of $\Delta^{36}S$.) These observations further suggested that the anomalous sulfur isotopic compositions obtained for shergottite CRS fractions were likely introduced by the extraction procedure, rather than representing true martian compositions.

**Table A-1. Sulfur Isotopic Compositions of Shergottite and Chassigny CRS**

(Isotope ratios normalized to CDT; 1σ uncertainties in parentheses)

| Meteorite | CRS yield (ppm) | $\delta^{34}S$ | $\Delta^{33}S$ | $\Delta^{36}S$ |
|---|---|---|---|---|
| *One-pot sequential extraction* | | | | |
| EET 79001A | 5 | -13.53 (0.15) | 0.124 (0.021) | 0.94 (0.19) |
| EET 79001B | 0 | n/a | n/a | n/a |
| NWA 2800 | 10 | -13.40 (0.15) | 0.098 (0.011) | -0.58 (0.15) |
| NWA 5718 | 0 | n/a | n/a | n/a |
| NWA 2975 | 12 | -7.90 (0.15) | 0.048 (0.013) | 0.50 (0.15) |
| NWA 2986 | ** | n/a | n/a | n/a |
| NWA 3171 | 8 | -13.98 (0.15) | 0.098 (0.008) | -0.58 (0.13) |
| NWA 5298 | 4 | -17.78 (0.15) | 0.131 (0.025) | 1.07 (0.24) |
| QUE 94201 | ** | n/a | n/a | n/a |
| Shergotty | 2 | -4.36 (0.15) | 0.077 (0.039) | 1.77 (0.66) |
| Los Angeles | 21 | -13.36 (0.15) | 0.095 (0.010) | -0.44 (0.15) |
| Zagami | 8 | -14.35 (0.15) | 0.078 (0.014) | -0.94 (0.15) |
| RBT 04261 | 10 | -13.06 (0.15) | 0.126 (0.008) | 0.30 (0.15) |
| LAR 06319 | 0 | n/a | n/a | n/a |
| Dhofar 019 | 4 | -11.45 (0.15) | 0.116 (0.021) | 1.29 (0.23) |
| NWA 5960 | ** | n/a | n/a | n/a |
| NWA 2990 | 8 | -15.66 (0.15) | 0.126 (0.011) | -0.34 (0.15) |
| NWA 5990 | ** | n/a | n/a | n/a |
| NWA 2046 | 11 | -8.63 (0.15) | 0.079 (0.008) | -0.29 (0.15) |
| NWA 4925 | 10 | -14.82 (0.15) | 0.115 (0.013) | -0.66 (0.15) |
| NWA 5789 | 0 | n/a | n/a | n/a |
| NWA 4468 | 11 | -15.66 (0.15) | 0.083 (0.012) | -0.84 (0.15) |
| NWA 6162 | ** | n/a | n/a | n/a |
| SaU 005 | 12 | -7.02 (0.15) | 0.053 (0.021) | -0.08 (0.16) |
| DaG 476 | 4 | -8.73 (0.15) | 0.065 (0.024) | 1.48 (0.44) |
| Y980459 | 0 | n/a | n/a | n/a |
| ALH 77005 | 1 | -10.20 (0.15) | 0.072 (0.009) | 1.28 (0.30) |
| NWA 6342 | ** | n/a | n/a | n/a |
| *Separate CRS Extraction* | | | | |
| Chassigny | < 1 | -0.59 (0.15) | 0.004 (0.008) | 0.42 (0.15) |
| Tissint | 4 | -0.12 (0.15) | -0.009 (0.008) | -0.03 (0.15) |
| NWA 7032 | < 1 | -0.09 (0.15) | 0.006 (0.056) | -- |

**= not recovered

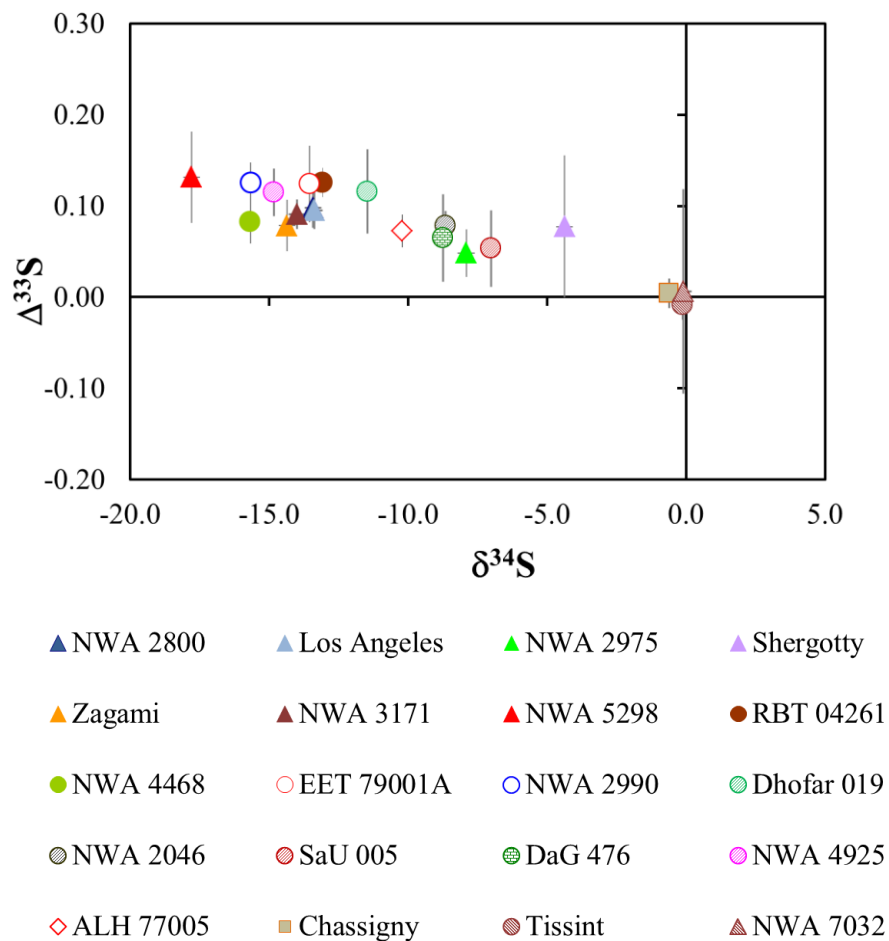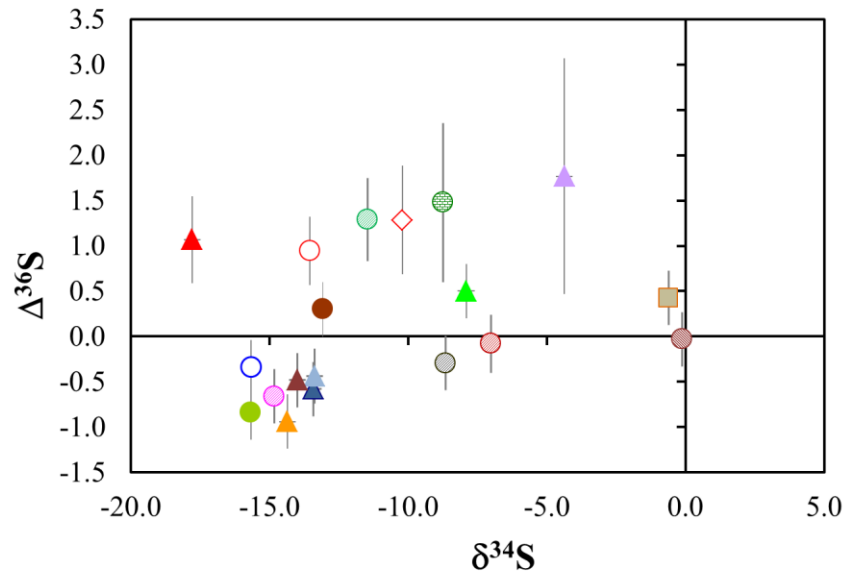-- = Sample too small for accurate measurement of this ratio

**Figure A-1(a).** $\Delta^{33}S$ vs. $\delta^{34}S$ for shergottites and Chassigny.

**Figure A-1(b). $\Delta^{36}S$ vs. $\delta^{34}S$ for shergottites and Chassigny.**

**($2\sigma$ error bars)**

Various possible explanations for the observed CRS isotope ratios were considered. First, it was hypothesized that the presence of ferric iron in the samples had oxidized a portion of the $H_2S$ produced from monosulfides during the AVS step to elemental sulfur, which was then extracted in the CRS step instead. If this were the source of the observed CRS anomaly, then there should be a correlation between the CRS isotopic compositions and the yields. Figure A-2 shows the variations in CRS $\Delta^{33}S$ and $\delta^{34}S$ versus CRS yield. As evident in the figure, no correlation is evident between the CRS isotopic composition and yield.

This idea was also investigated from another angle. If a portion of the monosulfides in the samples had been oxidized to elemental sulfur during the AVS step due to the presence of ferric iron, then there should be a correlation between the sulfur isotope ratios of the anomalous CRS products and the oxidation state of the samples. This is not the case, however. Figure A-3 graphically displays the variations in $\delta^{34}S$ and $\Delta^{33}S$ versus $fO_2$ for the CRS fractions, using $fO_2$ values for the meteorites reported in the literature (RBT 04261 – Usui et al., 2010; ALH 77005 – McCanta et al., 2009; Shergotty, Zagami, Los Angeles – Herd et al., 2001; EET 79001A, Dhofar 019, DaG 476, SaU 005 – Herd, 2003; NWA 2990 – Gross et al., 2012; NWA 4468 – Satake et al., 2009; NWA 3171 – Papike et al., 2009; NWA 5298 – Hui et al., 2011; NWA 2975 – He et al., 2011). As evident in the figure, there is no correlation between the sulfur isotopic compositions of the CRS fractions and magmatic $fO_2$ values, suggesting that partial oxidation of monosulfides to elemental sulfur during AVS reduction is not the source of the anomalous CRS compositions.

A second possibility considered was that the Thode reduction reactions for these meteorites had not run to completion, but had generated elemental sulfur intermediates that were then extracted during the CRS step. If this had occurred, then there should be a correlation between the CRS isotopic composition and the Thode yield, such that samples with incomplete Thode reductions should have the largest Thode yields. Plots of CRS sulfur isotopic composition versus Thode step yields are shown in Figure A-4. As evident from the figure, there is no correlation between the sulfur isotopic composition of the CRS products and the concentrations of acid-soluble sulfate extracted during Thode reduction, suggesting that this also is not the source of the anomalous CRS compositions.

As none of the preceding hypotheses can satisfactorily explain the anomalous CRS compositions, the leading possibility that remains is that the observed array in $\Delta^{33}S$-$\delta^{34}S$ space was produced by a complex reaction network facilitated by the presence of Thode solution during CRS reductions. The exact nature of this network is undetermined at this time, but it would presumably be analogous to the series of reactions that can occur during biologically-mediated dissimilatory sulfate reduction, producing similar anomalous sulfur isotopic compositions (Farquhar et al., 2007b).
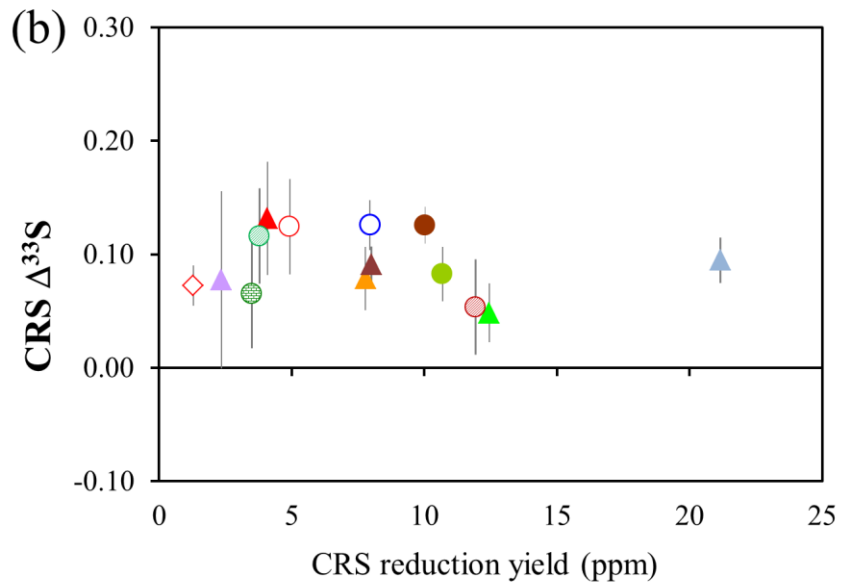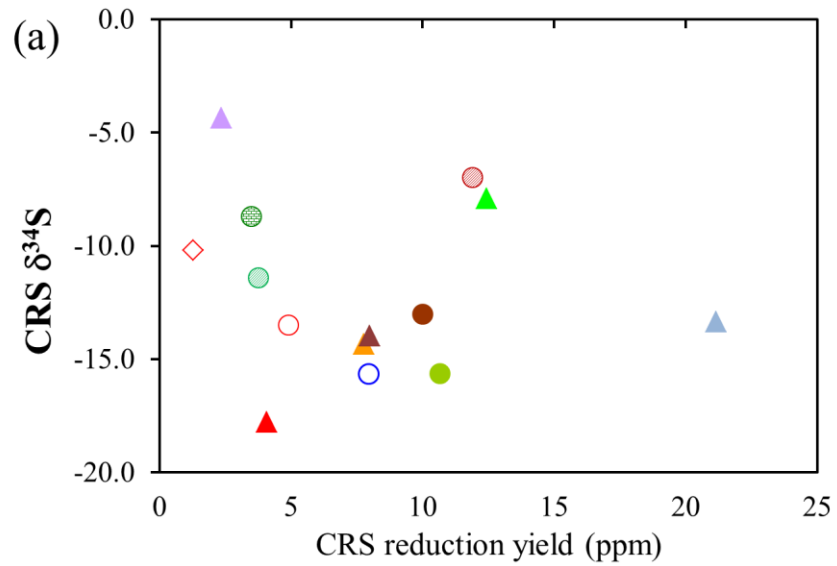
**Figure A-2. Sulfur isotopic composition of shergottite CRS vs. yield.**

(a) $\Delta^{33}$S vs. yield. (b) $\delta^{34}$S vs. yield. (2$\sigma$ error bars on $\delta^{34}$S and $\Delta^{33}$S)
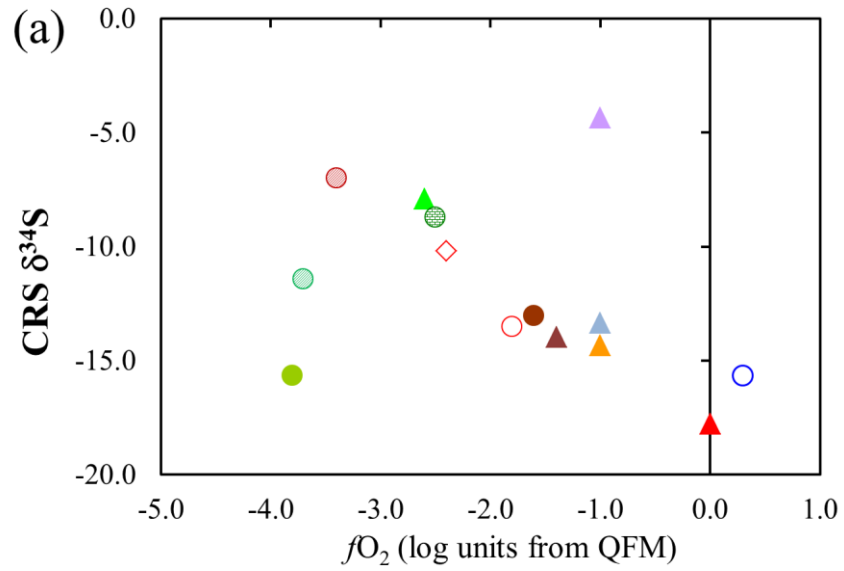
**Figure A-3. Sulfur isotopic composition of shergottite CRS vs. $fO_2$**

(a) $\Delta^{33}S$ vs. $fO_2$. (b) $\delta^{34}S$ vs. $fO_2$. (See text for references. $2\sigma$ error bars on $\delta^{34}S$ and $\Delta^{33}S$)

The anomalous CRS product generated through this reaction network would be mixed with the intrinsic signal from disulfide minerals in the meteorites, such as that presumed to have been measured during the CRS reductions of Chassigny, Tissint, and NWA 7032. Since the proportion of sulfur existing as disulfide minerals in the shergottites is so minor, even a small contribution from products of Thode-CRS interactions that possessed highly anomalous composition could readily overwhelm the intrinsic martian signal. However, the CRS fractions of the shergottites represent such an insignificant carrier of sulfur that this outcome does not alter any of the conclusions of this study.
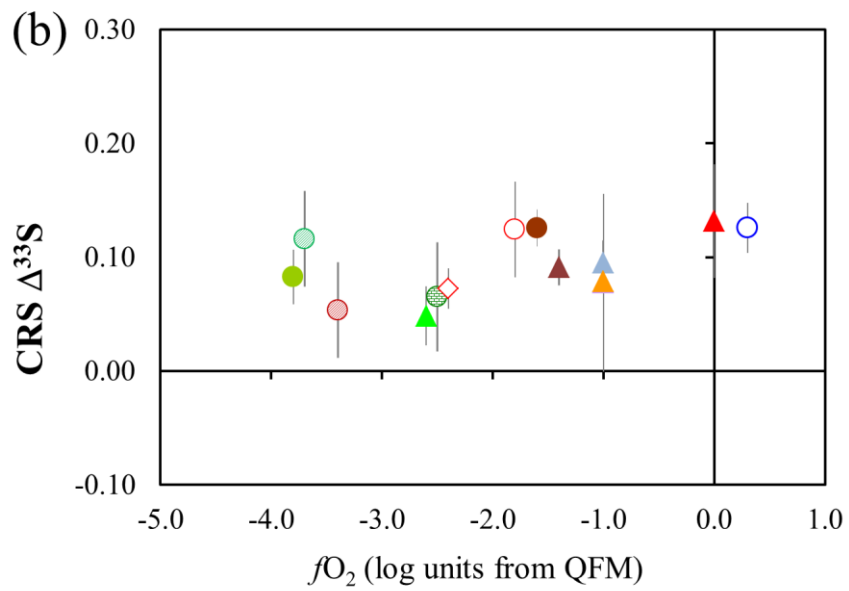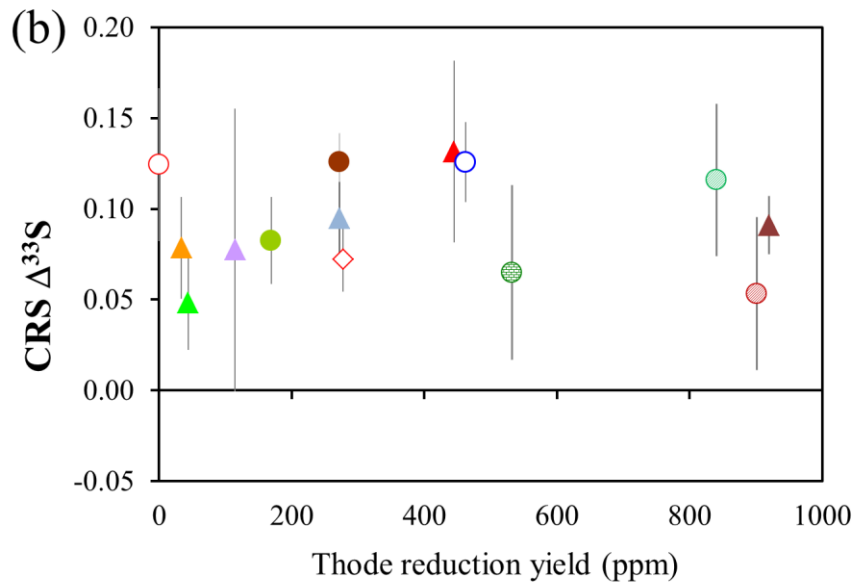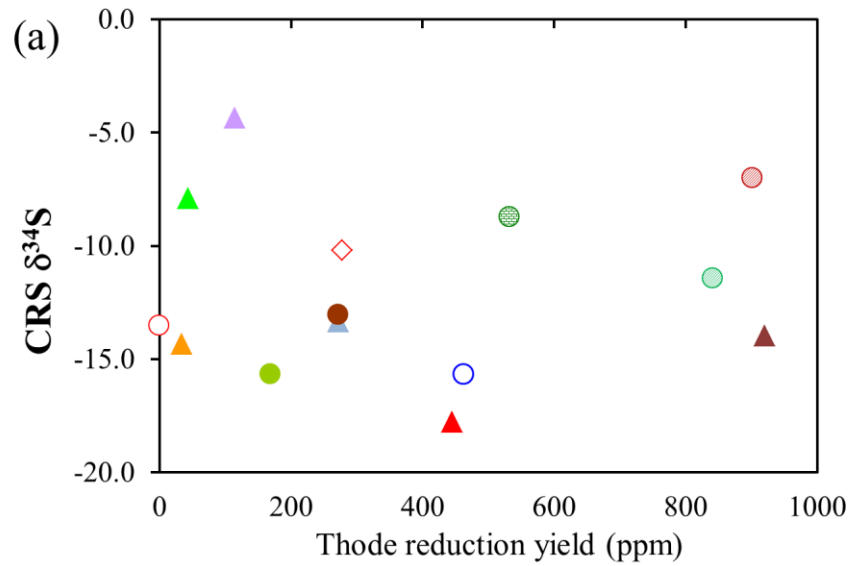
**Figure A-4. Sulfur isotopic composition of shergottite CRS vs. Thode yield**

(a) $\Delta^{33}$S vs. Thode yield. (b) $\delta^{34}$S vs. Thode yield. ($2\sigma$ error bars on $\delta^{34}$S and $\Delta^{33}$S)

## A.2   Ion Microprobe

Another technique for measuring multiple sulfur isotopes is secondary ion mass spectrometry (SIMS), also known as the ion microprobe. SIMS offers the best spatial resolution for *in situ* analysis of individual mineral grains for measurements of $\delta^{33}$S, $\delta^{34}$S, and $\Delta^{33}$S. This method was used to examine sulfides in nakhlites and ALH 84001, with the goal of determining whether the anomalous sulfur isotopic composition obtained via chemical extraction of bulk rock material was also evident in individual grains. The SIMS analyses described in this document were performed at the University of California at Los Angeles (UCLA), using a Cameca IMS 1270 high-resolution ion microprobe in multicollector mode. Polished meteorite samples first were mapped with reflected-light optical microscopy to locate sulfide grains large enough (i.e., > ~20 μm diameter) for SIMS analysis. Prior to loading in the ion microprobe sample chamber, the sections were cleaned by sonication in Milli-Q water and methanol, then coated with a ~100 Å layer of gold or carbon to ensure conductivity across the sample surface. Ion microprobe analyses in January 2012 utilized a 5 nA Cs$^+$ primary ion beam at 20 keV impact energy with 100 μm Kohler illumination, focused to a 25-30 μm spot. A mass resolving power of ~4000 and energy filtering were used to minimize the contributions from the $^{32}$SH$^-$ ion to the $^{33}$S$^-$ peak.  Positive charge buildup in the source was prevented by applying an electron flood gun normal to the primary beam. Prior to each analysis, the surface was pre-sputtered for up to 150 seconds, followed by 30 cycles (60 cycles in some cases) of 10-second integrations. The resulting secondary ions of $^{32}$S$^-$, $^{33}$S$^-$, and $^{34}$S$^-$ were

simultaneously collected by multiple Faraday cups, located in a temperature-controlled vacuum chamber (Mojzsis et al., 2003). Measurements of Nakhla in January 2008 employed similar operating conditions to those described above, but with mass resolution of ~6000.

The precision achieved during SIMS analysis is highly dependent on mineral grain and primary beam characteristics, which affect the number of sulfur ions produced. Isotope ratios determined by SIMS also exhibit a mass-dependent fractionation resulting from the measurement process, causing deviations from the true isotope ratios that can be predicted and corrected in a systematic manner. The fractionation may be due to the ionization process of sputtering, the transport of secondary ions to the detector, and mass-dependent detector response (Mojszis et al., 2003). These errors are corrected by calibration with matrix-matched standards under the same instrumental conditions. Note that fractionation due to matrix effects are solely mass-dependent and do not affect $\Delta^{33}S$ measurements.

Results for analyses of reference standards during these sessions are presented in Tables A-1 and A-2. Note that the $1\sigma$ errors listed in the tables represent only "internal" errors, or the standard error measured in an individual spot over the number of integration cycles. The true uncertainty in measurements of sulfide grains in the meteorite sections was taken as the greatest of the internal error, the standard error of repeated analyses of mineral standards (i.e., "external reproducibility"), or the standard error of multiple analyses of a given grain. Measurements of MIL 03346, NWA 6148, and ALH 84001 in January 2012 achieved average $1\sigma$ precision of $\pm$ 0.07‰ for $\Delta^{33}S$ and $\pm$ 0.07‰ for $\delta^{34}S$, based on repeatability of reference standards.

The uncertainty on $\Delta^{33}S$ measurements of ALH 84001 was a little higher, $\pm$ 0.25‰, due to smaller grain sizes. Average $1\sigma$ precision for Nakhla analyses in January 2008 was $\pm$ 0.04‰ for $\Delta^{33}S$ and $\pm$ 0.15‰ for $\delta^{34}S$.

**Table A-1. Sulfur isotopic composition of mineral standards - January 2008 SIMS sessions**

| Standard | $\delta^{33}$S (‰) | 1σ error (‰) | $\delta^{34}$S (‰) | 1σ error (‰) | $\Delta^{33}$S (‰) | 1σ error (‰) |
|---|---|---|---|---|---|---|
| *Session 1* | | | | | | |
| Cañon Diablo Troilite (CDT) | | | | | | |
| CDT-1 | -0.68 | ± 0.15 | -1.34 | ± 0.02 | 0.00 | ± 0.15 |
| CDT-2 | -0.70 | ± 0.15 | -0.76 | ± 0.02 | -0.32 | ± 0.15 |
| CDT-3 | -0.42 | ± 0.15 | -0.51 | ± 0.02 | -0.16 | ± 0.15 |
| CDT-4 | -0.44 | ± 0.15 | -0.96 | ± 0.02 | 0.04 | ± 0.15 |
| CDT-5 | -0.21 | ± 0.15 | -0.51 | ± 0.02 | 0.05 | ± 0.15 |
| CDT-6 | -0.47 | ± 0.15 | -0.35 | ± 0.02 | -0.29 | ± 0.15 |
| CDT-7 | -0.12 | ± 0.15 | -0.73 | ± 0.02 | 0.25 | ± 0.15 |
| CDT-8 | -0.29 | ± 0.15 | -0.89 | ± 0.02 | 0.16 | ± 0.15 |
| CDT-9 | -0.12 | ± 0.16 | 0.08 | ± 0.02 | -0.16 | ± 0.16 |
| CDT-10 | 0.26 | ± 0.16 | 0.69 | ± 0.02 | -0.09 | ± 0.16 |
| CDT-11 | 0.28 | ± 0.16 | 0.95 | ± 0.02 | -0.21 | ± 0.16 |
| CDT-12 | 0.02 | ± 0.16 | 0.18 | ± 0.02 | -0.07 | ± 0.16 |
| CDT-13 | 0.53 | ± 0.16 | 0.55 | ± 0.02 | 0.25 | ± 0.16 |
| CDT-14 | -0.09 | ± 0.16 | 0.11 | ± 0.02 | -0.15 | ± 0.16 |
| CDT-15 | 0.36 | ± 0.16 | 0.65 | ± 0.02 | 0.03 | ± 0.16 |
| CDT-16 | -0.36 | ± 0.15 | -0.83 | ± 0.02 | 0.06 | ± 0.16 |
| CDT-17 | 0.06 | ± 0.19 | 0.29 | ± 0.02 | -0.09 | ± 0.19 |
| CDT-18 | 0.05 | ± 0.20 | -0.01 | ± 0.02 | 0.05 | ± 0.20 |
| CDT-19 | -0.10 | ± 0.19 | 0.18 | ± 0.02 | -0.19 | ± 0.19 |
| CDT-20 | -0.01 | ± 0.20 | 0.13 | ± 0.02 | -0.07 | ± 0.20 |
| CDT-21 | 1.12 | ± 0.22 | 1.05 | ± 0.03 | 0.65 | ± 0.22 |
| CDT-22 | 0.66 | ± 0.22 | 0.99 | ± 0.03 | 0.16 | ± 0.22 |
| CDT-23 | 0.62 | ± 0.23 | 1.04 | ± 0.03 | 0.09 | ± 0.23 |
| | | | | | | |
| *Average* | *0.00* | | *0.00* | | *0.00* | |
| *(Standard deviation)* | *(0.46)* | | *(0.72)* | | *(0.21)* | |
| | | | | | | |
| Balmat pyrite | | | | | | |
| Balmat-1 | 7.17 | ± 0.11 | 14.47 | ± 0.01 | -0.15 | ± 0.11 |
| Balmat-2 | 7.46 | ± 0.11 | 14.44 | ± 0.01 | 0.16 | ± 0.11 |
| Balmat-3 | 7.29 | ± 0.11 | 14.53 | ± 0.01 | -0.07 | ± 0.11 |
| Balmat-4 | 7.45 | ± 0.11 | 14.42 | ± 0.01 | 0.15 | ± 0.11 |
| Balmat-5 | 7.18 | ± 0.11 | 14.42 | ± 0.01 | -0.12 | ± 0.11 |
| Balmat-6 | 7.85 | ± 0.12 | 15.57 | ± 0.01 | -0.03 | ± 0.12 |
| Balmat-7 | 7.92 | ± 0.12 | 15.60 | ± 0.01 | 0.03 | ± 0.12 |
| Balmat-8 | 7.67 | ± 0.13 | 15.40 | ± 0.02 | -0.12 | ± 0.13 |
| Balmat-9 | 7.89 | ± 0.15 | 15.49 | ± 0.02 | 0.06 | ± 0.15 |
| Balmat-10 | 7.85 | ± 0.15 | 15.64 | ± 0.02 | -0.058 | ± 0.15 |
| Balmat-11 | 8.02 | ± 0.15 | 15.96 | ± 0.02 | -0.049 | ± 0.15 |
| Balmat-12 | 8.17 | ± 0.15 | 15.99 | ± 0.02 | 0.09 | ± 0.15 |
| | | | | | | |
| *Average* | *7.66* | | *15.16* | | *-0.01* | |
| *(Standard deviation)* | *(0.34)* | | *(0.65)* | | *(0.11)* | |
| | | | | | | |
| CAR 123 pyrite | | | | | | |
| CAR-1 | 0.87 | ± 0.13 | 1.48 | ± 0.02 | 0.12 | ± 0.13 |

| | | | | | | |
|---|---|---|---|---|---|---|
| CAR-2 | 0.59 | ± 0.13 | 1.38 | ± 0.02 | -0.11 | ± 0.13 |
| CAR-3 | 0.58 | ± 0.13 | 1.52 | ± 0.02 | -0.19 | ± 0.13 |
| CAR-4 | 0.66 | ± 0.13 | 1.76 | ± 0.02 | -0.24 | ± 0.13 |
| CAR-5 | 0.81 | ± 0.13 | 1.21 | ± 0.02 | 0.19 | ± 0.13 |
| | | | | | | |
| *Average* | *0.70* | | *1.47* | | *-0.04* | |
| *(Standard deviation)* | *(0.13)* | | *(0.20)* | | *(0.19)* | |
| | | | | | | |
| P1 pyrrhotite | | | | | | |
| P1-1 | 4.56 | ± 0.13 | 9.17 | ± 0.02 | -0.09 | ± 0.13 |
| P1-2 | 4.74 | ± 0.13 | 9.15 | ± 0.02 | 0.10 | ± 0.13 |
| P1-3 | 4.55 | ± 0.13 | 9.01 | ± 0.02 | -0.02 | ± 0.13 |
| P1-4 | 3.98 | ± 0.13 | 7.50 | ± 0.02 | 0.18 | ± 0.13 |
| | | | | | | |
| *Average* | *4.46* | | *8.71* | | *0.05* | |
| *(Standard deviation)* | *(0.33)* | | *(0.81)* | | *(0.12)* | |

**Table A-2. Sulfur isotopic composition of mineral standards - January 2012 SIMS sessions**

| Standard | δ³³S (‰) | 1σ error (‰) | δ³⁴S (‰) | 1σ error (‰) | Δ³³S (‰) | 1σ error (‰) |
|---|---|---|---|---|---|---|
| *Session 1* | | | | | | |
| Cañon Diablo Troilite (CDT) | | | | | | |
| CDT-1 | 0.02 | ± 0.17 | 0.05 | ± 0.25 | 0.00 | ± 0.21 |
| CDT-2 | 0.09 | ± 0.17 | 0.22 | ± 0.25 | -0.02 | ± 0.21 |
| CDT-3 | -0.11 | ± 0.17 | -0.27 | ± 0.25 | 0.09 | ± 0.21 |
| | | | | | | |
| *Average* | *0.00* | | *0.00* | | *0.00* | |
| *(Standard deviation)* | *(0.10)* | | *(0.25)* | | *(0.02)* | |
| | | | | | | |
| Balmat pyrite | | | | | | |
| Balmat-1 | 7.52 | ± 0.41 | 14.92 | ± 0.25 | -0.03 | ± 0.43 |
| Balmat-2 | 7.83 | ± 0.41 | 15.28 | ± 0.25 | 0.09 | ± 0.43 |
| | | | | | | |
| *Average* | *7.68* | | *15.10* | | *0.03* | |
| *(Standard deviation)* | *(0.22)* | | *(0.25)* | | *(0.09)* | |
| | | | | | | |
| CAR 123 pyrite | | | | | | |
| CAR-1 | 0.75 | ± 0.42 | 1.36 | ± 0.46 | 0.05 | ± 0.48 |
| CAR-2 | 0.76 | ± 0.43 | 1.51 | ± 0.46 | -0.01 | ± 0.49 |
| CAR-3 | 0.68 | ± 0.43 | 1.41 | ± 0.46 | -0.04 | ± 0.49 |
| CAR-4 | 0.13 | ± 0.43 | 0.73 | ± 0.46 | -0.24 | ± 0.49 |
| CAR-5 | 1.26 | ± 0.42 | 2.03 | ± 0.46 | 0.23 | ± 0.48 |
| | | | | | | |
| *Average* | *0.72* | | *1.41* | | *0.00* | |
| *(Standard deviation)* | *(0.40)* | | *(0.46)* | | *(0.17)* | |
| | | | | | | |
| | | | | | | |
| *Session 2* | | | | | | |
| Cañon Diablo Troilite (CDT) | | | | | | |
| CDT-1 | -0.61 | ± 0.45 | -1.19 | ± 0.87 | -0.01 | ± 0.63 |
| CDT-2 | -0.52 | ± 0.45 | -0.91 | ± 0.87 | -0.06 | ± 0.63 |
| CDT-3 | -0.38 | ± 0.45 | -0.98 | ± 0.87 | 0.11 | ± 0.63 |
| | | | | | | |
| *Average* | *-0.51* | | *-1.03* | | *0.02* | |
| *(Standard deviation)* | *(0.11)* | | *(0.15)* | | *(0.09)* | |
| | | | | | | |
| Balmat pyrite | | | | | | |
| Balmat-1 | 7.11 | ± 0.40 | 13.94 | ± 0.74 | 0.05 | ± 0.54 |
| Balmat-2 | 7.15 | ± 0.40 | 14.11 | ± 0.74 | 0.01 | ± 0.54 |
| | | | | | | |
| *Average* | *7.13* | | *14.03* | | *0.03* | |
| *(Standard deviation)* | (0.03) | | *(0.12)* | | *(0.03)* | |
| | | | | | | |
| Anderson pyrrhotite | | | | | | |
| AND-1 | 1.30 | ± 0.98 | 2.47 | ± 1.83 | 0.05 | ± 1.34 |
| AND-2 | -0.42 | ± 0.98 | -0.54 | ± 1.83 | -0.15 | ± 1.34 |
| AND-3 | -0.28 | ± 0.98 | -0.65 | ± 1.83 | 0.05 | ± 1.34 |

| | | | | | |
|---|---|---|---|---|---|
| AND-4 | 1.56 | ± 0.98 | 3.05 | ± 1.83 | 0.01 | ± 1.34 |
| AND-5 | 1.40 | ± 0.98 | 2.66 | ± 1.83 | 0.05 | ± 1.34 |
| | | | | | | |
| *Average* | *0.71* | | *1.40* | | *0.00* | |
| *(Standard deviation)* | *(0.97)* | | *(1.83)* | | *(0.08)* | |
| | | | | | | |
| NWA standard #1 | | | | | | |
| NWA-1 | 12.42 | ± 0.16 | 24.48 | ± 0.03 | 0.05 | ± 0.16 |
| NWA-2 | 12.41 | ± 0.19 | 24.28 | ± 0.03 | 0.14 | ± 0.19 |
| NWA-3 | 12.56 | ± 0.31 | 24.79 | ± 0.06 | 0.04 | ± 0.31 |
| NWA-4 | 12.42 | ± 0.26 | 24.40 | ± 0.04 | 0.09 | ± 0.26 |
| NWA-5 | 12.55 | ± 0.19 | 24.60 | ± 0.03 | 0.12 | ± 0.19 |
| | | | | | | |
| *Average* | *12.47* | | *24.51* | | *0.09* | |
| *(Standard deviation)* | *(0.08)* | | *(0.20)* | | *(0.04)* | |
| **Session 3** | | | | | | |
| Cañon Diablo Troilite (CDT) | | | | | | |
| CDT-1 | 0.09 | ± 0.47 | 0.70 | ± 0.87 | -0.26 | ± 0.64 |
| CDT-2 | 0.54 | ± 0.46 | 0.77 | ± 0.87 | 0.15 | ± 0.63 |
| CDT-3 | 0.38 | ± 0.45 | 0.81 | ± 0.87 | -0.03 | ± 0.63 |
| CDT-4 | 0.23 | ± 0.47 | 0.47 | ± 0.87 | 0.00 | ± 0.64 |
| CDT-5 | 0.28 | ± 0.46 | 0.34 | ± 0.87 | 0.11 | ± 0.64 |
| | | | | | | |
| *Average* | *0.30* | | *0.61* | | *0.00* | |
| *(Standard deviation)* | *(0.17)* | | *(0.20)* | | *(0.16)* | |
| | | | | | | |
| Balmat pyrite | | | | | | |
| Balmat-1 | 7.73 | ± 0.40 | 15.36 | ± 0.74 | -0.05 | ± 0.55 |
| Balmat-2 | 7.75 | ± 0.39 | 15.27 | ± 0.74 | 0.02 | ± 0.54 |
| Balmat-3 | 7.94 | ± 0.39 | 15.65 | ± 0.74 | 0.02 | ± 0.54 |
| Balmat-4 | 8.00 | ± 0.40 | 15.67 | ± 0.74 | 0.07 | ± 0.55 |
| Balmat-5 | 8.04 | ± 0.40 | 15.71 | ± 0.74 | 0.09 | ± 0.54 |
| | | | | | | |
| *Average* | *7.89* | | *15.53* | | *0.03* | |
| *(Standard deviation)* | *(0.14)* | | *(0.20)* | | *(0.05)* | |
| | | | | | | |
| CAR 123 pyrite | | | | | | |
| CAR-1 | 0.68 | ± 0.37 | 1.54 | ± 0.53 | -0.10 | ± 0.45 |
| CAR-2 | 0.90 | ± 0.38 | 1.63 | ± 0.53 | 0.06 | ± 0.47 |
| CAR-3 | 1.14 | ± 0.33 | 2.23 | ± 0.53 | 0.00 | ± 0.43 |
| | | | | | | |
| *Average* | *0.91* | | *1.80* | | *-0.01* | |
| *(Standard deviation)* | *(0.23)* | | *(0.38)* | | *(0.08)* | |
| | | | | | | |
| NWA standard #2 | | | | | | |
| NWA-1 | -1.48 | ± 0.09 | -2.93 | ± 0.02 | -0.02 | ± 0.09 |
| *(one measurement)* | | | | | | |

## A.3   Electron Microprobe

The composition of sulfide grains analyzed via SIMS was verified using the JEOL JXA-8900 SuperProbe (EPMA) with a ZAF correction at the University of Maryland. Wavelength dispersive spectrometry (WDS) scans were performed with an accelerating potential of 15 kV, beam current of 10 nA, spot size of 1 μm, and dwell times of 20 s for iron and sulfur and 30 s for the remaining elements. Precision of sulfur and iron measurements based on repeated analyses of a pyrrhotite standard was approximately 0.2 wt% (1σ). EPMA analyses of MIL 03346 were performed by J. M. D. Day and S-T. Kim using similar instrument settings.

# Appendix B. Images of Sulfide Grains Analyzed by Ion Microprobe[1]

[1] All text and images in this appendix were written/created by H. B. Franz.

Prior to ion SIMS analysis, petrographic sections were studied and mapped with reflected light microscopy to locate sulfide grains large enough (> ~20 μm) for sulfur isotopic measurements with the ion microprobe. The grains were also imaged post-SIMS with scanning electron microscopy. Images of sulfide grains are shown in Figures B-1 through B-11. Note that high-resolution images of Nakhla sections pre-SIMS were not collected, so inly post-SIMS images of Nakhla sections are included. Images of MIL 03346 were taken by S-T. Kim. Images of NWA 6148 were taken by J. Farquhar. Abbreviations: BSE = backscattered electron; SEM = secondary electron microscope; RL = reflected light.
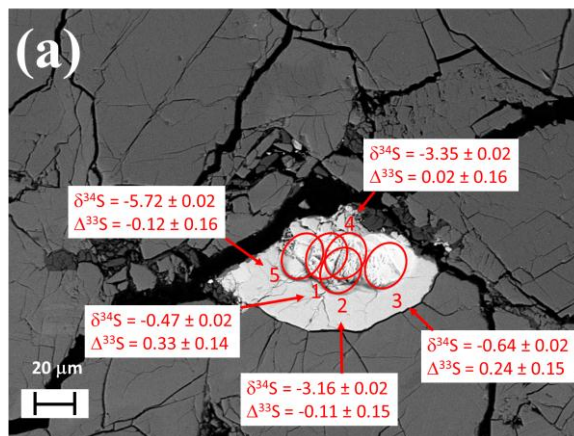


**Figure B-1. Sulfide grains in Nakhla section USNM-426-9.**

**BSE images post-SIMS analysis. (a) Grain 1. Spots of duplicate analyses are indicated.**
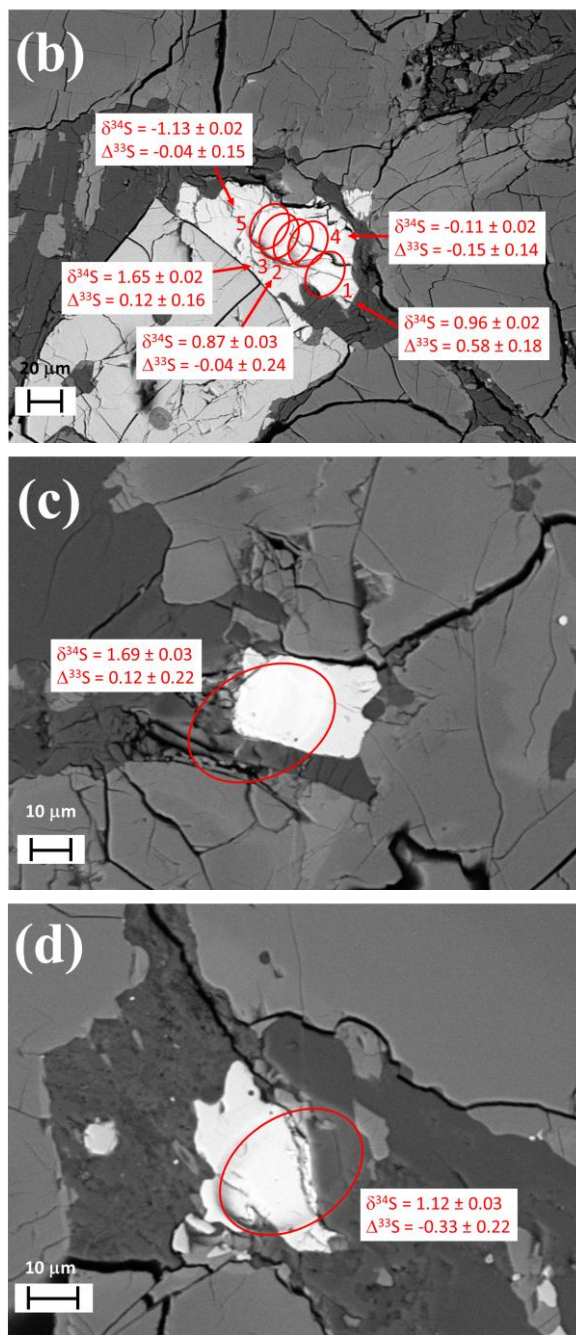
**Figure B-1, continued. Sulfide grains in Nakhla section USNM-426-9.**

**BSE images post- SIMS analysis. (b) Grain 4. Spots of duplicate analyses are indicated.**

**(c) Grain 11. (d) Grain 16.**
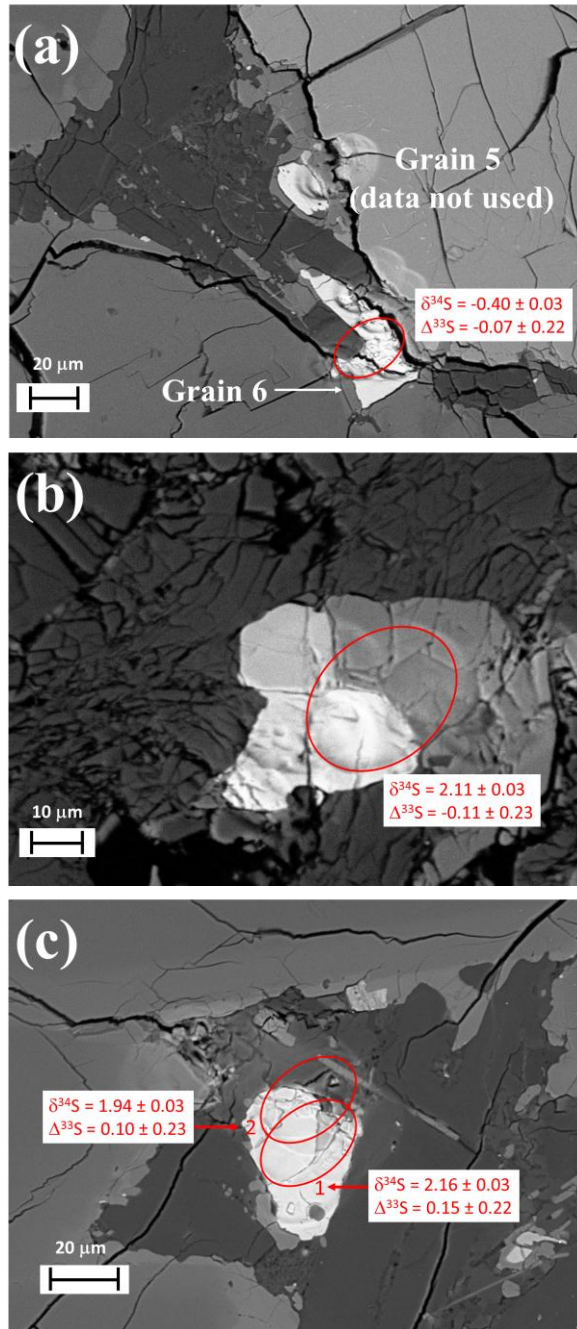
**Figure B-2. Sulfide grains in Nakhla section USNM-426-17.**

BSE images post- SIMS analysis. (a) Grain 6. (b) Grain 14. (c) Grain 19. Spots for

duplicate analyses are indicated.
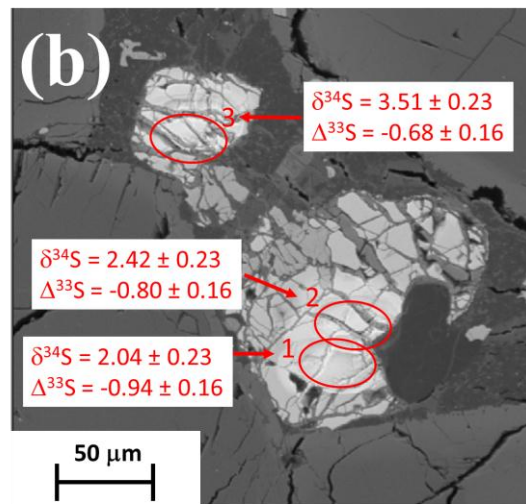
**Figure B-3. Sulfide grains in MIL 03346, section 6.**

**(a) Grain 6, RL image, pre-SIMS. (b) Grain 1, SEM image, post-SIMS. Spots of**

**duplicate analyses are indicated.**
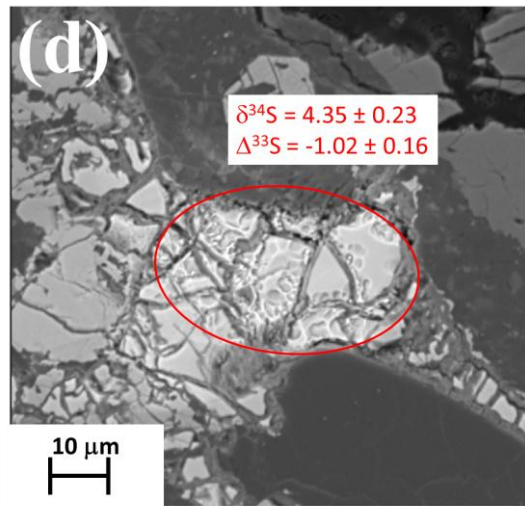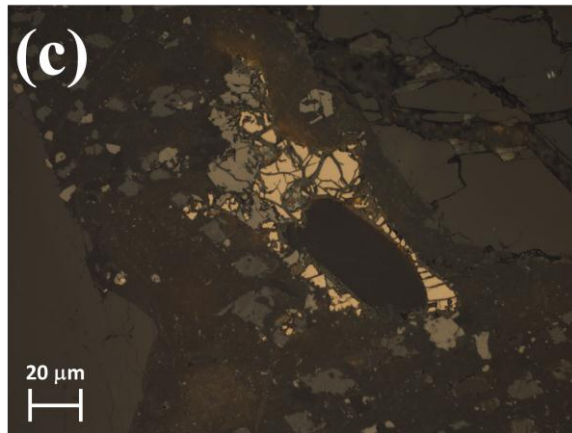
**Figure B-3, continued. Sulfide grains in MIL 03346, section 6.**

**(c) Grain 17, RL image, pre-SIMS. (d) Grain 17, SEM image, post-SIMS.**

$\delta^{34}S = 4.27 \pm 0.23$
$\Delta^{33}S = -0.97 \pm 0.13$

$\delta^{34}S = 2.45 \pm 0.23$
$\Delta^{33}S = -1.23 \pm 0.13$

**Figure B-4. Sulfide grains in MIL 03346, section 93.**

(a) Grain 2, RL image, pre-SIMS. (b) Grain 2, SEM image, post-SIMS. Data from uncircled spots were not used due to poor count rates. (c) Grain 5, RL image, pre-SIMS.

(d)

$\delta^{34}S = 3.75 \pm 0.23$
$\Delta^{33}S = -0.55 \pm 0.13$

20 μm

(e)

100 μm

(f)

$\delta^{34}S = 3.00 \pm 0.23$
$\Delta^{33}S = -0.68 \pm 0.13$

$\delta^{34}S = 2.89 \pm 0.23$
$\Delta^{33}S = -0.44 \pm 0.13$

50 μm
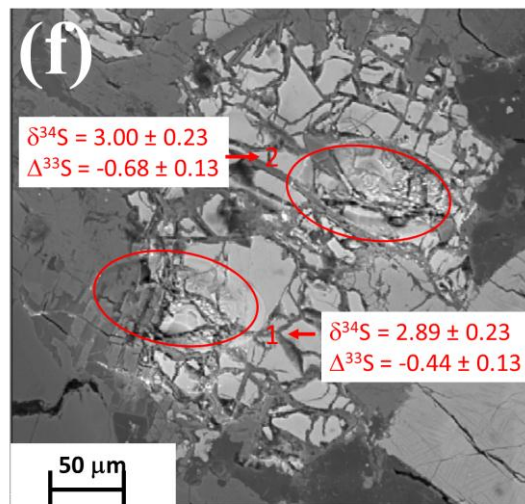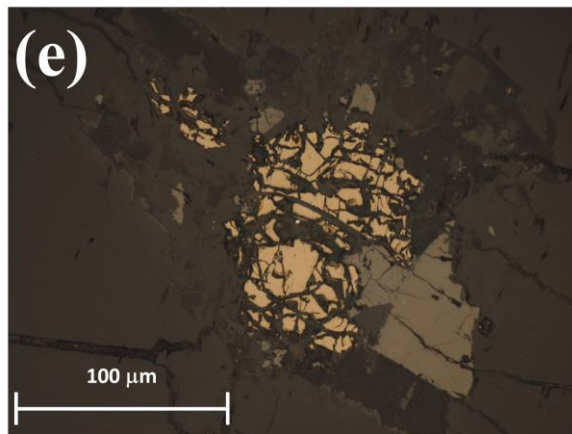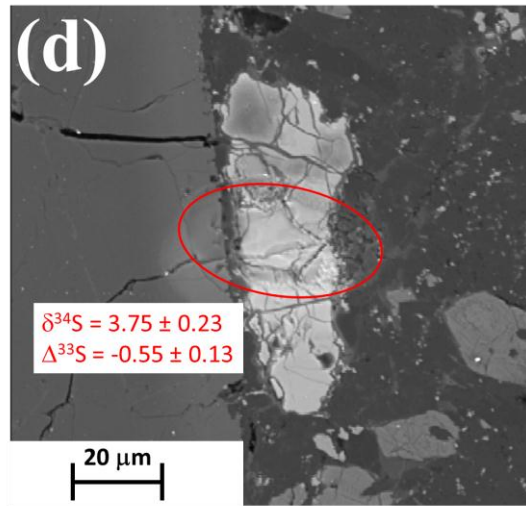
**Figure B-4, continued. Sulfide grains in MIL 03346, section 93.**

**(d) Grain 5, SEM image, post-SIMS. (e) Grain 7, RL image, pre-SIMS. (f) Grain 7, SEM**

**image, post-SIMS.**
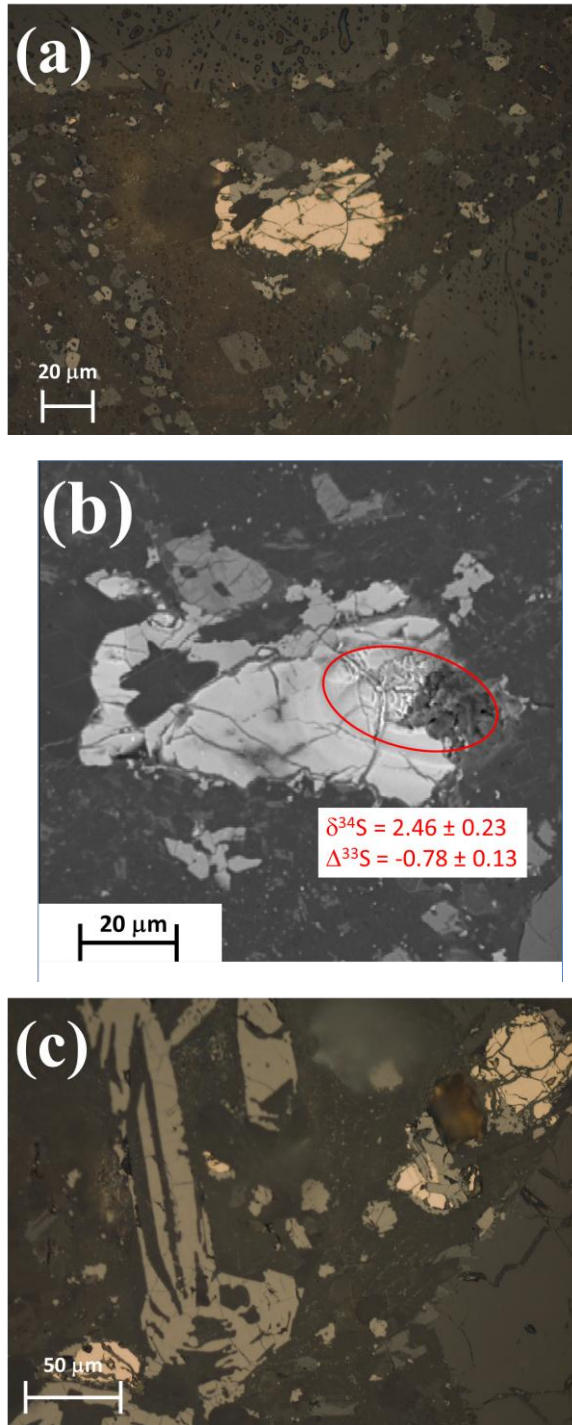
**Figure B-5. Sulfide grains in MIL 03346, section 104.**

**(a) Grain 2, RL image, pre-SIMS. (b) Grain 2, SEM image, post-SIMS. (c) Grain 6, RL image, pre-SIMS.**

$\delta^{34}S = 3.81 \pm 0.23$
$\Delta^{33}S = -0.30 \pm 0.13$

$\delta^{34}S = 5.95 \pm 0.23$
$\Delta^{33}S = -1.06 \pm 0.13$

50 µm



20 µm



$\delta^{34}S = 1.62 \pm 0.23$
$\Delta^{33}S = -0.71 \pm 0.13$

20 µm
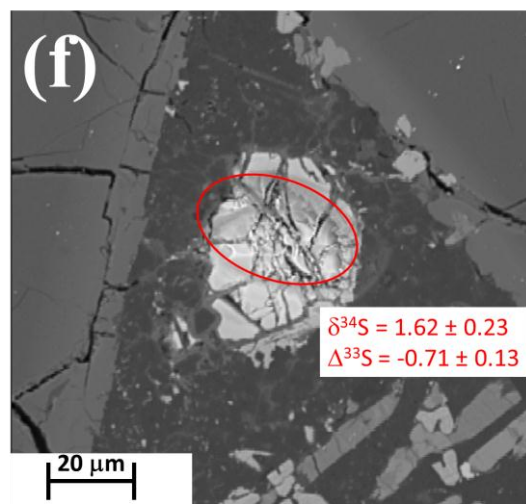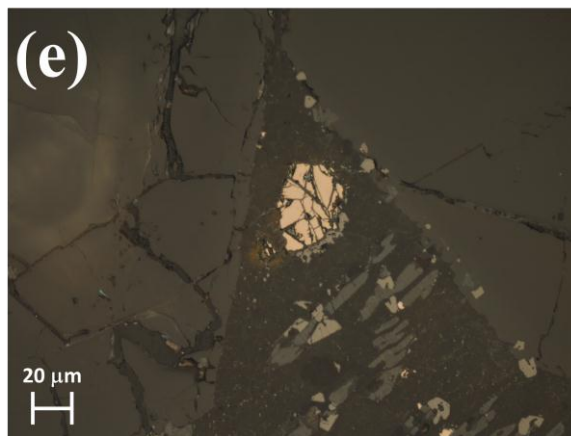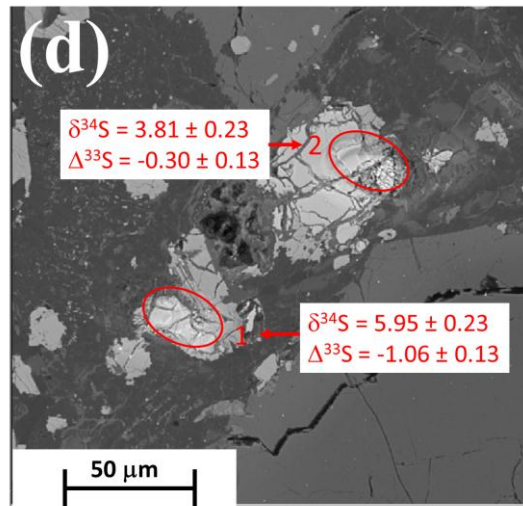
**Figure B-5, continued. Sulfide grains in MIL 03346, section 104.**

**(d) Grain 6, SEM image, post-SIMS. (e) Grain 8, RL image, pre-SIMS. (f) Grain 8, SEM**

**image, post-SIMS.**

$\delta^{34}S = 1.31 \pm 0.23$
$\Delta^{33}S = -0.46 \pm 0.13$

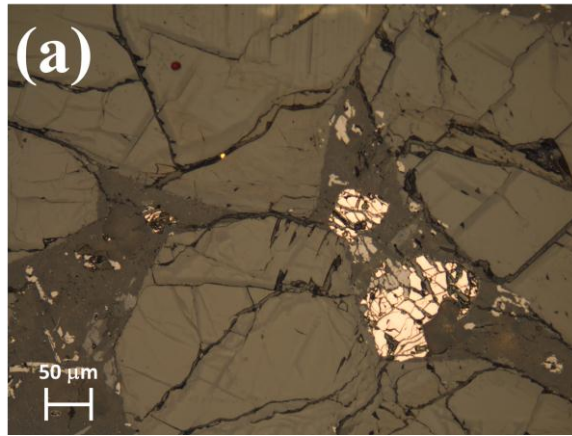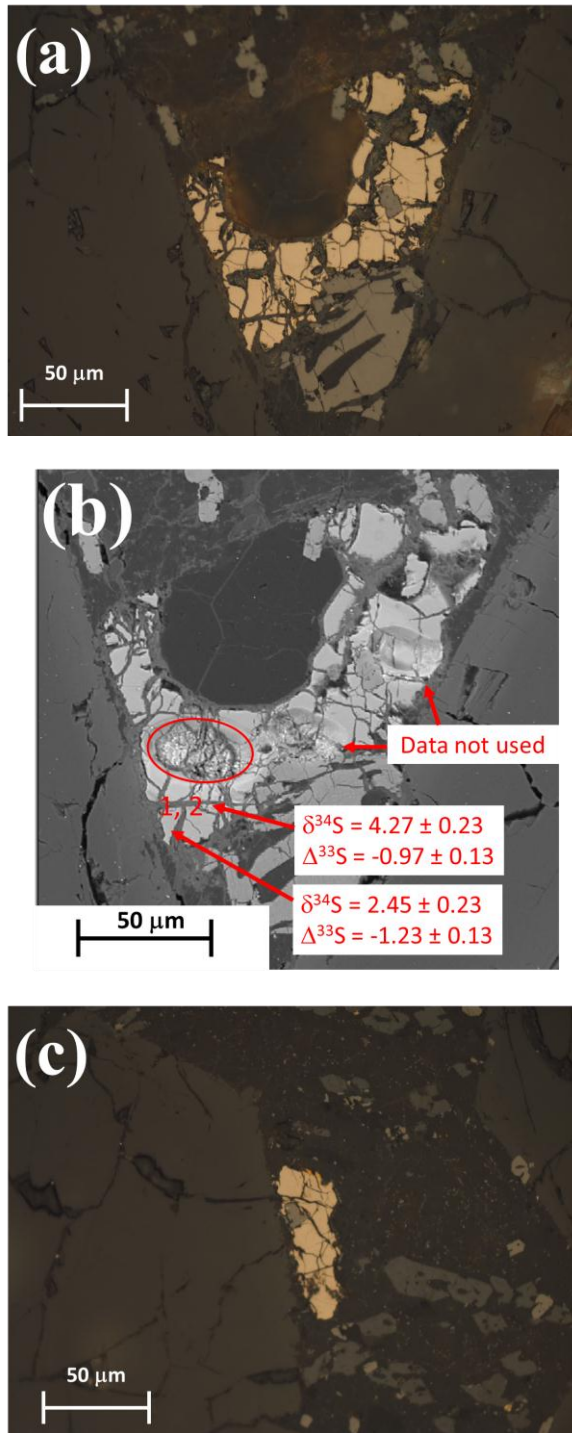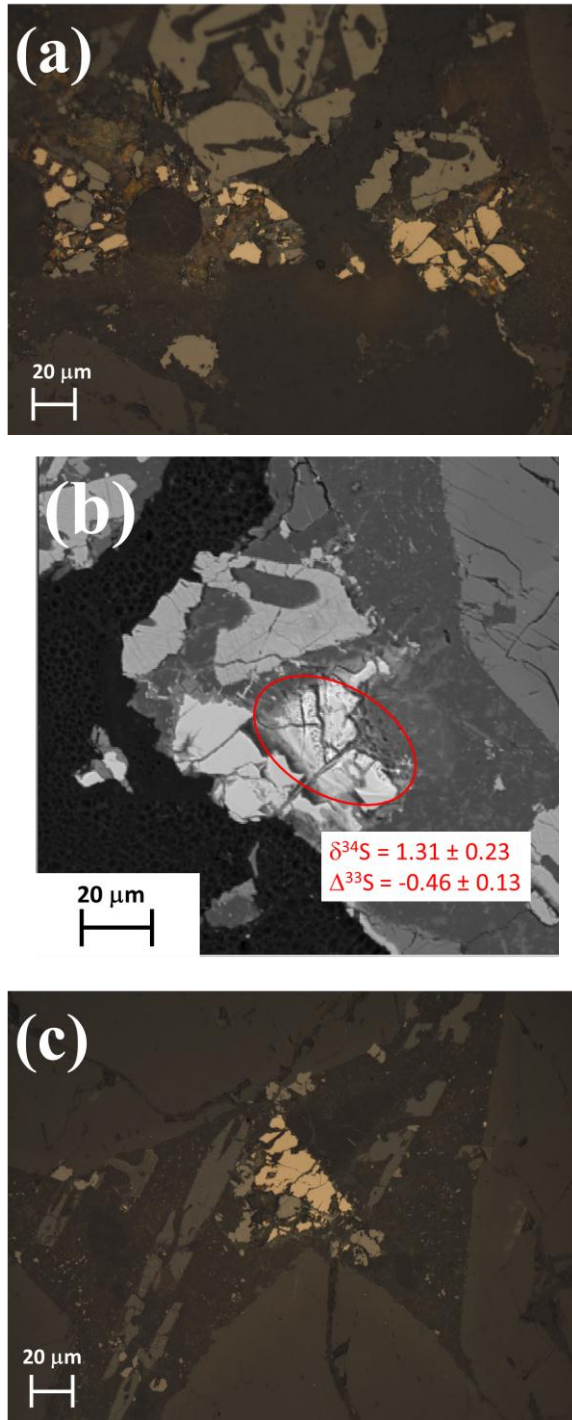**Figure B-6. Sulfide grains in MIL 03346, section 132.**

**(a) Grain 1, RL image, pre-SIMS. (b) Grain 1, SEM image, post-SIMS. (c) Grain 2, RL image, pre-SIMS.**

$\delta^{34}S = 0.89 \pm 0.23$
$\Delta^{33}S = -0.40 \pm 0.13$

20 μm



20 μm



$\delta^{34}S = 2.56 \pm 0.23$
$\Delta^{33}S = -0.73 \pm 0.13$

20 μm
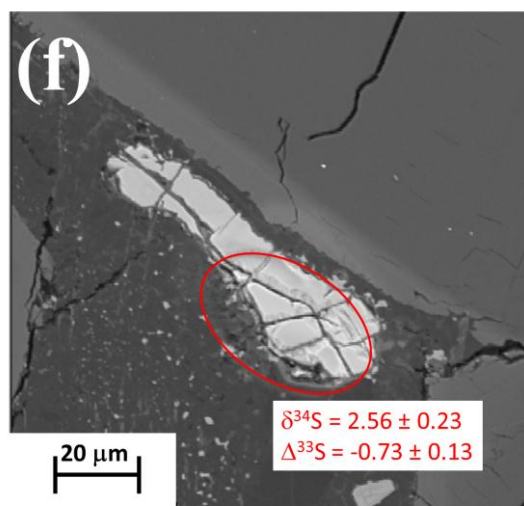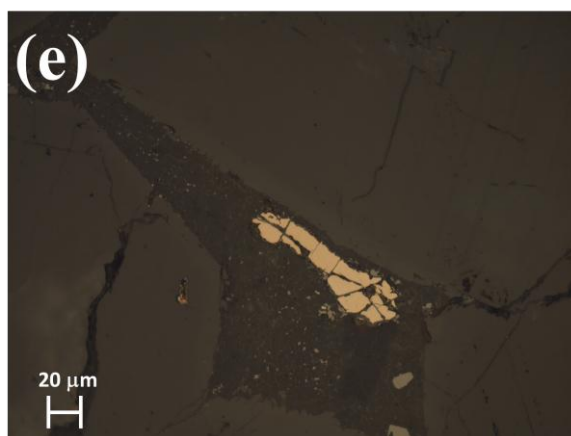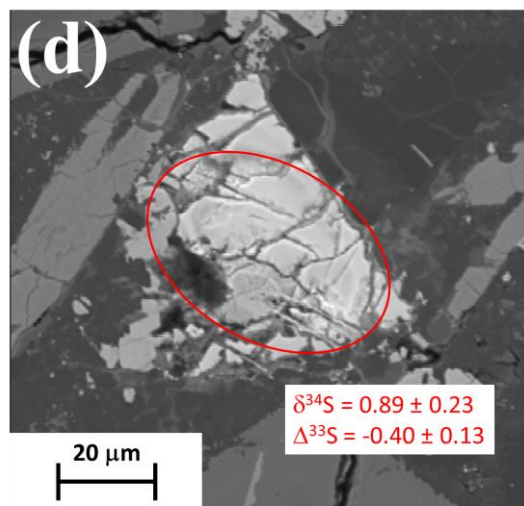
**Figure B-6, continued. Sulfide grains in MIL 03346, 132.**

**(d) Grain 2, SEM image, post-SIMS. (e) Grain 3, RL image, pre-SIMS. (f) Grain 3, SEM**

**image, post-SIMS.**

217
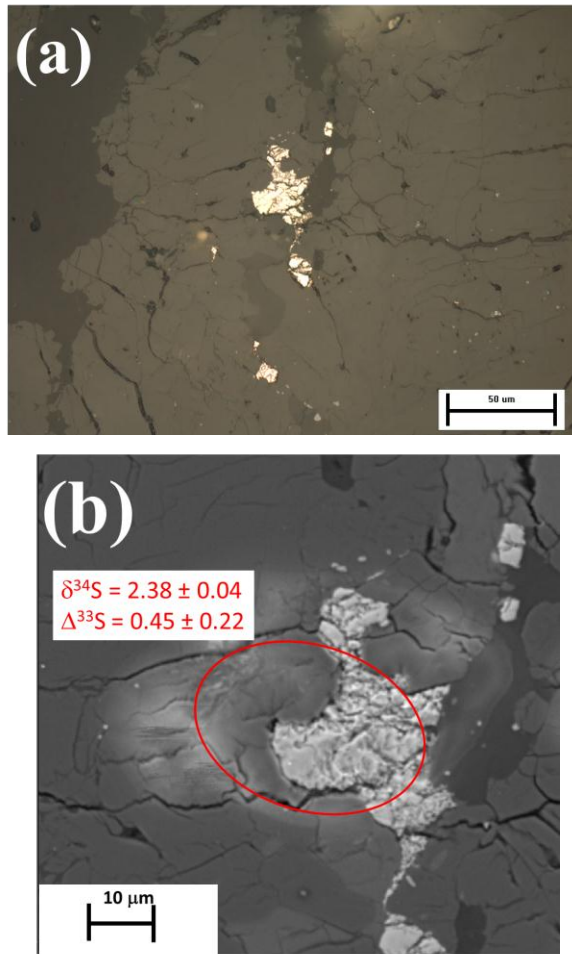
**Figure B-7. Sulfide grains in ALH 84001, section 352.**

**(a) Grain G6, RL image, pre-SIMS. (b) Grain G6, SEM image, post-SIMS.**
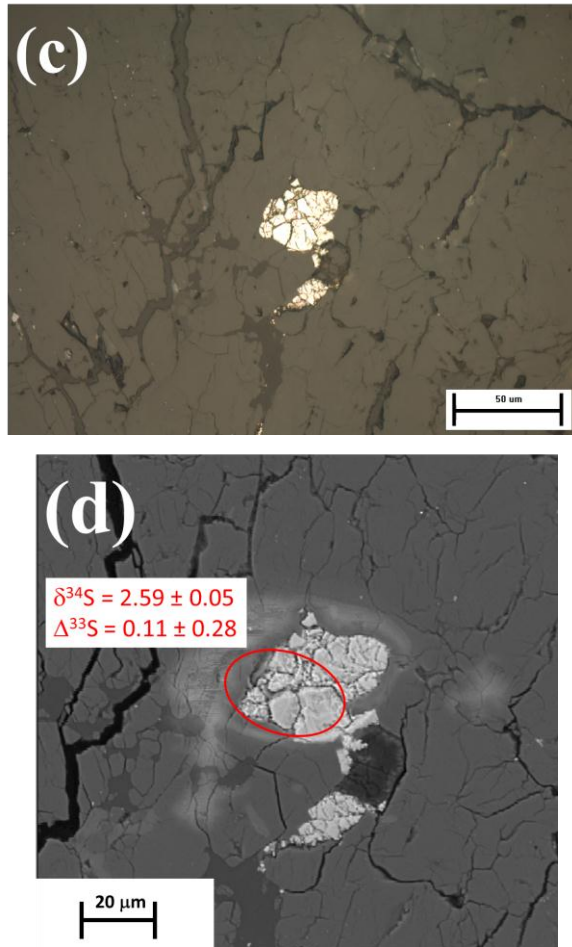
**Figure B-7, continued. Sulfide grains in ALH 84001, section 352.**

**(c) Grain G9, RL image, pre-SIMS. (d) Grain G9, SEM image, post-SIMS.**

# Bibliography

Allègre, C., Manhes, G., and Lewin, E. (2001) Chemical composition of the Earth and the volatility control on planetary genetics. *Earth and Planetary Science Letters* 185, 49-69.

Andrews-Hanna, J. C., Zuber, M. T., Arvidson, R. E. and Wiseman, S. M. (2010) Early Mars hydrology: Meridiani playa deposits and the sedimentary record of Arabia Terra. *Journal of Geophysical Research* 115, doi: 10.1029/2009JE003485.

Antonelli, M. A., Peters, M., and Farquhar, J. (2012) Sulfur isotopic compositions of magmatic and non-magmatic iron meteorites. Lunar and Planetary Institute #2081.

Archer, C.P., Elks, J.M., and Western, C.M. (2000) The $C^3\Pi$, $d^1\Pi$, and $e^1\Pi$ states of SO. *Journal of Chemical Physics* 112, 6293-6300.

Arvidson, R. E., Poulet, F., Morris, R. V., Bibring, J-P., Bell, III., J. F., Squyres, S. W., Christensen, P. R., Bellucci, G., Gondet, B., Ehlmann, B. L., Farrand, W. H., Fergason, R. L., Golombek, M., Griffes, J. L., Grotzinger, J., Guinness, E. A., Herkenhoff, K. E., Johnson, J. R., Klingelhöfer, G., Langevin, Y., Ming, D., Seelos, K., Sullivan, R. J., Ward, J. G., Wiseman, S. M., and Wolff, M. (2006) Nature and origin of the hematite-bearing plains of Terra Meridiani based on analyses of orbital and Mars Exploration Rover data sets. *Journal of Geophysical Research* 111, doi:10.1029/2006JE002728.

Ashwal L.D., Warner J.L., and Wood C.A. (1982) SNC meteorites: Evidence against an asteroidal origin. Proceedings of the 13th Lunar and Planetary Science Conference. *Journal of Geophysical Research* 87, A393-A400.

Baird, A.K., Toulmin III, P., Clark, B.C., Rose Jr., H.J., Keil, K., Christian, R.P., and Gooding, J.L. (1976) Mineralogic and petrologic implications of Viking geochemical results from Mars: interim report. *Science* 194, 1288-1293.

Bally, J. and Langer, W. D. (1982) Isotope-selective photodestruction of carbon monoxide. *Astrophysical journal* 255, 143-148.

Bandfield, J. L., Hamilton, V. E., and Christensen, P. R. (2000) A global view of martian surface compositions from MGS-TES. *Science* 287, 1626-1630.

Bandfield, J. L., Hamilton, V. E., Christensen, P. R., and McSween, H. Y., Jr. (2004) Identification of quartzfeldspathic materials on Mars. *Journal of Geophysical Research* 109, doi: 10.1029/2004JE002290.

Banin, A., Han, F.X., and Cicelsky, A. (1997) Acidic volatiles and the Mars soil. *Journal of Geophysical Research* 102 (E6), 13341–13356.

Bao, H. and Marchant, D.R. (2006) Quantifying sulfate components and their variations in soils of the McMurdo Dry Valleys, Antarctica. *Journal of Geophysical Research* 111, D16301.

Baroni, M., Savarino, J., Cole-Dai, J., Rai, V.K., and Thiemens, M.H. (2008) Anomalous sulfur isotope compositions of volcanic sulfate over the last millennium in Antarctic ice cores. *Journal of Geophysical Research* 113. D20112.

Barrat J.A., Blichert-Toft J., Nesbitt R.W. and Keller F. (2001c) Bulk chemistry of Saharan shergottite Dar al Gani 476. *Meteoritics & Planetary Science* 36, 23-29.

Barrat, J.A., Gillet, P., Sautter, V., Jambon, A., Javoy, M., Göpel, C., Lesourd, M., Keller, F. and Petit, E. (2002a) Petrology and geochemistry of the basaltic shergottite North West Africa 480. *Meteoritics & Planetary Science* 37, 487-499.

Barrat, J.A., Jambon, A., Bohn, M., Gillet, P., Sautte, V., Göpel, C., Lesourd, M. and Keller, F. (2002b) Petrology and chemistry of the picritic shergottite North West Africa 1068 (NWA 1068). *Geochimica et Cosmochimica Acta* 66, 3505-3518.

Beck, P., Barret, J., Gillet, P., Franchi, I.A., Greenwood, R.C., Van de Moortele, B., Reynard, B., Bohn, M. and Cotton, J. (2005) The Diderot meteorite: the second chassignite. *Lunar & Planetary Science* XXXVI, #1639.

Bell, J.F., III, McSween, H.Y., Jr., Crisp, J.A., Morris, R.V., Murchie, S.L., Bridges, N.T., Johnson, J.R., Britt, D.T., Golombek, M.P., Moore, H.J., Ghosh, A., Bishop, J.L., Anderson, R.C., Brückner, J., Economou, T., Greenwood, J.P., Gunnlaugsson, H.P., Hargraves, R.M., Hviid, S., Knudsen, J.M., Madsen, M.B., Reid, R., Rieder, R., and Soderblom, L. (2000) Mineralogic and compositional properties of Martian soil and dust: results from Mars Pathfinder. *Journal of Geophysical Research* 105 (E1), 1721-1755.

Berkley, J. L., Brown, H. G., IV, Keil, K., Carter, N. L., Mercier, J.-C., and Huss, G. (1976) The Kenna ureilite: An ultramafic rock with evidence for igneous, metamorphic, and shock origin. *Geochimica et Cosmochimica Acta* 40, 1429-1437.

Berkley, J.L. (1987) Petrology and compositional trends in five new Antarctic diogenites. *Lunar & Planetary Science* XVIII, 62-63.

Berkley, J.L., Keil, K. and Prinz, M. (1980) Comparative petrology and origin of Governador Valadares and other nakhlites. *Proceedings of Lunar & Planetary Science Conference* XI, 1089-1102.

Berman, D. C. and Hartmann, W. K. (2002) Recent fluvial, volcanic, and tectonic activity on the Cerberus Plains of Mars. *Icarus* 159, 1-17.

Bhattacharya, S.K. Savarino, J., and Thiemens, M.H. (2000) A new class of oxygen isotopic fractionation in Photodissociation of carbon dioxide: potential implication for atmospheres of Mars and Earth. *Geophysical Research Letters* 27, 1459-1462.

Bibring, J.-P., and Erard, S. (2001) The martian surface composition. *Chronology and Evolution of Mars*, Kallenbach et al., eds., 293-316.

Bibring, J.P., Langevin, Y., Gendrin, A., Gondet, B., Poulet, F., Berthé, M., Soufflot, A., Arvidson, R., Mangold, N., Mustard, J., Drossart, P., and the OMEGA team (2005) Mars surface diversity as revealed by the OMEGA/Mars Express observations. *Science* 307, 1576–1581.

Bibring, J.-P., Langevin, Y., Mustard, J. F., Poulet, F., Arvidson, R., Gendrin, A., Gondet, B., Mangold, N., Pinet, P., Forget, F., and the OMEGA team. (2006) Global mineralogical and aqueous Mars history derived from OMEGA/Mars Express data. *Science* 312, 400-404.

Boctor, N.Z., Wang, J., D'Alexander, C.M.O., Hauri, E., Bertka, C.M., Fei, Y. and Humayun, M. (1998) Petrology and hydrogen and sulfur isotope studies of mineral phases in Martian meteorite ALH 84001. *Lunar & Planetary Science* XXIX, #1787.

Bogard, D.D. and Johnson, P. (1983) Martian gases in an Antarctic meteorite? *Science* 221, 651-654.

Bogumil, K., Orphal, J., Homann, T., Voigt, S., Spietz, P., Fleischmann, O.C., Vogel, A., Hartmann, M., Kromminga, H., Bovensmann, H., Frefick, J., and Burrows, J.P. (2003) Measurements of molecular absorption spectra with the SCIAMACHY pre-flight model: instrument characterization and reference data for atmospheric remote-sensing in the 230-2380 nm region. *Journal of Photochemistry and Photobiology A: Chemistry* 157, 167-184.

Borg, L. E., Nyquist, L. E., Taylor, L. A., Wiesmann, H., and Shih, C. Y. (1997) Constraints on martian differentiation processes from Rb-Sr and Sm-Nd isotopic analyses of the basaltic shergottite QUE 94201. *Geochimica et Cosmochimica Acta* 61, 4915-4931.

Borg, L. E., and Draper, D. S. (2003) A petrogenetic model for the origin and compositional variation of the martian basaltic meteorites. *Meteoritics & Planetary Science* 38, 1713-1731.

Boynton, W. V., Feldman, W. C., Squyres, S. W. Prettyman, T. H., Brückner, J., Evans, L. G., Reedy, R. C., Starr, R., Arnold, J. R., Drake, D. M., Englert, P. A., Metzger, A. E., Mitrofanov, I., Trombka, J. I., d'Uston, C., Wänke, H., Gasnault, O.,

Hamara, D. K., Janes, D. M., Marcialis, R. L., Maurice, S., Mikheeva, I., Taylor, G. J., Tokar, R. I., and Shinohara, C. (2002) Distribution of hydrogen in the near surface of Mars: Evidence for subsurface ice deposits. *Science* 27, 81-85.

Bradley, J.P., Harvery, R.P., and McSween, Jr., H.Y. (1996) Magnetite whiskers and platelets in the ALH 84001 Martian meteorite: Evidence of vapor phase growth. *Geochimica et Cosmochimica Acta* 60, 5149-5155.

Brandon, A. D., Walker, R. J., Morgan, J. W., and Goles, G. G. (2000) Re-Os isotopic evidence for early differentiation of the martian mantle. *Geochimica et Cosmochimica Acta* 64, 4083-4095.

Brandon, A. D., Puchtel, I. S., Walker, R. J., Day, J. M. D., Irving, A. J., and Taylor, L. A. (2012) Evolution of the martian mantle inferred from the $^{187}$Re-$^{187}$Os isotope and highly siderophile element abundance systematics of shergottite meteorites. *Geochimica et Cosmochimica Acta* 76, 206-235.

Brearley, A.J. (2000) Hydrous phases in ALH 84001: Further evidence for preterrestrial alteration and a shock-induced thermal overprint. *Lunar & Planetary Sci*ence XXXI, # 1203.

Bridges, J. C., and Grady, M. M. (2000) Evaporite mineral assemblages in the nakhlite (martian) meteorites. *Earth and Planetary Science Letters* 176, 267-279.

Bridges, J. C. and Hicks, L. J. (2011) Amorphous gel in the nakhlites: Product of a rapidly cooled hydrothermal fluid. *Meteoritics & Planetary Science* 46, A30.

Brügmann. G. E., Naldrett, A. J., Asif, A., Lightfoot, P. C., Gorbechev, N. S., and Fedorenko, V. A. (1993) Siderophile and chalcophile metals as tracers of the evolution of the Siberian Trap in the Noril'sk region, Russia. *Geochimica et Cosmochimica Acta* 57, 2001-2018.

Buchachenko, A.L. (2001) Magnetic isotope effect: nuclear spin control of chemical reactions. *Journal of Physical Chemistry A* 105, 9995–10011.

Bunch, T.E. and Reid, A.M. (1975) The nakhlites, I. Petrography and mineral chemistry. *Meteoritics* 10**,** 303-315.

Burgess, R., Wright, I.P. and Pillinger, C.T. (1989) Distribution of sulphides and oxidized sulphur components in SNC meteorites. *Earth Planetary Science Lett*ers 93, 314-320.

Burghele, A., Dreibus, G., Palme, H., Rammensee, W., Spettel, B., Weckwerth, G., and Wänke, H. (1983) Chemistry of shergottites and the Shergotty Parent Body (SPB): Further evidence for the two component model of planet formation. Lunar and Planetary Institute, 80-81.

Burns, R. G. and Fisher, D. S. (1988) Weathering of sulfides on Mars. Lunar and Planetary Institute. WEVTV Workshop on Nature and Composition of Surface Units on Mars, 34-36.

Burns, R.G. (1993) Rates and mechanisms of chemical weathering of ferromagnesian silicate minerals on Mars. *Geochimica et Cosmochimica Acta* 57, 4555–4574.

Burns, R. G. and Fisher, D. S. (1993) Rates of oxidative weathering on the surface of Mars. *Journal of Geophysical Research* 98, E2, 3365-3372.

Canfield, D.E. and Raiswell, R. (1999) The evolution of the sulfur cycle. *American Journal of Science* 299, 697-723.

Carlson, R. W. and Irving, A. J. (2004) Pb-Hf-Sr-Nd isotopic systematics and age of nakhlite NWA 998. Lunar and Planetary Institute, #1442.

Carr, M. H. (1978) Formation of martian flood features by release of water from confined aquifers. *Journal of Geophysical Research* 84, 2995-3007.

Carr, M. H. and Head, J. W. III (2010) Geologic history of Mars. *Earth and Planetary Science Letters* 294, 185-203.

Carroll, M. R., and Rutherford, M. J. (1985) Sulfide and sulfate saturation in hydrous silicate melts. *Journal of Geophysical Research* 90, C601-C612.

Carroll, M., and Webster, J. D. (1994) Solubilities of sulfur, noble gases, nitrogen, chlorine, and fluorine in magmas. *Reviews in Mineralogy* 30, 231-280.

Cates, N.L. and Mojzsis, S.J. (2006) Chemical and isotopic evidence for widespread Eoarchean metasedimentary enclaves in southern West Greenland. *Geochimica et Cosmochimica Acta* 70, 4229-4257.

Changela, H. G., and Bridges, J. C. (2011) Alteration assemblages in the nakhlites: Variation with depth on Mars. *Meteoritics & Planetary Science* 45, 1847-1867.

Chevrier, V., Lorand, J.-P., and Sautter, V. (2011) Sulfide petrology of four nakhlites: Northwest Africa 817, Northwest Africa 998, Nakhla, and Governador Valadares. *Meteoritics & Planetary Science* 46, 769-784.

Clark, B.C., Baird, A.K., Rose Jr., H.J., Toulmin III, P., Keil, K., Castro, A.J., Kelliher, W.C., Rowe, C.D., and Evans, P.H. (1976) Inorganic analyses of Martian surface samples at the Viking lander sites. *Science* 194, 1283-1288.

Clark, B., and Baird, A.K. (1979) Is the Martian lithosphere sulfur-rich? *Journal of Geophysical Research* 84, 8395–8403.

Classen, N. (2009) An Up-to-Date List of Martian Meteorites. http://www.meteoris.de/mars/list.html.

Clayton, R.N. and Mayeda, T.K. (1983) Oxygen isotopes in eucrites, shergottites, nakhlites, and chassignites. *Earth and Planetary Science Letters* 62, 1-6.

Cline, J. D. (1969) Spectrophotometric determination of hydrogen sulfide in natural waters. *Limnology and Oceanography* 14, 454-458.

Colman, J.J., Xu, Xianping, Thiemens, M.H., and Trogler, W.C. (1996) Photopolymerization and mass-independent sulfur isotope fractionations in carbon disulfide. *Science* 273, 774-776.

Cooper, G.W., Thiemens, M.H., Jackson, T.L., and Chang, S. (1997) Sulfur and hydrogen isotope anomalies in meteorite sulfonic acids. *Science* 277, 1072-1074.

Craddock, R. A. and Howard, A. D. (2002) The case for rainfall on a warm, wet early Mars. *Journal of Geophysical Research* 107, doi:10.1029/2001JE001505.

Crowe, D. E., and Vaughn, R. G. (1996) Characterization and use of isotopically homogeneous standards for in situ laser microprobe analysis of $^{34}S/^{32}S$ ratios. *American Mineralogist* 81, 187-193.

Crozaz, G., Floss, C., and Wadhwa, M. (2003) Chemical alteration and REE mobilization in meteorites from hot and cold deserts. *Geochimica et Cosmochimica Acta* 67, 4727-4741.

Cull, S., Arvidson, R. E., Mellon, M. T., Skemer, P., Shaw, A., and Morris, R. V. (2010) Compositions of subsurface ices at the Mars Phoenix landing site. *Geophysical Research Letters* 37, doi: 10.1029/2010GL045372.

Danielache, S. O., Eskebjerg, C., Johnson, M. S., Ueno, Y., and Yoshida, N. (2008) High-precision spectroscopy of $^{32}S$, $^{33}S$, and $^{34}S$ sulfur dioxide: Ultraviolet absorption cross sections and isotope effects. *Journal of Geophysical Research* 113, doi:10.1029/2007JD009695.

Danielache, S. O. (2012) Personal communication.

Day, J. M. D., Taylor, L. A., Floss, C., and McSween, H. Y., Jr. (2006) Petrology and chemistry of MIL 03346 and its significance in understanding the petrogenesis of nakhlites on Mars. *Meteoritics & Planetary Science* 41, 581-606.

Debaille, V., Yin, Q.-Z., Brandon, A. D., and Jacobsen, B. (2008) Martian mantle mineralogy investigated by the $^{176}Lu$-$^{176}Hf$ and $^{147}Sm$-$^{143}Nd$ systematics of shergottites. *Earth and Planetary Science Letters* 269, 186-199.

Delaney, J.S. (1992) Petrological comparison of LEW88516 and ALHA77005 shergottites. *Meteoritics* 27, 213-214.

Ding, T., Valkiers, S., Kipphardt, H., de Bievre, P., Taylor, P.D.P., Gonfiantini, R., and Krouse, R. (2001) Calibrated sulfur isotope abundance ratios of three IAEA sulfur isotope reference materials and V-CDT with a reassessment of the atomic weight of sulfur. *Geochimica et Cosmochimica Acta* 65, 2433– 2437.

Dold, B. and Spangenberg, J.E. (2005) Sulfur speciation and stable isotope trends of water-soluble sulfates in mine tailings profiles. *Environmental Science & Technology* 39, 5650-5656.

Dreibus, G. and Palme, H. (1996) Cosmochemical constraints on the sulfur content in the Earth's core. *Geochimica et Cosmochimica Acta* 60, 1125-1130.

Dreibus, G., Huisl, W., Spettel, B. and Haubold, R. (2006) Halogens in Nakhlites: Studies of pre-terrestrial and terrestrial weathering processes. *Lunar & Planetary Science Conference* XXXVII, #1180.

Dyakonova M.I. and Kharitonova V.Y. (1960) Chemical analyses of some stoney and iron meteorites from the collection of the Academy of Sciences of the USSR. *Meteoritika* 18, 48-67.

Effenhauser, C.S., Felder, P., and Huber, J.R. (1990) Two-photon dissociation of sulfur dioxide at 248 and 308 nm. *Chemical Physics* 142, 311-320.

Ehlmann, B. L., Mustard, J. F., Murchie, S. L., Bibring, J.-P., Meunier, A., Fraeman, A. A., and Langevin, Y. (2011) Subsurface water and clay mineral formation during the early history of Mars. *Nature* 479, 53-60.

Elkins-Tanton, L. T., Hess, P. C., and Parmentier, E. M. (2005) Possible formation of ancient crust on Mars through magma ocean processes. *Journal of Geophysical Research* 110, doi: 10.1029/2005JE002480.

Encrenaz, T., Greathouse, T. K., Richter, M. J., Lacy, J. H., Fouchet, T., Bézard, B., Lefèvre, F., Forget, F., and Atreya, S. K. (2011) A stringent upper limit to $SO_2$ in the martian atmosphere. *Astronomy and Astrophysics* 530, A37, doi: 10.1051/0004-6361/201116820.

Eugster, O., Busemann, H., Lorenzetti, S., and Terribilini, D. (2002) Ejection ages from [81]Kr-[83]Kr dating and pre-atmospheric sizes of martian meteorites. *Meteoritics & Planetary Science* 37, 1345-1360.

Farquhar, J., Bao, H., and Thiemens, M.H. (2000a) Atmospheric influence of Earth's earliest sulfur cycle. *Science* 289, 756-758.

Farquhar, J., Savarino, J. Jackson, T.L., and Thiemens, M. H. (2000b) A $^{33}$S enrichment in ureilite meteorites: Evidence for a nebular sulfur component. *Geochimica et Cosmochimica Acta* 64, 1819-1825.

Farquhar, J., Savarino, J., Jackson, T. L. and Thiemens, M.H. (2000c) Evidence of atmospheric sulphur in the Martian regolith from sulphur isotopes in meteorites. *Nature* 404, 50-52.

Farquhar, J., Savarino, J., Airieau, S., and Thiemens, M.H. (2001) Observation of wavelength-sensitive mass-independent sulfur isotope effects during $SO_2$ photolysis: Implications for the early atmosphere. *Journal of Geophysical Research* 106 (E12), 32829-32839.

Farquhar, J., Wing, B.A., McKeegan, K.D., Harris, J.W., Cartigny, P., and Thiemens, M.H. (2002) Mass-independent sulfur of inclusions in diamond and sulfur recycling on early Earth. *Science* 298, 2369-2372.

Farquhar, J. and Wing, B.A. (2003) Multiple sulfur isotopes and the evolution of the atmosphere. *Earth and Planetary Science Letters* 213, 1-13.

Farquhar, J., Kim., S.T., and Masterson, A. (2007a) Implications from sulfur isotopes of the Nakhla meteorite for the origin of sulfate on Mars. *Earth and Planetary Science Letters* 264, 1-8.

Farquhar, J., Johnston, D. T., and Wing, B. A. (2007b) Implications of conservation of mass effects on mass-dependent isotope fractionations: Influence of network structure on sulfur isotope phase space of dissimilatory sulfate reduction. *Geochimica et Cosmochimica Acta* 71, 5862-5875.

Farquhar, J., Peters, M., Johnston, D. T., Strauss, H., Masterson, A., Wiechert, U., and Kaufman, A. J. (2007c) Isotopic evidence for Mesoarchean anoxia and changing atmospheric sulfur chemistry. *Nature* 449, 706-710.

Fassett, C. I. and Head, J. W. (2011) Sequence and timing of conditions on early Mars. *Icarus* 211, 1204-1214.

Fegley, B. Jr. (2000) Kinetics of gas-grain reactions in the solar nebula. *Space Science Reviews* 92, 177-200.

Felder, P., Haas, B.M., and Huber, J.R. (1993) Isotope specific photodissociation of $SO_2$ at 193.3 nm. *Chemical Physics Letters* 204, 248-256.

Feldman, W. C., Prettyman, T. H., Maurice, S., Plaut, J. J., Bish, D. L., Vaniman, D. T., Mellon, M. T., Metzger, A. E., Squyres, S. W., Karunatillake, S., Boynton, W. V., Elphic, R. C., Funsten, H. O., Lawrence, D. J., and Tokar, R. L. (2004) Global

distribution of near-surface hydrogen on Mars. *Journal of Geophysical Research* 109:E9, doi: 10.1029/2003JE002160.

Filiberto, J. and Dasgupta, R. (2011) $Fe^{2+}$-Mg partitioning between olivine and basaltic melts: Applications to genesis of olivine-phyric shergottites and conditions of melting in the martian interior. *Earth and Planetary Science Letters* 304, 527-537.

Filiberto, J., Chin, E., Day, J. M. D., Gross, J., Penniston-Dorland, S. C., Schwenzer, S. P., and Treiman, A. H. (2012) Geochemistry of intermediate olivine-phyric shergottite Northwest Africa 6234. Lunar and Planetary Institute, #1139.

Floran R.J., Prinz M., Hlava P.F., Keil K., Nehru C.E. and Hinthorne J.R. (1978) The Chassigny meteorite: A cumulate dunite with hydrous amphibole-bearing melt inclusions.

Forget, F., Haberle, R. M., Montmessin, F., Levrard, B., and Head, J. W. (2006) Formation or glaciers on Mars by atmospheric precipitation at high obliquity. *Science* 311, 368-371.

Forrest, J. and Newman, L. (1977) AG-110 microgram sulfate analysis for short time resolution of ambient levels of sulfur aerosol. *Analytical Chemistry* 49, 1579-1584.

Franchi, I.A., Wright, I.P., Sexton, A.S., and Pillinger, C.T. (1999) The oxygen-isotopic composition of Earth and Mars. *Meteoritics and Planetary Science* 34, 657-661.

Frey, H. (2008) Ages of very large impact basins on Mars: Implications for the late heavy bombardment in the inner solar system. *Geophysical Research Letters* 35, doi:10.1029/2008GL033515.

Gaillard, F. and Scaillet, B. (2009) The sulfur content of volcanic gases on Mars. *Earth and Planetary Science Letters* 279, 34-43.

Gao, X. and Thiemens, M.H. (1987) Multi-isotopic sulfur isotope ratios ($\delta^{33}$S, $\delta^{34}$S, and $\delta^{36}$S) in meteorites. *Meteoritics* 24, 269.

Gao. X. and Thiemens, M. (1990) Sulfur isotopic studies in meteorites. *Lunar & Planetary Science* XXI, #401.

Gao, X. and Thiemens, M.H. (1993) Variations in the isotopic composition of sulfur in enstatite and ordinary chondrites. *Geochimica et Cosmochimica Acta* 57, 3171-3176.

Garrison, D.H. and Bogard, D.D. (2000) Cosmogenic and trapped noble gases in the Los Angeles martian meteorite. *Meteoritics & Planetary Science* 35, A58.

Garrison, D. H. and Bogard, D. D. (2005) Ar-Ar ages of nakhlites Y000593, NWA 998, and Nakhla and CRE age of NWA 998. Lunar and Planetary Institute, #1137.

Gendrin, A., Mangold, N., Bibring, J.P., Langevin, Y., Gondet, B., Poulet, F., Bonello, G., Quantin, C., Mustard, J., Arvidson, R., and LeMouélic, S. (2005) Sulfates in Martian layered terrains: The OMEGA/Mars Express view. *Science* 307, 1587–1591.

Ghatan, G. J., Head, J. W., and Wilson, W. (2005) Mangala Valles, Mars: Assessment of early stages of flooding and downstream flood evolution. *Earth, Moon, Planets* 96, 1-57.

Gibson, E. K., Jr. and Moore, C. B. (1983) Sulfur in achondritic meteorites. Lunar and Planetary Institute, #247.

Gibson, E. K., Moore, C. B., Primus, T. M., and Lewis, C. F. (1985) Sulfur in achondritic meteorites. *Meteoritics* 20, 503-511.

Gilbert, A. and Baggott, J. (1991) *Essentials of Molecular Photochemistry*. Boca Raton: CRC Press, Inc.

Gillman, C., Lognonné, P., Chassefière, E., and Moreira, M. (2009) The present-day atmosphere of Mars: Where does it come from? *Earth and Planetary Science Letters* 277, 384-398.

Gillman, C., Lognonné, P., and Moreira, M. (2011) Volatiles in the atmosphere of Mars: The effects of volcanism and escape constrained by isotopic data. *Earth and Planetary Science Letters* 303, 299-209.

Golombek, M. P., Grant, J. A., Crumpler, L., Greeley, R., Arvidson, R., Bell J. F., III, Weitz, C. M., Sullivan, R., Christensen, P. R., Soderblom, I. A., and Squyres, S. W. (2006) Erosion rates at the Mars Exploration Rover landing sites and long-term climate change on Mars. *Journal of Geophysical Research* 111, doi:10.1029/2006JE002754.

Gooding, J.L. (1978) Chemical weathering on Mars: Thermodynamic stabilities of primary minerals (and their alteration products) from mafic igneous rocks. *Icarus* 33, 483-513.

Gooding, J.L. and Muenow, D.W. (1986) Martian volatiles in Shergottite EETA 79001: new evidence from oxidized sulfur and sulfur-rich aluminosilicates. *Geochimica et Cosmochimica Acta* 50, 1049-1059.

Gooding, J. L., Wentworth, S. J., and Zolensky, M. E. (1991) Aqueous alteration of the Nakhla meteorite. *Meteoritics* 26, 135-143.

Goodrich, C.A., vanNiekerk, D. and Morgan, M.L. (2003) Northwest Africa 1110: A new olivine-phyric shergottite possibly paired with Northwest Africa 1068. *Lunar & Planetary Science* XXXIV, #1266.

Graham, G.A., Kearsley, A.T., Wright, I.P., Grady, M.M., and Pillinger, C.T. (2000) Carbonates in the Los Angeles 001 Meteorite. *Meteoritics & Planetary Science* 35, A63.

Greeley, R., Kuzmin, R. O., and Haberle, R. M. (2001) Aeolian processes and their effects on understanding the chronology of Mars. *Space Science Reviews* 96, 393-404.

Greenwood, J.P., Riciputi, L.R. and McSween, H.Y. (1997a) Sulfur isotopic variations in sulfides from shergottites and ALH 84001 determined by ion microprobe: No evidence for life on Mars. *Lunar & Planetary Science* XXVIII, 459-460.

Greenwood J.P., Riciputi L.R. and McSween H.Y. (1997b) Sulfide isotopic compositions in shergottites and ALH 84001 and possible implications for life on Mars. *Geochimica et Cosmochimica Acta* 61, 4449-4453.

Greenwood, J.P., Riciputi, L.R. and McSween, H.Y. (1998a) Sulfur isotopic ratios in Nakhla and Chassigny sulfides determined by ion microprobe: Implications for the Martian sulfur cycle. *Lunar & Planetary Science* XXIX #1643.

Greenwood, J.P., Riciputi, L.R., Taylor, L.A. and McSween H.Y. (1998b) Hydrothermal modification of sulfides in Nakhla, Lafayette and Chassigny. *Meteoritics & Planetary Science* 33, A62-63.

Greenwood, J.P., Mojzsis, S.J., Coath, C.D. and Wasson, J.T. (1999) Measurements of Sulfur-32,33,34 in Allan Hills 84001 and Nakhla sulfides by multicollecter secondary ion mass spectrometry: Implications for Crustal-Atmospheric exchange and biogenic activity on Mars. *Ninth Annual V. M. Goldschmidt Conference,* #103.

Greenwood, J.P., Riciputi, L.R., McSween, H.Y. and Taylor, L.A. (2000a) Modified sulfur isotopic compositons of sulfides in the nakhlites and Chassigny. *Geochimica et Cosmochimica Acta* 64, 1121-1131.

Greenwood, J.P., Mojzsis, S.J. and Coath, C.D. (2000b) Sulfur isotopic compositions of individual sulfides in Martian meteorites ALH 84001 and Nakhla: implications for crust-regolith exchange on Mars. *Earth & Planetary Science Letters* 184, 23-35.

Greenwood, J.P., Mojzsis, S.J. and Coath, C.D. (2001) Development of the sulfur isotope biomarker for Mars sample return: Results from Los Angeles, Nakhla and ALH 84001. *Lunar & Planetary Science* XXXII, #1734.

Greenwood, J.P., Blake, R.E., and Coath, C.D. (2003) Ion microprobe measurements of $^{18}O/^{16}O$ ratios of phosphate minerals in the martian meteorites ALH 84001 and Los Angeles. *Geochimica et Cosmochimica Acta* 67 (12), 2289-2298.

Greenwood, J. P., and Blake, R. E. (2006) Evidence for an acidic ocean on Mars from phosphorus geochemistry of martian soils and rocks. *Geology* 34, 953-956.

Greenwood, J.P. (2007) Personal communication.

Greshake, A., Fritz, J. and Stöffler, D. (2004) Petrology and shock metamorphism of the olivine-phyric shergottite Yamato 980459: Evidence for a two-stage cooling and single-stage ejection history. *Geochimica et Cosmochimica Acta* 68, 2359-2377.

Gross, J., Filiberto, J., Treiman, A. H., Herd, C. D. K., Melwani Daswani, M., and Schwenzer, S. P. (2012) Petrography, mineral chemistry, and crystallization history of olivine-phyric shergottite NWA 6234: A new intermediate melt composition. Lunar and Planetary Institute, #2693.

Grossman, J. N. (1988) Meteorites – Chondrites and the solar nebula. *Nature* 334, 14-15.

Grotzinger, J.P., Arvidson, R.E., Bell, J.F., Calvin, W., Clark, B.C., Fike, D.A., Golombek, M., Greeley, R., Haldemann, A., Herkenhoff, K.E., Jolliff, B.L., Knoll, A.H., Malin, M., McLennan, S.M., Parker, T., Soderblom, L., Sohl-Dickstein, J.N., Squyres, S.W., Tosca, N.J., Watters, W.A. (2005) Stratigraphy and sedimentology of a dry to wet eolian depositional system, Burns formation, Meridiani Planum, Mars. *Earth and Planetary Science Letters* 240, 11–72.

Haggerty, S. E. (1976) Opaque mineral oxides in terrestrial igneous rocks. *Reviews in Mineralogy* 3, 101-300.

Halevy, I., Zuber, M., and Schrag, D. (2007) A sulfur dioxide climate feedback on early Mars. *Science* 318, 1903-1907.

Halevy, I., Johnston, D. T., and Schrag, D. P. (2010) Explaining the structure of the Archean mass-independent sulfur isotope record. *Science* 329, 204-207.

Hamilton, V.E., Christensen, P.R., McSween, H.Y., Jr., and Bandfield, J.L. (2003) Searching for the source regions of martian meteorites using MGS TES: Integrating martian meteorites into the global distribution of igneous materials on Mars. *Meteoritics & Planetary Science* 38, 871-885.

Hartmann, W.K., Malin, M., McEwen, A., Carr, M., Soderblom, L., Thomas, P., Danielson, E., James, P., Veverka, J. (1999) Evidence for recent volcanism on Mars from crater counts. *Nature* 397, 586–589.

Hartmann, W. K. and Neukum, G. (2001) Cratering chronology and the evolution of Mars. in *Chronology and Evolution of Mars*, Kallenbach et al., eds., 165-194.

Hartmann, W. K. (2003) *A Traveler's Guide to Mars*. New York: Workman Publishing.

Harvey, R.P. and McSween, Jr., H.Y. (1992a) Petrogenesis of the nakhlite meteorites: Evidence from cumulate mineral zoning. *Geochimica et Cosmochimica Acta* 56, 1655-1663.

Harvey, R. P., and McSween, H. Y., Jr. (1992b) The parent magma of the nakhlite meteorites: Clues from melt inclusions. *Earth and Planetary Science Letters* 111, 467-482.

Harvey, R.P., McCoy, T.J. and Leshin, L.A. (1996) Shergottite QUE94201: Texture, mineral compositions, and comparison with other basaltic shergottites. *Lunar & Planetary Science* XXVII, 497-498.

Haughton, D. R., Roeder, P. L., and Skinner, B. J. (1974) Solubility of sulfur in mafic magmas. *Economic Geology* 69, 451-467.

He, Q., Hsu, W., Xiao, L., and Guan, Y. (2011) Petrography and geochemistry of the shergottite Northwest Africa 2975. Lunar and Planetary Institute, #1646.

Herd, C. D. K., Papike, J. J., and Brearley, A. J. (2001) Oxygen fugacity of martian basalts from electron microprobe oxygen and TEM-EELS analyses of Fe-Ti oxides. *American Mineralogist* 86, 1015-1024.

Herd, C. D. K., Borg, L. E., Jones, J. H., Papike, J. J. (2002) Oxygen fugacity and geochemical variations in the martian basalts: Implications for martian basalt petrogenesis and the oxidation state of the upper mantle of Mars. Geochimica et Cosmochimica Acta 66, 2025-2036.

Herd, C. D. K. (2003) The oxygen fugacity of olivine-phyric martian basalts and the components within the mantle and crust of Mars. *Meteoritics & Planetary Science* 38, 1793-1805.

Herd, C. D. K. (2004) Oxygen in martian meteorites: A review of results from mineral equilibria oxybarometers. *Lunar and Planetary Institute,* Oxygen in the Terrestrial Planets, #3026.

Herd, C.D.K. (2006) An occurrence of jarosite in MIL 03346: Implications for conditions of Martian aqueous alteration. *Meteoritics & Planetary Science* 41, A74.

Hobbs, S. W., Pauli, D. J., and Bourke, M. C. (2010) Aeolian processes and dune morphology in Gale Crater. *Icarus* 210, 102-115.

Horneck, G. (2000) The microbial world and the case for Mars. Planetary and Space Science 48, 1053-1063.

Hu, G., Rumble, D., and Wang, P. (2003) An ultraviolet laser microprobe for the in situ analysis of multisulfur isotopes and its use in measuring Archean sulfur isotope mass-independent anomalies. *Geochimica et Cosmochimica Act*a 67 (17), 3101-3117.

Hulston, J. R. and Thode, H. G. (1965) Variations in the $S^{33}$, $S^{34}$, and $S^{36}$ contents of meteorites and their relation to chemical and nuclear effects. *Journal of Geophysical Research* 70, 3475-3484.

Hurowitz, J.A., McLennan, S.M., Tosca, N.J., Arvidson, R.E., Michalski, J.R., Ming, D.W., Schröder, C., and Squyres, S.W. (2006) In situ and experimental evidence for acidic weathering of rocks and soils on Mars. *Journal of Geophysical Research* 111, E02S19.

Hutchison, R. (2004) *Meteorites: A Petrologic, Chemical, and Isotopic Synthesis.* New York: Cambridge University Press.

Iishi, K., Torigoe, K., and Han, X. (1997) Oriented precipitate complexes in iron-rich olivines produced experimentally in aqueous oxidizing environment, *Physics and Chemistry of Minerals* 25, 8 – 14.

Ikeda, Y. (1997) Petrology of the Yamato 793605 lherzolitic shergottite. *Meteoritics & Planetary Science* 32, A64.

Imae, N. and Ikeda, Y. (2005) Comparative petrology of Yamato and MIL 03346 Nakhlites. *Meteoritics & Planetary Science* 40, A72.

Imae, N., and Ikeda, Y. (2007) Petrology of the Miller Range 03346 nakhlite in comparison with the Yamato-000593 nakhlite. *Meteoritics & Planetary Science* 42, 171-184.

Irving, A. J., Kuehner, S. M., Rumble, D. III, Carlson, R. W., Hupé, A. C., and Hupé, G. M. (2002) Petrology and isotopic composition of orthopyroxene-bearing nakhlite NWA 998. *Meteoritics & Planetary Science* 37, A70.

Irving, A.J., Kuehner, S.M., Hupé, A.C. and Hupé, G.M. (2002a) Olivine-phyric basaltic shergottite NWA1195: a very primitive Martian lava. *Meteoritics & Planetary Science* 37, A69.

Irving, A. J., Kuehner, S. M., Rumble, D. III, Carlson, R. W., Hupé, A. C., and Hupé, G. M. (2002b) Petrology and isotopic composition of orthopyroxene-bearing nakhlite NWA 998. *Meteoritics & Planetary Science* 37, A70.

Irving, A. J., Herd, C. D. K., Kuehner, S. M., Gregory, D. A., and Aaronson, A. A. (2004) Petrology and redox state of basaltic shergottite NWA 3171. *Meteoritics & Planetary Science* 39, A49.

Irving, A.J., and Kuehner, S. M. (2008) Northwest Africa 5298: A strongly shocked basaltic shergottite equilibrated at QFM and high temperature. *Meteoritics & Planetary Science* 43, A63.

Irving, A.J. (2012a) Martian Meteorites. [http://www.imca.cc/mars/martian-meteorites.htm](http://www.imca.cc/mars/martian-meteorites.htm).

Irving, A. J., Kuehner, S. M., Tanaka, R., Herd, C. D. K., Chen, G., and Lapen, T. L. (2012b) The Tissint depleted permafic olivine-phyric shergottite: Petrologic, elemental and isotopic characterization of a recent martian fall in Morocco. *Lunar and Planetary Institute,* #2510.

Irving, A. J., Kuehner, S. M., Herd. C. D. K., Gellison, M., Korotev, R. L., Puchtel, I., Walker, R. J., Lapen, T. J., and Rumble, D., III. (2010) Petrologic, elemental, and multi-isotopic characterization of permafic olivine-phyric shergottite Northwest Africa 5789: A primitive magma derived from depleted martian mantle. Lunar and Planetary Institute, #1547.

Irving, A. J., Herd, C. D. K., Gellissen, M., Kuehner, S. M., and Bunch, T. E. (2011) Paired fine-grained, permafic olivine-phyric shergottites Northwest Africa 2990/5960/6234/6710: Trace element evidence for a new type of martian mantle source of complex lithospheric assimilation process. *Meteoritics & Planetary Science* 46, A108.

Jakosky, B. M., and Carr, M. H. (1985) Possible precipitation of ice at low latitudes of Mars during periods of high obliquity. *Nature* 315, 559-561.

Jambon, A., Barrat, J.-A., Bollinger, C., Sautter, V., Boudouma, O., Greenwood, R. C., Franchi, I. A., and Badia, D. (2010) Northwest Africa 5790. Top Sequence of the nakhlite pile. Lunar and Planetary Institute, #1696.

Jensen, M.L. (1962) Sulfur isotopes. *Science* 137, 470-472.

Johnson, J.R., Bell III, J.F., Cloutis, E., Staid, M., Farrand, W.H., McCoy, T., Rice, M., Wang, A., and Yen, A. (2007) Mineralogic constraints on sulfur-rich soils from Pancam spectra at Gisev crater, Mars. *Geophysical Research Letters* 34, L13202.

Johnson, S. S., Mischna, M. A, Zuber, M. T., and Grove, T. L. (2008) Sulfur-induced greenhouse warming in early Mars. *Journal of Geophysical Research* 113, doi:10.1029/2007JE002962.

Johnson, S. S., Pavlov, A. A., and Mischna, M. A. (2009) Fate of $SO_2$ in the ancient martian atmosphere: Implications for transient greenhouse warming. *Journal of Geophysical Research* 114, doi:10.1029/2008JE003313.

Johnston, D.T., Puolton, S.W., Fralick, P.W., Wing, B.A., Canfield, D.E., and Farquhar, J. (2006) Evolution of the oceanic sulfur cycle at the end of the Paleoproterozoic. *Geochimica et Cosmochimica Acta* 70, 5723-5739.

Jones, J. H. (1989) Isotopic relationships among the shergottites, the nakhlites and Chassigny. Proceedings of the 19th LPSC, Lunar and Planetary Institute, 465-474.

Jugo, P. J., Luth, R. W., and Richards, J. P. (2005) Experimental data on the speciation of sulfur as a function of oxygen fugacity in basaltic melts. *Geochimica et Cosmochimica Acta* 69, 497-503.

Jugo, P. J. (2009) Sulfur content at sulfide saturation in oxidized magmas. *Geology* 37, 415-418.

Kallenbach, R., Geiss, J., and Hartmann, W. K. ed. (2001) *Chronology and Evolution of Mars*. Dordrecht: Kluwer Academic Publishers.

Karlsson, K.R., Clayton, R.N., Gibson, E.K., and Mayeda, T.K. (1992) Water in SNC meteorites — evidence for a Martian hydrosphere. *Science* 255, 1409–1411.

Kasting, J. F., Zahnle, K. J., Pinto, J. P., and Young, A. T. (1989) Sulfur, ultraviolet radiation, and the early evolution of life. *Origins of Life and Evolution of the Biosphere* 19, 95-108.

Kaufman, A.J., Johnston, D.T., Farquhar, J., Masterson, A.L., Lyons, T.W., Bates, S., Anbar, A.D., Arnold, G.L., Garvin, J., and Buick, R. (2007) Late Archean Biospheric Oxygenation and Atmospheric Evolution. *Science* 317, 1900-1903.

Kawasaki, M. and Sato, H. (1987) Photodissociation of molecular beams of $SO_2$ at 193 nm. *Chemical Physics Letters* 139, 585-588.

Kim, S.-T., and Farquhar, J. (2008) Multiple sulfur isotope compositions in Martian meteorite MIL 03346. Lunar Planetary Institute, #2151.

Klingelhöfer, G., Morris, R.V., Bernhardt, B., Schröder, S., Rodionov, D.S., de Souza Jr., P.A., Yen, A., Gellert, R., Evlanov, E.N., Zubkov, B., Foh, J., Bonnes, U., Kankeleit, E., Gütlich, P., Ming, D.W., Renz, F., Wdowiak, T., Squyres, S.W., and Arvidson, R.E. (2004) Jarosite and hematite at Meridiani Planum from Opportunity's Mössbauer spectrometer. *Science* 306, 1740–1745.

Knappenberger, K.L. and Castleman, A.W. (2004) Photodissociation of sulfur dioxide: the E# state revisited. *Journal of Physical Chemistry A* 108, 9-14.

Knauth, L.P., Burt, D.M., and Wohletz, K.H. (2005) Impact origin of sediments at the opportunity landing site on Mars. *Nature* 438, 1123–1128.

Krasnopolsky, V. A. (2005) A sensitive search for $SO_2$ in the martian atmosphere: Implications for seepage and origin of methane. *Icarus* 178, 487-492.

Krasnopolsky, V. A. (2012) Search for methane and upper limits to ethane and $SO_2$ on Mars. *Icarus* 217, 144-152.

Lane, M. D., Dyar, M. D., and Bishop, J. L. (2004) Spectroscopic evidence for hydrous iron sulfates in the Martian soil. *Geophysical Research Letters* 31, #119702.

Langevin, Y., Poulet, F., Bibring, J.P., and Gondet, B. (2005) Sulfates in the North Polar region of Mars detected by OMEGA/Mars Express. *Science* 307, 1584–1586.

Lapen, T. J., Righter, M., Brandon, A. D., Debaille, V., Beard, B. L., Shafer, J. T., and Peslier, A. H. (2010) A younger age for ALH 84001 and its geochemical link to shergottite sources in Mars. *Science* 328, 347-351.

Laskar, J., Correia, A. C. M., Gastineau, M., Joutel, F., Levrard, B., and Robutel, P. (2004) Long term evolution and chaotic diffusion of the insolation quantities on Mars. *Icarus* 170, 343-364.

Le Deit, L., Flahaut, J., Quantin, C., Hauber, E., Mège, D., Bourgeois, O., Gurgurewicz, J., Massé, M., and Jaumann, R. (2012) Extensive surface pedogenic alteration of the martian Noachian crust suggested by plateau phyllosilicates around Valles Marineris. *Journal of Geophysical Research* 117, doi:10.1029/2011JE003983.

Lee, D.-C. and Halliday, A. N. (1997) Core formation on Mars and differentiated asteroids. *Nature* 388, 854-857.

Lee, C. C-W., Savarino, J., and Thiemens, M. H. (2001) Mass-independent oxygen isotopic composition of atmospheric sulfate: Origin and implications for the present and past atmosphere of Earth and Mars. *Geophysical Research Letters* 28, 1783-1786.

Lentz, R. C. F., McCoy, T. J., and Taylor, G. J. (2005) Multiple nakhlite lava flows? *Meteoritics & Planetary Science* 40, A91.

Levine, J. S. and Summers, M. E. (2003) Non-equilibrium thermodynamic chemistry and the composition of the atmosphere of Mars. Lunar and Planetary Institute, Sixth International Conference on Mars, #3055.

Levy, J., Head, J., and Marchant, D. (2009) Thermal contraction crack polygons on Mars: Classification, distribution, and climate implications from HiRISE observations. *Journal of Geophysical Research* 114:, doi: 10.1029/2008JE003273.

Lichtenberg, K. A., Arvidson, R. E., Morris, R. V., Murchie, S. L., Bishop. J. L., Fernandez Remolar, D., Glotch, T. D., Noe Dobrea, E., Mustard, J. F., Andrews-Hanna. J., and Roach, L. H. (2010) Stratigraphy of hydrated sulfates in the sedimentary deposits of Aram Chaos, Mars. *Journal of Geophysical Research* 115, doi:10.1029/2009JE003353.

Lodders, K. and Fegley, B. Jr. (1997) An oxygen isotope model for the composition of Mars. *Icarus* 126, 373-394.

Longhi, J. (1991) Complex magmatic processes on Mars: Inferences from the SNC meteorites. Proceedings of Lunar and Planetary Science, 21, 695-709.

Lorand, J.-P., Chevrier, V., and Sautter, V. (2005) Sulfide mineralogy and redox conditions in some shergottites. *Meteoritics & Planetary Science* 40, 1257-1272.

Lottermoser, B. G. (1992) Rare earth elements and hydrothermal ore formation processes. *Ore Geology Reviews* 7, 25-41.

Lyons, J. R. (2007) Mass-independent fractionation of sulfur isotopes by isotope-selective photodissociation of $SO_2$. *Geophysical Research Letters* 28, 3231-3234.

Lyons, J. R. (2009) Atmospherically-derived mass-independent sulfur isotope signatures, and incorporation into sediments. *Chemical Geology* 267, 164-174.

Macnamara, J. and Thode, H.G. (1950) Comparison of the isotopic constitution of terrestrial and meteoritic sulfur. *Physical Review* 78, 307-308.

Malin, M. C. and Edgett, K. S. (2000) Sedimentary rocks of early Mars. *Science* 290, 1927-1937.

Marini, L., Moretti, R., and Accornero, M. (2011) Sulfur isotopes in magmatic-hydrothermal systems, melts, and magmas. *Reviews in Mineralogy & Geochemistry* 73, 423-492.

Masterson, A. M., Farquhar, J., and Wing, B. A. (2011) Sulfur mass-independent fractionation patterns in the broadband UV photolysis of sulfur dioxide: Pressure and third body effects. *Earth and Planetary Science Letters* 306, 253-260.

Mayer, B. and Krouse, H.R. (2004) Procedures for sulfur isotope abundance studies. In: de Groot, P. (Ed.), *Handbook of Stable Isotope Analytical Techniques, Vol. 1*, 538-596.

Mayne, R.G., Fayek, M., and McSween, H.Y. (2003) Sulfur isotopic compositions in pyrrhotite grains from the Los Angeles meteorite. AGU Fall meeting, #P12B-1065.

McCanta, M. C., Elkins-Tanton, L., and Rutherford, M. J. (2009) Expanding the application of the Eu-oxybarometer to the lherzolitic shergottites and nakhlites: Implications for the oxidation state heterogeneity of the martian interior. *Meteoritics & Planetary Science* 44, 725-745.

McCubbin, F. M., Tosca, N. J., Smirnov, A., Nekvasil, H., Steele, A., Fries M., and Lindsley, D. H. (2009) Hydrothermal jarosite and hematite in a pyroxene-hosted melt inclusion in martian meteorite Miller Range (MI) 03346: Implications for magmatic-hydrothermal fluids on Mars. *Geochimica et Cosmochimica Acta* 73, 4907-4917.

McDonough, W. F. and Sun, S. S. (1995) The composition of the Earth. *Chemical Geology* 120, 223-253.

McGill, G.E. and Squyres, S. W. (1991) Origin of the martian crustal dichotomy: Evaluating hypotheses. *Icarus* 93, 386-393.

McKay, D.S., Gibson, Jr., E.K., Thomas-Keprta, K.L., Vali, H., Romanek, C.S., Maechling, C.R., and Zare, R.N. (1996) Search for past life on Mars: Possible relic biogenic activity in Martian meteorite ALH 84001. *Science* 273, 924-930.

McKenzie, D. (1985) Extraction of magma from the crust and mantle. *Earth and Planetary Science Letters* 74, 81-91.

McSween, H. Y., Jr. (1994) What we have learned about Mars from SNC meteorites. *Meteoritics* 29, 757-779.

McSween, H. Y., Jr., Eisenhour, D. D., Taylor, L. A., Wadhwa, M., and Crozaz, G. (1996) QUE94201 shergottite: Crystallization of a martian basaltic magma. *Geochimica et Cosmochimica Acta* 60, 4563-4569.

McSween, H. Y., Jr. (1999) *Meteorites and Their Parent Planets*, 2nd edition. New York: Cambridge University Press.

McSween, H. Y. , Jr., Grove, T. L., Lentz, R. C. F., Dann, J. C., Holzheid, A. H., Riciputi, L. R., and Ryan, J. G. (2001) Geochemical evidence for magmatic water within Mars from pyroxenes in the Shergotty meteorite. *Nature* 409, 487-490.

Mellon, M. T., and Jakosky, B. M. (1995) The distribution and behavior of martian ground ice during past and present epochs. *Journal of Geophysical Research* 100, 11781-11799.

Meyer, C. (2006) Mars Meteorite Compendium. *JSC #27672 Revision C*.

Mikouchi, T. (2000) Pyroxene and Plagioclase in the Los Angeles Martian meteorite: Comparison with the Queen Alexandra Range 94201 Martian meteorite and the Asuka 881757 Lunar meteorite. *Meteoritics & Planetary Science* 35, A110.

Mikouchi, T. and Miyamoto, M. (2001) Northwest Africa 817: A new nakhlite similar to others but distinct. *Meteoritics & Planetary Science* 36, A134.

Mikouchi, T. and Miyamoto, M. (2002) Comparative cooling rates of nakhlites as inferred from iron-magnesium and calcium zoning of olivines. Lunar and Planetary Institute #1343.

Mikouchi, T., Koizumi, E., Monkawa, A., Ueda, Y., and Miyamoto, M. (2003) Mineralogy and petrology of Yamato 000593: Comparison with other Martian nakhlite meteorites. *Antarctic Meteorite Research* 16, 34-57.

Mikouchi, T., Koizumi, E., McKay, G., Monkawa, A., Ueda, Y., Chokai, J., and Miyamoto, M. (2004) Yamato 980459: Mineralogy and petrology of a new shergottite-related rock from Antarctica. *Antarctic Meteorite Research* 17, 13-34.

Mikouchi, T., Miyamoto, M., Koizumi, E., Makishima, J., and McKay, G. (2006) Relative burial depths of nakhlites: An update. Lunar and Planetary Institute, #1865.

Mikouchi, T., Makishima, J., Kurihara, T., Hoffman, V. H., and Miyamoto, M. (2012) Relative burial depth of nakhlites revisited. Lunar and Planetary Institute, #2363.

Milliken, R. E., Grotzinger, J. P., and Thomson, B. J. (2010) Paleoclimate of Mars as captured by the stratigraphic record in Gale Crater. *Geophysical Research Letters* 37, doi:10.1029/2009GL041870.

Misawa, K., Shih, C.-Y., Wiesmann, H., and Nyquist, L. E. (2003) Crystallization and alteration ages of the Antarctic nakhlite Yamato 000593. Lunar and Planetary Institute, #1556.

Misener, D. J. (1974) Cationic diffusion in olivine to 1400 ℃ and 35 kb. In *Geochemical Transport and Kinetics* (eds. A. Hoffman, B. Giletti, H. Yoder and R. Yund). Carnegie Institute of Washington, p. 117-129.

Mojzsis, S.J., Coath, C.D., Greenwood, J.P., McKeegan, K.D., and Harrison, T.M. (2003) Mass-independent isotope effects in Archean (2.5 to 3.8 Ga) sedimentary sulfides determined by ion microprobe analysis. *Geochimica et Cosmochimica Acta* 67 (9), 1635-1658.

Muhkin, L. M., Koscheev, A. O., Dikov, Y. P., Huth, J., and Wänke, H. (1996) Experimental simulations of the photodecomposition of carbonates and sulphates on Mars. *Nature* 379, 141-143.

Mullin, A. S. (2006) Unpublished notes.

Murchie, S. L., Mustard, J. F., Ehlmann, B. L., Milliken, R. E., Bishop, J. L., McKeown, N. K., Noe Dobrea, E. Z., Seelos, F. P., Buczkowski, D. L., Wiseman, S. M., Arvidson, R. E., Wray, J. J. Swayze, G., Clark, R. N., DesMarais, D. J., McEwen, A. S., and Bibring, J.-P. (2009) A synthesis of martian aqueous mineralogy after 1 Mars year of observations from the Mars Reconnaissance Orbiter. *Journal of Geophysical Research* 114, doi:10.1029/2009JE00342.

Murchie, S., Roach, L., Seelos, F., Milliken, R., Mustard, J., Arvidson, R., Wiseman, S., Lichtenberg, K., Andrews-Hanna, J., Bishop, J., Bibring, J-P., Parente, M., and Morris, R. (2009) Evidence for the origin of layered deposits in Candor Chasma, Mars, from mineral composition and hydrologic modeling. *Journal of Geophysical Research* 114, doi:10.1029/2009JE003343.

Nakagawa, H., Kasaba, Y., Maezawa, H., Hashimoto, A., Sagawa, H., Murata, I., Okano, S., Aoki, S., Moribe, N., Mizuno, A., Momose, M., Ohnishi, T., Mizuno, N., and Nagahama, T. (2009) Search for $SO_2$ in the martian atmosphere by ground-based submillimeter observation. *Planetary and Space Science* 57, 2123-2127.

Nakamura, N., Unruh, D. M., Tatsimoto, M., and Hutchison, R. (1982) Origin and evolution of the Nakhla meteorite inferred from the Sm-Nd and U-Pb systematics and REE, Ba, Sr, Rb abundances. *Geochimica et Cosmochimica Acta* 46, 1555-1573.

Navrotsky, A., Forray, F. L., and Drouet, C. (2005) Jarosite stability on Mars. *Icarus* 176, 250-253.

Nelson, G.E. and Borkman, R.F. (1975) Effect of oxygen-18 substitution upon electronic relaxation in the $^3B_1$ state of $SO_2$. *Journal of Chemical Physics* 63, 208-211.

Neukum, G., Basilevsky, A. T., Kneissl, T., Chapman, M. G., van Gasselt, S., Michael, G., Jaumann, R., Hoffman, H., and Lanz, J. K. (2010) The geologic evolution of Mars: Episodicity of resurfacing events and ages from cratering analysis of image data and correlation with radiometric ages of martian meteorites. *Earth and Planetary Science Letters* 294, 204-222.

Nimmo, F., Hart, S. D., Korycansky, D. G., and Agnor, C. B.(2008) Implications of an impact origin for the martian hemispheric dichotomy. *Nature* 453, 1220-1223.

Nishiizumi, K., Caffee, M.W., and Masarik, J. (2000) Cosmogenic Radionuclides in the Los Angeles martian meteorite. *Meteoritics & Planetary Science* 35, A120.

Noguchi, T., Nakamura, T., Misawa, K., Imae, N., Aoki, T., and Toh, S. (2009) Laihunite and jarosite in the Yamato 00 nakhlites: Alteration products on Mars? *Journal of Geophysical Research* 114, doi:10.1029/2009JE00364.

Nyquist, L.E. (1995) "Martians" young and old: Zagami and ALH84001. *Lunar & Planetary Science* XXVI, 1065-1066.

Ohmoto, H. and Lasaga, A.C. (1982) Kinetics of reactions between aqueous sulfates and sulfides in hydrothermal systems. Geochimica *et Cosmochimica Acta* 46, 1727-1745.

Ohmoto, H. and Goldhaber, M.B. (1997) Sulfur and carbon isotopes. In *Geochemistry of Hydrothermal Ore Deposits*. New York: John Wiley, pp. 517-611.

Okabe, H. (1978) *Photochemistry of Small Molecules*, John Wiley, New York.

Ono, S., Beukes, N.J., Rumble, D., and Fogel, M.L. (2006a) Early evolution of atmospheric oxygen from multiple-sulfur and carbon isotope records of the 2.9 Ga Mozaan Group of the Pongola Supergroup, Southern Africa. *Journal of Geology* 109, 97-108.

Ono, S., Wing, B., Rumble, J., and Farquhar, J. (2006b) High precision analysis of all four stable isotopes of sulfur ($^{32}$S, $^{33}$S, $^{34}$S, and $^{36}$S) at nanomole levels using a laser fluorination isotope-ratio-monitoring gas-chromatography-mass spectrometry. *Chemical Geology* 225, 30-39.

Ono, S., Wing, B., Johnston, D., Farquhar, J., and Rumble, D. (2006c) Mass-dependent fractionation of quadruple stable sulfur isotope system as a new tracer of sulfur biogeochemical cycles. *Geochimica et Cosmochimica Acta* 70, 2238-2252.

Ono, S. (2007) Personal communication.

Oppenheimer, C., Scaillet, B. and Martin, R. S. (2011) Sulfur degassing from volcanoes: Source conditions, surveillance, plume chemistry and Earth systems impact. *Reviews in Mineralogy* 73, 363-421.

Palme, H., and Jones, A. (2003) Solar system abundances of the elements. *Treatise on Geochemistry* 1, 41-61.

Papanastassiou, D. A., and Wasserburg, G. J. (1974) Evidence for late formation and young metamorphism in the achondrite Nakhla. *Geophysical Research Letters* 1, 23-26.

Papike, J. J., Karner, J. M., Shearer, C. K., and Burger, P. V. (2009) Silicate mineralogy of martian meteorites. *Geochimica et Cosmochimica Acta* 73, 7743-7485.

Paytan, A., Kastner, M., Campbell, D., and Thiemens, M. H. (1998) Sulfur Isotopic Composition of Cenozoic Seawater Sulfate. *Science* 282, 1459-1462.

Penniston-Dorland, S. C., Wing, Boswell A., Nex, P. A. M., Kinnaird, J. A., Farquhar, J., Brown, M., and Sharman, E. R. (2008) Multiple sulfur isotopes reveal a magmatic origin for the Platreef platinum group element deposit, Bushveld Complex, South Africa. *Geology* 36, 979-982.

Pepin, R. O. (2006) Atmospheres on the terrestrial planets: Clues to origin and evolution. *Earth and Planetary Science Letters* 252, 1-14.

Peters, M., Strauss, H., Farquhar, J., Ockert, C., Eickmann, B., and Jost, C. L. (2010) Sulfur cycling at the Mid-Atlantic Ridge: A multiple sulfur isotope approach. *Chemical Geology* 269, 180-196.

Philippot, P., Van Zuilen, M., Lepot, K., Thomazo, T., Farquhar, J., and Van Kranendonk, M.J. (2007) Early Archean microorganisms preferred elemental sulfur, not sulfate. Science 317, 1534-1537.

Phillips, R. J., Zuber, M. T., Solomon, S. C., Golombek, M. P., Jakosky, B. M., Banerdt, W. B. Smith, D. E., Williams, R. M., Hynek, B. M., Aharonson, O., and Hauck, S. A. (2001) Ancient geodynamics and global-scale hydrology on Mars. *Science* 291, 2587-2591.

Plescia, J. B. (1993) An assessment of volatile release from recent volcanism in Elysium, Mars. *Icarus* 104, 20-32.

Postawko, S. E. and Kuhn, W. R. (1986) Effect of the greenhouse gases ($CO_2$, $H_2O$, $SO_2$) on martian paleoclimate. *Journal of Geophysical Research – Solid Earth and Planets* 91, B4, D431-D438.

Prinz, M., Hlava, P. H. and Keil, K. (1974) The Chassigny meteorite: A relatively iron-rich cumulate dunite. *Meteoritics* 9, 393-394.

Rai, V.K., Jackson, T.L., and Thiemens, M.H. (2005) Photochemical mass-independent sulfur isotopes in achondritic meteorites. *Science* 309, 1062-1065.

Rai, V.K. and Thiemens, M.H. (2007) Mass independently fractionated sulfur components in chondrites. *Geochimica et Cosmochimica Acta* 71, 1341-1354.

Ramdohr, P. (1972) The highly reflecting and opaque components in the mineral content of the Haveroe meteorite. *Meteoritics* 7, 565-571.

Rapp, J. F., Draper, D. S., and Mercer, C. (2012) Crystallization of Yamato 980459 at 0.5 GPa: Are residual liquids like QUE 94201? Lunar and Planetary Institute, #2108.

Rieder, R., Economou, T., Wänke, H., Turkevich, A., Crisp, J., Brückner, J. Dreibus, G., and McSween Jr., H.Y. (1997) The chemical composition of Martian soils and

rocks returned by the mobile alpha proton X-ray spectrometer: preliminary results from the X-ray mode. *Science* 278, 1771-1774.

Rieder, R., Gellert, R., Anderson, R.C., Brückner, J., Clark, B.C., Dreibus, G., Economou, T., Klingelhöfer, G., Lugmair, G.W., Ming, D.W., Squyres, S.W., d'Uston, C., Wänke, H., Yen, A., and Zipfel, J. (2004) Chemistry of rocks and soils at Meridiani Planum from the alpha particle X-ray spectrometer. *Science* 306, 1746-1749.

Righter, K., Pando, K., and Danielson, L. R. (2009) Experimental evidence for sulfur-rich martian magmas: Implications for volcanism and surficial sulfur sources. *Earth and Planetary Science Letters* 288, 235-243.

Robinson, B.W. (1993) Sulfur isotope standards. Reference and inter-comparison materials for stable isotopes of light elements. Proceedings of a consultants meeting held in Vienna, December 1993, pp. 39-45.

Rochette, P., Gattacceca, J., Chevrier, V., Hoffman, V., Lorand, J. P., Funaki, M., and Hochleitner, R. (2005) Matching Martian crustal magnetization and magnetic properties of Martian meteorites. *Meteoritics & Planetary Science* 40, 529-540.

Romanek, C.S., Grady, M.M., Wright, I.P., Mittlefehldt, D.W., Socki, R.A., Pillinger, C.T., and Gibson, Jr., E.K. (1994) Record of fluid-rock interactions on Mars from the meteorite ALH 84001. *Nature* 372, 655-657.

Romero, A.B. and Thiemens, M.H. (2003) Mass-independent sulfur isotopic compositions in present-day sulfate aerosols. *Journal of Geophysical Research* 108, 8-17.

Rubin, A.E., Warren, P.H., Greenwood, J.P., Verish, R.S., Leshin, L.A., Hervig, R.L., Clayton, R.N., and Mayeda, T.K. (2000) Los Angeles: The most differentiated basaltic martian meteorite. *Geology* 28, 1011.

Rumble, D., III, and Hoering, T.C. (1994) Analysis of oxygen and sulfur isotope ratios in oxide and sulfide minerals by spot heating with a carbon dioxide laser in a fluorine atmosphere. *Accounts of Chemical Research* 27, 237-241.

Rumble, D., III, and Irving, A.J. (2009) Dispersion of oxygen isotopic compositions among 42 Martian meteorites determined by laser fluorination: Evidence for assimilation of (ancient) altered crust. Lunar & Planetary Institute, #2293.

Russell, S. S., Zolensky, M., Righter, K., Folco, L., Jones, R., Connolly, H. C., Jr., Grady, M. M., and Grossman, J. N. (2005) The Meteoritical Bulletin, No. 89, 2005 September. *Meteoritics & Planetary Science* 40, Supplement, A201-A263.

Russell, P. S. and Head, J. W. (2007) The martian hydrologic system: Multiple recharge centers at large volcanic provinces and the contribution of snowmelt to outflow channel activity. *Planetary and Space Science* 55, 315-332.

Sakai, H. (1957) Fractionation of sulphur isotopes in nature. *Geochimica et Cosmochimica Acta* 12, 150-169.

Sakai, H. (1957) Fractionation of sulphur isotopes in nature. *Geochimica et Cosmochimica Acta* 12, 150-169.

Sakai, H., Casadevall, T.J., and Moore, J.G. (1982) Chemistry and isotope ratios of sulfur in basalts and volcanic gases at Kilauea Volcano, Hawaii. *Geochimica et Cosmochimica Acta* 46, 729-738.

Sanloup, C., Jambon, A., and Gillet, P. (1999) A simple chondritic model of Mars. *Physics of the Earth and Planetary Interiors* 112, 43-54.

Sarbadhikari, A. B., Day, J. M. D., Liu, Y., Rumble, D. III, and Taylor, L. A. (2009) Petrogenesis of olivine-phyric shergottite Larkman Nunatak 06319: Implications for enriched components in martian basalts. *Geochimica et Cosmochimica Acta* 73, 2190-2214.

Satake, W., Mikouchi, M., Makishima, J., and Miyamoto, M. (2009) Comparison of redox states between geochemically-intermediate and enriched lherzolitic shergottites. Lunar and Planetary Institute, #1717.

Sato, T., Kinugawa, T., and Arikawa, T. (1992) Two-photon dissociation of $SO_2$ in the ultraviolet region. *Chemical Physics* 165, 173-182.

Scott, D. H. and Carr, M. H. (1978) Geologic map of Mars. U.S. Geological Survey, Misc. Invest. Ser. Map I-1083.

Scott, D. H., and Tanaka, K. L. (1986) Geologic map of the western equatorial region of Mars. U.S. Geological Survey, Misc. Invest. Ser. Map I-1802-A.

Settle, M. (1979) Formation and deposition of volcanic sulfate aerosols on Mars. *Journal of Geophysical Research* 84, 8343-8354.

Shearer, C.K., Layne, G.D., Papike, J.J. and Spilde, M.N. (1996) Sulfur isotopic systematics in alteration assemblages in Martian meteorite ALH 84001. *Geochimica et Cosmochimica Acta* 60, 2921-2926.

Shih, C.-Y., Wiesmann, H., Nyquist, L. E., and Misawa, K. (2002) Crystallization age of Antarctic nakhlite Y000593: Further evidence of nakhlite launch pairing. Antarctic Meteorites XXVII, National Institute of Polar Research, Tokyo, 151-153.

Shih, C.Y., Nyquist, L.E., Wiesmann, H., and Misawa, H. (2004) Rb-Sr and SM-Nd isotopic studies of shergottite Y980459 and a petrogenetic link between depleted shergottites and nakhlites. *Lunar & Planetary Science* XXXV, #1814.

Shih, C.-Y., Nyquist, L. E., Reese, Y., and Jambon, A. (2010) Sm-Nd isotopic studies of two nakhlites, NWA 5790 and Nakhla. Lunar and Planetary Institute, #1367.

Shirai, N. and Ebihara, M. (2008) Chemical characteristics of nakhlites: Implications to the geological setting for nakhlites. Lunar and Planetary Institute, #1643.

Shu, F. H., Shang, H., and Lee, T. (2006) Toward an astrophysical theory of chondrites. *Science* 271, 1545-1552.

Shu, F. H., Shang, H., Glassgold, A. E., and Lee, T. (2007) X-rays and fluctuating x-winds from protostars. *Science* 277, 1475-1479.

Speth, R.S., Braatz, C., and Tiemann, E. (1998) REMPI spectroscopy of SO singlet states. *Journal of Molecular Spectroscopy* 192, 69-74.

Squyres, S. W. and Kasting, J. F. (1994) Early Mars: How warm and how wet? *Science* 265, 744-749.

Squyres, S.W., Arvidson, R.E., Bell, J.F., III, Brückner, J., Cabrol, N.A., Calvin, W., Carr, M.H., Christensen, P.R., Clark, B.C., Crumpler, L., Des Marais, D.J., d'Uston, C., Economou, T., Farmer, J., Farrand,W., Folkner, W., Golombeck, M., Gorevan, S., Grant, J.A., Greeley, R., Grotzinger, J., Haskin, L., Herkenhoff, K.E., Hviid, S., Johnson, J., Klingelhöfer, G., Knoll, A.H., Landis, G., Lemmon, M., Li, R., Madsen, M.B., Malin, M.C., McLennan, S.M., McSween Jr., H.Y., Ming, D.W., Moersch, J., Morris, R.V., Parker, T., Rice, J.W., Jr., Richter, L., Rieder, R., Sims, M., Smith, M., Smith, P., Soderblom, L.A., Sullivan, R., Wänke, H., Wdowiak, T., Wolff, M., and Yen, A. (2004) The Opportunity rover's Athena science investigation at the Meridiani Planum, Mars. *Science* 306, 1698–1703.

Stauffer, H. (1962) On the production rates of rare gas isotopes in stone meteorites. *Journal of Geophysical Research* 67, 2003-2008.

Stöffler, D. and Ryder, G. (2001) Stratigraphy and isotope ages of lunar geologic units: Chronological standard for the inner solar system. in *Chronology and Evolution of Mars*, Kallenbach et al., eds., 9-54.

Swindle, T. D., Treiman, A. H., Lindstrom, D. J., Burkland, M. K., Cohen, B. A., Grier, J. A., Li, B., and Olson, E. K. (2000) Noble gases in iddingsite from the Lafayette meteorite: Evidence for liquid water on Mars in the last few hundred million years. *Meteoritics & Planetary Science* 35, 107-115.

Szymanski, A., Brenker, F. E., Palme, H., and El Goresy, A. (2010) High oxidation state during formation of martian nakhlites. *Meteoritics & Planetary Science* 45, 21-31.

Tanaka, K.L. (1986) The stratigraphy of Mars. *Journal of Geophysical Research* 91:B13, E139-E158.

Taylor, F. W. (2011) Comparative planetology, climatology, and biology of Venus, Earth, and Mars. *Planetary and Space Science* 59, 889-899.

Thiemens, M. H. (1999) Mass-independent isotope effects in planetary atmospheres and the early solar system. *Science* 283, 341-345.

Thiemens, M.H. and Heidenreich III, J.E., (1983) The mass-independent fractionation of oxygen: A novel effect and its possible cosmochemical implications. *Science* 219, 1073-1075.

Thode, H.G., Macnamara, J., and Collins, C.B. (1949) Natural variations in the isotopic content of sulphur and their significance. *Canadian Journal of Research* B 27, 361-373.

Thode, H.G., Macnamara, J., and Fleming, W.H. (1953) Sulphur isotope fractionation in nature and geological and biological time scales. *Geochimica et Cosmochimica Acta* 3, 235-243.

Thode, H.G., Monster, J., and Dunford, H.B. (1961) Sulphur isotope geochemistry. *Geochimica et Cosmochimica Acta* 25, 150-174.

Tian, F., Claire, M. W., Haqq-Misra, J. D., Smith, M., Crisp, D. C., Catling, D., Zahnle, K., and Kasting, J. F. (2010) Photochemical and climate consequences of sulfur outgassing on early Mars. *Earth and Planetary Science Letters* 295, 412-418.

Tirsch, D., Jaumann, R., Pacifici, A., and Poulet, F. (2011) Dark aeolian sediments in martian craters: Composition and sources. *Journal of Geophysical Research* 116, doi: 10.1029/2009JE003562.

Treiman, A. H., Barrett, R. A., and Gooding, J. L. (1993) Preterrestrial aqueous alteration of the Lafayette (SNC) meteorite. *Meteoritics* 28, 86-97.

Trieman, A.H. (1995) A petrographic history of Martian meteorite ALH 84001: Two shocks and an ancient age. *Meteoritics* 30, 294-302.

Treiman, A. H., and Goodrich, C. A. (2002) Preterrestrial aqueous alteration of the Y-000749 nakhlite meteorite. Antarctic Meteorites XXVII, National Institute of Polar Research, Tokyo, 166-167.

Treiman, A. H., and Irving, A. J. (2008) Petrology of martian meteorite Northwest Africa 998. *Meteoritics & Planetary Science* 43, 829-854.

Ueno, Y., Johnson, M. S., Danielache, S. O. Eskebjerg, C., Pandey, A. and Yoshida, N. (2009) Geological sulfur isotopes indicate elevated OCS in the Archean atmosphere, solving faint young sun paradox. *Proceedings of the National Academy of Sciences* 106, 14784-14789.

Usui, T., Sanborn, M., Wadhwa, M., and McSween, H. Y., Jr. (2010) Petrology and trace element geochemistry of Robert Massif 04261 and 04262 meteorites, the first examples of geochemically enriched lherzolitic shergottites. *Geochimica et Cosmochimica Acta* 74, 7283-7306.

Vaniman, D.T., Bish, D.L., Chipera, S.J., Fialips, C.I., Carey, J.W., and Feldman, W.C. (2004) Magnesium sulphate salts and the history of water on Mars. *Nature* 431, 663–665.

Vicenzi, E. P., Fries, M., Fahey, A., Rost, D., Greenwood, J. P., and Steele, A. (2007a) Detailed elemental, mineralogical, and isotopic examination of jarosite in martian meteorite MIL 03346. *Lunar and Planetary Institute* #2335.

Vicenzi, E. P., Fries, M., Fahey, A., Rost, D., Greenwood, J. P., and Steele, A. (2007b) Evidence for young jarosite precipitation on Mars. *Meteoritics & Planetary Science* 42, A157.

Wadhwa, M. and Crozaz, G. (1995) Trace and minor elements in minerals of nakhlites and Chassigny: Clues to their petrogenesis. *Geochimica et Cosmochimica Acta* 59, 3629-3647.

Wadhwa, M. (2001) Redox state of Mars' upper mantle and crust from Eu anomalies in shergottite pyroxenes. *Science* 291, 1527-1530.

Wadhwa, M., Crozaz, G., and Barrat, J.-A. (2004) Trace element distributions in the Yamato 000593/000749, NWA 817 and NWA 998 nakhlites: Implications for their petrogenesis and mantle source on Mars. *Antarctic Meteorite Research* 17, 97-116.

Walker, R. J. (2009) Highly siderophile elements in the Earth, Moon and Mars: Update and implications for planetary accretion and differentiation. *Chemie der Erde* 69, 101-125.

Walker, R. J. (2012) Personal communication.

Walther, J. V. (2005) *Essentials of Geochemistry.* Sudbury, MA: Jones and Bartlett Publishers.

Wallace, P., and Carmichael, I. S. E. (1992) Sulfur in basaltic magmas. *Geochimica et Cosmochimica Acta* 56, 1863-1874.

Walton, E.L. and Spray, J.G. (2003) Mineralogy, microtexture, and composition of shock-induced melt pockets in the Los Angeles basaltic shergottite. *Meteoritics & Planetary Science* 39 (12), 1865-1875.

Warren, P. H., Greenwood, J. P., and Rubin, A. E. (2004) Los Angeles: A tale of two stones. *Meteoritics & Planetary Science* 39, 137-156.

Watson L.L., Hutcheon I.D., Epstein S. and Stolper E.M. (1994) Water on Mars: Clues from deuterium/hydrogen and water contents of hydrous phases in SNC meteorites. *Science* 265, 86-90.

Wendlandt, R. F. and Harrison, W. J. (1979) Rare earth partitioning between immiscible carbonate and silicate liquids and $CO_2$: Results and implications for the formation of light rare earth-enriched rocks. *Contributions to Mineralogy and Petrology* 69, 409-419.

Wentworth S.J. and Gooding J.L. (1994) Carbonates and sulfates in the Chassigny meteorite: Further evidence for aqueous chemistry on the SNC parent planet. *Meteoritics* 29, 860-863.

Whitehill, A. R., Lin, Y., Cordner, E., and Ono, S. (2010) Mass-independent fractionation of sulfur isotopes during experimental photolysis of sulfur dioxide and carbonyl sulfide. *Geochimica et Cosmochimica Acta* 74, A1129.

Wilhelms, D. E. and Squyres, S. W. (1984) The martian hemispheric dichotomy may be due to a giant impact. *Nature* 309, 138-140.

Wiseman, S. M., Arvidson, R. E., Andrews-Hanna, J. C., Clark, R. N., Lanza, N. L., Des Marais, D., Marzo, G. A., Morris, R. V., Murchie, S. L., Newsom, H. E., Noe Dobrea, E. Z., Ollila, A. M., Poulet, F., Roush, T. L., Seelos, F. P., and Swayze, G. A. (2008) Phyllosilicate and sulfate-hematite deposits within Miyamoto crater in southern Sinus Meridiani, Mars. *Geophysical Research Letters* 35, doi:10.1029/2008GL035363.

Wisniewski, E.S. and Castleman, A.W. (2002) Femtosecond photodissociation dynamics of excited-state SO. *Journal of Physical Chemistry A* 106, 10843-10848.

Wu, C.Y.R., Yang, B.W., Chen, F.Z., Judge, D.L., Caldwell, J., and Trafton, L.M. (2000) Measurements of high-, room-, and low-temperature photoabsorption cross sections of $SO_2$ in the 2080- to 2950-Å region, with application to Io. *Icarus* 145, 289-296.

Xirouchakis, D., Draper, D.S., Schwandt, C.S., and Lanzirotti, A. (2002) Crystallization conditions of Los Angeles, a basaltic Martian meteorite. *Geochimica et Cosmochimica Acta* 66, 1867-1880.

Zmolek, P., Xu, X., Jackson, T., Thiemens, M.H., and Trogler, W.C. (1999) Large mass independent sulfur isotope fractionations during the photopolymerization of $^{12}CS_2$ and $^{13}CS_2$. *Journal of Physical Chemistry* 103, 2477-2480.

Zolotov, M.Y. and Shock, E.L. (2005) Formation of jarosite-bearing deposits through aqueous oxidation of pyrite at Meridiani Planum, Mars. *Geophysical Research Letters* 32, doi: 10.1029/2005GL024253.